Vol. 278, No. 1, June 6, 1993

ISSN 0003-2670

ANALYTICA CHIMICA ACTA

An international journal devoted to all branches of analytical chemistry

ELSEVIER

ANALYTICA CHIMICA ACTA

Scope. *Analytica Chimica Acta* publishes original papers, preliminary communications and reviews dealing with every aspect of modern analytical chemistry. Reviews are normally written by invitation of the editors, who welcome suggestions for subjects. Preliminary communications of important urgent work can be printed within four months of submission, if the authors are prepared to forego proofs.

Submission of Papers

Americas

Prof. Harry L. Pardue
Department of Chemistry
1393 BRWN Bldg, Purdue University
West Lafayette, IN 47907–1393
USA
Tel:(+1-317) 494 5320
Fax:(+1-317) 496 1200

Computer Techniques

Prof. J.T. Clerc
Universität Bern
Pharmazeutisches Institut
Baltzerstrasse 5, CH-3012 Bern
Switzerland
Tel:(+41-31) 654171
Fax:(+41-31) 654198

Other Papers

Prof. Alan Townshend
Department of Chemistry
The University
Hull HU6 7RX
Great Britain

Tel:(+44-482) 465027
Fax:(+44-482) 466410

Prof. Willem E. van der Linden
Laboratory for Chemical Analysis
Department of Chemical Technology
Twente University of Technology
P.O. Box 217, 7500 AE Enschede
The Netherlands
Tel:(+31-53) 892629
Fax:(+31-53) 356024

Prof. Paul Worsfold
Dept. of Environmental Sciences
University of Plymouth
Plymouth PL4 8AA
Great Britain

Tel:(+44-752) 233006
Fax:(+44-752) 233009

Submission of an article is understood to imply that the article is original and unpublished and is not being considered for publication elsewhere. *Anal. Chim. Acta* accepts papers in English only. There are no page charges. Manuscripts should conform in layout and style to the papers published in this issue. See inside back cover for "Information for Authors".

Publication. *Analytica Chimica Acta* appears in 14 volumes in 1993. The subscription price for 1993 (Vols. 267–280) is Dfl. 4214.00 plus Dfl. 462.00 (p.p.h.) (total approx. US$ 2672.00). *Vibrational Spectroscopy* appears in 2 volumes in 1993. The subscription price for *Vibrational Spectroscopy* (Vols. 4 and 5) is Dfl. 700.00 plus Dfl. 66.00 (p.p.h.) (total approx. US$ 437.75). The price of a combined subscription (*Anal. Chim. Acta* and *Vib. Spectrosc.*) is Dfl. 4592.00 plus Dfl. 528.00 (p.p.h.) (total approx. US$ 2925.75). All earlier volumes (Vols. 1–266) except Vols. 23 and 28 are available at Dfl. 259.50 (US$ 148.25), plus Dfl. 18.00 (US$ 10.25) p.p.h., per volume. The Dutch guilder price is definitive. The U.S. dollar price is subject to exchange-rate fluctuations and is given only as a guide. Subscriptions are accepted on a prepaid basis only, unless different terms have been previously agreed upon.
Our p.p.h. (postage, packing and handling) charge includes surface delivery of all issues, except to subscribers in the U.S.A., Canada, Australia, New Zealand, China, India, Israel, South Africa, Malaysia, Thailand, Singapore, South Korea, Taiwan, Pakistan, Hong Kong, Brazil, Argentina and Mexico, who receive all issues by air delivery (S.A.L.–Surface Air Lifted) at no extra cost. For Japan, air delivery requires 25% additional charge of the normal postage and handling charge; for all other countries airmail and S.A.L. charges are available upon request.

Subscription orders. Subscription orders can be entered only by calendar year and should be sent to: Elsevier Science Publishers B.V., Journals Department, P.O. Box 211, 1000 AE Amsterdam, The Netherlands. Tel: (+31-20) 5803 642, Telex: 18582, Telefax: (+31-20) 5803598, to which requests for sample copies can also be sent. Claims for issues not received should be made within six months of publication of the issues. If not they cannot be honoured free of charge. Readers in the U.S.A. and Canada can contact the following address: Elsevier Science Publishing Co. Inc., Journal Information Center, 655 Avenue of the Americas, New York, NY 10010, U.S.A. Tel: (+1-212) 633 3750, Telefax: (+1-212) 633 3990, for further information, or a free sample copy of this or any other Elsevier Science Publishers journal.
Advertisements. Advertisement rates are available from the publisher on request.

Detailed "Instructions to Authors" for *Analytica Chimica Acta* was published in Volume 256, No. 2, pp. 373–376. Free reprints of the "Instructions to Authors" of *Analytica Chimica Acta* and *Vibrational Spectroscopy* are available from the Editors or from: Elsevier Science Publishers B.V., P.O. Box 330, 1000 AH Amsterdam, The Netherlands. Telefax: (+31-20) 5862845.

US mailing notice – Analytica Chimica Acta (ISSN 0003-2670) is published biweekly by Elsevier Science Publishers (Molenwerf 1, Postbus 211, 1000 AE Amsterdam). Annual subscription price in the USA US$ 2672.00 (subject to change), including air speed delivery. Second class postage paid at Jamaica, NY 11431. *USA Postmasters*: Send address changes to Anal. Chim. Acta, Publications Expediting, Inc., 200 Meacham Av., Elmont, NY 11003. Airfreight and mailing in the USA by Publication Expediting.

ANALYTICA CHIMICA ACTA

An international journal devoted to all branches of analytical chemistry

(Full texts are incorporated in CJELSEVIER, a file in the Chemical Journals Online database available on STN International; Abstracted, indexed in: Aluminum Abstracts; Anal. Abstr.; Biol. Abstr.; BIOSIS; Chem. Abstr.; Curr. Contents Phys. Chem. Earth Sci.; Engineered Materials Abstracts; Excerpta Medica; Index Med.; Life Sci.; Mass Spectrom. Bull.; Material Business Alerts; Metals Abstracts; Sci. Citation Index)

VOL. 278 NO. 1 CONTENTS JUNE 6, 1993

(Continued overleaf)

Contents (continued)

ANALYTICA CHIMICA ACTA
VOL. 278 (1993)

ANALYTICA CHIMICA ACTA

An international journal devoted to all branches of analytical chemistry
Revue internationale consacrée à tous les domaines de la chimie analytique
Internationale Zeitschrift für alle Gebiete der analytischen Chemie

Anal. Chim. Acta, Vol. 278 (1993)

ELSEVIER, Amsterdam–London–New York–Tokyo

0003-2670/93/$06.00

Analytica Chimica Acta, 278 (1993) 1–2
Elsevier Science Publishers B.V., Amsterdam

Guest Editorial

An ode to Laitinen: wherefore art thou, chemistry?

Most analytical chemists, if they are sufficiently old, remember Herb Laitinen for his two principal roles: as the editor of the "other" journal in analytical chemistry and as the author (with W.E. Harris) of the classic textbook titled "Chemical Analysis". I cannot claim to have been professionally mature when Laitinen was at the zenith of his editorial prowess. But I did suffer through the none-too-easy problems at the end of each chapter in Laitinen and Harris as much as any other aspiring analytical chemist of my generation. I discovered Laitinen the editor quite by accident. Hunting for a dated article, I stumbled upon the editorial page. I glanced through it and could not help but finish reading it. I skipped over to the next month's issue and read the editorial. Then I read the next one. By the time I left the stacks, I had not found the article I came for but I had read several dozen Laitinen editorials.

Reading editorials can become addictive over the years, I suppose. *Analytica Chimica Acta* now publishes guest editorials. The views are not always convergent on what should be important to analytical chemists. Mottola [1] seeks greater importance of equilibrium and kinetic aspects in the "core" discipline. Meanwhile Deming [2] feels that modern analytical chemistry relies less and less on chemical reactions.

I remember my Laitinen [3]. Some 17 years ago, he was commenting on a remark of H.A. Liebhafsky (which Laitinen already classified as "now classic"), namely that "Like it or not, chemistry is going out of analytical chemistry". He then paraphrased R.C. Chirnside in that it is not so much that chemistry is going out but that physics is coming in. Laitinen went on to point out all the areas in instrumental analysis where chemistry is ill understood and where work is still needed. (As it stands, nearly two decades later, with all the blessings of physics, electronics and chemometrics, the same problems still remain unsolved!)

Chemistry, whether related to equilibrium, kinetics, or new reactions, is indeed going out of graduate-level analytical chemistry classrooms. I, for one, think it is a sad state of affairs because chemistry, in all its glory, is more important than ever before in all frontiers of research. Two decades ago, Laitinen [4] took to task a conference speaker who maintained that analytical chemistry passed its zenith during the Manhattan project. The only rational basis for making such a comment, Laitinen retorted, is to pretend that there were no changes in what was required of analytical chemists in the intervening period. The present day analytical chemist is asked to determine things in quantities smaller than ever before and with a specificity unimaginable a decade ago. Without innovative ingenious chemistry, no amount of electronics or chemometrics would have accomplished that objective. The lion's share of the credit for the vast enhancement in the power and scope of chromatography that has taken place in the last two decades goes to the clever chemistry that has resulted in ingenious new stationary phases. Postcolumn reaction detection and precolumn derivatization have become routine and it is all due to chemistry.

There is little doubt that the most challenging frontier in analytical chemistry today is in the biological sciences. It is necessary to differentiate between molecules which differ from each other by 0.01% and then quantitate them at trace levels. Perhaps we do not think of it that way, but there is little doubt that the task of designing such specific probes and carrying out such quantitation *is* analytical chemistry, more than anything else. And the marketplace is certainly more than anxious for such chemists: there is a thriving

company whose sole business is to design specific probes and dyes that undergo specific binding (Molecular Probes, Eugene, OR).

I go to Laitinen again: "...Our field is so broad, in fact in some respects broader than chemistry as a whole, that it is relatively immune to the shift of emphasis from one area to another..." [5]. The human genome project is the grandest analytical chemistry project to date, far larger in scope and consequences indeed, than the Manhattan project. I admire those with the audacity of even undertaking such a project and I am proud as a fellow analytical chemist. I am not proud, however, when I see that the only way many of our chemistry students can answer the question "Is this a copper ore?" is to look for an atomic absorption spectrometer. I am glad that geology majors still can respond to such a challenge.

My own mentor, Philip W. West, long time editor of this journal, lamented that increasingly the teaching of chemistry involves teaching as little reaction chemistry as possible. The freshmen are so busy learning why and how carbon dioxide is linear and sulfur dioxide is angular that there is never any time to learn about their chemical reactions. Ironically, I cannot remember a single instance where anything I have ever done in my career as a chemist with sulfur dioxide or carbon dioxide has been affected by the knowledge of their shapes. It is indeed sad that so little chemistry is taught in analytical chemistry. Because they have had no previous exposure to it, many students of analytical chemistry regard the knowledge many of us "older" folks as akin to alchemical. It is a process of discovery for an average present day student to realize that there is little difference in coating an air sampling filter or a denuder tube with NaOH rather than Na_2CO_3: the former becomes the latter in a few minutes!

Surely physics, electronics, computer science and chemometrics have done much to enhance analytical chemistry and each or all of them should be studied by an analytical chemist depending on the subdiscipline (s)he is specializing in. Are any of them more important to analytical chemistry than chemistry? At best, they can be equally important if one's aspirations are limited to becoming a technician, not an analytical chemist. Is chemistry really disappearing out of analytical chemistry? Well, there seems to be a concerted effort to make that a self-fulfilling prophecy, by deleting it from all required curricula. Should I advise students to study molecular biology to participate in the frontiers of analytical chemistry? Would Laitinen have approved?

REFERENCES

1 H.A. Mottola, Anal. Chim. Acta, 242 (1991) 1.
2 S.N. Deming, Anal. Chim. Acta, 249 (1991) 303.
3 H.A. Laitinen, Anal. Chem., 47 (1975) 2073.
4 H.A. Laitinen, Anal. Chem., 44 (1972) 1929.
5 H.A. Laitinen, Anal. Chem., 45 (1973) 1.

Purnendu K. Dasgupta
Department of Chemistry and Biochemistry,
Texas Tech University,
Lubbock, TX 79409-1061 (USA)

Analytica Chimica Acta, 278 (1993) 3–4
Elsevier Science Publishers B.V., Amsterdam

Obituary

Wilhelm Simon
26th September 1929–17th November 1992

On 17th November 1992, Wilhelm Simon, Professor of Analytical Chemistry at the ETH Zürich and one of the most prominent analytical chemists of our time, died after a long period of illness.

Wilhelm Simon was born on 26th September 1929 in Fahrwangen, Switzerland. He studied chemistry at the Swiss Federal Institute of Technology (ETH) in Zürich, where he graduated in 1953. In 1956 he obtained his PhD at the Organic Chemistry Laboratory at ETH with Professor Edgar Heilbronner. He remained in the Department of Organic Chemistry, where he obtained the "venia legendi" in 1961, and was promoted to full Professor in 1972. Despite the fact that his work was focused on analytical chemistry, his Chair was called "Special Organic Chemistry", the field of analytical chemistry being traditionally in the domain of inorganic chemistry, where the Traedwells (father and son) and Schwarzenbach had made their essential contributions to the field. His group always remained in the organic chemistry section, but was renamed the Laboratory for Analytical Chemistry in 1985. This recognition of analytical chemistry as an independent field at ETH is one of Willy Simon's more important political achievements.

His initial field of interest was automation and miniaturization of analytical procedures. In particular, he developed a fully automated apparatus for the acidimetric titration of micro samples [1]. In connection with this project he then became interested in the sensors used in this instrument, i.e., in the glass electrode. The target was to develop low-resistance electrodes with low alkaline errors [2]. In the early 1960s he began the development of a fully automated CHN analyser [3]. This project resulted in a successful commercial product. The concurrent research project on the determination of molecular weights by vapour osmometry was also concluded with a successful commercial apparatus [4]. At about the same time, research work on pyrolysis combined with gas chromatography and mass spectrometry was initiated [5,6]. He was also among the first to realize the synergistic effects of the combination of different methods of molecular spectroscopy for the structure elucidation of organic compounds. This resulted in an ongoing series of

books [7]. Also new (photoelectron spectroscopy [8]) and uncommon (magneto-optical rotatory dispersion [9]) methods in molecular spectroscopy were studied.

A new and even more successful period in Simon's scientific work started with the use of antibiotics for ion-selective electrodes [10]. One of the first practical results in this field was the potassium-selective valinomycin-based electrode [11], which has been used ever since in clinical chemistry. Theoretical [12] and experimental [13] studies provided the basis for highly successful synthetic work in the field of ion-selective ligands [14]. Already in 1975 the first enantioselective sensor was described [15]. Successful miniaturization made possible the application of ion-selective sensors for measurements in living cells [16] and as detectors in chromatographic systems [17]. In more recent years the development of optical sensors also became a prominent research topic [18].

Willy Simon was not only a successful scientist, he was also a devoted teacher and educator. He developed and realized a curriculum for undergraduate chemists specializing in analytical chemistry. In his group he trained 115 doctoral students, many of whom today hold high positions in industrial and governmental laboratories or are in academic positions. He was a member of about 20 national and international learned societies and 30 scientific committees and advisory boards. In particular he served for many years on the Editorial Board of *Analytica Chimica Acta*.

For his co-workers he was always available, giving help and advice if required. He was a demanding but very liberal boss. If someone wanted to commit an error, he pointed out the consequences, and gave his advice as what he would do in the given situation, but he never forced his views upon his colleagues. This turned out to be quite unnecessary, as he was second to none in his ability to motivate his co-workers.

Despite the many honours he recived and besides his scientific rigour, he always remained human. We all, students, friends and colleagues, will remember Willy Simon and thank him for his scientific achievements, his political engagement for the education of the younger generation and for his friendship.

E. Pretsch
J.T. Clerc

REFERENCES

1 W. Simon, E. Kováts, L.H. Chopard-dit-Jean and E. Heilbronner, Helv. Chim. Acta, 37 (1954) 1872.
2 W. Simon and D. Wegmann, Helv. Chim. Acta, 41 (1958) 2099.
3 J.T. Clerc, R. Dohner, W. Sauter and W. Simon, Helv. Chim. Acta, 46 (1963) 2369.
4 Ch. Cylewsky and W. Simon, Helv. Chim. Acta, 47 (1964) 515.
5 H. Giacobbo and W. Simon, Pharm. Acta Helv., 39 (1964) 162.
6 J.A. Völlmin, P. Kriemler, I. Omura, J. Seibl and W. Simon, Microchem. J., 11 (1966) 73.
7 W. Simon and J.T. Clerc, Strukturaufklärung organischer Verbindungen mit spektroskopischen Methoden, Akademische Verlagsgesellschaft, Frankfurt am Main, 1967.
8 P.C. Meier and W. Simon, Analytical Applications of Photo-Electron Spectroscopy, in P. Hepple (Ed.), Molecular Spectroscopy, Institute of Petroleum, London, 1971, pp. 53–60.
9 H.-K. Wipf, J.T. Clerc and W. Simon, Helv. Chim. Acta, 51 (1968) 1051.
10 Z. Stefanac and W. Simon, Chimia, 20 (1966) 436; Mikrochem. J., 12 (1967) 125.
11 L.A.R. Pioda and W. Simon, Chimia, 23 (1969) 72.
12 W.E. Morf and W. Simon, Helv. Chim. Acta, 54 (1971) 2683; G. Corongiu, E. Clementi, E. Pretsch and W. Simon, J. Chem. Phys., 70 (1979) 1266.
13 P.U. Früh, J.T. Clerc and W. Simon, Helv. Chim. Acta, 54 (1971) 1445; R. Büchi, E. Pretsch, W.E. Morf and W. Simon, Helv. Chim. Acta, 59 (1976) 2407.
14 D. Amman, E. Pretsch and W. Simon, Tetrahedron Lett., (1972) 2473.
15 A.P. Thoma, Z. Cimerman, U. Fiedler, D. Bedekovic, M. Güggi, P. Jordan, K. May, E. Pretsch, V. Prelog and W. Simon, Chimia, 29 (1975) 344.
16 R.C. Thomas, W. Simon and M. Oehme, Nature (London), 258 (1975) 754.
17 A. Manz and W. Simon, J. Chromatogr. Sci., 21 (1983) 326.
18 W.E. Morf, K. Seiler, B. Lehmann, Ch. Beringer, K. Hartmann and W. Simon, Pure Appl. Chem., 61 (1989) 1613.

Analytica Chimica Acta, 278 (1993) 5–16
Elsevier Science Publishers B.V., Amsterdam

Development of a flow-through electrochemical detector for glucose based on a glucose oxidase-modified microelectrode incorporating redox and conducting polymer materials

Ellen Rohde [1], Eithne Dempsey, Malcolm R. Smyth and Johannes G. Vos

School of Chemical Sciences, Dublin City University, Dublin 9 (Ireland)

Hendrik Emons

Department of Chemistry, University of Leipzig, 7010 Leipzig (Germany)

(Received 26th October 1992; revised manuscript received 8th January 1993)

Abstract

The preparation of a reagentless glucose oxidase-based biosensor for application in a flow system is described. The enzyme was first codeposited with the redox polymer $[Os(bpy)_2(PVP)_{10}Cl]Cl$ (bpy = bipyridyl, PVP = poly-4-vinylpyridine) and glutaraldehyde on the surface of a platinum electrode, and subsequently covered with an electropolymerized layer of pyrrole, also containing glucose oxidase. The electron transfer from the reduced $FADH_2$ group in the core of the enzyme to the electrode surface is facilitated via the redox polymer/polypyrrole system. Due to the high permeability of both layers the amperometric detection of β-D-glucose can be carried out directly. Qualitative and quantitative investigations to optimize the composition of the solution for adsorption and electropolymerisation were performed. The characterisation of the sensor in terms of linearity, reproducibility, pH dependence, stability and the response to interfering substances was also carried out.

Keywords: Biosensors; Flow system; Glucose oxidase; Microelectrode; glucose oxidase-modified

Owing to its high selectivity, low cost and ruggedness, glucose oxidase (GOD) has been most employed in the development of glucose biosensors [1,2]. The enzyme [EC 1.1.3.4.] consists of two identical subunits, each of them containing a firmly bound flavine adenosine dinucleotide (FAD) group, which acts both as a prosthetic group and as a coenzyme. In its function as a coenzyme, this flavoprotein confers the redox properties to the enzyme. As a glycoprotein it contains up to 12% carbohydrate residues which are mostly arranged around the centre as an oligosaccharide shell. GOD shows a high selectivity towards β-D-glucose as reducing agent. The reaction rate with the anomer α-D-glucose is almost zero; reactions with derivatives and epimers of glucose, such as 2-deoxy-D-glucose, are negligible [3]. The overall reaction of β-D-glucose catal-

Correspondence to: M.R. Smyth, School of Chemical Sciences, Dublin City University, Dublin 9 (Ireland).
[1] Permanent address: Department of Chemistry, University of Leipzig, 7010 Leipzig (Germany).

ysed by the enzyme has a turnover rate of 10^{-3} s^{-1} and is as follows:

$$\beta\text{-D-glucose} + O_2 \longrightarrow \beta\text{-D-gluconolactone} + H_2O_2 \quad (1)$$

It has been shown that this happens in two consecutive steps with FAD as the reactive centre and ubiquitous oxygen as electron acceptor.

$$\text{E-FAD} + \beta\text{-D-glucose} \longrightarrow \text{E-FADH}_2 + \beta\text{-D-gluconolactone} \quad (2)$$

$$\text{E-FADH}_2 + O_2 \longrightarrow \text{E-FAD} + H_2O_2 \quad (3)$$

Since the first sensors based on this enzymatic reaction were introduced [4,5], a wide variety of glucose sensors based on optical, calorimetric and electrochemical principles has been developed. In practice, the electrochemical approach seems to be the most promising.

When working with amperometric glucose sensors, one is faced with the problem of how to directly detect the electron exchange occurring during the redox reaction between glucose and the enzyme. The FAD coenzyme in this reaction is known to be situated almost in the centre of the protein. Once the glucose substrate has reached this active site and reaction 2 has taken place, the flavine group is in its reduced state $FADH_2$. For its reoxidation, an electron acceptor is needed. Nature provides therefore oxygen, which is reduced to the chemically and electrochemically active species H_2O_2. Either the oxygen uptake or the increase in the peroxide concentration can be monitored amperometrically by an electrode that has the enzyme immobilized on its surface. The potential required to detect H_2O_2 is around +0.8 (vs. SCE). Many commercial available sensors work on this latter principle [6]. The amperometric determination of H_2O_2, however, has several disadvantages. Firstly, there is the necessity for a relatively high working potential which causes interferences by species which are present in real samples and are oxidized at potentials less positive than +0.8 V. Secondly, the high reactivity of the peroxide has proved to be damaging to the enzyme [7], which might be one reason for the loss of sensitivity of such sensors in the course of time. Therefore, attempts have been made to detect the redox reaction at lower potentials. The oxidation of the $FADH_2$ group is theoretically [8] as follows:

$$\text{FADH}_2 \longrightarrow \text{FAD} + 2H^+ + 2e^- \quad E^0 = 0.05 \text{ V (vs. SHE)} \quad (4)$$

However, this oxidation cannot be performed efficiently at solid electrodes. Since the redox centre is buried deep in the macromolecule, the electrons fail to overcome the distance between the inner core of the enzyme and the surface of a metallic electrode at acceptable transfer rates. The rate of electron transfer decreases exponentially with increasing distance between two redox centres [9]. Even if the enzyme is at the electrode surface there is practically no exchange of electrons, implicating a lack of measurable current. To establish the electron transfer, small and mobile redox couples like ferrocene, derivatives of ferrocene, quinones, conducting salts, and organic Os and Ru complexes have been immobilized together with the enzyme in the vicinity of the electrode surface to act as electron mediators diffusing between the redox centres. By means of this mechanism, this generation of glucose sensors gave signals linearly related to glucose concentrations, indicating that the rate of the electron transfer was enhanced sufficiently. However, due to their small size, the mediator molecules tend to diffuse through semi-permeable membranes or out of gels into the bulk solution. This causes not only a drop in the sensitivity of such sensors, but prevents their application in biological systems, since the substances have toxic properties and severely disturb the electron transport chain in the organism.

In recent studies, redox macromolecules have served as mediators. Polypyrrole (PPy) and modified derivatives of PPy were used to achieve both the entrapment of the biocatalyst and the enhanced electron transfer after the glucose conversion [10–14]. The positively charged PPy backbone incorporates anions in order to maintain electroneutrality. The entrapment of the polyanionic glucose oxidase within the positively charged network is probably based both on electrostatic forces and simple physical enclosure. The three

dimensional layer grown on the electrode surface is fairly stable and has been proved not to decrease the enzyme activity [11].

In the latest approach, workers have developed non-diffusionally mediated electron transfer in glucose oxidase-based biosensors, where a direct electrical connection between the enzyme's redox centre and the electrode is established via "relay" molecules. Hale et al. [15,16] used ferrocene derivatives bound to insoluble siloxane polymers to incorporate the enzyme and facilitate high electron transfer rates, while Heller and co-workers [17–20] reported on attempts with modified enzymes based on covalent bonding of enzyme and polymers containing a fast redox couple. In this so called "molecular wiring" on the electrode surface, hydrogels of long and flexible $[Os(bpy)_2Cl]^{+/2+}$ poly(vinylpyridine) molecules (Os–PVP) are formed, which penetrate the enzyme deeply enough to reduce the distance for the required electron transfer. Apart from this complexation, the enzyme is physically attached to the electrode surface and covalently bound via crosslinks or functionalized polymer side chains to the three dimensional network. For such deposited films the observed current densities are higher than those obtained with systems employing diffusional mediators. In addition the stability is reported to be good. The kinetics of this system, which is a function of several processes, is controlled by the transport rate of the electrons through the biomolecule and surrounding network [20].

Our approach has been to develop an amperometric glucose sensor dedicated for application in flow-injection analysis (FIA). The aim was to place the enzyme in close proximity to the electrode surface. Based on the results of Heller's group and the outcome of recent studies on polypyrrole coated electrodes, this approach has been modified and extended. The utilized redox polymer has a molecular mass of 230 kD without the Os complex in the side chain, and its structure is shown in Fig. 1 [21]. One in ten of the polymer units bears the fast and stable $Os^{2+/3+}$ redox couple.

This report describes work on the optimisation and characterisation of the sensor produced by wiring glucose oxidase with polymers designed to support the electrical communication between the enzyme and the electrode. It reports the results obtained from pH, flow-rate and stability studies. The electrode response to interfering substances like ascorbic acid, uric acid, acetaminophen and glutathione, which are common in real samples, has also been investigated.

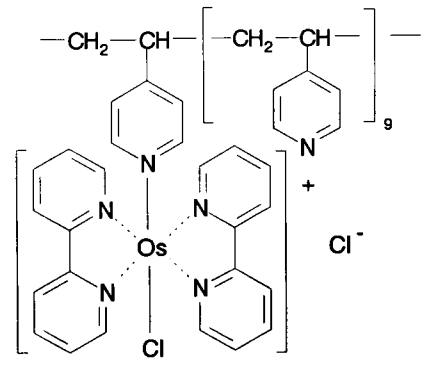

Fig. 1. Structure of the utilized redox polymer $[Os(bpy)_2(PVP)_{10}Cl]Cl$.

EXPERIMENTAL

Chemicals

Glucose oxidase (GOD) [EC 1.1.3.4.] from *Aspergillus* niger had an activity of 150 000 U g^{-1} and was obtained as a lyophilized powder from Sigma and stored below 0°C. A unit is defined as the amount of enzyme which oxidizes 1 micromole of β-D-glucose to D-gluconic acid and H_2O_2 per minute at pH 5.1 at 35°C. For these studies the redox polymer $[Os(bpy)_2(PVP)_{10}Cl]Cl$ (Os polymer) was synthesized as reported elsewhere [21] and used as 1% (w/w) solution in methanol. Pyrrole (Riedel-de-Haen; 98%, v/v) was first distilled and collected under nitrogen before use and store at 4°C.

Reagent grade K_2HPO_4 and KH_2PO_4 were obtained from Riedel-de-Haen, and used to prepare 0.1 M phosphate buffer. The pH was then adjusted to 7.5. β-D-Glucose was obtained from BDH. After the preparation of a 1 M solution, it was allowed to mutarotate for 24 h at room temperature. Afterwards the solution was stored

at 4°C. From this stock solution dilutions of the appropriate amount were made in 0.1 M phosphate buffer, pH 7.5. Glutaraldehyde was obtained from Aldrich as a 25% solution in water, and bovine serum albumin (BSA) was obtained from Sigma. For the study of interfering substances, L-ascorbic acid and uric acid were obtained from Aldrich, paracetamol from BDH and glutathione from Sigma. The alumina for polishing the electrode was obtained from Metrohm. Deionized water was used for preparation of all solutions, and was obtained by passing distilled water through a Milli Q-water purification system (Millipore).

Apparatus

For the electropolymerisation of pyrrole and electroanalytical measurements, an EG&G Princeton Applied Research EC Model 400 detector was used. Currents were recorded on a WPA Model CQ95 recorder. FIA was carried out in a system consisting of a Minipuls 3 peristaltic pump (Gilson), a two-way injection valve (Rheodyne) with a 20-μl loop and the flow cell designed by Hua et al. [22]. For stability studies, a Shimadzu SIL 9A autosampler and C-R6A integrator were added to the manifold. The injection valve was connected to the flow cell through a 18-cm polyethylene tubing with a diameter of 0.5 mm.

Procedures

The working electrode was prepared in a similar manner reported by Hua et al. [22]. A piece of platinum wire (diameter 0.5 mm, length 6 mm) was first polished with alumina on a wet cloth, rinsed with deionized water and ultrasonicated for 5 min. A polyethylene tube (diameter 3 mm, length 3 cm) was punctured vertically and the platinum wire was inserted in the hole. The gap between the wire and the tube was closed by gently heating and melting the polyethylene and wrapping it with strips of parafilm. For the electrical connection the platinum was soldered onto copper wire. The Ag/Ag_3PO_4 (1 M H_3PO_4) reference electrode was also prepared according to Hua et al. [22]. The potential of this electrode is 286 mV vs. the standard hydrogen electrode (SHE). The stainless-steel tube in the flow cell acted as the counter electrode.

The three electrodes were then mounted into the flow cell, as shown in Fig. 2 [22]. The electrolyte solution used as a carrier stream was air-saturated.

Prior to the actual modification, the platinum wire was preanodized at a potential of +1000 mV for 60 s. Subsequently a solution consisting of a mixture of 100 μl of GOD (150 U) in 5% BSA, 50 μl of 2.5% glutaraldehyde in phosphate buffer and 10 μl of 1% Os polymer in methanol was mixed, pumped into the system and allowed to adsorb onto the platinum surface for 30 min. After this a fast stream of air was pumped through the flow cell for 60 min in order to dry the adsorbed layer. Before the electropolymerisation of pyrrole was performed, the electrode was gently rinsed with 0.1 M glycine for about 3 min in order to remove residues of glutaraldehyde from the layer. Meanwhile 200 μl of 0.1 M pyrrole in 0.5 M NaCl were added to 100 μl of GOD solution (150 U) and deoxygenated by bubbling through nitrogen for 8 min. This mixture was pumped into the flow cell so that the working electrode was surrounded by the plug of pyrrole and GOD, while the other electrodes were immersed in phosphate buffer. The flow was stopped and the electropolymerisation was carried out by applying a constant potential of 950 mV for 20 min. For optimisation studies, one of the constituents of the mixtures was replaced by the same volume of its solvent (qualitative optimisation), or the concentration of this species was varied (quantitative optimisation). After this procedure, the plug of pyrrole containing GOD was cleared out of the flow cell and the electrode was

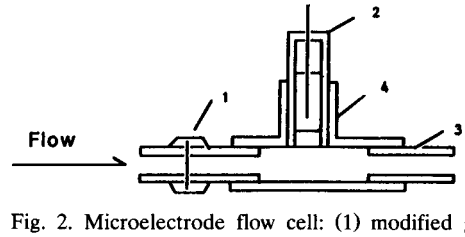

Fig. 2. Microelectrode flow cell: (1) modified glucose electrode; (2) reference electrode, $Ag/Ag_3PO_4/H_3PO_4$ (1 M); (3) auxiliary electrode, (stainless-steel tube); (4) T-junction.

stored in phosphate buffer at 4°C for 24 h to allow the electrode to equilibrate. When this time had expired the electrode was ready for all the types of measurements described below.

To evaluate the behavior of the electrode, voltammetric studies of the response to increasing concentrations of glucose at a fixed potential of 400 mV were performed. Initially the response to high concentrations in the range between 0.05 and 1 M was tested. After a proper response was obtained, the experiment was extended into the concentration range from 1 to 20 mM. The electrode response to 0.01 M glucose at potentials between 200 and 700 mV was used to produce hydrodynamic voltammograms.

After applying the potential the background current was allowed to decline until the baseline was stable. 20-μl glucose samples were then injected into the stream of phosphate buffer (0.7 ml min^{-1}) and the current was recorded versus time. For evaluation purposes the peak height measured between the baseline and the tip of the peak was used. In further experiments the electrode behaviour for 0.1 M glucose in dependence to changes in the pH, flow-rate and time was tested. Long time stability studies for this new type of electrode were carried out over a period of 105 h. For these studies the recorder and the injection valve were replaced by a Shimadzu autosampler and integrator which were connected with the manifold. Samples of 20 μl of 10 mM glucose were injected every 15 min into the buffer stream with a flow-rate of 0.3 ml min^{-1}.

RESULTS AND DISCUSSION

The procedure we have developed combines the use of both polypyrrole and an Os-containing PVP-based polymer immobilization of the enzyme. Initially the Os–PVP was mixed with glucose oxidase and allowed to adsorb physically to the platinum surface. A three-dimensional network was formed by means of the bifunctional glutaraldehyde. The reaction of aldehyde groups with free amino groups of the enzyme leads to Schiff's base linkages. During the crosslinking process, a network is formed around the already existing polymer molecules on the surface of the electrode. The interaction between the enzyme and the redox mediator is assumed to be of an electrostatic nature. In the next step the first layer is covered with electropolymerized polypyrrole containing glucose oxidase. This additional step is to achieve a high loading of enzyme on the electrode surface and to improve the overall turnover of the analyte. The features of the electrical conducting PPy layer, coupled with those of the three-dimensional network underneath, are to improve the electron transfer process, and the electrode stability. Activity losses of 25–75% can occur when redox polymers are covalently bound to the enzyme [17]. By using our method, the loss of enzyme activity can be minimized. Furthermore, we are able to operate the sensor near the potential of the Os-containing mediator molecule.

The glucose sensor exhibits currents which are linearly dependent on the concentration of the substrate. After the glucose diffuses into the bilayer, it is oxidized at the FAD group of the enzyme. Then, according to the conduction mechanism of each layer, the electrons are transferred to the nearby electrode surface.

The "wiring" procedure and the subsequent measurements were performed in a flow cell. This cell was developed earlier by Hua et al. [22] for use in connection with microelectrodes. Using FIA, fast and reproducible results can be obtained, and only a small sample volume is needed. Also, the fact that flow systems are easy to adapt to a wide range of detection methods, has made flow injection analysis eligible for application in clinical chemistry.

Qualitative optimisation

The term "qualitative optimisation" represents attempts to find out which substances are necessary to create a glucose sensor based on the principles mentioned above. The basic ideas about the content of the solutions for adsorption and polymerisation were derived from reports of experiments using electrodes modified with PPy [23–26] or metal-containing redox polymers [17,18], which were adapted for used in the flow cell. The adsorption solution used in the first step of the electrode preparation has to contain glu-

cose oxidase, glutaraldehyde and $[Os(bpy)_2(PVP)_{10}Cl]Cl$. The electropolymerisation in the second step has to be carried out a solution of sodium chloride, pyrrole and glucose oxidase. Afterwards, electrodes were prepared, where one or more of these compounds were omitted. The electrodes were tested by holding at a potential of 400 mV (vs. Ag/Ag_3PO_4, 1 M H_3PO_4) and their response to relatively high concentrations of glucose injection was monitored (Fig. 3).

Electrodes prepared without the enzyme showed almost no response to glucose. At a bare Pt wire, no direct oxidation of glucose at the applied potential was observed (Fig. 3a). Electrodes modified with only $[Os(bpy)_2(PVP)_{10}Cl]Cl$ or PPy film did not give any response (Fig. 3b and c respectively). This is in agreement with results obtained when electrodes with a similar polymer film and in the absence of GOD were tested by Gregg and Heller [18]. A fourth electrode prepared with all compounds except GOD again exhibited only very small currents to glucose injections (Fig. 3d). This emphasizes the fact, that no glucose conversion at +0.4 V occurs in the absence of GOD. When adding GOD to the modifying mixtures, however, a significant current after injection of the analyte was observed (Fig. 3e). A solution of 0.1 M glucose gave rise to a response of about 200 nA, clearly showing that electron transfer is triggered by the redox reaction in the reactive centre of the enzyme. The response of an electrode without the redox active $[Os(bpy)_2(PVP)_{10}Cl]Cl$ gave evidence of its necessity and demonstrated furthermore the conducting properties of PPy (Fig. 3f). Only a very few electrons could be shuttled to the electrode surface via the polymer chains. Testing an electrode containing enzyme and $[Os(bpy)_2(PVP)_{10}Cl]Cl$, but without a PPy layer, gave initially a response to 0.1 M glucose of about 150 nA. The response decreased dramatically after the electrode was left longer than 30 min in the buffer stream. This leads to the assumption that the network formed by crosslinking with glutaraldehyde was not stable enough, and components were washed out and carried away with the electrolyte stream. In a further preparation, the first wiring step was carried out without adding glutaraldehyde to the solution (Fig. 3g). The electrode subsequently gave almost no response to glucose. The absence of the cross-linking agent prevents a spatial network to be erected, indictating that a three-dimensional structure is essential for the electron transfer process to occur.

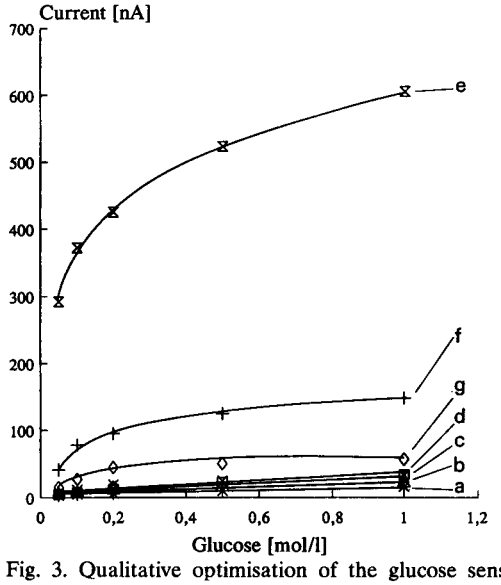

Fig. 3. Qualitative optimisation of the glucose sensor; constructed electrodes: (a) bare platinum wire, (b) only $[Os[(bpy)_2(PVP)_{10}Cl]Cl$, (c) only $[Os[(bpy)_2(PVP)_{10}Cl]Cl$ and PPy, (d) without enzyme, (e) complete electrode, (f) without redox polymer, (g) without glutaraldehyde.

Quantitative optimisation

In this part of the investigation particular attention was paid to the influence of varied parameters of the modifying process towards the electrode properties.

Variation of the cross-linking glutaraldehyde between 0.39 and 1.56% showed an optimum at a concentration of 0.78% (Fig. 4). One can assume that lower concentrations are not sufficient to form intermolecular bridges between the enzyme molecules, thereby giving a poor network structure. The electrodes prepared with 1.56% glutaraldehyde showed smaller currents than those with 0.78% glutaraldehyde content. Thus an increase of the cross-linker concentration leads to a deterioration in sensitivity, which might be traced back to a loss of enzyme activity. The enzyme

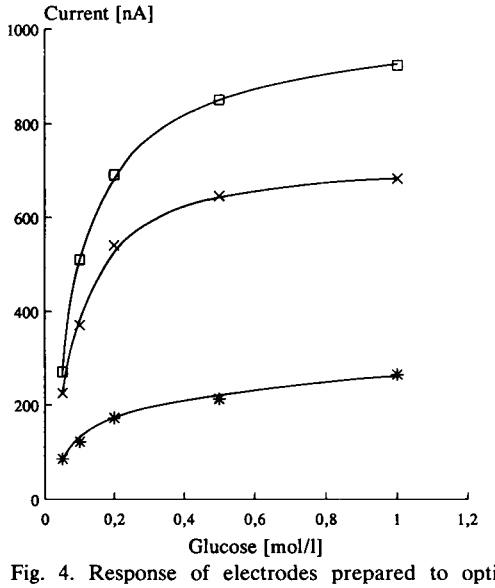

Fig. 4. Response of electrodes prepared to optimize the cross-linker concentration in the adsorption solution. □, 0.78% glutaraldehyde, ×, 1.56% glutaraldehyde, *, 0.39% glutaraldehyde.

structure can undergo changes after reacting with an excess of glutaraldehyde. In addition, too rigid a network can also inhibite substrate transfer within the layer.

Electrodes prepared with contents of 0.06, 0.12 and 0.24% (w/w) $[Os(bpy)_2(PVP)_{10}Cl]Cl$ in the adsorption solution gave different responses to substrate injections. Unexpectedly, the highest peaks were obtained from electrodes with the lowest $[Os(bpy)_2(PVP)_{10}Cl]Cl$ concentration. We had assumed that increasing the amount of redox polymer would increase the current. In contrast, electrodes with a high loading of redox centres gave rise to smaller, tailed peaks.

The concentration of the enzyme was then varied in both modification solutions. Electrodes prepared with a GOD content of 90 U in 100 μl of adsorption solution and 50 U in the 100 μl polymerisation solution, respectively, showed greater responses. Halving or doubling the amount of GOD immobilized on the electrode surface gave rise to smaller responses to reactions with glucose. A simple calculation shows how the ratio of the redox centres of the enzyme and the polymer changes when the enzyme concentration is varied. The utilized redox polymer has an average chain length of 2200 units. Every tenth unit is derivatized with an Os complex so that there are 220 redox centres per molecule. The overall molecular weight of the hydrated polymer is 375 kD, while the molecular weight of glucose oxidase is 155 kD. In a mixture of both containing $[Os(bpy)_2(PVP)_{10}Cl]Cl$ and GOD in a ratio of 1:2.5, theoretically 36 redox centres would be available for one enzyme molecule. This ratio is lowered when the enzyme concentration increases. A 1:5 ratio of the compounds implicates 18 Os centres for one enzyme molecule, whereas a ratio of 1:10 means that 9 redox centres can be used for enhancement of the electron transfer per enzyme. The best electrodes were prepared with a Os polymer to GOD ratio of 1:10 (see Fig. 5). This seems to be the optimum of the interaction of different factors like electrostatic attraction and repulsion in the complexation of the enzyme by the $[Os(bpy)_2(PVP)_{10}Cl]Cl$, chain constitution of the redox polymer, number of electron relays available and network structure under the constant interaction with the second layer on top. Several publications reporting about the modification of an enzyme electrode with redox

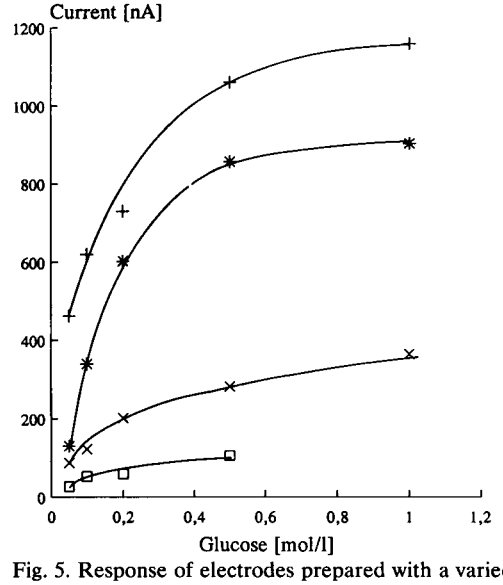

Fig. 5. Response of electrodes prepared with a varied ratio of $Os[(bpy)_2PVP_{10}Cl]Cl$–GOD (w/w). +, 1:10; *, 1:20; ×, 1:5; □, 1:2:5.

polymers only give Os polymer to GOD ratios of 7:3 (w/w) and 1:1 (w/w), respectively, as their optimum [18,19]. This contradiction may be caused by different experimental conditions, e.g., the use of redox polymers with smaller molecular weight, higher redox centre loading, functionalized side chains and utilized cross-linking agent. A major factor to explain these differences probably lies however in the higher complexity of our bilayer electrode.

This must be born in mind when it comes to the interpretation of the results from variations in the polymerisation process. From evaluation of monomer concentrations, a 0.06 M solution of pyrrole seemed to be optimal. Other groups have reported about their methods working in a concentration area from 0.1 to 0.5 M. Although it was recognized that lower pyrrole concentrations slow down the rate of the film growth [10], in the present case a sufficient PPy layer was formed after a constant polymerisation time of 20 min. A rather high potential of 950 mV was also used for this purpose.

Since the ionic strength is known to influence both the action of the enzyme and the redox polymer, we performed the electropolymerisation in NaCl solutions with ionic strengths of 0.05, 0.1 and 0.2 M (Fig. 6). The PPy formation from the lowest concentration gave the electrode with the best efficiency. Following the proposed inclusion mechanism for GOD into the polycationic PPy structure, a lower concentration of anionic competitors from the electrolyte is expected to favour enzyme entrapment. This result of the electropolymerisation is in agreement with the fact stated in other papers that GOD can be successfully incorporated into PPy [27].

Since there is expected to be an interaction between the PPy layer and the Os polymer, the electric field of the ions can influence the structure of the Os–PVP layer. The coiling of the cationic redox polymer caused by attracted anions is normally reversible [26]. Assuming that the PPy network penetrates the already established first layer and adsorbs to the electrode surface as well, the rigidity of these segments may hinder a part of the OsPVP to recoil when in solution with lower ionic strength.

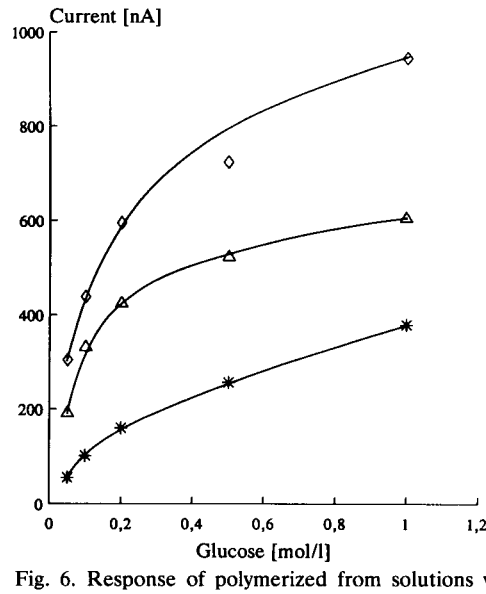

Fig. 6. Response of polymerized from solutions with varied ionic strength. ◇, 0.05 M; △, 0.1 M; *, 0.2 M.

As a result of this process of optimisation, enzyme electrodes have been prepared which gave responses twice as high as initially found. The mechanism of electron transfer seems to be different from that observed in electrodes with only a single type of immobilisation. Because the data to explain the electron transport in this bilayer are limited, the exact mechanism remains uncertain.

Characteristics of the glucose sensor

In Fig. 7 some of the electrode's features are shown. The hydrodynamic voltammogram (Fig. 7a) obtained from the catalyzed reaction of 10 mM glucose at different potentials shows that +0.4 V is the most efficient working potential. The standard potential of the Os polymer utilized as a redox mediator is +0.23 V vs. Ag/Ag_3PO_4 [28]. This is well above the potential necessary for the reoxidation of the $FADH_2$ group in the enzyme. As soon as the Os centres in the polymer are oxidized electrochemically the sensor gives a response to glucose injections. This proves the importance of the codeposition of the enzyme and the redox polymer for the electron transfer process. The potential of the mediator allows the electrode to be held at a lower potential than

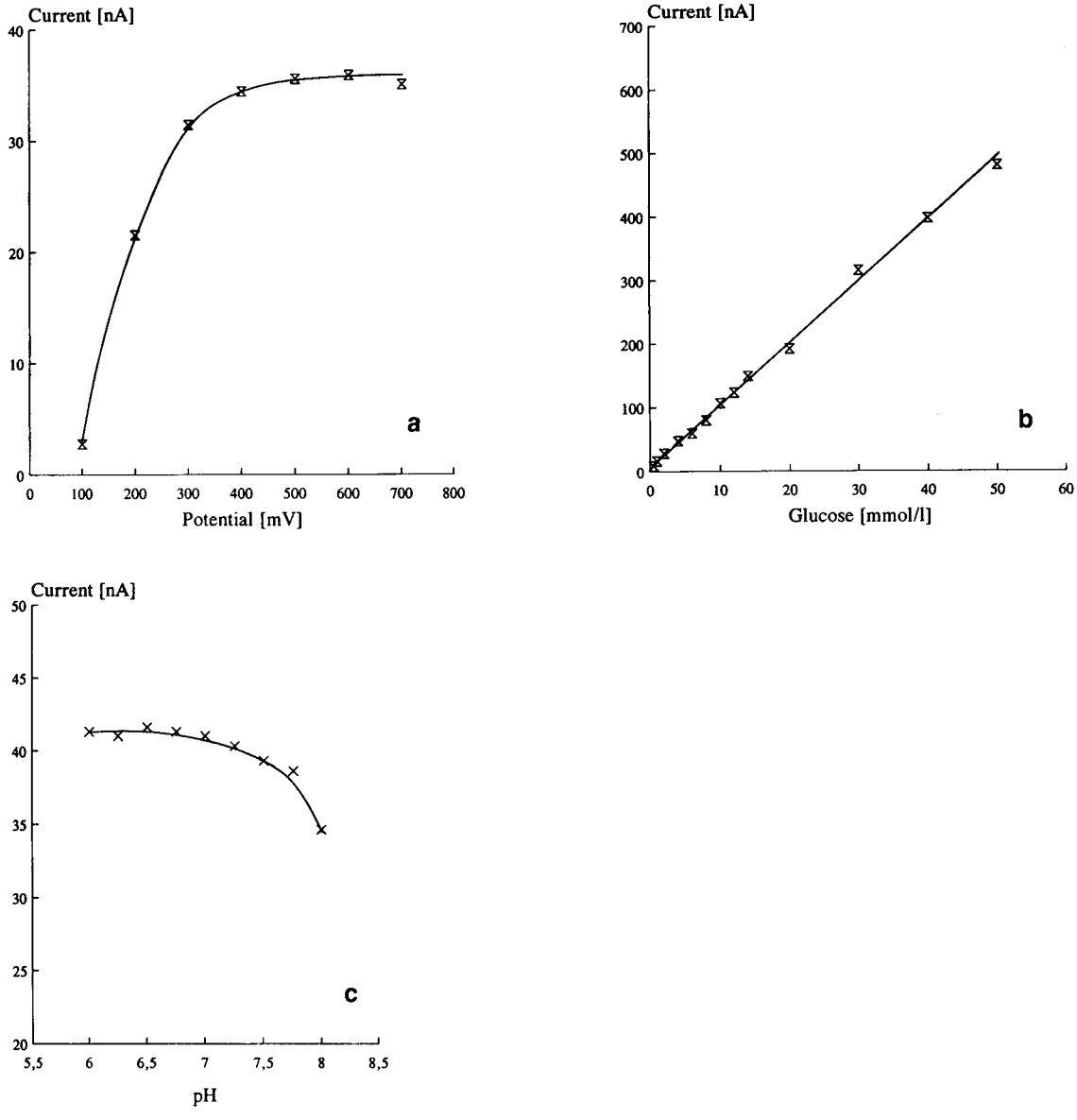

Fig. 7. Characteristics of the novel glucose sensor. (a) Hydrodynamic voltammogram for 10 mM glucose. (b) Electrode response to increasing concentrations of glucose at a potential of +0.4 V. (c) pH dependence of glucose sensor; 10 mM glucose; +0.4 V.

+0.8 V, the potential which is commonly used for the electrochemical oxidation of H_2O_2. This is desirable for the suppression of interferences.

From the calibration graph (Fig. 7b) the range within which the electrode responds linearly to glucose in the flow cell can be seen. This range between 1 and 50 mM includes that of biological importance. The calibration curve is characteristic for the average of the prepared electrodes with a slope of 12.2 nA dm^3 mol^{-1} and an intercept of 1.17 nA. The detection limit defined as a signal to noise ratio of 3 : 1 was usually 1 mM glucose. A few electrodes exhibited exceptionally good characteristics and were applicable for determinations of 10 μM glucose in buffer solution.

The reproducibility of the electrode response

was evaluated for 10 repeated injections of glucose standards with three different concentrations in a flow of an ideal carrier. The mean of the current for a 4 mM glucose dilution was found to be 3.0 nA with a relative standard deviation (R.S.D.) of 2.97 nA. The means for 10 mM and 100 mM solutions were 134 and 570 nA with R.S.D. values of 3.25 and 0.9 nA, respectively.

The influence of pH (Fig. 7c) on the electrode behaviour was then investigated. The free enzyme shows greatest activity at pH 6.5. After enzyme immobilisation a shift of the pH optimum towards higher values is generally observed. Any mediator used to transport electrons from the active site to the electrode will have an influence on the overall behaviour of glucose sensors [2] with respect to changing concentrations of hydrogen ions. The present sensor tested at pH values from 6.0 to 8.0 worked over most of this range without change of sensitivity. Only at pH > 7.75 did the peak height of 10 mM glucose injections decline. Changes in the tertiary structure maintained by H bridges can be regarded as the reason for this loss of stability. For an anticipated use in clinical chemistry the near physiological pH 7.5 was chosen as the basis of the phosphate buffer solutions and glucose standards.

The effect of the carrier flow-rate was then investigated. Lower flow-rates were found to enhance the sensitivity of the electrode but broadened the peak width simultaneously. From studies of flow-rates between 0.2 and 1.6 ml min^{-1}, a hyperbolic shaped curve was obtained. Normally a flow-rate of 0.7 ml min^{-1} was used, which was a compromise between the achieved peak height and the frequency of injection.

Despite the bilayer structure of the modified electrode, the response was found to be relatively fast. Times of 10 s and less were obtained for the electrode response to glucose concentrations up to 20 mmol l^{-1}. The time the sample plug spends in the tubing between the injection valve and the working electrode was determined by the fast electrode reaction of the redox couple $Fe^{2+/3+}$ and accordingly subtracted. This indicates that the redox reaction and the following electron transfer proceed relatively rapidly, aided by the porous structure and the redox active properties of the immobilisation matrix.

The stability of the developed glucose sensor was investigated in two ways (Fig. 8). Firstly, response curves for glucose were monitored in the first three days the electrode was in use. Thereby a decrease from the first day's slope of the calibration line of 9.90 to the third day's slope of 4.65 nA dm^3 mol^{-1} was observed (Fig. 8a). This decrease in sensitivity, however, levelled off and the same sensor tested after four weeks still maintained a useful response to glucose. This tendency can also be derived from a second experiment involving automatic injections of 10 mM glucose every 15 min. The experiment lasted 105 h; the response in the first 72 h is depicted in Fig. 8b. The reason for the 50–60% decline of the initial sensor response can be a gradual leaching

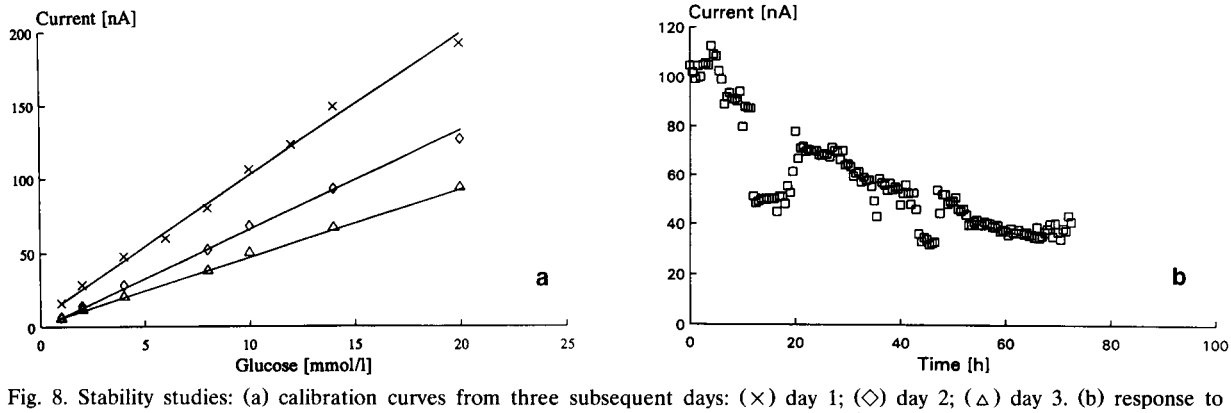

Fig. 8. Stability studies: (a) calibration curves from three subsequent days: (×) day 1; (◇) day 2; (△) day 3. (b) response to injections of 10 mM glucose every 15 min at a potential of +0.4 V; flow-rate 0.3 ml min^{-1}.

of the GOD from the upper layer, since the average pore size of the PPy network is reported to be the same order of magnitude as the enzyme diameter [10,12]. The enzyme is probably not firmly bound to its surrounding and is therefore subjected to diffusion processes in the porous outer layer. Because GOD is very stable, the factor of decreasing enzyme activity seems to be of less importance. The glucose sensor was always stored under cold conditions when not in use. Although many workers use their PPy-based glucose sensors immediately after preparation, we agree with the findings of Hämmerle et al. [14], that initially the response decreases within the first day after preparation, as a result of enzyme settlement in the new microenvironment. Changes in the structure of both the polymers and the enzyme towards more favourable and reactive conformations accelerate ongoing processes in the heterogeneous layer on the surface. Diffusion of excess substances out of the bilayer, although not favoured by the low storage temperatures, is likely to play a role in the improvement of the signal height and shape.

Influence of interfering substances

A sensor designed for practical applications has to cope with the influence of a different environment once in contact with a real sample. This is of special importance for an amperometric glucose sensor with an anticipated use in clinical laboratories, or for an in vivo application. Media to be investigated like whole blood, plasma, serum, urine and spinal fluid are composed of a variety of organic and inorganic substances, some of them interacting physically or chemically with the electrode. At a constant potential of +0.4 V, the electrode was found to be highly sensitive to ascorbic acid, uric acid and acetominophen. Neither the barrier effect of the PPy layer nor the lowered working potential can prevent the occurrence of extremely high pseudo currents caused by the oxidation of such substances at the underlying electrode surface. Considerations have to be made therefore on how to prepare a more selective sensor system. Work has been carried out to investigate and to improve the size-exclusion properties of PPy by modifying the conditions for the electropolymerisation [14]. Also, suggestions have been made for selective preoxidation of the interferants [19,29]. We also intend to modify the chemical structure of redox polymer in order to decrease the redox potential of the mediator.

Conclusions

A glucose sensor for application in a flowing system has been constructed. The flow cell, as well as the sensor, are easy to prepare. For the modification of the electrode, two simple techniques of enzyme immobilisation are employed under near physiological conditions. In the first step the enzyme is simultaneously entrapped in a polymer network and electrically connected to the electrode surface. After this "wiring" procedure, the Os-containing redox polymer acts as a relay system reducing the distances for electrons to be overcome and facilitates the electrical communication between the redox centre of the enzyme and the electrode surface. The three-dimensional structure is extended by electropolymerisation of pyrrole out of an aqueous GOD-containing solution. Although the enzyme is only physically attached, the electron shuttling mechanism is enhanced and electrons are transferred at sufficient rates to the electrode. Investigations of the sensor characteristics gave good linearity, sensitivity and reproducibility.

A problem that still has to be addressed is the loss of sensitivity within the first day of use. Further work is needed to improve the cross-linking of enzyme in the PPy layer and to improve the uniformity of the network. The latter could also contribute to the elimination of the relatively high response to potential interferants in real samples.

This work was supported by a grant (SC/90/118) from EOLAS (The Irish Science and Technology Agency) under the Scientific Research Programme. E.R. gratefully acknowledges support from the Gottlieb Daimler- und Benz-Stiftung, Ladenburg, Germany.

REFERENCES

1 A.E.G. Cass, Biosensors – A Practical Approach, IRL Press, Oxford University Press, pp. 116–118.

2 R. Wilson and A.P.F. Turner, Biosensors Bioelectronics, 7 (1992) 165.
3 P.W. Carr and L.D. Bowers, Immobilized Enzymes in Analytical and Clinical Chemistry – Fundamentals and Applications, Wiley, New York, 1980, p. 62.
4 L.C. Clark and C. Lyons, Ann. N.Y. Acad. Sci., 102 (1962) 29.
5 S.J. Updike and G.P. Hicks, Nature, 214 (1967) 986.
6 K. Bertermann, F. Scheller, D. Pfeiffer, M. Jähnchen and J. Lutter, Z. Med. Labor.-Diagn., 22 (1981) 83.
7 P.H.S. Tse and D.A. Gongu, Biotechnol. Bioeng., 29 (1987) 705.
8 L.F. Fieser and M. Fieser, Organic Chemistry, Reinhold, New York, 1956, 460.
9 A. Heller, J. Phys. Chem., 96 (1992) 3579.
10 M. Umana and J. Waller, Anal. Chem., 58 (1986) 2979.
11 N.C. Foulds and C.R. Lowe, J. Chem. Soc. Faraday Trans, 1, 82 (1986) 1259.
12 W. Schumann, R. Lämmert, B. Uhe and H.-L. Schmidt, Sensors Actuators B, 1 (1990) 537.
13 W. Schuhmann, Sensors Actuators B, 4 (1991) 41.
14 M. Hämmerle, W. Schuhmann and H.L. Schmidt, Sensors Actuators B, 6 (1992) 106.
15 P.D. Hale, L.J. Boguslavsky, T. Inagaki, H.J. Karan, H.S. Lee, T.A. Skotheim and Y. Okamoto, Anal. Chem., 63 (1991) 677.
16 P.D. Hale, T. Inagaki, H.J. Karan, Y. Okamoto and T.A. Skotheim, J. Am. Chem. Soc., 111 (1989) 3482.
17 Y. Degany and A. Heller, J. Am. Chem. Soc., 110 (1988) 2615.
18 B.A. Gregg and A. Heller, Anal. Chem., 62 (1990) 258.
19 M.V. Pishko, A.C. Michael and A. Heller, Anal. Chem., 63 (1991) 2268.
20 A. Heller, J. Phys. Chem., 96 (1992) 3579.
21 R.J. Forster and J.G. Vos, Macromolecules, 23 (1990) 4372.
22 C. Hua, K.A. Sagar, K. McLaughlin, M. Jorge, M. Meaney and M.R. Smyth, Analyst, 116 (1991) 1117.
23 J.M. Slater and E.J. Watt, Anal. Proc., 26 (1989) 397.
24 Y. Ikariyama and W.R. Heineman, Anal. Chem., 58 (1986) 1803.
25 Y. Ikariyama, C. Galiatsatos and W.R. Heineman, Sensors Actuators, 12 (1986) 455.
26 Y. Degany and A. Heller, J. Am. Chem. Soc., 111 (1989) 2357.
27 M.D. Imisides, R. John, P.J. Riley and G.G. Wallace, Electroanalysis, 3 (1991) 879.
28 R.J. Forster and J.G. Vos, Electrochim. Acta, 37 (1992) 159.
29 R. Maidan and A. Heller, J. Am. Chem. Soc., 113 (1992) 9003.

Analytica Chimica Acta, 278 (1993) 17–23
Elsevier Science Publishers B.V., Amsterdam

Flow-injection analysis of glucose at an amperometric glucose sensor based on electrochemical codeposition of palladium and glucose oxidase on a glassy carbon electrode

Qijin Chi and Shaojun Dong

Laboratory of Electroanalytical Chemistry, Changchun Institute of Applied Chemistry, Chinese Academy of Science, Changchun, Jilin 130022 (China)

(Received 29th September 1992; revised manuscript received 7th December 1992)

Abstract

A glassy carbon electrode (GCE) modified with palladium provides excellent electrocatalytic oxidation of hydrogen peroxide. When the electrolyte contains palladium chloride and glucose oxidase, the GCE can be modified by electrochemical codeposition at a given potential. The resulting modified surface was coated with a thin film of Nafion to form a glucose sensor. Such a glucose sensor was successfully used in the flow-injection analysis of glucose with high stability and anti-poisoning ability. It gave a detection limit of 1×10^{-7} M injected glucose, with a linear concentration range of 0.001–8 mM. There is no obvious interference from substances such as ascorbate and saccharides.

Keywords: Amperometry; Biosensors; Flow injection; Enzymatic methods; Enzyme electrodes; Glucose

Since the development of the first glucose sensor designed by Clark and Lyons [1] and fabricated by Updike and Hicks [2], there has been considerable interest in amperometric enzyme electrodes, particularly for the monitoring of glucose [3–8]. This widespread attention arises from the need for and importance of such a sensor in clinical [9] and industrial [10] fields and from commercial aspects. Glucose oxidase (GOD), being a flavoprotein, is responsible for the biocatalytic oxidation of glucose in the presence of dioxygen. The overall enzymatic reaction may be described as follows:

$$\text{glucose} + \text{GOD(FAD)} \rightarrow \text{glucose acid} + \text{GOD(FADH}_2\text{)} \quad (1)$$

$$\text{GOD(FADH}_2\text{)} + \text{O}_2 \rightarrow \text{GOD(FAD)} + \text{H}_2\text{O}_2 \quad (2)$$

where FAD is flavine adenine dinucleotide. Hence the level of glucose may be determined by monitoring either the consumption of oxygen or the formation of hydrogen peroxide. In the latter, if the generated hydrogen peroxide is directly detected at a bare electrode, a large overpoten-

Correspondence to: Shaojun Dong, Laboratory of Electroanalytical Chemistry, Changchun Institute of Applied Chemistry, Chinese Academy of Science, Changchun, Jilin 130022 (China).

tial for the oxidation of hydrogen peroxide will be required. Chemically modified electrodes (CMEs) provide an effective means for the electrocatalytic oxidation of hdyrogen peroxide. The electrocatalytic ability of rhodium and platinum black particles deposited on glassy carbon electrode (GCE) surfaces for the oxidation of peroxide has been documented [11–13]; moreover, these CMEs have been applied to the fabrication of glucose sensors [7,14]. In addition, Gorton and co-workers [15–17] showed that effective electrocatalysis for the oxidation of hydrogen peroxide can be achieved by sputtering a mixture of palladium and gold on carbon electrodes, and the resulting CMEs were used in the amperometric determination of hydrogen peroxide and as the substrate of glucose sensors.

In the glucose sensor devices, GOD is usually immobilized by covalent cross-linking with glutaraldehyde and bovine serum albumin on the electrode surface [18,19]. Recently, many new methods of enzyme immobilization have been developed, including the use of silicon dioxide [20] and the entrapment of GOD within electropolymerized films [21–26]. However, few reports of the codeposition of metal particles and GOD on a substrate have appeared [27]. This paper describes a simple fabrication of a glucose sensor based on the electrochemical codeposition of palladium particles and GOD on a GCE surface. This simple approach produces a highly active surface area of the electrode and shows powerful electrocatalytic activity for the detection of the hydrogen peroxide liberated from enzymatic reactions. A very sensitive response to glucose and a large current output are obtained. When a thin film of Nafion is coated on the outermost surface of the GOD electrode, the resulting glucose sensor is suitable for the determination of glucose in a flow system.

EXPERIMENTAL

Materials and apparatus

Glucose oxidase (*Aspergillus niger*, 35300 U g^{-1}, EC 1.1.3.4) was obtained from Sigma. β-D-(+)-Glucose, bovine serum albumin, lactose, maltose, sucrose and fructose were purchased from the Shanghai Institute of Biochemistry, Chinese Academy of Science. A 5% (w/w) Nafion 117 solution (Aldrich) in lower aliphatic alcohols–water (90 + 10) was diluted to 1% (w/w) with ethanol–water (90 + 10). Other reagents used were of analytical-reagent grade. All solutions were prepared with doubly distilled, deionized water. A stock solution of β-D-glucose was allowed to mutarotate at room temperature for 24 h before use. The exact concentration of hydrogen peroxide was determined by titration against standard potassium permanganate solution.

A three-electrode system was employed with a saturated calomel electrode (SCE) as reference electrode, a platinum wire as auxiliary electrode and a glassy carbon rod (3 mm diameter, bare and modified) as working electrode. Electrochemical experiments were conducted on a PAR Model 370 electrochemistry system with a Gould Series-60000 *X–Y* recorder (Shenyang, China). Flow-injection experiments were performed with a Model 510 pump and a U6K injector (Waters) and a BAS TL-5A thin-layer cell (Bioanalytical Systems). The potentials were monitored with a laboratory-made bipotentiostat. PTFE mixing tubing between the injector and the detection cell was 30 cm × 0.5 mm i.d. The carrier solution was 0.1 M phosphate buffer (pH 7.2) delivered at a given flow-rate. All experiments were carried out at room temperature.

The surfaces of the working electrodes, including the modified films, were examined by scanning electron microscopy (SEM) with a Model JXA-840 instrument (JEOL, Japan), operated at a 5 kV accelerating voltage.

Preparation of palladium–GOD modified GCE

Prior to use, the GCE was polished to a mirror finish with a polishing cloth impregnated with a 1.0-μm alumina powder suspension, followed by ultrasonication in water. In a stirred phosphate buffer solution (pH 5.0) containing 350 U ml^{-1} glucose oxidase and 0.5 mM palladium chloride, the enzyme electrode (GOD–Pd/GCE) was fabricated by potentiostatic codeposition at a potential of −0.9 V for 15 min. A 1-μl volume of 1%

Nafion solution was coated on the surface of the GOD–Pd/GCE to form a glucose sensor. Between experiments, the glucose sensor was immersed in 0.1 M phosphate buffer (pH 7.2) at 4°C. A palladium-coated GCE (Pd/GCE) was prepared in a similar fashion, but in the absence of GOD.

A mixture of GOD (2.0 mg) and bovine serum albumin (3.0 mg) was dissolved in 0.2 ml of 0.1 M phosphate buffer (pH 7.2), and then 5 μl of 25% glutaraldehyde solution were added with vigorous stirring. A yellowish transparent solution containing GOD and cross-linking agent was obtained. The GOD was immobilized by dip coating a small drop (2 μl) of the yellowish transparent solution on the surface of the bare GCE. This enzyme electrode (GOD/GCE) was used for comparison with the new glucose sensor (GOD–Pd/GCE).

RESULTS AND DISCUSSION

Features of the electrode surfaces

To obtain further insight into the structural features of the palladium- and the GOD-modified films, the surfaces of the electrodes were characterized by SEM at 5000 × magnification. These examinations were performed at three different stages of the modification procedure: after polishing with 1.0-μm alumina and ultrasonication in water; after depositing palladium particles; and after immobilization in water; after depositing palladium particles; and after immobilization of GOD by codeposition of palladium particles and GOD, as shown in Fig. 1. From Fig. 1(1), it is clear that the black spots represent the clean carbon surface and the lighter stripes come from the polishing with alumina, and such a surface is beneficial for depositing palladium particles and GOD on it. After deposition of palladium particles, a very porous structure [Fig. 1(2)] consisting of aggregates of fine palladium particles is observed, and a huge increase in the microscopic area of this surface is obtained. The structural differences between the Pd- and GOD–Pd-coated electrodes indicate that GOD is immobilized on the electrode surface. Because of aggregates of palladium particles forming many open "micropockets", GOD is strongly adsorbed on the three-dimensional palladium matrix [Fig. 1(3)]. Further, the large GOD molecules cover and connect the palladium aggregates.

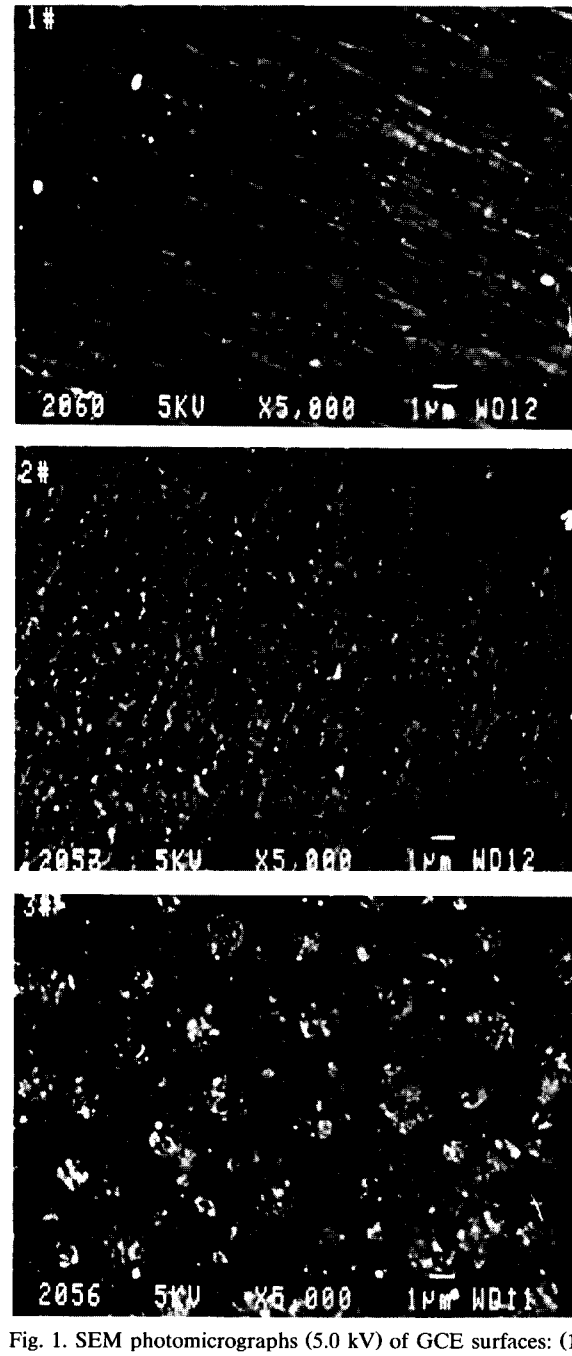

Fig. 1. SEM photomicrographs (5.0 kV) of GCE surfaces: (1) polished; (2) palladium-coated; (3) Pd–GOD-coated.

Electrocatalytic oxidation of hydrogen peroxide

Preliminary experiments were undertaken with an enzyme-free palladium-deposited GCE. Cyclic voltammetry was employed to examine whether such a modified electrode possesses electrocatalytic activity toward the oxidation of hydrogen peroxide. Typical cyclic voltammograms obtained for hydrogen peroxide at the GCE and Pd/GCE are shown in Fig. 2A and B, respectively. At the bare GCE, oxidation of hydrogen peroxide is observed only above +0.7 V with a small current. In contrast, the Pd/GCE exhibits an anodic response to hydrogen peroxide starting at + 0.20 V, reaching maximum value at +0.7 V. The palladium deposition results in a substantial (ca. 500 mV) decrease in the overvoltage, and also a large increase (over 1000-fold) in the oxidation current. When GOD is present on the electrode surface, no influence is observed on the electrocatalytic oxidation of hydrogen peroxide, but the anodic peak shifts positively ca. 50 mV (Fig. 2C), which is due to the slight increase in resistance of the GOD film.

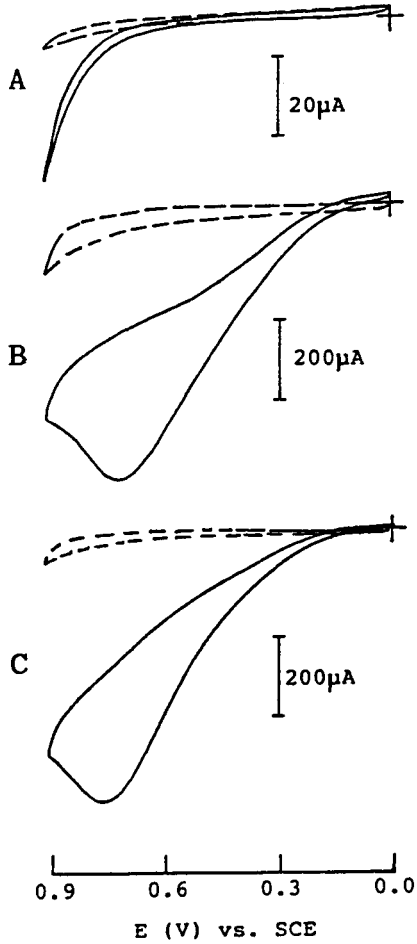

Fig. 2. Cyclic voltammograms for 2.5×10^{-2} M hydrogen peroxide at the (A) bare GCE, (B) Pd/GCE and (C) GOD–Pd/GCE. The dashed lines indicate the response of the blank solution. Scan rate, 50 mV s^{-1}; electrolyte, 0.1 M phosphate buffer (pH 7.2).

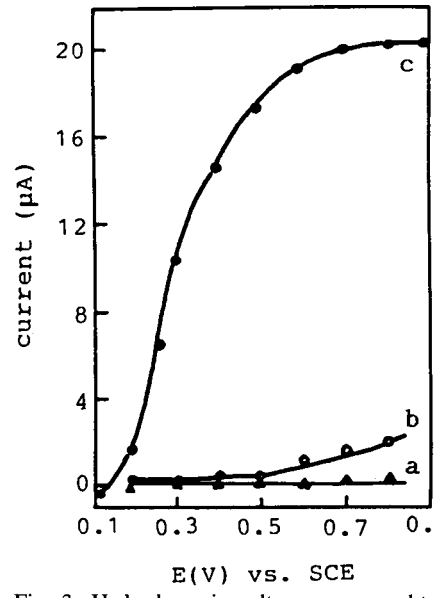

Fig. 3. Hydrodynamic voltammograms obtained at the (a) bare, (b) GOD-modified and (c) GOD–Pd-deposited GCEs for 2.0 mM glucose.

Response of GOD–Pd / GCE to glucose

Figure 3 shows the dependence of the response to glucose on the applied potential of the (a) GCE, (b) GOD/GCE and (c) GOD–Pd/GCE. As expected, no response is observed at the bare GCE over the entire range examined and a small current is obtained at the GOD/GCE only above +0.65 V. However, at the GOD–Pd/GCE the response to glucose starts at +0.20 V and reaches a maximum value at potentials higher than +0.70 V. Such a potential-dependent profile, which is in agreement with the cyclic voltammetric results in Fig. 2, supports further

the excellent catalytic ability of the palladium-coated surface towards hydrogen peroxide. In order to minimize the interference from relevant electroactive species, an operating potential of +0.3 V was selected.

Figure 4 shows the (A) chronoamperometric and (B) amperometric response (at +0.3 V) of the GOD–Pd/GCE to successive concentration increments of glucose. The GOD–Pd/GCE rapidly responds to these millimolar changes in substrate concentration and reaches a steady state within a few seconds. The response time and the detection limit under amperometric conditions are less than 5 s and 5×10^{-5} M, respectively. The resulting calibration graphs are shown in Fig. 4C; the response current increases linearly with increasing substrate concentration in the range 0.1–2.5 mM for both amperometric and chrono-amperometric conditions.

Flow-injection analysis (FIA) of hydrogen peroxide and glucose

It was of interest to determine whether the catalytic response at the GOD–Pd/GCE to glucose can be used in a flow-injection analysis system. Initial efforts to use the GOD–Pd/GCE failed, mainly owing to GOD gradually leaving the surface of the modified electrode in a flow system. However, when a thin film of Nafion was coated on the outermost surface of the GOD–Pd/GCE to form a Nafion–GOD–Pd/GCE, the loss of GOD from the electrode surface was effectively prevented by the Nafion film, and the resulting sensor can be successfully applied to determine glucose by FIA. Figure 5 shows the influence of the responses to glucose on (A) the solution pH and (B) the flow-rate. The current response reaches a maximum value in the pH range 7.2–7.5 and decreases with increasing flow-rate up to 0.7 ml min^{-1}. Therefore, a solution pH of 7.2 and the a flow-rate of 0.7 ml min^{-1} were chosen as optimum operating conditions.

The amperomertic determination of hydrogen peroxide was performed using FIA, and a linear concentration range of 1×10^{-7}–9×10^{-4} M with a detection limit of 5×10^{-8} M was obtained. Similarly, Fig. 6 shows the FIA responses to step increases in the concentration of glucose, with a linear range of 1×10^{-6}–8×10^{-3} M and a detection limit of 1×10^{-7} M. Obviously, by using

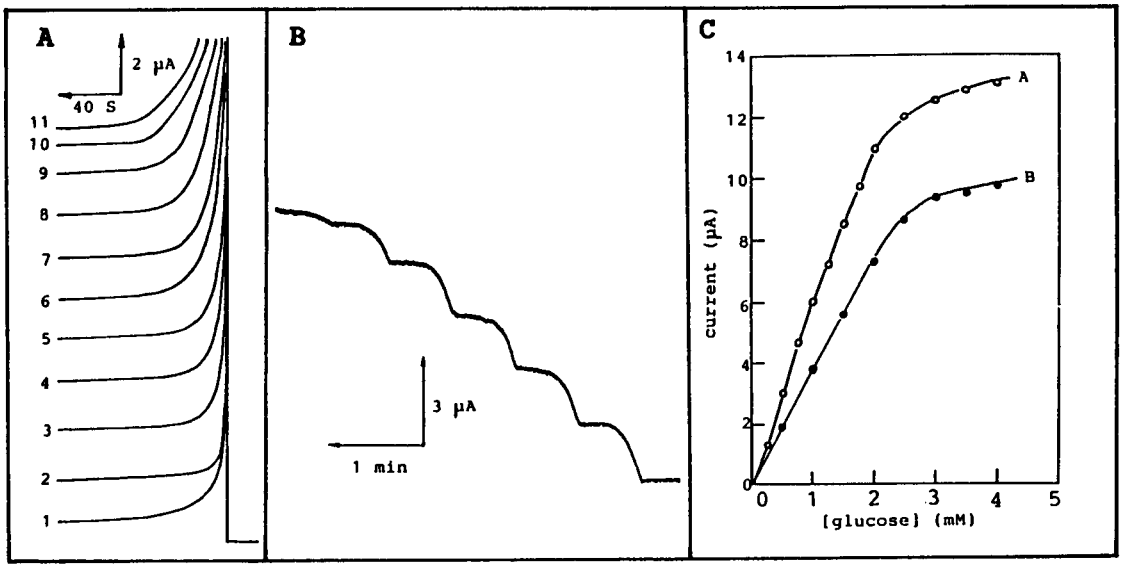

Fig. 4. Current–time curves recorded with step increases in the concentration of glucose: (A) chronoamperometric response for concentrations of (1) 0, (2) 0.25, (3) 0.50, (4) 0.75, (5) 1.00, (6) 1.25, (7) 1.50, (8) 2.0, (9) 2.5, (10) 3.0 and (11) 4.0 mM; (B) amperometric response for increments of 0.25 mM glucose. Operating potential, +0.3 V. (c) Resulting calibration graphs.

FIA the glucose sensor can obtain a lower detection limit and a wider linear concentration range in the response to glucose.

The reproducibility of the response to glucose at the Nafion–GOD–Pd/GCE was examined by ten successive injections of 10 μl of 8 mm glucose solution; the relative standard deviation was only 0.85%.

When the glucose sensor is stored in 0.1 M phosphate buffer (pH 7.2) at 4°C, the long-term stability was examined by measuring the response to 8 mM glucose every 5 days. Only 5% decrease in the initial response was observed after 25 days.

Several saccharides, including lactose, maltose, sucrose and fructose, were examined at the glucose sensor by FIA, and no response was observed. As is known, the determination of glucose in biological systems, such as blood [28] and brain fluid [29], is a principal area of application for the glucose sensor. A serious problem associated with such analyses is the interferences from ascorbic acid [30] and uric acid [31], which may oxidize directly on the electrode surface. As the concentrations of these two substances change continuously in biological tissues and fluids [32], it is necessary to reduce or eliminate these effects in the development of a reliable glucose sensor. In the present experiments, it was found that the presence of ascorbic acid or uric acid does not cause any observable interference to the response to glucose at +0.3 V. Nafion is a typical cation-exchange polymer, which may play an important role in the exclusive effect from anions, such as ascorbic and uric acid.

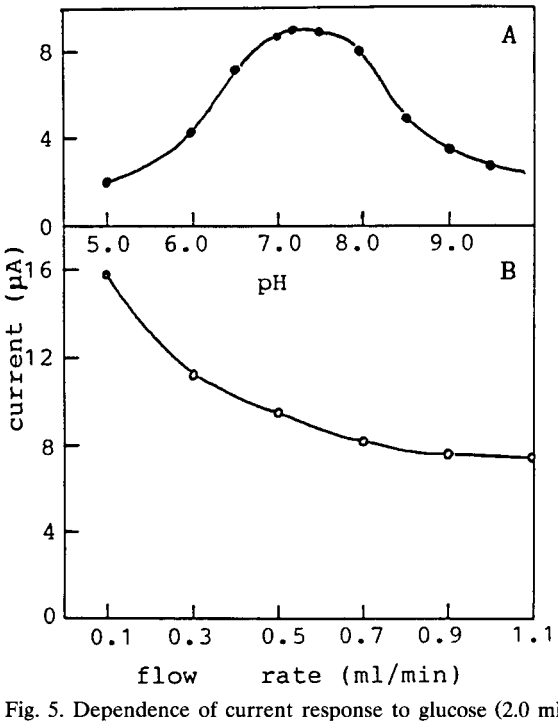

Fig. 5. Dependence of current response to glucose (2.0 mM) on (A) the solution pH and (B) the flow-rate. Operating potential, +0.3 V; flow-rate, 0.7 ml min^{-1} in (A).

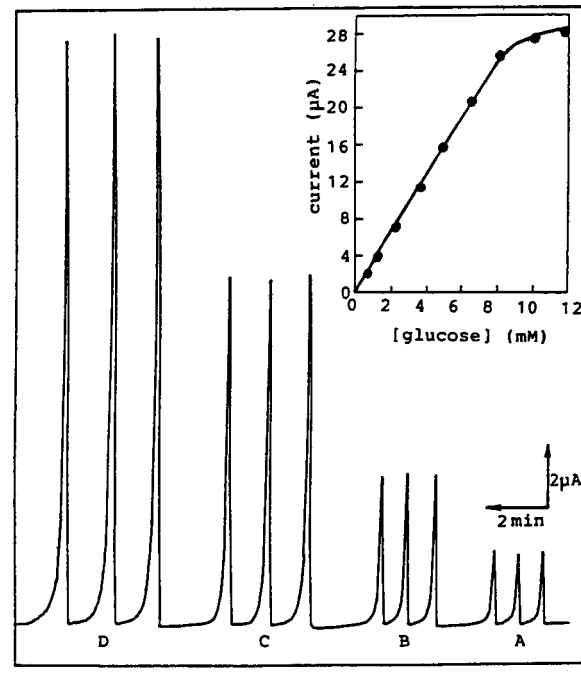

Fig. 6. FIA responses to glucose obtained at various concentrations: (A) 1.0; (B) 2.0; (C) 4.0; (D) 6.0 mM. Operating potential, +0.3 V; flow-rate, 0.7 ml min^{-1}; mobile phase, 0.1 M phosphate buffer (pH 7.2). Inset: resulting calibration graph.

Conclusion

A glucose sensor has been fabricated by electrochemical codeposition of palladium particles together with GOD on a GCE surface. Such a simple approach gives a highly active surface area and yields a powerful electrocatalytic surface for the detection of hydrogen peroxide. A very rapid response and a large current output to glucose

are obtained. When a thin film of Nafion is coated on the outermost surface of the GOD–Pd/GCE, the resulting sensor can be used for the detection of glucose by FIA. A linear response was obtained over the range 0.001–8 mM glucose with a detection limit of 1×10^{-7} M. The glucose sensor retained its activity with only slight variations over a test period of 25 days. Interferences from ascorbic or uric acid can be neglected. Apparently, the Nafion film effectively prevents the transport of ascorbic or uric acid to the electrode surface.

The method for the fabrication of this sensor is expected to be used in the immobilization of other oxidases, such as amino acid oxidase and xanthine oxidase.

The support of the National Science Foundation of China is gratefully acknowledged.

REFERENCES

1 L.C. Clark and C. Lyons, Ann. N.Y. Acad. Sci., 102 (1962) 29.
2 S.J. Updike and G.P. Hicks, Nature, 214 (1967) 986.
3 K. Narasimhan and L.B. Wingard, Jr., Anal. Chem., 58 (1986) 2984.
4 T. Yao, Anal. Chim. Acta, 148 (1983) 27.
5 S. Dong and T. Kuwana, Electroanalysis, 3 (1991) 485.
6 N.C. Foulds and C.R. Lowe, Anal. Chem., 60 (1988) 2473.
7 H. Gunasingham and C.B. Tan, Electroanalysis, 1 (1989) 223.
8 P.C. Pandey, J. Chem. Soc., Faraday Trans. 1, 84 (1988) 2259.
9 M.E. Meyerhoff, Clin. Chem., 36 (1990) 36.
10 M. Senda, Ann. N.Y. Acad. Sci., 613 (1990) 79.
11 R.A. Simon, T.E. Mallouk, K.A. Daube and M.S. Wrighton, Inorg. Chem., 24 (1985) 3119.
12 D. Cukman and M. Vukovic, J. Electroanal. Chem., 279 (1990) 273.
13 G.H. Heider, S.V. Sasso, K.M. Huang, A.M. Yacynych and H.J. Wieck, Anal. Chem., 62 (1990) 1106.
14 J. Wang, R. Li and M.S. Lin., Electroanalysis, 1 (1989) 151.
15 L. Gorton, Anal. Chim. Acta, 178 (1985) 247.
16 L. Gorton and T. Svensson, J. Mol. Catal., 38 (1986) 49.
17 L. Gorton and G. Jonsson, J. Mol. Catal., 38 (1986) 157.
18 M. Nanijo and G.G. Guilbault, Anal. Chim. Acta, 73 (1974) 367.
19 G. Nagy, L.H. Von Storp and G.G. Guilbault, Anal. Chim. Acta, 66 (1973) 443.
20 K. Yokoyama, E. Tamiya and I. Karube, Electroanalysis, 3 (1991) 469.
21 M. Umana and J. Waller, Anal. Chem., 58 (1986) 2979.
22 H. Shinohara, T. Chiba and M. Aizawa, Sensors Actuators, 13 (1987) 79.
23 P. Janda and J. Weber J. Electroanal. Chem., 300 (1991) 119.
24 N.C. Foulds and C.R. Lowe, J. Chem. Soc., Faraday Trans. 1, 82 (1986) 1259.
25 P.N. Bartlett and R.G. Whitaker, J. Electroanal. Chem., 224 (1987) 27.
26 P.N. Bartlett and R.G. Whitaker, J. Electroanal. Chem., 224 (1987) 37.
27 Y. Ikariyama, S. Yamauchi, T. Yukiashi and H. Ushiodo, J. Electrochem. Soc., 136 (1989) 702.
28 D. Ross, L. Heinemann and E.A. Chantelau, Diabetes Res. Clin. Pract., 10 (1990) 281.
29 M.G. Boutelle, C. Stanford, M. Fillenz, M.J. Albery and P.N. Bartlett, Neurosci. Lett., 72 (1986) 283.
30 R.A. Grunewald, R.D. O'Neill, M. Fillenz and M.J. Albery, Neurochem. Int., 5 (1983) 773.
31 R. Cespuglio, N. Sarda, A. Gharib, H. Faradji and N. Chastrette, Exp. Brain Res., 64 (1986) 589.
32 R.D. O'Neill, Brain Res., 507 (1990) 267.

Analytica Chimica Acta, 278 (1993) 25–33
Elsevier Science Publishers B.V., Amsterdam

Simultaneous use of dehydrogenases and hexacyanoferrate(III) ion in electrochemical biosensors for L-lactate, D-lactate and L-glutamate ions

Marielle Montagné, Hélène Durliat and Maurice Comtat

Laboratoire de Génie Chimique et Electrochimie (URA CNRS 192), Université Paul Sabatier, 118 Route de Narbonne, 31062 Toulouse Cédex (France)

(Received 7th September 1992; revised manuscript received 4th January 1993)

Abstract

The L-lactate, D-lactate and L-glutamate selective amperometric electrochemical biosensors presented were designed so that the last electron-transfer step is hexacyanoferrate(II) oxidation on a platinum electrode. A single enzyme sensor is described for L-lactate assay, where a lactate dehydrogenase extracted from yeast, immobilized on a membrane, will accept potassium hexacyanoferrate(III) as an electronic relay. It is possible to determine L- and D-lactate using bienzymatic sensors with NAD^+-dependent dehydrogenases immobilized or in solution. In such a case, a second enzymatic reaction [a diaphorase-catalysed NADH oxidation by hexacyanoferrate(III)] enabled the detection limit to be lowered. For the L-glutamate-specific sensor, the two preceding enzymes were associated with a third one that catalyses a substrate product transformation, making it possible to exploit the enzyme amplification phenomenon. In each instance, the required presence of hexacyanoferrate(III) in the samples to be assayed makes it possible to suggest a simple apparatus with two slightly polarized electrodes. The advantages of enzyme fixation in increasing sensor stability and lowering the detection limit are also highlighted.

Keywords: Amperometry; Biosensors; Dehydrogenases; Enzyme reactor; Glutamate; Lactate

There are a great number of electrochemical biosensors with either potentiometric or amperometric detection that use an enzyme as a catalyst [1,2]. They are applied in various fields of analysis such as in chemistry, clinical biology, the food industry and the environment. Urea electrodes are typical examples of potentiometric detection sensors whereas glucose electrodes are examples of amperometric detection. The performance of such sensors is characterized by response time, (linear) concentration range, useful lifetime, the number of assays they allow, sensitivity and accuracy.

It is clear that amperometric sensors are the most accurate because of the proportionality between intensity and concentration. They fall into two main groups according to whether the enzyme is an oxidase, leading to the detection of the oxygen consumed or of the hydrogen peroxide produced, or a dehydrogenase. The second type of enzyme implies detection of an enzymatic cofactor or of an oxidoreduction mediator that catalyses the electron transfer between the electrode and the cofactor [3,4].

In most of these sensors the enzyme is immobilized on a membrane in order to increase both the concentration range and electrode stability

Correspondence to: M. Comtat, Laboratoire de Génie Chimique et Electrochimie (URA CNRS 192), Université Paul Sabatier, 118 Route de Narbonne, 31062 Toulouse Cédex (France).

[5,6]. Over the last few years, bienzyme sensors have been developed with various objectives: modulation of the enzyme activity by using another enzyme to break down an inhibitor of the first enzyme, e.g., catalase is used with glucose oxidase, and hydrogen peroxide formed in the glucose oxidation reaction is an inhibitor of glucose oxidase and catalase destroys excess of this compound [7,8]; extension of the range of accessible substrates, where a first enzyme catalyses a reaction producing a second substrate that is easily detected by a standard biosensor, e.g. bienzyme electrodes have appeared for the detection of lecithin, choline, acetylcholine [9], glucosinolates [10] and aspartate [11]; and improving the specificity, accuracy and selectivity of an oxidoreductase electrode by making use of the enzyme amplification phenomenon, where the product of the first enzyme reaction becomes the substrate of the second enzyme reaction and vice versa [12–14].

L-Lactate assay is important in various clinical and medicine-related sectors such as sports medicine, emergency states and cardiovascular surgery. Some sensors have been proposed previously, using lactate dehydrogenase from muscle [15,16], lactate dehydrogenase extracted from baker's yeast [17,18] or lactate oxidase [19–23].

D-Lactate ion detection has not been the subject of intense research despite the fact that this ion plays an important role in various fermentation processes and in the control of food production processes. This can be explained by the fact that commercially available enzymes are not sufficiently pure. However, two sensors have been described: one is a continuous-flow reactor associated with amperometric detection that uses *Lactobacillus leichmannii* D-lactate dehydrogenase and diaphorase to lower the electrode potential [24], and the other is an electrode that simultaneously uses lactate dehydrogenase and NADH oxidase [25].

L-Glutamate plays a role in many neurological processes such as in schizophrenia, depression, amnaesia and morphine-induced muscular rigidity [26]. The food processing industry uses it as a taste enhancer. The proposed sensors used L-glutamate decarboxylase [27] and L-glutamate oxidase with glutamate transaminase or with pyruvate glutamate transaminase [28,29].

Finally, the need for a high level of accuracy is responsible for the appearance of a new type of sensor that operates by exploiting signals linked to the glutamate receptor ionic channels, reconstituted in a lipidic bilayer [30,31].

This paper presents amperometric electrodes for the detection of L- and D-lactate and L-glutamate using dehydrogenases. A second enzyme is used in order to improve the selectivity by lowering the potential at which the detection is done. The use of a third enzyme makes it possible to increase the sensitivity by exploiting the enzyme amplification phenomenon.

In all instances the set-up of the assay is simple with two slightly polarized electrodes obtained through the use of the hexacyanoferrate(III) ion, which is the final electron relay in the catalytic process. The hexacyanoferrate(II) formed is oxidized by constant-potential electrolysis performed on a platinum electrode. As the hexacyanoferrate(III) can be added to the sample to be assayed in a great excess over the concentration of hexacyanoferrate(II) formed in enzymatic reactions, the cathode potential is virtually independent of the intensity of the current within the circuit. This electrode can be used as the reference electrode and there is no need for a three-electrode system. In the same way, a stable power supply can be substituted for the potentiostat traditionally used to regulate the potential of the enzymatic electrode. These principles have already proved their value in with L-lactate [18,32] and L-carnitine [33] selective electrodes.

A further objective was to exploit enzyme fixation on polymeric supports in order to lower the electrode detection limit and increase the operational stability.

GENERAL PRINCIPLES

Figure 1 shows the various types of sensor studied. There are two categories of sensors: those with the enzymes in solution in a reaction chamber whose volume is defined by the flat electrode surface and a semi-permeable membrane, and

Electrode	Reaction chamber	Membrane	Analysed solution
Potential Nature of the material	Thickness Enzyme concentration	Thickness Permeability	Concentration of the different species Stirring

a

Electrode	Electrolyte film	Membrane	Analysed solution
Potential Nature of the material	Thickness	Position and Concentration of the enzymes	Concentration of the different species Stirring

b

Fig. 1. Scheme of the two types of sensors considered. The more important parameters are indicated. (a) The enzyme(s) is (are) in solution; (b) the enzyme(s) is (are) immobilized on a preactivated membrane.

those with the enzymes immobilized on a membrane in contact with the electrode. In all instances the membrane is held in place with an O-ring. Figure 1 also presents the parameters that condition sensor performance levels.

Various types of reaction are involved. With a single enzyme electrode, the substrate S reacts with the hexacyanoferrate(III):

$$S + Fe(CN)_6^{3-} \rightarrow P + Fe(CN)_6^{4-}$$

Such is the case for L-lactate with baker's yeast L-lactate dehydrogenase. With bienzyme sensors, the dehydrogenase catalyses the following reaction:

$$S + NAD^+ \rightarrow P + NADH + X$$

NADH is electroactive on a platinum electrode at around 0.75 V vs. SCE. In order to decrease the considerable overvoltage corresponding to the direct detection of NADH through anodic oxidation, a second reaction is introduced, the oxidation of NADH catalysed by a diaphorase:

$$NADH + 2Fe(CN)_6^{3-} \rightarrow$$

$$NAD^+ + 2Fe(CN)_6^{4-} + H^+ \quad (1)$$

These three examples concern the L- and D-lactate and L-glutamate ion assay.

As long as there is an enzyme capable of catalysing a substrate regeneration reaction from the species X:

$$X + A \rightarrow S + B$$

the presence of a third enzyme within the sensor makes it possible to use the enzymatic amplification phenomenon. This was the principle used for L-glutamate. In each instance electrochemical detection concerns the $Fe(CN)_6^{4-}$ ion on a platinum electrode that is used as a transducer:

$$Fe(CN)_6^{4-} \rightarrow Fe(CN)_6^{3-} + e^-$$

On the second electrode occurs the reaction

$$Fe(CN)_6^{3-} + e^- \rightarrow Fe(CN)_6^{4-}$$

from hexacyanoferrate(III) added in excess to the solution to be assayed. The sensor response curve shows the electrolysis current variation as a function of time, with 80 mV imposed between the two electrodes.

EXPERIMENTAL

Apparatus

Spectrophotometric measurements were made on a Hewlett-Packard Model 8451 spectrophotometer with a thermoregulated cell. A Tacussel PRT 20 × 2X potentiostat was used as a power supply to impose 80 mV between the enzyme electrode and the auxiliary electrode. A Sefram Luxytrace recorder was used to record the response curves.

Chemicals

The pure salts used to prepare solutions were obtained from Merck. The following solutions were used: pH 7.0, a mixture of monopotassium and disodium phosphate, 0.1 M phosphate; pH 8.3, 0.1 M 3-[(1,1-dimethyl-2-hydroxyethyl)amino]-2-hydroxypropanesulphonic acid (AMPSO) acidified with HCl; and pH 9.1, 0.1 M AMPSO acidified with HCl or a mixture of mono- and disodium carbonate with a carbonate concentration of 0.1 M.

The biochemical reagents and the enzymes were obtained from Sigma, with the exception of the L-lactate dehydrogenase extracted from baker's yeast, of the *Hansenula anomala* strain, which was supplied by Sétric Génie Industriel (Toulouse). The diaphorase EC 1.8.1.4 was extracted from *Clostridium kluyveri*, the L-lactate dehydrogenase (L-LDH) EC 1.1.1.27 was extracted from rabbit muscle, the D-lactate dehydrogenase (D-LDH) EC 1.1.1.28 was extracted from *Leuconostoc mesenteroides*, the L-glutamate dehydrogenase (L-GDH) EC 1.4.1.3 was extracted from beef liver and the glutamate oxaloacetic transaminase EC 2.6.1.1 was extracted from pig heart.

Enzymatic reactions

The specific L-lactate single enzyme electrode implemented the following reaction:

$$CH_3CHOHCOO^- + 2Fe(CN)_6^{3-} \rightarrow CH_3COCOO^- + 2Fe(CN)_6^{4-} + 2H^+ \quad (2)$$

The oxidation reactions of lactate and glutamate by NAD^+ were as follows:

$$CH_3CHOHCOO^- + NAD^+ \rightarrow CH_3COCOO^- + NADH + H^+ \quad (3)$$

$$^-OOCCH(NH_2)CH_2CH_2COO^- + NAD^+ + H_2O \rightarrow {}^-OOCCOCH_2CH_2COO^- + NADH + NH_4^+ \quad (4)$$

In order to benefit from the amplification phenomenon, in the case of this last substrate, it was necessary to involve a third reaction catalysed by an oxaloacetate transaminase glutamate reaction:

$$^-OOCCOCH_2CH_2COO^- + {}^-OOCCH_2CH(NH_2)COO^- \rightarrow {}^-OOCCH(NH_2)CH_2CH_2COO^- + {}^-OOCCOCH_2COO^- \quad (5)$$

Measurement of enzymatic activity

Enzymatic activity, deduced from the initial rate of the reaction catalysed by the enzyme, was expressed by the variation in the number of micromoles of substrate transformed per minute and per cm^3 of enzyme (U cm^{-3}). It was measured under the various sensor operating conditions.

For diaphorase, the solution, of either pH 8.3 or 9.1, contained 1.2 mM hexacyanoferrate(III) and 0.2 mM NADH. The reaction involved was reaction 1 and the disappearance of the hexacyanoferrate(III) was followed by measuring the decrease in the absorbance at 420 nm with time.

For L-lactate dehydrogenase from yeast, the solution of pH 7.0 contained 0.2 mM substrate and 1.5 mM hexacyanoferrate(III). The lactate oxidation reaction was reaction 2. The reaction progress was followed by measuring the absorbance at 420 nm.

For NAD^+-dependent D- and L-lactate dehydrogenases, the solution of pH 9.1 contained 0.2 mM substrate and 1 mM NAD^+. The lactate oxidation reaction, catalysed by the enzyme, was reaction 3. The appearance of NADH was followed by measuring the increase in absorbance at 340 nm.

For L-glutamate dehydrogenase, the solution of pH 8.3 contained 0.2 mM L-glutamate and 1 mM NAD^+. The substrate oxidizing reaction was reaction 4. The appearance of NADH made it possible to follow the reaction.

Immobilization of the enzymes on the membrane

The preactivated membrane was of the Immunodyne TM type (Pall Industries, ref. BIA065HC5). The immobilization procedure was as follows: 10 μl of enzymatic solution were placed on the membrane for 10 min. Two rinsing procedures were applied with the carbonate solution, the first rinse being performed in the presence of 1 M KCl. With the membrane dipped into a solution with the required compounds, each of the enzymes present on the membrane catalysed the specific reaction described above and it was possible to follow the reaction progress using spectrophotometry. Regular stirring made it possible to assume that there was no concentration gradient in the solution. The amount of enzyme fixed was correlated with the initial rate (v) of the substrate disappearance reaction and this initial rate was measured every 3 h. Between each measurement, the membrane was stored in the phosphate solution. A decrease in the initial rate of the reaction with time together with an increase in enzyme activity in the storage solution indicated the enzyme had dropped off the membrane.

Storage of electrodes and enzymatic solutions

The various solutions were stored at 4°C. The electrodes were used at 25°C and when not required the L- and D-lactate electrodes were stored at 4°C in phosphate buffer (pH 7.0) while the L-glutamate electrodes were stored at 4°C in AMPSO (pH 8.3) when not in use.

Standardization of operating conditions

Assays were performed in 2.5-cm^3 volume solutions with the temperature regulated at 25°C. During an assay, the electrode was successively dipped into a stirred solution containing the reagents 20 mM NAD^+, 20 mM $Fe(CN)_6^{3-}$ and (where reaction 5 was involved) 10 mM L-aspartic acid so that they were present in the reaction chamber after diffusion through the membrane; and a solution, whether stirred or not, containing the reagents, except the NAD^+ cofactor, to which the substrate was added. It was checked that response was identical whether the NAD^+ was in the solution or only present in the reaction chamber. The procedure used makes it possible to limit NAD^+ consumption and this is an advantage given the fact that it is a costly product. Between assays the electrode was rinsed with its storage solution.

RESULTS AND DISCUSSION

Previous work has already made it possible to determine several parameters [17]. The thickness of the reaction chamber for enzymes in solution should be of the order of 30 μm. Similarly, the semi-permeable membrane, which serves as a diffusion barrier for the substrates, is made from Cellophane with a thickness of ca. 40 μm. The measurement temperature is regulated to 25°C. However, this parameter has hardly any influence on the responses of the proposed sensors as the slow step of the global process is the diffusion of the substrate through the membrane, a reaction whose rate is not particularly sensitive to temperature. Enzymatic activity only influences the sensor response when it falls below a given value.

Various parameters were studied. Figure 2 provides an example of response curves obtained with a D-lactate specific bienzymatic sensor, with the solution containing the substrate (a) stirred or (b) not stirred. In the former instance the intensity becomes constant, whereas in the latter it decreases continuously when a diffusion layer forms between the membrane external surface and the solution to be assayed. The intensity considered as the sensor response corresponds to

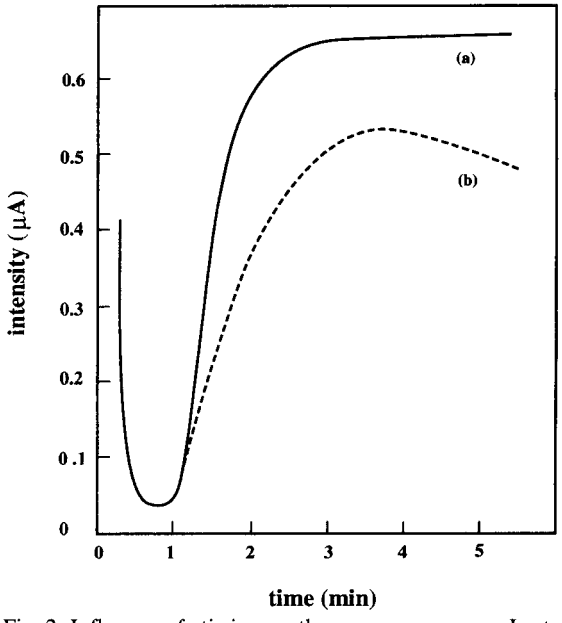

Fig. 2. Influence of stirring on the response curve. D-Lactate dehydrogenase and diaphorase are in solution. D-Lactate, 0.5 mM. (a) Stirred solution; (b) unstirred solution.

the value where there is a plateau or a maximum. Stirring the solution also leads to an increase in the intensity measured and a slight decrease in the response time. All the experiments presented below involved stirring the solution, using a magnetic stirrer with a sufficient bar rotation rate to avoid concentration gradients near the membrane.

Figure 3 shows an example of response curves for an L-lactate-specific bienzymatic sensor. The two enzymes are fixed either (a) on the same side of the membrane or (b) on each of the two sides. For the two sensors proposed here, the optimum layout is co-immobilization on the same side of the membrane which should be opposite to the platinum disc. The layer of enzymes is protected as it is no longer in contact with the solution. The electrolyte thickness between the electrode and the membrane is the lowest possible in order to minimize the cell electric resistance.

The diaphorase activity to dehydrogenase activity ratio is an important parameter. With the enzymes in solution, the response is best with a value of this ratio of ca. 8 for the D-lactate and 12 for the L-glutamate-specific sensor. The watertight connection between the reaction chamber and the analyte solution is not perfect because of the O-ring seal. Further, enzymes slowly become denatured with time. The sensor lifetime is thus longer if the initial activity is high. Commercially available enzymes unfortunately do not always guarantee a high activity level and this limits the sensor performance. The activity levels of the various enzymes used are as follows: D-lactate dehydrogenase, 8 U cm^{-3} and diaphorase 60 U cm^{-3}; L-glutamate dehydrogenase 10 U cm^{-3} and diaphorase 120 U cm^{-3}; and oxaloacetate transaminase glutamate 15 U cm^{-3}.

When the enzymes are immobilized, the amount of enzyme fixed on the membrane varies with the concentrations of enzyme solution used to deposit and the ratio of the amount deposited to the solution concentration varies with the nature of the enzyme molecule. For the sensors envisaged, the best responses were obtained with the following solutions: 350 U cm^{-3} diaphorase and 100 U cm^{-3} L-lactate dehydrogenase; 150 U cm^{-3} diaphorase and 6 U cm^{-3} D-lactate dehy-

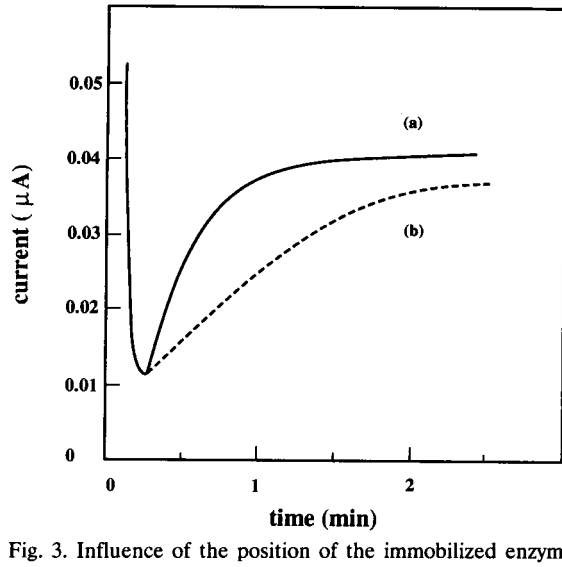

Fig. 3. Influence of the position of the immobilized enzymes on the response curve. L-Lactate, 0.1 mM. L-Lactate dehydrogenase and diaphorase from muscle are (a) on the same side of the membrane near the reaction chamber and (b) each on a different side.

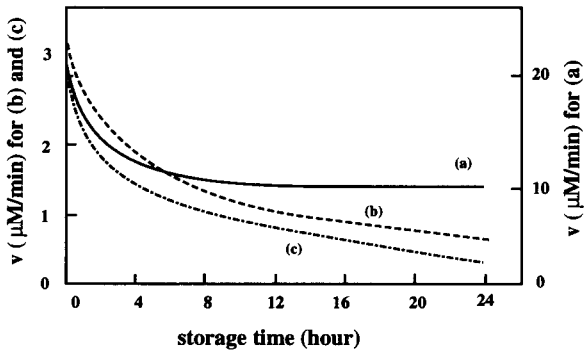

Fig. 4. Variation of the initial rate v (see text) with time. Activity of the deposited enzymatic solution: (a) diaphorase 150 U cm^{-3}; (b) L-lactate dehydrogenase from muscle 100 U cm^{-3}; (c) D-lactate dehydrogenase 6 U cm^{-3}.

drogenase; and 40 U cm^{-3} yeast L-lactate dehydrogenase.

With commercially available enzymes, as they are not pure, there is a considerable drop off linked to the variation of v (defined above) with time (Fig. 4). This is confirmed by the increase in enzyme activity of the solution in which the membrane is stored. However, if very pure, yeast L-lactate dehydrogenase remains fixed on the membrane.

Figure 5 illustrates the amplification phenomenon encountered with the L-glutamate three enzyme-specific sensor.

Table 1 summarizes the essential results obtained with these sensors; some of these results have already been published [17,33].

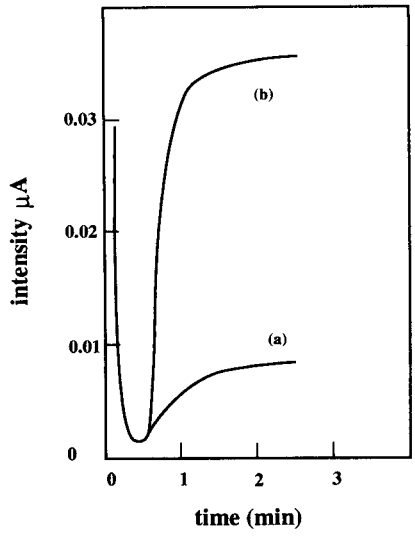

Fig. 5. Amplification response for L-glutamate biosensor. L-Glutamate, 0.02 mM. The enzymes are in solution. (a) L-Glutamate dehydrogenase 10 U cm^{-3} and diaphorase 60 U cm^{-3}; (b) glutamic–oxaloacetic transaminase 15 U cm^{-3} added to the previous solution.

The reproducibility of the results depends on the number of enzymes used either in solution or immobilized on membrane. It is about 2% on the basis of 50 measurements with the use of one enzyme and becomes 4% when two or three enzymes are used. In general, the response times vary between 0.5 and 5 min with the shortest times corresponding to highest enzyme activity levels. However, even the longest times are compatible with the applications planned for the sen-

TABLE 1

Specifications of the biosensors for L-lactate, D-lactate and L-glutamate

Substrate	Enzyme	Mode of enzyme confinement	Linearity range (mM)	Response time (min)	Stability (days)	Initial slope ($\mu A\ l\ mmol^{-1}$)
L-Lactate	Yeast L-LDH	Immobilized	2×10^{-3}–5	0.5	60	1.1
	Yeast L-LDH	In solution [17]	0.1–10	0.5	30	0.8
	Muscle L-LDH + diaphorase	Immobilized	5×10^{-3}–0.15	1	2	0.25
	Muscle L-LDH + diaphorase	In solution [32]	0.2–8	1	30	0.5
D-Lactate	D-LDH + diaphorase	Immobilized	5×10^{-3}–0.15	1	2	0.2
	D-LDH + diaphorase	In solution	2×10^{-2}–6	3	40	0.9
L-Glutamate	L-GDH + diaphorase	In solution	2×10^{-2}–2	5	28	0.3
	L-GDH + diaphorase + transaminase	In solution	5×10^{-3}–0.20	2	21	2

TABLE 2

Evolution of the slopes of the calibration graphs (μA l mmol^{-1}) with time for the different biosensors studied

Time (days)	Substrate					
	L-Lactate		D-Lactate		L-Glutamate	
	Yeast L-LDH (immobilized)	Muscle L-LDH + diaphorase (immobilized)	D-LDH + diaphorase (in solution)	D-LDH + diaphorase (immobilized)	L-GDH + diaphorase (in solution)	L-GDH + diaphorase + transaminase (in solution)
0	1.10	0.24	0.90	0.20	0.3	2
2	1.05	0.02	0.89	0.03	0.28	1.5
4	1.03	0	0.91	0	0.28	1.1
7	1.03	–	0.88	–	0.25	0.55
14	1.04	–	0.86	–	0.20	0.44
21	1.02	–	0.65	–	0.11	0.23
28	1.03	–	0.52	–	0.05	0
42	1.01	–	0.2	–	0	–
49	0.88	–	0	–	–	–

sors described here. Comparison of the results obtained by spectrophotometric enzyme assays and by using the sensors shows a difference of less than 4% on the basis of 50 measurements. The concentration ranges in which there is a linear response are sufficiently extensive (2–3 decades) for routine applications of these sensors. The corresponding linear calibration graphs are characterized by their slope (Table 2) and this provides an indication of the sensor stability. Indeed, as long as the response is independent of enzyme concentration, the slope value is constant. The enzyme concentration decreases with time (owing to denaturation, leaks due to sensor geometry in the case of enzymes in solution and dropping off of fixed enzymes) and when the slope starts to decrease daily calibration becomes necessary. The sensor stability is greater with immobilized enzymes, on condition that the enzyme solution deposited on the membrane is pure, otherwise it is preferable to use a sensor with enzymes in solution. Enzyme fixation makes it possible to lower the sensor detection threshold as opposed to where enzymes are in solution; the same applies where the amplification phenomenon is implicated through the use of a third enzyme.

The electrodes presented have various fields of applications. The L-lactate electrode with one immobilized enzyme will be used in sports medicine where it will replace the commercial sensor. The bienzyme D-lactate sensor has some applications in the field of malate–lactate fermentation. The L-glutamate three-enzyme electrode is being used in order to follow the concentration of the substrate during a cell culture experiment.

This work was supported by a grant from the Ministère de la Recherche et de la Technologie. The authors thank Professor P.R. Coulet of the University of Lyon I (France) for helpful discussions of the problem of enzyme immobilization on membranes.

REFERENCES

1 A.P.F. Turner, I. Karube and G.S. Wilson, Biosensors: Fundamentals and Applications, Oxford University Press, Oxford, 1987.
2 F. Scheller and F. Schubert, Biosensors, Elsevier, New York, 1990.
3 A.E.G. Cass, G. Davis, G.D. Francis, H.A.O. Hill, W.J. Aston, I.J. Higgins, E.V. Plotkin, L.D.L. Scott and A.P.F. Turner, Anal. Chem., 56 (1984) 667.
4 A.E.G. Cass, Biosensors: a Practical Approach, IRL, Oxford, 1990.
5 M. Akhtar, I.J. Higgins and C.R. Lowe (Eds.), Biosensors, Proceedings of a Royal Society Discussion, London, 1987, p. 3.
6 D.R. Thévenot, R. Sternberg, P.R. Coulet, J. Laurent and D.G. Gautheron, Anal. Chem., 51 (1979) 96.

7 R. Rennenberg, F. Scheller, K. Riedel, E. Litschko and M. Richter, Anal. Lett., 16 (1983) 877.
8 D. Pfeiffer, F. Scheller, M. Jänchen, K. Bertermann and H. Weise, Anal. Lett., 13 (1980) 1179.
9 R.M. Morelis and P.R. Coulet, Anal. Chim. Acta, 231 (1990) 27.
10 A. Koshy, H.P. Bennetto, G.M. Delaney, A.J. MacLeod, J.R. Mason, J.L. Stirling and C.F. Thurston, Anal. Lett., 21 (1988) 2177.
11 R.L. Villarta, G. Palleschi, G.J. Lubrano, A.A. Suleiman and G.G. Guilbault, Anal. Chim. Acta, 245 (1991) 63.
12 F. Schubert, F. Scheller and N.G. Krasteva, Electroanalysis, 2 (1990) 347.
13 J.J. Kulys, V.-S.A. Laurinavicius, M.V. Pesliakiene and V.V. Gureviciene, Anal. Chim. Acta, 148 (1983) 13.
14 J.J. Kulys and R.D. Schmid, Biosensors Bioelectron., 6 (1991) 43.
15 W.J. Blaedel and R.A. Jenkins, Anal. Chem., 48 (1976) 1240.
16 F.S. Cheng and G.D. Christian, Clin. Chim. Acta, 51 (1979) 100.
17 H. Durliat and M. Comtat, Anal. Chim. Acta, 85 (1976) 31.
18 H. Durliat, M. Comtat and A. Baudras, Clin. Chem., 22 (1976) 1802.
19 G. Bardeletti, F. Sechaud and P.R. Coulet, Anal. Chim. Acta, 187 (1986) 47.
20 T. Tatsuma and T. Watanabe, Anal. Chim. Acta, 242 (1991) 85.
21 I. Adamowicz and C. Burstein, Biosensors, 3 (1987/88) 27.
22 I. Katakis and A. Heller, Anal. Chem., 64 (1992) 1008.
23 H. Durliat and M. Comtat, Anal. Chem., 52 (1980) 2109; 54 (1982) 856; 56 (1984) 148.
24 T. Yao and T. Wasa, Anal. Chim. Acta, 175 (1985) 301.
25 F. Mizutani, S. Yakubi and T. Katsura, Anal. Sci., 7 (1991) 871.
26 J.T. Greenamyre, Arch. Neurol., 43 (1986) 1058.
27 W.-M. Lu and W.-C. Chen, Proc. Natl. Sci. Counc. ROC (A), 13 (1989) 120.
28 J.H.T. Luong, A. Mulchandani and K.B. Male, Enzyme Microb. Technol., 13 (1991) 116.
29 T. Yao, N. Kobayashi and T. Wasa, Electroanalysis, 2 (1990) 563.
30 M. Uto, E.K. Michaelis, I.F. Hu, Y. Umezanea and T. Kuwana, Anal. Sci., 6 (1990) 221.
31 H. Minami, M. Sugawara, K.O. Odashima and Y. Umezawa, Anal. Chem., 63 (1991) 2787.
32 H. Durliat, C. Causserand and M. Comtat, Anal. Chim. Acta, 231 (1990) 309.
33 M. Comtat, M. Galy, P. Goulas and J. Souppe, Anal. Chim. Acta, 208 (1988) 295.

Analytica Chimica Acta, 278 (1993) 35–40
Elsevier Science Publishers B.V., Amsterdam

Amperometric biosensor for determination of lactate in sweat

Mohammad H. Faridnia, Giuseppe Palleschi [1] and Glenn J. Lubrano
Universal Sensors, Inc., 5258 Veterans Blvd., Suite D, Metairie, LA 70006 (USA)

George G. Guilbault
Department of Chemistry, University of New Orleans, 2000 Lakeshore Dr., New Orleans, LA 70148 (USA)

(Received 2nd January 1992; revised manuscript received 29th December 1992)

Abstract

An amperometric hydrogen peroxide based biosensor has been developed for non-invasive determination of L-lactate. The biosensor utilizes lactate oxidase immobilized between a polycarbonate membrane and a polytetrafluoroethylene (PTFE) blocking membrane to effectively eliminate electrochemical interferences. Both the steady state current and maximum rate of current change were measured. The response times were 2 min and 10 s, respectively. Because of the addition of polycarbonate and PTFE membranes, the linear range of lactate was extended up to 140 mg dl^{-1} and the apparent Michaelis–Menten constant was almost two orders of magnitude higher than that of the free enzyme. The biosensor was applied to the analysis of sweat L-lactate content of healthy subjects during physical exercise.

Keywords: Amperometry; Biosensors; Body fluids; Lactate

Increasing demand for non-invasive, fast and reliable methods for metabolite determination in body fluids resulted in extensive research in this area. L-Lactate is one of the most important metabolites in clinical analysis for medical patients with respiratory failures [1] and in sport medicine [2–8], in which the blood L-lactate level is used to monitor the maximum performance level of an athlete. We have previously reported development of an amperometric L-lactate biosensor for determination of lactate in saliva samples [9]. There are two major limitations in using salvia as a medium for lactate determination; the low saliva to blood L-lactate ratio [10] and the presence of bacteria in saliva [11,12]. To overcome these limitations, very sensitive and highly selective electrodes are required and the analysis must be carried our promptly after sample collection. Sweat, on the other hand, has a much higher sweat to blood L-lactate ratio [10].

Electrochemical biosensors have been shown to be specific, selective and easy to use and many L-lactate selective electrodes have been reported [1–9]. Presently, there are four enzymes available for detection of L-lactate: lactate dehydrogenase (LDH) [13–15], cytochrome b_2 [16], lactate monooxygenase (LMO) and lactate oxidase (LOD) [17–22]. Bienzyme systems such as LOD/LDH [23,24] and cytochrome b_2/LDH [25] have also been proposed.

Although dehydrogenases are highly selective in many cases, the difficulty in oxidation of coen-

Correspondence to: M.H. Faridnia, Universal Sensors Inc., 5258 Veterans Blvd., Suite D, Metairie, LA 70006 (USA).
[1] Present address: DISTAAM, Università del Molise, Via Tiberio 21, 86100 Campobasso (Italy).

zyme (NADH or NADPH) poses a problem as an additional parameter to be optimized.

Biosensors utilizing immobilized lactate monooxygenase and lactate oxidase attached to oxygen or hydrogen peroxide electrodes measure the rate of oxygen consumption or hydrogen peroxide production [17–22]. In addition, some biosensors utilize microbial cells [26,27]. Microbial cells, although functional as L-lactate biosensors, suffer from limited operating life time due to deactivation.

We have developed an amperometric biosensor for L-lactate determination. The sensor utilizes lactate oxidase chemically immobilized on a polycarbonate membrane. The electrochemical interferents have been eliminated by the use of a hydrophobic blocking membrane that was permeable to hydrogen peroxide. The biosensor was applied to the analysis of sweat samples of healthy subjects, before and after physical exercise.

The electrochemical lactate biosensor operates according to the following reaction:

$$\text{L-Lactate} + O_2 + H_2O \xrightarrow{\text{Lactate oxidase}} \text{Pyruvate} + H_2O_2$$

This reaction is catalyzed by the enzyme lactate oxidase and the hydrogen peroxide generated is measured at a platinum electrode poised at +650 mV vs. Ag/AgCl electrode.

EXPERIMENTAL

Instrumentation

An amperometric biosensor detector (ABD) (Catalog No. 2001) and a hydrogen peroxide electrode with combined working (Pt) and reference (Ag/AgCl) electrode (Catalog No. 4006) were from Universal Sensors (New Orleans, LA). For temperature studies, a jacketed glass wall beaker was thermostated by an MS-20 Lauda heating circulator from Brinkmann Instruments. The sample temperature was monitored with a Thermometrics 10 kΩ thermistor (MC50F103A) connected to a digital voltmeter.

Chemicals

Lactate oxidase from *Pediococcus sp.* (EC 1.1.3.2) 30 units mg^{-1} and a spectrophotometric lactate kit (No. 826-UV) were purchased from Sigma. Bovine serum albumin (BSA, 98–99%, Catalog No. A-7906, lot No. 18F-0409) and 25% glutaraldehyde, grade II (Catalog No. G6257, lot No. 116F-5027), were also purchased from Sigma. All other chemicals not listed were reagent grade.

Materials

Microporous polycarbonate membrane (0.015 μ) was obtained from Nuclepore. The hydrophobic blocking membrane, polytetrafluoroethylene (PTFE), 4 mil thickness (Catalog No. 4106) was from Universal Sensors.

Solutions

Phosphate buffered saline (PBS) was used for all measurements and electrode storage. The PBS contained the following salt concentrations in deionized water: 137 mM NaCl, 2.7 mM KCl, 8.0 mM Na_2HPO_4 and 1.5 mM KH_2PO_4 (pH 7.45 ± 0.10). BSA and glutaraldehyde immobilization solutions were prepared in 0.10 M phosphate buffer, pH 7.5.

Enzyme immobilization

A 2-cm^2 piece of polycarbonate membrane was attached to the electrode jacket with its dull side facing out and secured in place with an O-ring. A 10-μl volume of a solution of 5% BSA in 0.1 M phosphate buffer (pH 7.5) was used to dissolve 10 units of lactate oxidase. The enzyme solution was then placed on the polycarbonate membrane and 1 μl of 2.5% glutaraldehyde was added and the reaction mixture quickly stirred and spread out over the membrane surface with a small glass rod to form a 6-mm diameter disk. The enzyme membranes were air dried (approximately 2 h). They were then washed once with PBS, soaked for a few minutes in PBS containing 0.1 M glycine, then washed and stored in PBS.

Electrode construction

The biosensor was constructed with the PTFE membrane innermost, and the immobilized lactate oxidase sandwiched between it and the polycarbonate membrane. It has the following configuration: Pt/PTFE/LOD/polycarbonate.

Test method

The applied potential was set at 0.650 V vs. Ag/AgCl. A 5000 mg dl^{-1} L-lactate stock solution in PBS was used to calibrate the biosensor. Appropriate volumes of the stock solution were pipetted into 5 ml of PBS and the current monitored with a strip chart recorder. The maximum, initial rate of reaction was read from the display of the ABD. The change in current was calculated by subtraction of background current from the steady state current. The steady state current was taken as the current at 2 min. All measurements were carried out at room temperature and no adjustments for temperature were made.

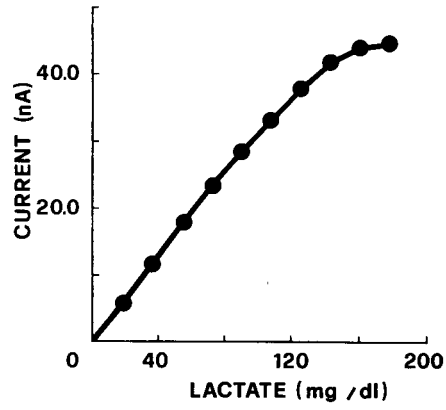

Fig. 2. Calibration curve of L-lactate biosensor, given as the steady state current vs. the L-lactate concentration.

RESULTS AND DISCUSSION

Electrode response

Typical response curves of the lactate electrode are given in Fig. 1. The time to 95% or better of the steady state current was 2 min. The maximum initial rate of current change occurred at 10 s. A typical calibration curve of steady state current vs. concentration is given in Fig. 2. The membranes used extended the linear range of the lactate up to 140 mg dl^{-1}. Conventional lactate probes based on oxygen or hydrogen peroxide electrodes assembled with the same enzyme [18,28] used in this work have been used in clinical medicine. In these papers a lactate probe has a linear range up to 5 mg dl^{-1}. With this electrode, the linearity goes up to 140 mg dl^{-1}.

We did not use the initial rate for calibration because the steady state current method was more reproducible (5 vs. 10%). Thus, the steady state method was used throughout. The initial rate method is good enough to measure the lactate variation in sweat within 10 s, but for our purposes, this fast procedure was unnecessary.

Because the enzyme is immobilized and not used in a homogeneous solution and because there is a substrate diffusion restricting membrane between the sample and the enzyme, the K_m of the electrode system (140 mg dl^{-1} lactate) is referred to as an apparent K_m, which is almost two orders of magnitude larger than the K_m of corresponding homogeneous systems. This is consistent with the results of other biosensors.

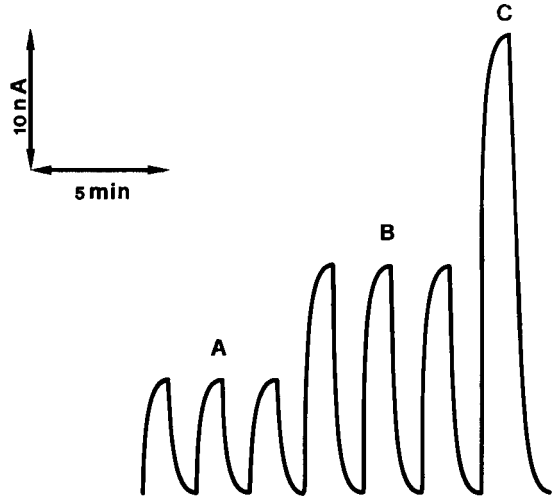

Fig. 1. Response curves of the L-lactate biosensor. (A) 20 mg dl^{-1}, (B) 40 mg dl^{-1}, and (C) 80 mg dl^{-1}.

Interference study

Effects of the following interferents on the L-lactate biosensor were investigated: ascorbic acid, acetaminophen, acetylsalicylic acid, uric acid, valine, lysine, histidine, leucine, tyrosine, threonine, arginine, sodium, chloride, calcium and potassium. The electrode was highly selective against these compounds. For all these interferents, the electrode response was less than detectable (i.e., less than 0.01 nA) at concentrations 10 times higher that present in sweat.

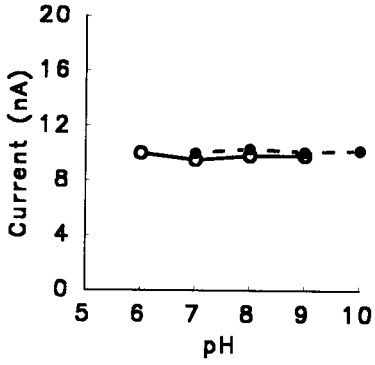

Fig. 3. Steady state response of the L-lactate biosensor to 20 mg dl^{-1} L-lactate at different pH values: (○) = 0.1 M phosphate buffer; (●) = 0.1 M Tris buffer.

pH study

The response to 20 mg dl^{-1} L-lactate was measured at different pH values. Fig. 3 is a plot of steady state current vs pH. Phosphate buffer (0.1 M) and Tris buffer (0.1 M) were used for pH 6–9 and 8–11, respectively. Within this range, there was no noticeable change in response.

Temperature study

The response to 20 mg dl^{-1} L-lactate was measured at 5°C intervals from 25 to 45°C. The effect of temperature on response is given in Fig. 4. Although response is higher at higher temperatures, the analyses were carried out at ambient temperature, since extended exposure to high temperature results in more rapid denaturation of the enzyme. Denaturation due to extreme temperature is usually irreversible, resulting in permanent loss of enzyme activity.

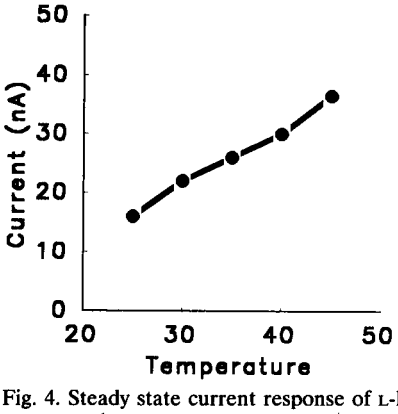

Fig. 4. Steady state current response of L-lactate biosensor to 20 mg dl^{-1} L-lactate at different temperatures.

Application

Subjects. The participants in this study were males, ages 24–36 years, accustomed to moderate exercise and were not professional athletes.

Sample collection and analysis. Sweat samples, 1–2 ml, were collected in 5-ml disposable vials, capped and either immediately assayed or kept at 0°C until assay. During each experiment, samples were collected from upper parts of legs and arms, area covering Gluteus Maximas and Biceps respectively. To establish a baseline response, at least three samples were collected before exercise, while the subject was at rest. The subject then ran at a speed of 4–6 miles h^{-1} for 30 min. Sweat samples were collected immediately after the run and thereafter at 5-min intervals, until the sweat lactate level returned to normal. The biosensor was calibrated before the analysis and 20 mg dl^{-1} L-lactate controls were run throughout the study. 100 μl of each sample was pipetted into 5.00 ml of stirring PBS and the steady state current and maximum initial rate responses were monitored. The steady state current was measured within 2 min and the initial rate of reaction was measured in less than 10 s.

A typical plot of sweat L-lactate vs. time is given in Fig. 5. The values of lactate concentration reported in the figure were calculated considering the dilution of 100 μl sweat sample injected into 5 ml of buffer solution. The values calculated according with the dilution attained were always in the linearity range of the probe. All subjects had an increase in sweat lactate after the physical exercise and the concentration decreased during he resting period. This finding is in agreement with that reported by many researchers on L-lactate metabolism after a physical exercise [2–8]. Location of sample collection is crucial and the concentration of L-lactate depends on the type of exercise. The samples collected from subjects' arms and legs showed the

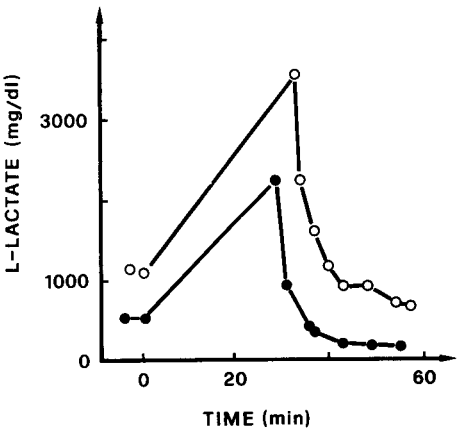

Fig. 5. L-lactate metabolism curve presented as sweat L-lactate concentration (mg dl^{-1}) vs. time (min), samples were collected from the subject's legs (○) and arms (●) before and after a physical exercise.

same trend, but the former showed much lower baseline level and peaked at a lower maximum value.

Stability. The short term stability of sweat L-lactate was investigated by storage at 2–4°C for 22 h and 25°C for 5 h. The latter's L-lactate concentration was periodically measured over the 5-h period. No decrease in L-lactate concentration was observed for either storage condition. This allowed the samples to be collected and stored at 2–4°C, and analyzed at a later time. No preservatives were added to enhance stability.

Conclusion

We have developed an amperometric hydrogen peroxide based L-lactate biosensor, that has shown good characteristics in terms of its selectivity, indifference to pH change and extended linearity. The biosensor was applied to the non-invasive determination of sweat L-lactate of subjects before and after physical exertion. The results were comparable to that reported by others doing the same type of experiment, but measuring blood L-lactate content.

Dr. Palleschi gratefully acknowledges the CNR (Conciglio Nazionale delle Ricerche) Progetto Finalizzato Biotecnologie e Biostrumentazione, Sottoprogetto Biostrumentazione, Contratto No. 90,0061,PF 70

REFERENCES

1 A.L. Herrick, B.M. Fisher, M.R. Moore, S. Cathcart, K.E.L. McColl and A. Goldberg, Clin. Chim. Acta, 190 (1990) 157.
2 G. Pallesclhi, R. Pilloton, M. Mascini, L. Bernardi, G. Bombardieri, A.M. Deluca and P. Zippilli, J. Biosensors, 14 (1989) 3.
3 K. Wasserman and M.B. Mcilroy, Am. J. Cardiol., 14 (1964) 844.
4 J. Karlsson, L.O. Nordesio, L. Jiorfeldt and B. Saltin, J. Appl. Physiol., 33 (1972) 199.
5 J. Karlsson and I. Jacobs, Int. Sports Med., 3 (1982) 190.
6 G. Palleschi, M. Mascini, L. Bernardi and P. Zeppilli, Med. Biol. Eng. Comput., 38 (1990) B25.
7 C. Juel, J. Bangsbo, T. Graham and B. Saltin, Physiol. Scand., 140 (1990) 147.
8 N. Shimojo, K. Fujino, S. Kitahashi, M. Nakao, K. Naka and K. Okuda, Clin. Chem., 37 (1991) 1978.
9 G. Palleschi, M.H. Faridnia, G.J. Lubrano and G.G. Guilbault, Anal. Chim. Acta, 245 (1991) 151.
10 D.S. Dittmer (Ed.), Blood and Other Body Fluids, Federation of American Societies for Experimental Biology, Washington DC, 1961, p. 400.
11 J.O. Tenovuo, Human Saliva: Clinical Chemistry & Microbiology, Vol. I, CRC Press, Boca Raton, FL, 1989.
12 J.O. Tenovuo, Human Saliva: Clinical Chemistry & Microbiology, Vol. II, CRC Press, Boca Raton, FL, 1989.
13 W.J. Blaedel and R.A. Jenkins, Anal. Chem., 48 (1976) 1240.
14 W.J. Blaedel and R.C. Engstrom, Anal. Chem., 52 (1986) 1691.
15 M.F. Suaud-Chagny and F.G. Gonon, Anal. Chem., 58 (1986) 412.
16 J.J. Kulys and G.J.S. Svirmickas, Anal. Chim. Acta, 117 (1980) 115.
17 N. Shimozo, K. Naka, C. Nakajima, C. Yoshikawa, K. Okuda and K. Okada, Clin. Chem., 35 (1989) 1992.
18 M. Mascini, S. Fortunati, D. Moscone, G. Palleschi, M. Massi-Benedetti and P. Fabietti, Clin. Chim., 31 (1985) 451.
19 J. Wandrup, K. Tvede, J. Grinsted and H. Jordening, Clin. Chem., 35 (1989) 1740.
20 M. Mascini, F. Mazzel, D. Moscone, G. Calabresel and M. Massi-Benedetti, Clin. Chem, 33 (1987) 591.
21 G. Bardeletti, F. Sechaud and R. Coulet, Anal. Chim. Acta., 187 (1986) 47.
22 R. Pilloton, T.N. Nwosou and M. Mascini, Anal. Lett., 21 (1988) 747.
23 F. Mizutani, T. Yamanaka and Y. Tanabe, Chem. Lett., 2 (1984 199.
24 F. Mitzutani, Y. Yamanda, Y. Tanabe and K. Tsuda, Anal. Chim. Acta, 177 (1985) 153.

25 F. Schubert, D. Kirtein, K.L. Schoder and F.W. Scheller, Anal. Chim. Acta, 169 (1985) 391.
26 J.H.T. Luong, M. Mulchandani and C.A. Groom, J. Biotechnol., 10 (1989) 241.
27 J.H.T. Luong, M. Mulchandani and C.A. Groom, J. Biotechnol. Scand., 140 (1990) 147.
28 G. Palleschi, M. Mascini, L. Bernardi, G. Bombardieri and A.M. De Luca, Anal. Lett., 22 (1989) 1209.

Analytica Chimica Acta, 278 (1993) 41–51
Elsevier Science Publishers B.V., Amsterdam

Cathodic stripping voltammetric behaviour of copper complexes of glycylglycyl-L-histidine at a hanging mercury drop electrode

Determination of trace amounts of glycylglycyl-L-histidine

Arnold G. Fogg, F. Nil Ertas and Josino C. Moreira [a]

Department of Chemistry, Loughborough University of Technology, Loughborough, Leicestershire LE11 3TU (UK)

Jiri Barek

UNESCO Laboratory of Environmental Electrochemistry, Department of Analytical Chemistry, Charles University, Prague (Czech Republic)

(Received 10th June 1992; revised manuscript received 17th December 1992)

Abstract

The behaviour of copper complexes with glycylglycyl-L-histidine (GGH) was investigated using cyclic voltammetry and adsorptive differential pulse cathodic stripping voltammetry. The nature of the observed cathodic and anodic peaks was established and optimum conditions have been found for the determination of nanomolar levels of GGH by means of differential pulse cathodic stripping voltammetry after accumulation in the presence of excess copper at −0.20 V vs. Ag–AgCl reference electrode and using the stripping peak around −0.40 V which corresponds to the reduction of the copper(I)–GGH complex.

Keywords: Cyclic voltammetry; Stripping voltammetry; Copper complexes; Glycylglycyl-L-histidine

Tripeptides containing the histidine residue are of interest as models of bioactive polypeptides and proteins. Glycylglycyl-L-histidine (GGH) is of particular interest since it is used as a low-molecular-weight mimic of human and bovine serum albumin (BSA) [1]. The involvement of copper in the redox processes of many of these biological systems is well established. The complexing ability of GGH towards copper(II) has been studied extensively, mainly by means of pH titrimetry in which the loss of protons on complexation is monitored [1–6]. It follows from these studies that GGH forms a 1:1 complex with copper(II) within the pH range 6.6–11.0. Crystallography has indicated that in this complex GGH is tetradentate, complexing the copper via its amino nitrogen, two amido nitrogens (after loss of their hydrogen atoms) and the pyridine-like imidazole nitrogen.

Although many authors have reported on the structures of these complexes (see reviews [1,2]), there are few reports on their electrochemical

Correspondence to: A.G. Fogg, Department of Chemistry, Loughborough University of Technology, Loughborough, Leicestershire LE11 3TU (UK).

[a] Present address: Departamento de Quimica da UFRRJ, Antiga Rio–SP Km 47, Itaguai (Brazil)

behaviour. The reduction of Cu(II) complexes of histidine and histidyl peptides at mercury electrodes was investigated by Bilewicz [7] and anomalous current fluctuations in the reduction process of Cu(II)–GGH complex was studied by Takehara and Ide [8,9]. No attempts to investigate the adsorptive stripping voltammetric behaviour of Cu(II)–GGH complexes and to use them for the determination of trace amounts of either copper or the tripeptide have so far been reported. Our previous studies on the cathodic stripping voltammetric behaviour of copper complexes with imidazole [10] and histidine [11] have led to interesting results and an extremely sensitive method for the determination of histidine. Therefore, a detailed study of the adsorptive stripping voltammetric behaviour of Cu(II)–GGH complexes was carried out and is reported in the present paper. In addition to the better understanding of the redox behaviour of these biologically interesting complexes on the surface of a mercury drop, which can be treated as a hydrophobic substrate model of a physiological redox site [7], the possibility of developing a sensitive method for voltammetric determination of trace amounts of polarographically inactive GGH was kept in mind.

EXPERIMENTAL

Apparatus and reagents

Adsorptive stripping voltammetry was carried out with a Metrohm 626 Polarecord with a 663 VA stand using a multi-mode electrode in the hanging mercury drop electrode (HMDE) mode. The three-electrode system was completed by means of a glassy carbon auxiliary electrode and an Ag–AgCl reference electrode. All potentials given are relative to this Ag–AgCl electrode. The cyclic voltammetric experiments were carried out by connecting the electrodes on the Metrohm 663 VA stand to a PAR 174A polarographic analyser (Princeton Applied Research); the multimode-electrode (HMDE) was still activated by means of the Metrohm 626 Polarecord. The pH measurements were made with a Corning combined pH/reference electrode and a Radiometer PHM 64 pH meter.

Supporting electrolytes and buffers were prepared using analytical grade reagents supplied by BDH. A 1×10^{-2} M solution of glycylglycyl-L-histidine was prepared by dissolving precisely weighed amounts of pure substance supplied by Sigma in 5 ml of deionised water with sonication. It was kept in a refrigerator and prepared freshly each day. Standard solutions of copper(II) were prepared by diluting SpectrosoL atomic absorption standard solution (BDH). Stock solutions of copper(I) were prepared by dissolving copper(I) chloride in hydrochloric acid [12]. Sodium hydrogencarbonate buffer solution (0.1 M) was used for voltammetric measurements at pH 8.3.

Procedures

The general procedure used to obtain adsorptive stripping voltammograms was as follows. A 20 ml aliquot of 0.1 M sodium hydrogencarbonate buffer solution was placed in a voltammetric cell and the required amounts of standard GGH and copper(II) solutions were added. The stirrer was switched on and the solution was purged with nitrogen for 5 min. After forming a new HMDE, accumulation was effected for the required time at the appropriate potential while stirring the solution. Maximum drop size and stirrer speed were used throughout. At the end of the accumulation period the stirrer was switched off, and, after 20 s had elapsed to allow the solution to become quiescent, a negative potential scan was initiated between the accumulation potential and -0.8 V. When the adsorptive accumulation was carried out at more negative potentials, the potential was changed immediately to -0.1 V from where a negative potential scan was initiated.

Cyclic voltammetry was carried out either immediately after forming a new HMDE or after preceding accumulations at different potentials for different times while stirring the solution. Either negative or positive scans were initiated after accumulation depending on the potential of accumulation.

Sampled direct current polarography was performed using the static dropping mercury electrode mode with a drop time of 1 s and scan rate 5 mV s^{-1}.

RESULTS AND DISCUSSION

GGH was shown to be electrochemically inactive over the pH and potential ranges studied. Sampled DC polarograms of the copper(II)–GGH complex obtained in the presence of excess GGH showed a single wave of constant height over the pH range 6.0–11.8, in which range the 1:1 complex is known to be formed [1,2]: 1:1 complex formation at pH 8.3 was confirmed by the fact that the height of the wave of a 1×10^{-5} M solution of uncomplexed copper(II) solution decreased by 50% after addition of GGH (0.5×10^{-5} M) and to zero when the GGH concentration was increased to 1×10^{-5} M. The differential pulse polarographic peak potential varied linearly from −0.39 to −0.69 V between pH 6.0 and 11.8. The polarographic maximum observed was readily removed by means of Triton X-100.

Cyclic voltammetric behaviour of copper complexes of glycylglycyl-L-histidine

Typical cyclic voltammograms obtained at a HMDE with 5×10^{-7} M copper(II) and 1×10^{-5} M GGH in a pH 8.3 hydrogencarbonate buffer are shown in Fig. 1. Fig. 1a and b show multiple scans between 0 and −0.8 V after holding the potential initially at 0 and −0.7 V, respectively, for 2 min. Two reduction peaks are observed, around −0.4 and −0.6 V, the exact position of which slightly depends on both GGH and copper(II) concentration. Moreover, the height of these two peaks was found to be dependent on the concentration of GGH and copper(II), poten-

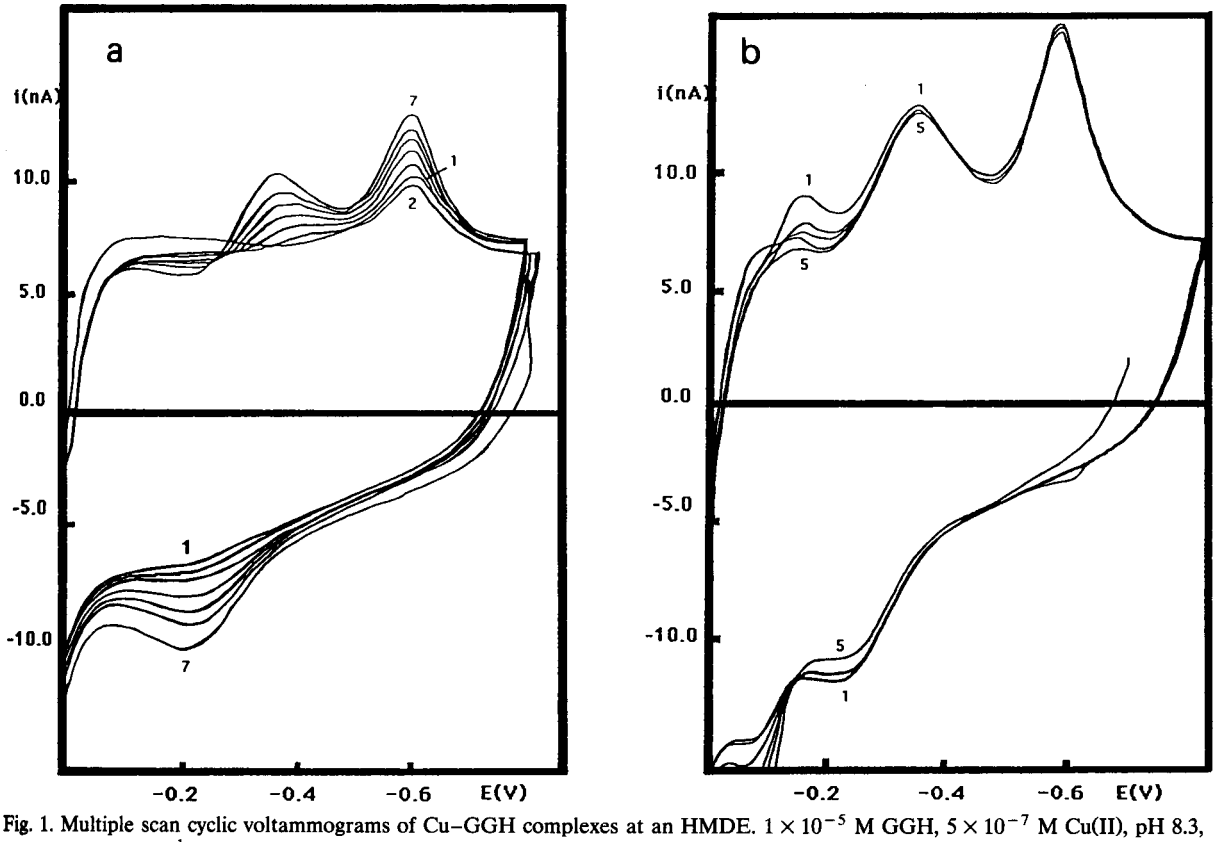

Fig. 1. Multiple scan cyclic voltammograms of Cu–GGH complexes at an HMDE. 1×10^{-5} M GGH, 5×10^{-7} M Cu(II), pH 8.3, scan rate 50 mV s^{-1}, accumulation time (where applied) 2 min in stirred solution, the scan number is indicated on the plot. (a) Accumulation potential 0.0 V, cycling between 0.0 and −0.8 V; (b) accumulation potential −0.7 V, cycling between 0.0 and −0.8 V; (c) accumulation potential 0.0 V, cycles 1–3 between 0.0 and −0.4 V, cylces 4–6 between 0.0 and −0.7 V; (d) accumulation potential −0.5 V, cycling between −0.5 V and 0.0 V; (e) accumulation potential −0.7 V, scan to 0.0 V, cycles 1–2 between 0.0 and −0.9 V, scan 3 and 4 held at 0.0 V for 1 and 2 min, respectively, before scanning.

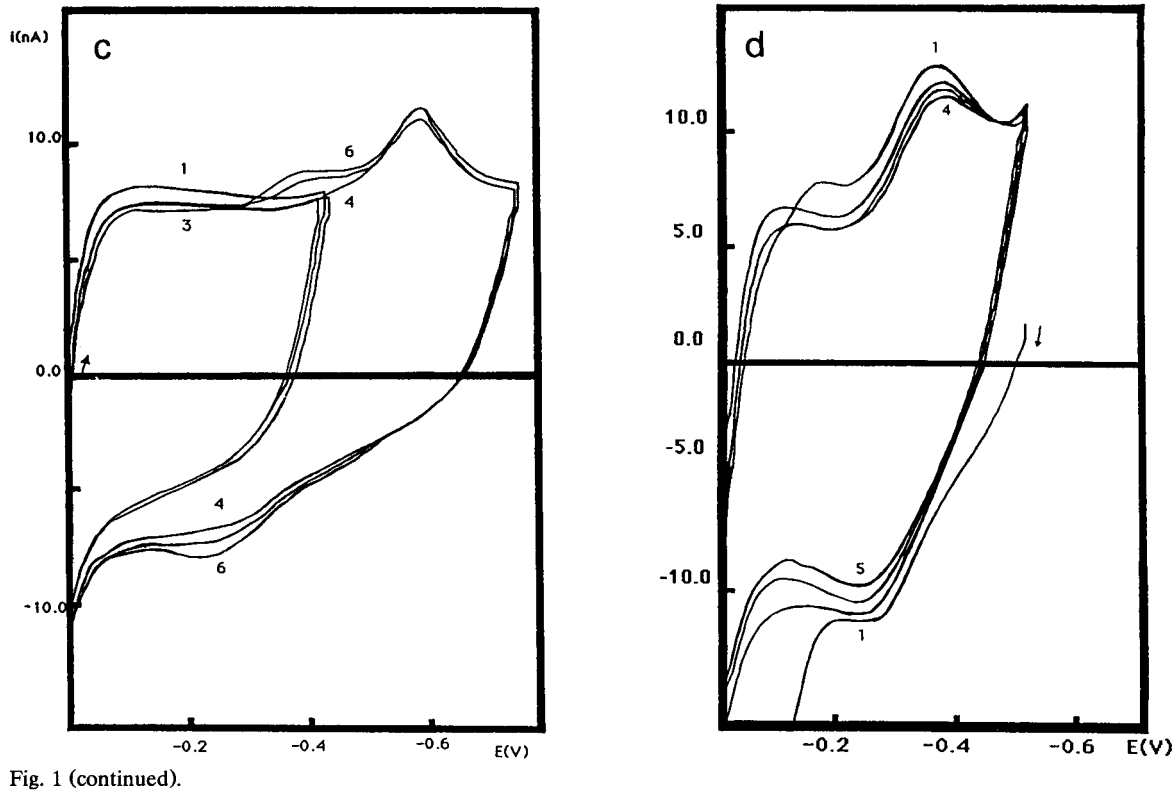

Fig. 1 (continued).

tial and time of accumulation, scan rate, direction and switching potentials of subsequent cyclic voltammetric scans. On the basis of DC and differential pulse polarographic behaviour of Cu(II)–GGH complex, the second peak around −0.6 V can be assigned to the reduction of the Cu(II)–GGH complex to Cu amalgam. This assumption is supported by the fact that Cu amalgam is accumulated when the potential is held at −0.7 V which is clear from the appearance of the anodic peak at −0.07 V corresponding to reoxidation of Cu amalgam to free copper(II), and from the free Cu(II) cathodic peak obtained at −0.12 V in the subsequent cathodic scan (see Fig. 1b). The first peak, around −0.4 V, is not present during the first scan after holding the potential at 0.0 V (see scan 1 in Fig. 1a). In subsequent scans, however, the first peak increases continuously in size, as does the second peak. The morphology of these two peaks and their dependence on the scan rate suggest that they correspond to the reduction of adsorbed species.

A single reoxidation peak is observed on the reversed scan at −0.25 V; the shape of this peak indicates a diffusion-controlled process. The nature of this anodic peak was established using 1 min accumulation at −0.8 V in a solution containing 1×10^{-7} M copper(II) without GGH. In the anodic scan after this accumulation, a single anodic peak at −0.07 V is observed, which corresponds to the reoxidation of Cu amalgam formed during the accumulation step. However, when after the same accumulation step GGH is added so that its total concentration was equal to 1×10^{-4} M, a single anodic peak at −0.22 V is observed, the shape of which suggests a diffusion-controlled process. No cathodic peak around −0.4 V was observed in the subsequent cathodic scan with switching potential −0.15 V. Thus, the possibility that the peak at −0.22 V corresponds to the reoxidation of Cu amalgam to the species

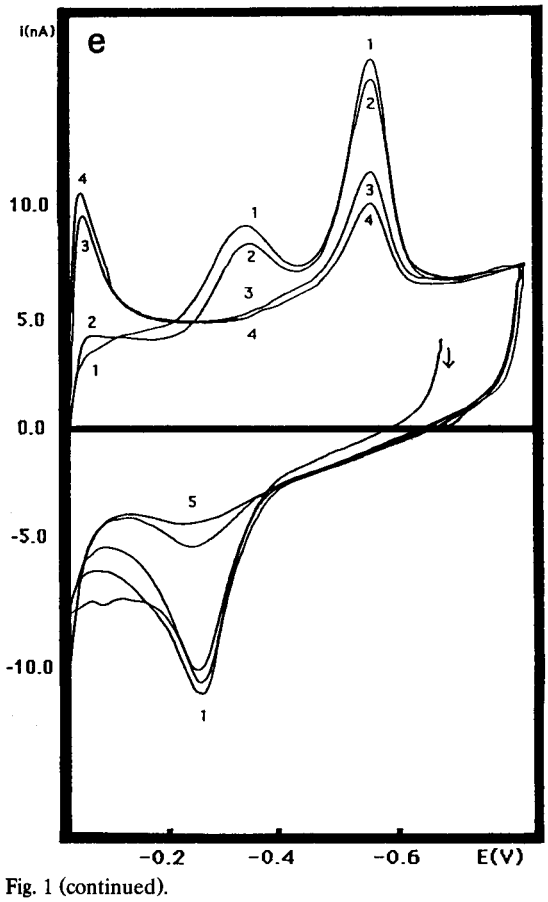

Fig. 1 (continued).

responsible for the cathodic peak at −0.4 V can be excluded. However, the second cathodic peak, around −0.6 V, can clearly be seen in the subsequent cathodic scan. Therefore, we can assume that the anodic peak at −0.22 V corresponds to reoxidation of Cu amalgam to the Cu(II)–GGH complex.

No experimental findings support the assumption of Takehara and Ide [9] that oxidation of a Cu–GGH complex to a Cu(II)–GGH complex is involved under these conditions. Nevertheless, in accordance with their findings, it can be assumed that, at pH 8.3 and at potentials more negative than −0.6 V, GGH is desorbed because of its negative charge and the strong repulsive force caused by the high negative charge on the HMDE. This explains why reoxidation of Cu amalgam to Cu(II)–GGH complex is a diffusion controlled process in contrast to the adsorption controlled processes corresponding to the cathodic peaks around −0.4 and −0.6 V. (However, readsorption of GGH will occur during subsequent anodic or cathodic scans at potentials closer to the electrocapillary zero.)

The Cu amalgam formed on electrolysis at the more negative potentials is reoxidised to copper(II) on cycling to 0 V, and the two cathodic peaks around −0.4 and −0.6 V remain of constant height during the first and subsequent scans. The free copper(II) cathodic peak at −0.12 V observed clearly during the first scan gradually disappears during subsequent scans. This indicates that whereas the species responsible for the peaks around −0.4 and −0.6 V are adsorbed at the electrode surface, the uncomplexed copper(II) diffuses away from the surface. Cycling the potential between 0 and −0.4 V produced no peak around −0.4 V (see Fig. 1c), but holding the potential at −0.5 V and subsequent cycling between 0 and −0.5 V did (see Fig. 1d). The formation of both peaks on scanning to −0.7 V is also shown in Fig. 1c for comparison. When accumulation was effected at −0.7 V and the potential was then held for 1 or 2 min at 0 V before cycling between 0 and −0.9 V, the peak around −0.4 V disappeared and the peak around −0.6 V was decreased in height (see Fig. 1e). Clearly, the dissolution of Cu amalgam (which is formed during accumulation at −0.7 V) at 0.0 V results in the desorption of the species responsible for the cathodic stripping peaks. When the experiment illustrated in Fig. 1b was repeated using 1×10^{-7} and 3×10^{-7} M copper(II), the two peaks were again obtained of constant height on cycling, but became proportionately smaller as the copper(II) concentration was decreased. However, when the copper(II) concentration was only 5×10^{-8} M, the peak around −0.4 V was not present and the capacitance background current was higher than in Fig. 1a.

The species responsible for the cathodic peak around −0.6 V was barely or only weakly accumulated under these conditions (i.e., with excess of GGH) using the accumulation potential 0.0 or −0.4 V (see Fig. 2a and b). However, with 1×10^{-7} M copper(II) and an equal concentration of

GGH, the second peak, whose potential was shifted to −0.54 V, was increased with longer accumulation times at −0.1 or −0.2 V. Practically no accumulation could be seen at 0.0 V. Moreover, no accumulation was observed for the second peak at higher concentrations (1×10^{-6} M) of both Cu(II) and GGH. This can be explained by the preferred accumulation of GGH rather than its Cu(II) complex under these conditions.

The cyclic voltammograms shown in Fig. 2b were obtained by accumulating at −0.4 V and then cycling the potential to −0.8 V and then through 0 V and back to −0.4 V. With no accumulation at −0.4 V, neither reduction peak was obtained. As little as 15 s accumulation, however, caused full formation of the small second peak at −0.6 V for the first part of the scan to −0.8 V; this peak was slightly smaller with accumulation times of 1 and 2 min. These longer accumulation times, however, caused the first peak at −0.4 V to increase significantly in size. It seems probable that both copper amalgam and GGH are accumulated at −0.4 V; the reoxidation, on the positive-going scan, is largely reoxidation of Cu amalgam to the Cu(II)–GGH complex. Signs of reoxidation of Cu amalgam to free Cu(II) are only seen after 2 min accumulation.

Figure 3 shows voltammograms obtained by accumulating at various potentials between 0.0 and −0.6 V, before immediately changing the potential to 0.0 V and scanning from 0 to −1.0 V. The peak around −0.6 V increases in size gradually between accumulation potentials 0 and −0.3 V, and then, from −0.4 to −0.6 V, the peak around −0.4 V appears at an appreciable fixed height as does the peak around −0.6 V. The progressive increase in the height of the second peak, while the first peak is still being established, at lower accumulation potentials indicates a need for a greater accumulation of Cu amalgam, and the resulting greater concentration of free copper(II) at the electrode surface on cycling to 0.0 V, for formation of the species responsible for the peak around −0.4 V. This is confirmed by the voltammograms shown in Fig. 4. These were obtained at increasing accumulation times at −0.4 V, and scanning immediately from

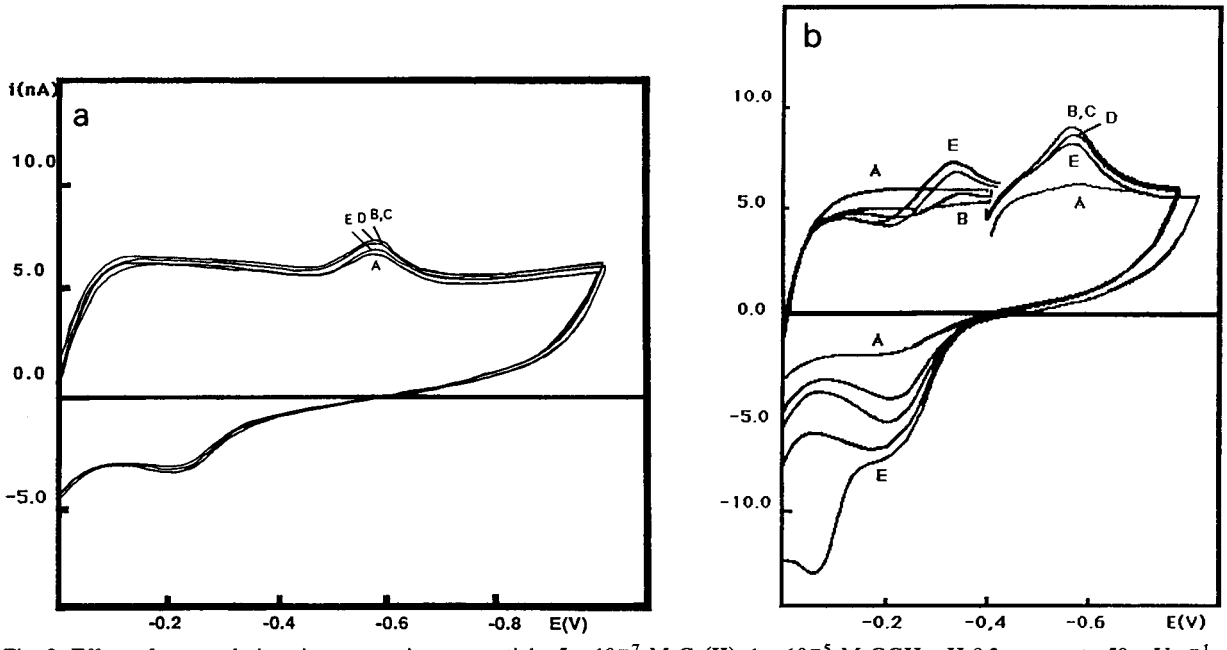

Fig. 2. Effect of accumulation times at various potentials. 5×10^{-7} M Cu(II), 1×10^{-5} M GGH, pH 8.3, scan rate 50 mV s^{-1}, accumulation time: (A) 0 s; (B) 15 s; (C) 30s; (D) 1 min; (E) 2 min. (a) Accumulation potential 0.0 V, scanning between 0.0 and −1.0 V; (b) accumulate potantial −0.4 V, scanning from −0.4 to −0.8 V to 0.0 and back to −0.4 V.

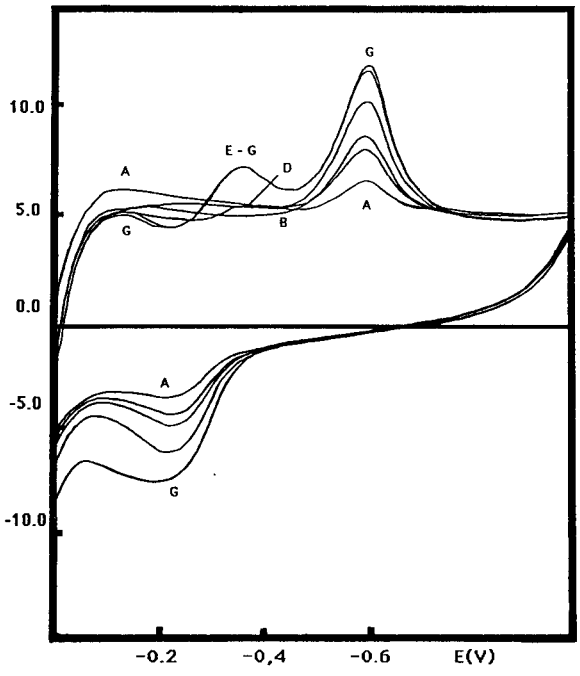

Fig. 3. Effect of accumulation potential. 5×10^{-7} M Cu(II), 1×10^{-5} M GGH, pH 8.3, accumulation time 1 min in stirred solution, after accumulation all scans were made immediately from 0.0 V at scan rate 50 mV s^{-1}, accumulation potential: (A) 0; (B) −0.1; (C) −0.2; (D) −0.3; (E) −0.4; (F) −0.5; (G) −0.6 V.

0.0 to −0.8 V. One minute accumulation gave full formation of both peaks for accumulation at −0.4 V and more negative potentials (compare Fig. 3). In the voltammograms in Fig. 4, the more rapid increase of the second peak at the lower accumulation times is clear.

In Fig. 5 the effect of accumulating copper amalgam at −0.4 V in the absence of GGH, which was then added whilst the cell was on open circuit before scanning from 0.0 V to more negative potentials, is shown; this is compared with the voltammogram obtained similarly without addition of GGH. Clearly the first and second peak can be formed, using these bulk concentrations of copper(II) and GGH, from accumulated Cu amalgam (subsequently reoxidised), without the need to accumulate GGH.

The effect of gradually increasing the GGH concentration with accumulation at −0.8 V is shown in Fig. 6. The peak around −0.4 V is clearly seen for a ten- and twenty-fold ratio of GGH to copper(II) in the bulk solution, but at higher ratios still the first peak disappears whilst the second peak continues to increase in size. Note that the GGH to copper(II) ratio at the electrode surface during the scan from 0.0 to −0.4 V will be considerably less than in the bulk solution owing to the accumulation of Cu amalgam at −0.8 V and its subsequent reoxidation to free copper(II) at the beginning of the scan from 0.0 V. Nevertheless, at a sufficiently high GGH to Cu(II) ratio in the bulk solution, the ratio at the electrode surface, even after the above mentioned accumulation and subsequent reoxidation of copper, is evidently too high for the first peak to be formed. Note also that the suppression of the peak around −0.4 V coincides with the loss of the oxidation peak at −0.07 V on the anodic scan which corresponds to the oxidation of Cu amalgam to free copper(II). It would appear that if copper(II) ion is not released during the anodic

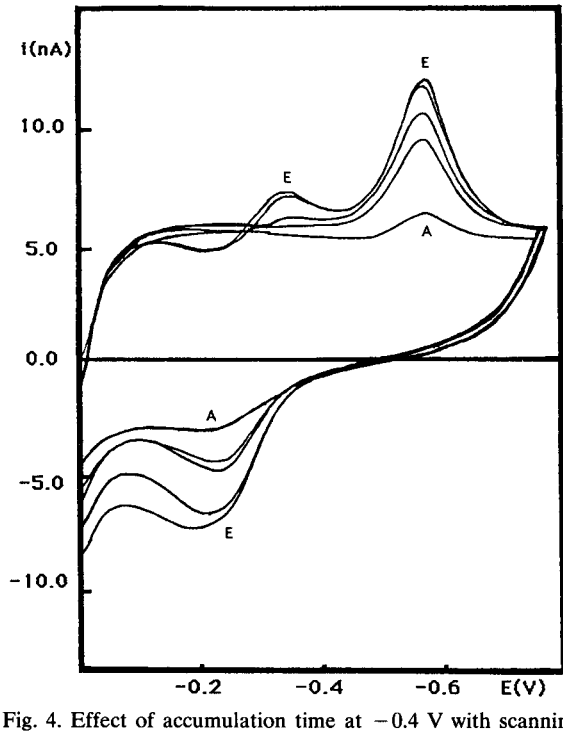

Fig. 4. Effect of accumulation time at −0.4 V with scanning from 0.0 V at scan rate 50 mV s^{-1}. 5×10^{-7} M Cu(II), 1×10^{-5} M GGH; pH 8.3, accumulation time: (A) 0 s; (B) 15 s; (C) 30 s; (D) 1 min; (E) 2 min.

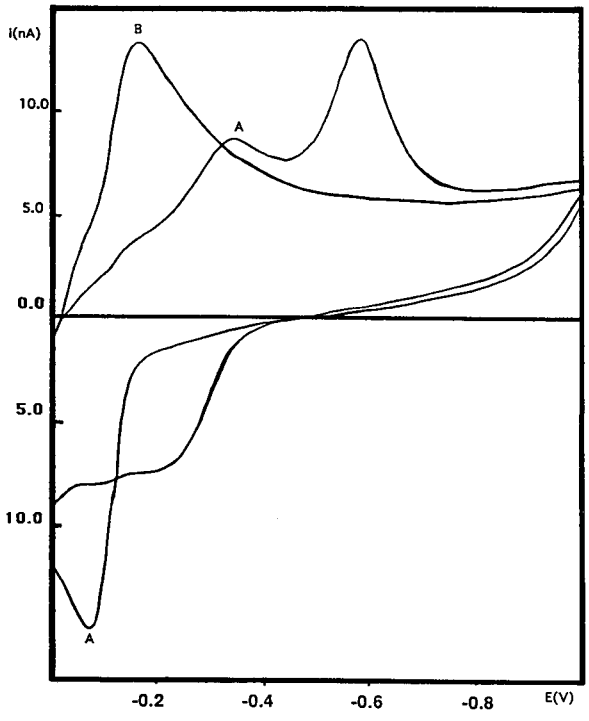

Fig. 5. Effect of accumulating copper in absence of GGH. (A) Accumulation in absence of GGH at −0.4 V for 2 min before going to open circuit, addition of GGH and scanning from 0.0 to −1.0 V at scan rate 50 mV s^{-1}. (B) The same but without addition of GGH. 5×10^{-7} M Cu(II); 1×10^{-5} M GGH [only (A)]; pH 8.3.

scan then the species responsible for the cathodic peak around −0.4 V is not formed and accumulated.

It can be assumed, therefore, that this species is a Cu(I)–GGH complex which is formed on the surface of the HMDE from free copper(II) and copper amalgam. The polarographic behaviour of copper(I) complexes with histidine [13] and the electrochemical evidence for the generation of Cu(I) complexes as intermediates in the polarographic reduction of copper(II) complexes with various amino acids [14] were reported earlier. Moreover, Bilewicz [7] presented evidence that the copper(I) complex with β-alanyl-L-histidine is stabilised by adsorption at the mercury surface. The fact that the Cu(I)–GGH complex is more easily reducible than the Cu(II)–GGH complex can be explained in terms of the different structures of these complexes, copper(I) preferring coordination number two in complexes with monodentate imidazole [15] and some histidine derivatives [16].

To prove the assumption that the Cu(I)–GGH complex is responsible for the cathodic peak around −0.4 V, an attempt was made to prepare a solution of the Cu(I)–GGH complex and investigate its polarographic and voltammetric behaviour. However, after addition of 0.020 ml of 1×10^{-3} M copper(I) chloride solution to 20 ml of 1×10^{-4} M GGH in 0.1 M $NaHCO_3$, only the cathodic peak around −0.6 V was observed. This means that the disproportionation of Cu(I) into

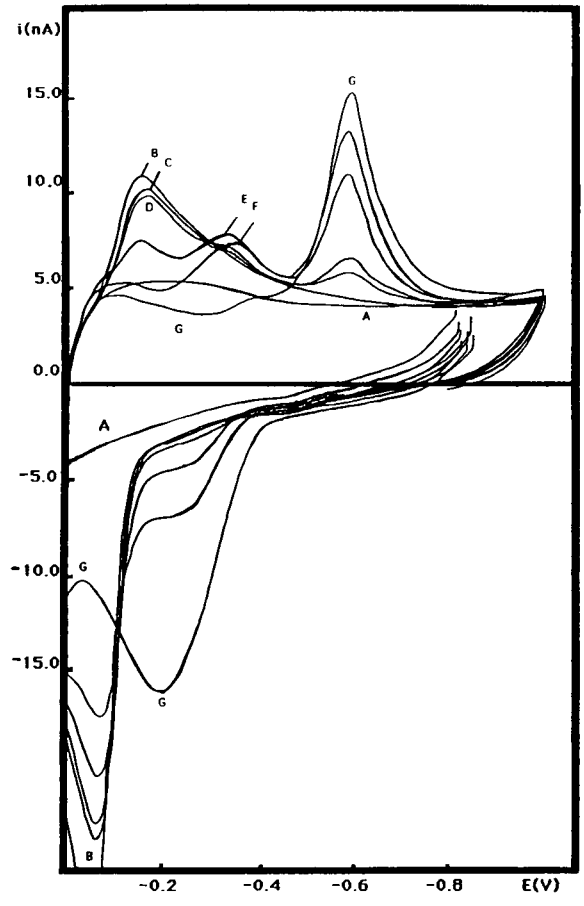

Fig. 6. Effect of GGH concentration on the formation of the cathodic peak around −0.4 V. Accumulation for 2 min at −0.8 V before scanning to 0 V and back to −1.0 V. (A) buffer (pH 8.3) only; (B–G) 5×10^{-7} M Cu(II); GGH concentration: (B) 0; (C) 5×10^{7}; (D) 1×10^{-6}; (E) 5×10^{-6}; (F) 1×10^{-5}; (G) 5×10^{-5} M.

Cu and Cu(II) is faster than the formation of the Cu(I)–GGH complex. Therefore, later, 0.1 M $NaHCO_3$ buffer in 1 M KCl was used, as it is well known that chloride ions stabilise copper(I). In this medium (with no added GGH), 5×10^{-5} M copper(II) gives two waves with current sampled DC polarography. The first one, which coalesces with the dissolution of mercury, corresponds to Cu(II) to Cu(I) reduction, while the second one, with the half-wave potential around −0.2 V, corresponds to Cu(I) to Cu amalgam reduction. After addition of GGH (total GGH concentration 1×10^{-4} M), only the wave around −0.6 V is observed, which corresponds to the reduction of Cu(II)–GGH complex to Cu amalgam. Cu(I) (5×10^{-5} M) gives in this medium in absence of GGH just one wave around −0.2 V corresponding to Cu(I) to Cu amalgam reduction. The half-wave potential of this wave shifts towards more negative values ($E_{1/2} = -0.21$, −0.23, −0.26, and −0.30 V in 1×10^{-5}, 2×10^{-5}, 5×10^{-5}, and 1×10^{-4} M GGH, respectively) and the wave height decreases as the result of lower diffusion coefficient of Cu(I)–GGH complex as compared with that of free copper(I). Cyclic voltammetry of 1×10^{-5} M Cu(I) in 0.1 M $NaHCO_3$ and 1 M KCl provided just one peak at −0.22 V which obviously corresponds to Cu(I) chloride complex reduction to Cu amalgam. After addition of GGH, a new cathodic peak around −0.3 V was formed which clearly corresponds to the reduction of the Cu(I)–GGH complex to Cu amalgam. Simultaneously, a cathodic peak around −0.5 V corresponding to the reduction of Cu(II)–GGH complex to Cu amalgam was observed, probably as the result of partial disproportionation of Cu(I) to Cu and Cu(II). The peaks around −0.2 and −0.3 V are diffusion controlled as confirmed by the linear dependence of their height on the square root of the scan rate. On the contrary, the peak around −0.5 V is adsorption controlled its height being proportional to the scan rate. After exposing the investigated solution to air oxygen, the height of the peak around −0.3 V markedly decreased which confirms that this peak corresponds to the easily oxidisable Cu(I)–GGH complex. The fact that the adsorptive stripping voltammetric peaks of this complex are shifted towards more negative potentials as compared with the cyclic voltammetric peaks confirms its strong adsorption on the surface on the HMDE.

Adsorptive differential pulse cathodic stripping voltammetric determination of trace amounts of glycylglycyl-L-histidine

From the above data it follows that the Cu(I)–GGH complex responsible for the peak around −0.4 V is only formed in the presence of excess of copper(II). These are the conditions required for the adsorptive cathodic stripping determination of trace levels of GGH using adsorptive accumulation of the Cu(I)–GGH complex at a hanging mercury drop electrode. Some accumulation at 0.0 V of Cu(I)–GGH complex was observed using these conditions, but significantly increased accumulation of the species responsible

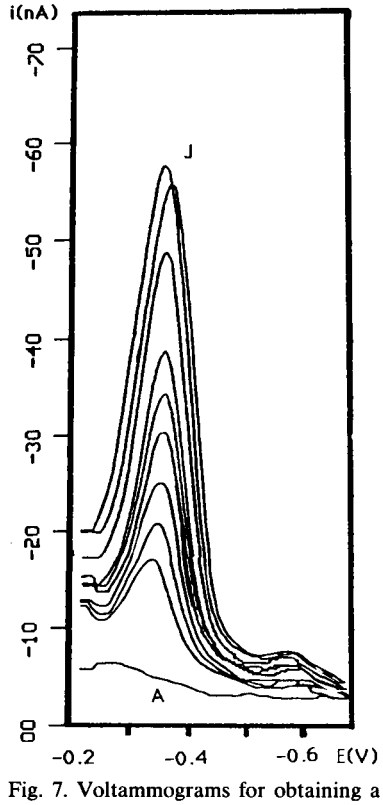

Fig. 7. Voltammograms for obtaining a calibration graph for the determination of GGH. Accumulation potential, −0.20 V. Accumulation time, 2 min. (B–J) [Cu^{2+}]: 1×10^{-6} M. [GGH]: (B) 0; (C) 1; (D) 2; (E) 3; (F) 4; (G) 5; (H) 7; (I) 9; (J) 10×10^{-8} M. pH 8.4.

for the peak around −0.4 V was obtained using accumulation potentials very slightly more positive than its reduction potential. Note that the differential pulse voltammetric peaks are shifted towards more positive potentials ($E_p = -0.32$) as compared with the cyclic voltammetric peaks, in agreement with theory [17].

On the basis of preliminary investigations involving the influence of the accumulation time on the peak height, the following optimum conditions have been found for the determination of GGH in the concentration region $(1–10) \times 10^{-8}$ M: 0.1 M $NaHCO_3$ (pH 8.3) as base electrolyte; 1×10^{-6} M Cu(II); accumulation potential, −0.2 V; accumulation time, 2 min in stirred solution. Calibration graphs obtained in this way were rectilinear with the slope 0.414 A mol^{-1} and intercept 0.5 nA. For the determination of GGH at even lower concentrations, it was necessary to prolong the accumulation time to 3 min in stirred solutions keeping all other conditions as given above. The calibration graph thus obtained was again rectilinear in the concentration range 2–10 $\times 10^{-9}$ M GGH with the slope 1.40 A mol^{-1} and intercept 2.7 nA. The limit of detection calculated as three times the standard deviation of the determination of GGH at 4×10^{-9} M was about 3×10^{-9} M. Coefficients of variation at the 1×10^{-8} M level are typically < 2% (5 determinations). Typical differential pulse cathodic stripping voltammograms for GGH calibration are shown in Fig. 7. The effect of accumulation time on peak height is illustrated by the voltammograms in Fig. 8: saturation of the mercury drop is clearly approaching after 1 min accumulation at this concentration of GGH.

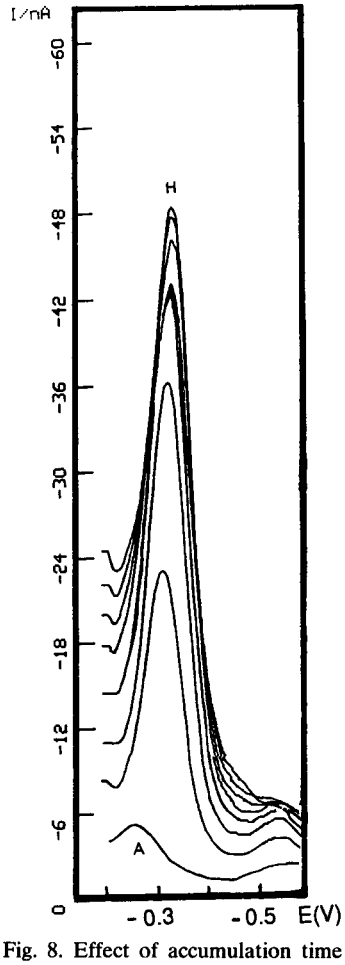

Fig. 8. Effect of accumulation time under the conditions of GGH determination. Accumulation potential, −0.20 V. $[Cu^{2+}]$, 1×10^{-6} M. [GGH], 5×10^{-8} M. Accumulation time: (A) 0; (B) 30; (C) 60; (D) 90; (E) 120; (F) 150; (G) 180; (H) 210 s.

Conclusions

Using adsorptive differential pulse cathodic stripping voltammetry, low levels of glycylglycyl-L-histidine down to 3×10^{-9} M were determined as the copper(I)–GGH complex formed at the HMDE surface. Polarographically active substances that are reduced at potentials around −0.4 V vs. Ag–AgCl reference electrode would interfere. Surface active agents interfere by inhibiting adsorption of the Cu(I)–GGH complex. Chelating agents would interfere by masking the added copper(II), an excess of which over GGH is required for successful determination. Zinc and some other doubly charged ions would interfere by competing with copper(I) for GGH [1,2] and some amino acids could interfere owing to the adsorption of their copper(II) complexes [11]. This lack of selectivity, inherent in most voltammetric techniques, would require a preliminary separation step in the analysis of practical samples. However, the high sensitivity of the proposed method can be successfully exploited for the determination of low concentrations of glycylglycyl-

L-histidine in simple matrices which can be the case in many biologically relevant model studies involving this important tripeptide. Furthermore, the usefulness of adsorptive stripping voltammetry in the investigation of redox processes of biologically important complexes of copper is clearly demonstrated in this paper. Studies are continuing on the cathodic stripping voltammetry of metal complexes of other simple peptides.

FNE thanks EGE University, Turkey, for financial support and leave of absence. J.B. thanks Charles University, Prague, for leave of absence.

REFERENCES

1 R.J. Sundberg and R.B. Martin, Chem. Rev., 74 (1974) 471.
2 H. Sigel and R.B. Martin, Chem. Rev., 82 (1982) 385.
3 H. Aiba, A. Tokoyama and H. Tanaka, Bull. Chem. Soc. Jpn., 47 (1974) 1437.
4 R.P. Agarwal and D.D. Perrin, J. Chem. Soc. Dalton Trans., (1977) 53.
5 T. Sakurai and A. Nakahara, Inorg. Chem., 19 (1980) 847.
6 E. Farkas, I. Sovago, T. Kiss and A. Gergely, J. Chem. Soc. Dalton Trans., (1984) 611.
7 R. Bilewicz, J. Electroanal. Chem. Interfacial Electrochem., 267 (1989) 231.
8 K. Takehara and Y. Ide, Inorg. Chim. Acta, 186 (1991) 73.
9 K. Takehara and Y. Ide, Inorg. Chim. Acta, 183 (1991) 195.
10 F.N. Ertas, J.C. Moreira and A.G. Fogg, Analyst, 116 (1991) 369.
11 J.C. Moreira and A.G. Fogg, Analyst, 115 (1991) 41.
12 G. Svehla, Vogel's Qualitative Inorganic Analysis, Longmans, Singapore, 6th edn., 1979, p. 288.
13 D.G. Davis and W.R. Bordelon, Anal. Lett., 3 (1970) 449.
14 G. Thomas and P.S. Zacharias, Polyhedron, 4 (1985) 811.
15 S. Kitagawa and M. Munakata, Bull. Chem. Soc. Jpn., 59 (1986) 2751.
16 L. Casella and L. Rigoni, J. Chem. Soc., Chem. Commun., (1985) 1668.
17 A.J. Bard and L.R. Faulkner, Electrochemical Methods, Wiley, New York, 1980.

Analytica Chimica Acta, 278 (1993) 53–58
Elsevier Science Publishers B.V., Amsterdam

Catalytic kinetic determination of trace amounts of ascorbic acid with single-sweep oscillopolarography

Zhi-Liang Jiang

Laboratory of Instrumental Analysis, Department of Chemistry, Guangxi Normal University, Guilin (China)

Ai-Hui Liang

Guilin 3rd Pharmaceutical Factory, Guilin (China)

(Received 23rd June 1992; revised manuscript received 13th October 1992)

Abstract

A highly sensitive and selective catalytic method with single-sweep d.c. oscillopolarographic detection is described for the determination of ascorbic acid, based on its activation effect on the slow vanadium(V)-catalysed reaction of BrO_3^- and methyl orange in sulphuric acid medium at 60°C. The oxidation product of methyl orange exhibits a polarographic wave at −0.40 V vs. SCE in the supporting electrolyte of sodium hydroxide, and was chosen as the indicator component for the indicator reaction. A calibration graph between 8 and 160 ng ml^{-1} ascorbic acid was obtained by the fixed-time procedure. The detection limit was 4 ng ml^{-1}. Possible interferences by co-existing substances were examined.

Keywords: Catalytic methods; Kinetic methods; Polarography; Ascorbic acid; Oscillopolarography

Ascorbic acid (vitamin C) is important and widely applied in the food science, medical science and chemical fields, and a highly sensitive, selective, simple, rapid and broadly applicable method for its determination is required.

A number of methods have been reported for the determination of ascorbic acid [1–10]. Titrimetry with 2,6-dichlorophenolindophenol is the most extensively used method. Although this method is rapid, the reagent itself is unstable and must be standardized before use. Moreover, the application of the method to coloured samples is difficult [1]. Several direct or indirect spectrophotometric methods for ascorbic acid have been reported. Some of them are not simple or rapid; the reaction varies with time, acidity and temperature. Some sensitive methods for the determination of ascorbic acid include fluorimetry and liquid chromatography; however, the equipment required is not always widely available. A polarographic method has been proposed, based on the fact that dehydroascorbic acid reacts with phenoniamidine to produce an electroactive species at a dropping mercury electrode (DME), but the detection limit is poor and the procedure is long and inconvenient [10].

Catalytic methods with single-sweep d.c. polarographic detection represent a new branch of catalytic kinetic analysis [11,12]. A method for the determination of several inorganic substances has been reported [11–17], but no method seems to have been developed for organic compounds. This paper describes a sensitive, selective and rapid catalytic method with oscillopolarographic detec-

Correspondence to: Zhi-Liang Jiang, Laboratory of Instrumental Analysis, Department of Chemistry, Guangxi Normal University, Guilin (China).

tion for the accurate determination of ascorbic acid in vitamin C and tomato juice samples, based on its activation effect on the slow vanadium(V)-catalysed reaction of BrO_3^- with methyl orange (MO) in sulphuric acid medium at 60°C. The oxidation product of methyl orange (MO_{ox}), chosen as indicator component, exhibits a good single-sweep oscillopolarographic wave at −0.40 V vs. SCE in a solution of the supporting electrolyte, sodium hydroxide.

EXPERIMENTAL

Apparatus

A Model JP-2 single-sweep oscillopolarograph (Chendu Instrumental Factory) was used for single-sweep d.c. polarographic measurements. The settings were drop time = 7 s, time for drop growth = 5 s, scan rate = 250 mV in the negative direction, scan range = 500 mV and measurement of I_p'' (second-derivative wave). A three-electrode system was employed with a DME as working electrode, SCE as reference electrode and a platinum counter electrode. A thermostated bath was used to control the reaction temperature.

Reagents

A stock standard solution of ascorbic acid (AA) (1 mg ml^{-1}) was prepared by dissolving the reagent in doubly distilled water and then standardizing the solution by iodimetry. A working standard solution was prepared by dilution shortly before use. Solutions of 1.00×10^{-4} M MO, 0.10 M potassium bromate, 0.10 M sulphuric acid and 1.0 g ml^{-1} V(V) were prepared.

Procedure

Into a 25-ml graduated test-tube fitted with a glass stopper, 1.0 ml of 0.10 M sulphuric acid, 0.80 ml of 1.0 μg ml^{-1} V(V) solution, 0.70 ml of 1.00×10^{-4} M MO solution and 12–2400 ng of ascorbic acid were transferred, and the solution was diluted accurately to 10 ml with water. A 2.5 ml volume of 0.010 M potassium bromate solution was added and the mixture was placed in a thermostated bath at 60°C in order to start the reaction. After 10 min, 2.5 ml of 1.0 M sodium hydroxide solution were added and the mixture was cooled with tap water to quench the reaction. A portion of the solution was transferred into a polarographic cell and the second-derivative peak current, $(I_p'')_{a,t}$, was measured. The $(I_p'')_{b,t}$ for the blank was measured in a similar manner.

The $\Delta(I_p'') = (I_p'')_{a,t} - (I_p'')_{b,t}$ values for a range of ascorbic acid concentration were plotted as a function of ascorbic acid concentration to prepare a calibration graph.

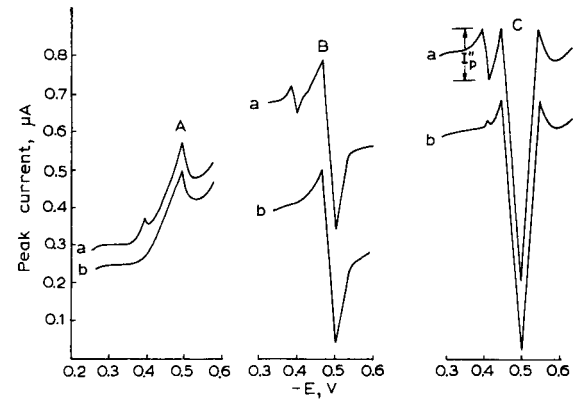

Fig. 1. Oscillopolarograms for MO_{ox} and MO. (a) Activation reaction system (33.3 ng ml^{-1} AA); (b) the blank solution. (A) Normal wave; (B) first derivative; (C) second derivative.

RESULTS AND DISCUSSION

Principle of the determination of ascorbic acid

Under the chosen conditions, ascorbic acid has very strong activation effect on the slow vanadium(V)-catalysed reaction of BrO_3^- with MO in sulphuric acid medium at 60°C, and the oxidation product of MO exhibits a good single-sweep oscillopolarographic wave at −0.40 V vs. SCE in a sodium hydroxide supporting electrolyte. Figure 1 shows the normal, first-derivative and second-derivative waves. The second-derivative wave shape is best and its peak current is largest, so it was chosen for use.

In a separate study, the polarographic behaviour of the product was considered in detail [16]. The influence of BrO_3^-, Br^- and ascorbic acid on the oscillopolarographic measurement of MO_{ox} in sodium hydroxide medium was exam-

ined, and no effect was observed. The indicator reaction is very slow in sodium hydroxide or sulphuric acid medium at room temperature, and can be quenched by cooling with tap water or adding sodium hydroxide. I_p'' becomes constant ≤ 120 min after quenching the reaction as described. The fixed reaction-time procedure appears suitable for the indicator reaction and was chosen for use.

In the analytical solution, the non-catalytic, catalytic and activation reactions take place simultaneously:

$$MO + BrO_3^- \xrightarrow[H^+,\ 60°C]{\text{slow}} MO_{ox} + Br^- \quad (1)$$

$$MO + BrO_3^- \xrightarrow[H^+,\ 60°C]{\text{slow, V(V) cat.}} MO_{ox} + Br^- \quad (2)$$

$$MO + BrO_3^- \xrightarrow[H^+,\ 60°C]{\text{fast, V(V)–AA cat.}} MO_{ox} + Br^- \quad (3)$$

The rate equation for the analytical solution may be

$$d[MO_{ox}]/dt = k_u + k_c + k_a[AA] \quad (4)$$

$$\text{or } d[MO_{ox}] = (k_u + k_c + k_a[AA])\, dt \quad (5)$$

where k_u, k_c and k_a are the apparent rate constants of the uncatalysed, catalytic and activation reactions, respectively, for a solution containing a fixed concentration of MO, potassium bromate, V(V) and sulphuric acid. Integration of Eqn. 5 gives

$$[MO_{ox}]_{a,t} = (k_u + k_c + k_a[AA])t + [MO_{ox}]_{a,0} \quad (6)$$

where $[MO_{ox}]_{a,t}$ and $[MO_{ox}]_{a,0}$ are the concentrations of MO_{ox} in the analytical solution at times t and 0, respectively. If [AA] = 0, then Eqn. 6 has the form

$$[MO_{ox}]_{b,t} = (k_u + k_c)t + [MO_{ox}]_{b,0} \quad (7)$$

where $[MO_{ox}]_{b,t}$ and $[MO_{ox}]_{b,0}$ are the concentrations of MO_{ox} in the blank solution at reaction time t and 0 min, respectively. As $[MO_{ox}]_{b,0}$ is equal to $[MO_{ox}]_{a,0}$, Eqns. 6 and 7 are combined to obtain

$$[MO_{ox}]_{a,t} - [MO_{ox}]_{b,t} = (k_a t)[AA] \quad (8)$$

According to the Randles–Sevčik equation, $I_p'' = k'[MO_{ox}]$, where k' is a constant, and Eqn. 8 can be rewritten as

$$\Delta(I_p'') = (I_p'')_{a,t} - (I_p'')_{b,t} = (k' k_a t)[AA] \quad (9)$$

Equation 9 demonstrates that $\Delta(I_p'')$ is proportional to the ascorbic acid concentration, with the other variables and the reaction time and temperature held constant for a given system. This is in agreement with the experimental results.

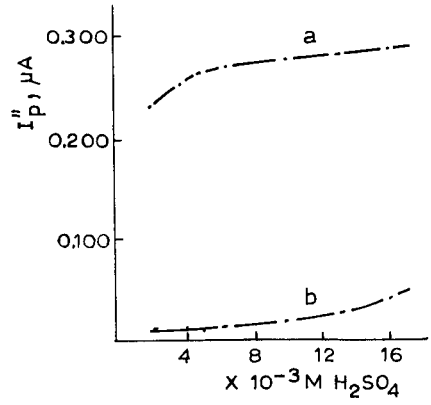

Fig. 2. Effect of H_2SO_4 concentration. (a) Analytical solution (66.7 ng ml^{-1} AA); (b) blank solution. For other conditions, see text.

Effect of variables

The effects of the concentrations of sulphuric acid, potassium bromate, MO and V(V) and the reaction time and temperature on the $(I_p'')_{a,t}$ and

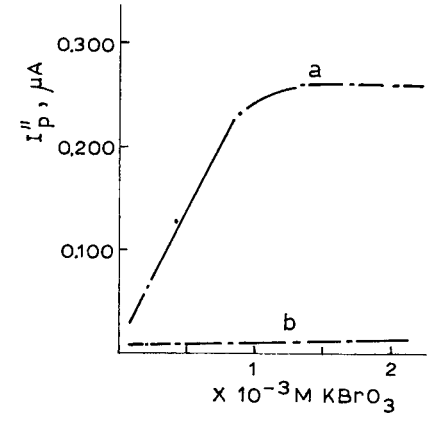

Fig. 3. Effect of $KBrO_3$ concentration. (a) Analytical solution (66.7 ng ml^{-1} AA); (b) blank solution.

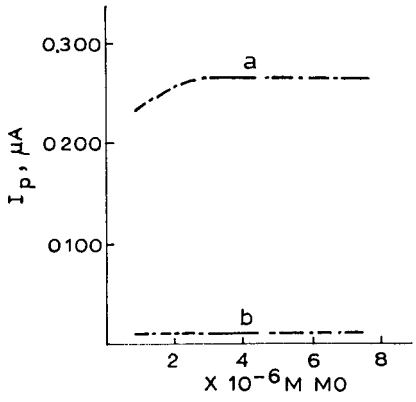

Fig. 4. Effect of MO concentration. (a) Analytical solution (66.7 ng ml^{-1} AA); (b) blank solution.

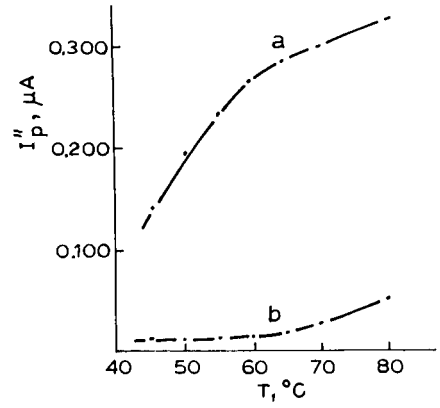

Fig. 6. Effect of reaction temperature. (a) Analytical solution (66.7 ng ml^{-1} AA); (b) blank solution.

$(I''_p)_{b,t}$ were investigated. In general, the conditions chosen were so as to make $(I''_p)_{a,t}$ larger and $(I''_p)_{b,t}$ smaller.

Several reaction media, including sulphuric acid, hydrochloric acid and perchloric acid, were tested. The results showed that sulphuric acid is the best. Figure 2 shows the relationship between I''_p and sulphuric acid concentration. A 6.7×10^{-3} M sulphuric acid concentration was selected as optimum.

$(I''_p)_{a,t}$ increases considerably with increasing concentration of potassium bromate until the latter reaches 1.3×10^{-3} M, then $(I''_p)_{a,t}$ changed only negligibly with further increase in concentration (Fig. 3). A concentration of 1.67×10^{-3} M was adopted.

The effect of MO concentration on I''_p is shown in Fig. 4. $(I''_p)_{a,t}$ and $(I''_p)_{b,t}$ are constant when the MO concentration is greater than about 3×10^{-6} M. An MO concentration of 4.7×10^{-6} M was adopted.

Figure 5 shows that $(I''_p)_{a,t}$ increases linearly with increasing concentration of V(V) up to 40 ng ml^{-1}; although $(I''_p)_{b,t}$ also increases linearly with increasing concentration of V(V), the slope is

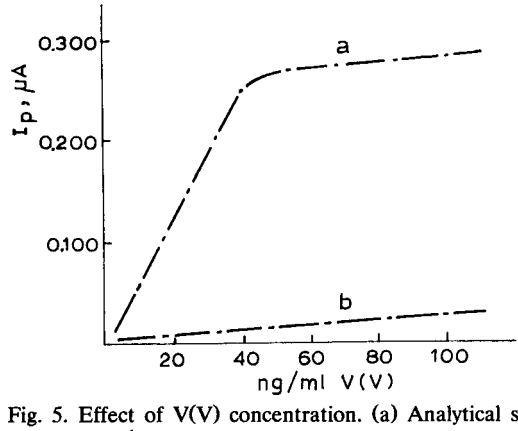

Fig. 5. Effect of V(V) concentration. (a) Analytical solution (66.7 ng ml^{-1} AA); (b) blank solution.

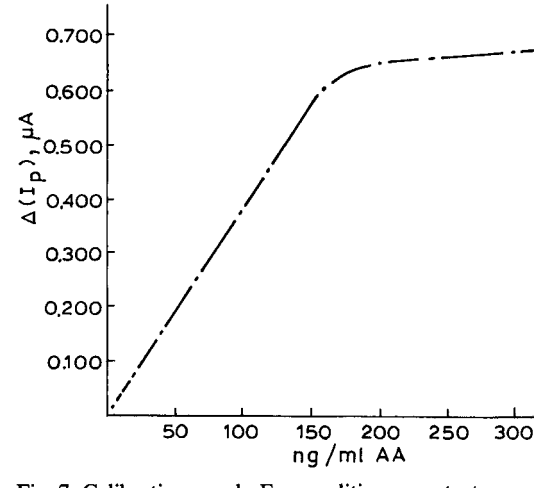

Fig. 7. Calibration graph. For conditions, see text.

TABLE 1

Influence of foreign substances on the determination of ascorbic acid (66.7 ng ml^{-1})

Tolerance limit, [foreign substance]/[AA]	Foreign substance added
2.5×10^3	Ca(II), Mg(II), Zn(II), NH_4^+, SO_4^{2-}, Cl^-
1.5×10^3	Al(III), PO_4^{3-}, SiO_3^{2-}
1.0×10^3	Starch
6.0×10^2	Hydroxylammonium chloride, acetate
2.0×10^2	SO_3^{2-}, urea, sucrose, Fe(III)
80	Glucose, nicotic acid, glutamic acid, aspartic acid, uric acid
20	Vitamin B_1, adipic acid, tartaric acid
10	Oxalic acid, citric acid

very small. A concentration of 53.3 ng ml^{-1} V(V) was selected as the optimum.

The effects of reaction temperature and time on I_p'' were also considered. A reaction temperature of 60°C, which gives a lower blank value, was chosen (Fig. 6). A fixed reaction time of 10 min was selected for use, giving a good compromise between high sensitivity and short analysis time.

Under the conditions chosen, the relationship between $\Delta(I_p'')$ and the concentration of ascorbic acid is as shown in Fig. 7. A linear calibration graph was obtained by the fixed-time procedure at concentrations from 8 to 160 ng ml^{-1}. The detection limit is 4 ng ml^{-1}. The relative standard deviations for 33.3, 66.7 and 100 ng ml^{-1} AA samples were 3.7%, 3.1% and 2.4%, respectively (ten replicates).

Effect of foreign substances

The influence of foreign substances on the catalytic analysis of a 66.7 ng ml^{-1} ascorbic acid sample was studied. The results are given in Table 1 and indicate that the method has good selectivity. The tolerance limit is that ratio giving not more than a ±6% error.

Analysis of real samples

The proposed catalytic method was applied to the determination of ascorbic acid in vitamin C injection liquid and tomato juice samples, which

TABLE 2

Analysis results and recovery of added AA

Sample	AA added (μg)	AA found (μg)	Recovery (%)	Content (mg ml^{-1})	
				Proposed method	Reference method [18]
Vitamin C	–	0.246		246	
injection liquid	–	0.250		250	255
	–	0.250		250	
	0.200	0.450	100		
	0.400	0.645	99.0		
	1.00	1.24	99.1		
Tomato juice	–	0.120		0.120	
	–	0.125		0.125	0.128
	–	0.127		0.127	
	0.100	0.220	96.0		
	0.200	0.320	98.0		
	0.400	0.532	102		

were also analysed by a reference method [18]. The recoveries of standard additions of ascorbic acid to each sample were also measured. The results are given in Table 2.

REFERENCES

1 L.J. Harris and S.N. Ray, Biochem. J., 27 (1933) 303.
2 M.M. Aly, Anal. Chim. Acta, 106 (1979) 379.
3 M. Eldawy, A.S. Tawfik and S. Elshabouri, Anal. Chem., 47 (1975) 461.
4 M. Schmall, C.W. Pifer and E.G. Wollish, Anal. Chem., 25 (1955) 1486.
5 M.J. Deutsch and C.E. Weeks, J. Assoc. Off. Anal. Chem., 48 (1965) 1248.
6 R.C. Williams, D.R. Baker and J.A. Schmidt, J. Chromatogr. Sci., 11 (1973) 618.
7 F. Salinas and T. Galeano Diaz, Analyst, 113 (1988) 1657.
8 E.S. Elnenaey and R. Soliman, Talanta, 26 (1979) 1164.
9 A. Besada, Talanta, 34 (1988) 731.
10 H.-K. Wang, Shipin Jianyan Yu Fenxi, Qianggongye Publishing House, Beijing, 1989, p. 103.
11 Z.-L. Jiang and B. Lu, Fenxi Huaxue, 19 (1991) 339.
12 Z.-L. Jiang, Guijinshu, 12 (1991) 24.
13 C.-Z. Qin, X.-J. Li and Z.-L. Jiang, Chin. Chem. Lett., 2 (1991) 641.
14 Z.-L. Jiang and A.-H. Liang, Talanta, 37 (1990) 1077.
15 Z.-L. Jiang, Huaxue Xuebao, 50 (1992) 484.
16 Z.-L. Jiang, H.-C. Qin and D.-Q. Wu, Talanta, 39 (1992) 1239.
17 Z.-L. Jiang, Talanta, 38 (1991) 621.
18 H.-K. Wang, Shipin Jianyan Yu Fenxi, Qianggongye Publishing House, Beijing, 1989, p. 100.

Analytica Chimica Acta, 278 (1993) 59–70
Elsevier Science Publishers B.V., Amsterdam

Electrochemical kinetic simulations of mixed diffusion/homogeneous reaction problems by the Saul'yev finite difference algorithms

Lesław K. Bieniasz [1] and Dieter Britz

Kemisk Institut, Aarhus Universitet, Langelandsgade 140, 8000 Aarhus C (Denmark)

(Received 6th October 1992; revised manuscript received 18th December 1992)

Abstract

The validity of the Saul'yev finite difference integration schemes for the simulation of electrokinetic diffusion/homogeneous reaction problems has been investigated. Respective algorithms have been formulated for typical examples involving first and second order homogeneous reactions. Their numerical properties have been examined in calculations and compared with those of the classic explicit, second order Runge–Kutta and Crank–Nicolson methods. The averaged ⟨LR,RL⟩ Saul'yev algorithm has been found to be especially attractive, showing efficiency comparable with the Crank–Nicolson method but at lower programming effort. The general, method-oriented formulation of Saul'yev algorithms is also presented.

Keywords: Kinetic methods; Electrochemical kinetic simulations; Saul'yev finite difference algorithms

The Saul'yev method of finite difference integration [1,2] has recently been proposed for the solution of kinetic partial differential equations (PDEs) in electroanalytical chemistry [3–7]. The examination of several simple pure diffusion kinetic problems showed that certain combinations of the basic variants (LR or RL) of this method, such as the alternated LR–RL or averaged ⟨LR,RL⟩ algorithms, have a speed and accuracy comparable with those of the implicit Crank–Nicolson technique, but are significantly easier to implement, as they do not require solution of large systems of simultaneous equations for the concentrations of reacting species at new time levels. In addition, the method is unconditionally stable (in the von Neumann sense [2]) when pure diffusion equations are considered [1,2].

Taking into account these results, the examination of the validity of the Saul'yev method for the simulation of more complicated electrokinetic phenomena appears to be important. This refers in particular to the mixed diffusion/homogeneous reaction problems, which are frequent in electroanalytical chemistry. The investigation of the Saul'yev method in this respect becomes especially interesting, in view of the matrix solution technique [8], which allows the implicit finite difference methods to be successfully applied to solve PDEs coupled by homogeneous kinetic terms. This was not feasible until now with the

Correspondence to: D. Britz, Kemisk Institut, Aarhus Universitet, Langelandsgade 140, 8000 Aarhus C (Denmark).
[1] On leave from the Institute of Physical Chemistry of the Polish Academy of Sciences, Molten Salts Laboratory, ul. Zagrody 13, 30-318 Cracow (Poland).

traditional fully implicit or Crank–Nicolson algorithms [3]. The technique [8] requires extensive matrix operations, however, significantly increasing the computational effort. Therefore, it is interesting to compare its efficiency with that of the simpler Saul'yev method.

The unconditional stability of the Saul'yev method in the presence of homogeneous kinetic terms has been confirmed theoretically in the previous paper [9], using the von Neumann method. Therefore, in the present work the Saul'yev algorithms are formulated for several example kinetic problems and their numerical properties are compared with those for the classic explicit [2,3,10], Runge–Kutta second order [3,11] and Crank–Nicolson [2,3,12] algorithms. As an example of the first order homogeneous kinetics the standard catalytic mechanism [13] has been selected, which represents features typical for the considered class of problems (formation of a reaction layer) and for which analytical solutions are available, which simplifies the accuracy comparisons. As an example of the second order homogeneous kinetics the Pedersen and Svensmark system [3,14] has been chosen. Semi-infinite diffusion conditions and planar electrodes have been assumed in both cases.

ALGORITHMS

The algorithms for electrochemical kinetic simulations can be formulated using the traditional, problem-oriented approach or the recently proposed method-oriented one [15]. Both of them were used in the present work. Below, the traditional formulation for the selected example electrode reaction mechanisms is outlined. The method-oriented formulation is presented in the Appendix. This formulation yields algorithms of a general, problem-independent structure and multiple potential applications to electrokinetic phenomena [15]. Hence, the Appendix can be useful for those readers who will decide to apply the Saul'yev method to problems other than examples discussed below. This refers either to the use of the program developed in Ref. 15 or to the preparation of other programs.

The catalytic mechanism, traditional formulation

The standard pseudo-first order catalytic mechanism involves formally two species A and B:

$$\begin{aligned} &A + e^- \underset{\kappa_b}{\overset{\kappa_f}{\rightleftharpoons}} B \\ &B \underset{\kappa_b}{\overset{}{\rightleftharpoons}} A \end{aligned} \qquad (1)$$

for which the kinetic PDEs are:

$$\frac{\partial c_A(x,t)}{\partial t} = D\frac{\partial^2 c_A(x,t)}{\partial x^2} - \kappa_b c_A(x,t) + \kappa_f c_B(x,t) \qquad (2)$$

$$\frac{\partial c_B(x,t)}{\partial t} = D\frac{\partial^2 c_B(x,t)}{\partial x^2} + \kappa_b c_A(x,t) - \kappa_f c_B(x,t) \qquad (3)$$

where $c_A(x,t)$ and $c_B(x,t)$ denote concentrations of the species A and B, respectively, dependent on space coordinate x and time t. Equal diffusion coefficients D have been assumed for simplicity. Taking constant integration steps h and δt for the space and time coordinates and the "point" formulation of the finite difference algorithms [3], the discrete representation of the Eqns. 2 and 3 in the case of the Saul'yev LR (left-right) method can be written:

$$c'_{A_i} - c_{A_i} = \lambda(c'_{A_{i-1}} - c'_{A_i} - c_{A_i} + c_{A_{i+1}}) - \xi_b\left(\frac{c_{A_i} + c'_{A_i}}{2}\right) + \xi_f\left(\frac{c_{B_i} + c'_{B_i}}{2}\right) \qquad (4)$$

$$c'_{B_i} - c_{B_i} = \lambda(c'_{B_{i-1}} - c'_{B_i} - c_{B_i} + c_{B_{i+1}}) + \xi_b\left(\frac{c_{A_i} + c'_{A_i}}{2}\right) - \xi_f\left(\frac{c_{B_i} + c'_{B_i}}{2}\right) \qquad (5)$$

where $\lambda = D\delta t/h^2$, $\xi_b = \kappa_b \delta t$ and $\xi_f = \kappa_f \delta t$. The subscripts refer to the discrete positions x_i along the x axis, whereas a new time level is denoted with a prime, according to the convention from Ref. 3. The kinetic terms in Eqns. 4 and 5 have been discretized in a way which assures an unconditionally λ-stable approximation of Eqns. 2 and 3 [9]. Other representations of these terms are possible but they lead to conditionally stable approximations only [9].

For any discrete space point x_i the unknown variables in Eqns. 4 and 5 are c'_{A_i} and c'_{B_i}. These variables occur in both equations simultaneously which necessitates a solution of this linear system of equations. The situation looks better, however, than in the case of fully implicit or Crank–Nicolson techniques, where unknown concentrations for all the points x_i occur simultaneously in the equation set. Using Saul'yev the unknowns correspond to the single point x_i. In the case of relatively simple mechanisms, such as the two considered in the present work, it is reasonable to solve Eqns. like 4 and 5 analytically for c'_{A_i} and c'_{B_i} and use the obtained formulas for the calculations at every point x_i. In the method-oriented approach to be considered in the Appendix, where any complex mechanisms may be expected, it is easier to solve the set 4–5 numerically at every point x_i, although this is less efficient.

Thus, following the first approach, one gets from Eqns. 4 and 5 in the matrix notation:

$$\mathbf{c}'_i = \mathbf{A}_1(\mathbf{c}'_{i-1} + \mathbf{c}_{i+1}) + \mathbf{A}_2\mathbf{c}_i \tag{6}$$

where $\mathbf{c}_i$, $\mathbf{c}_{i+1}$, etc. are vectors containing concentrations of the species A and B, i.e.:

$$\mathbf{c}_i = [c_{A_i}, c_{B_i}]^T \tag{7}$$

etc. and $\mathbf{A}_1$ and $\mathbf{A}_2$ denote the matrices:

$$\mathbf{A}_1 = \frac{1}{(1+\lambda)[2(1+\lambda)+\xi]} \times \begin{bmatrix} \lambda[2(1+\lambda)+\xi_f] & \lambda\xi_f \\ \lambda\xi_b & \lambda[2(1+\lambda)+\xi_b] \end{bmatrix} \tag{8}$$

$$\mathbf{A}_2 = \frac{1}{(1+\lambda)[2(1+\lambda)+\xi]} \begin{bmatrix} e_1 & 2\xi_f \\ 2\xi_b & e_2 \end{bmatrix} \tag{9}$$

with $\xi = \xi_f + \xi_b$, and the matrix element expressions $e_1 = (1-\lambda)[2(1+\lambda)+\xi_f-(1+\lambda)\xi_b$ and $e_2 = (1-\lambda)[2(1+\lambda)+\xi_b-(1+\lambda)\xi_f$.

Equation 6 is the matrix counterpart of the scalar Eqn. 3 in Ref. 6. When $\xi_f = \xi_b = 0$ the non-diagonal elements of the matrices $\mathbf{A}_1$ and $\mathbf{A}_2$ disappear and Eqn. 6 decomposes into two independent scalar equations of the form of Eqn. 3 from Ref. 6. This formal analogy to the pure diffusion problems allows the calculation of the concentration vectors $\mathbf{c}'_1, \mathbf{c}'_2, \mathbf{c}'_3, \cdots$ in a left-right scan by a successive application of the matrices $\mathbf{A}_1$ and $\mathbf{A}_2$ to the previously determined concentration vectors $\mathbf{c}_1, \mathbf{c}_2, \mathbf{c}_3, \cdots$ and $\mathbf{c}'_0$. Therefore, the method can be treated as an explicit one. The matrices $\mathbf{A}_1$ and $\mathbf{A}_2$ contain only constant elements which depend neither on x, t nor on concentrations. Therefore, these matrices can be precalculated and stored for further use, before the iterations along the time coordinate are started.

The right-left variant (RL) of the method is analogous. In that case one can write:

$$\mathbf{c}'_i = \mathbf{A}_1(\mathbf{c}_{i-1} + \mathbf{c}'_{i+1}) + \mathbf{A}_2\mathbf{c}_i \tag{10}$$

where all the concentrations $\mathbf{c}_{i-1}$, $\mathbf{c}'_{i+1}$ and $\mathbf{c}_i$ are known at the moment when $\mathbf{c}'_i$ is calculated.

The alternated LR–RL algorithm requires that Eqns. 6 and 10 be used alternately at successive time levels. In the averaged ⟨LR,RL⟩ algorithm one calculates the concentrations $\mathbf{c}'_i$ in an LR scan and stores them in a separate memory area, without modifying the concentrations $\mathbf{c}_i$ from the previous time level. The RL scan is then performed, using old concentrations $\mathbf{c}_i$ and the results for $\mathbf{c}'_i$, obtained in both cases, are averaged. This roughly doubles the necessary memory as compared with the LR–RL algorithm.

The analogy of the Eqns. 6 and 10 with the scalar case [6] extends further to the calculation of boundary concentrations at $x = 0$. If the boundary conditions at $x = 0$ involve spatial derivatives, one is advised to use the general n-point approximations for the gradients [3, p. 63]. One should also perform implicit calculations of $\mathbf{c}'_0$, as this assures a better accuracy of the results [16, 3]. This is not a problem in the RL case, since $\mathbf{c}'_1, \mathbf{c}'_2, \cdots$ are already determined when it comes to the calculation of $\mathbf{c}'_0$ [6]. However, in the LR case the concentrations $\mathbf{c}'_1, \mathbf{c}'_2, \cdots$ etc., needed for the gradient approximations must be determined together with $\mathbf{c}'_0$. This problem can be overcome by introducing the quantities $\mathbf{v}_i$, $\mathbf{u}_i$, $\mathbf{P}$ and $\mathbf{Q}$ [6]. In the present case $\mathbf{v}_i$ is a matrix:

$$\mathbf{v}_i = \begin{cases} \mathbf{I} & \text{for } i = 0 \\ \mathbf{A}_1^i & \text{for } i = 1, 2, \ldots, n-1 \end{cases} \tag{11}$$

and $\mathbf{u}_i$ is a vector:

$$\mathbf{u}_i \begin{cases} \mathbf{0} \quad \text{for } i = 0 \\ \mathbf{A}_1(\mathbf{u}_{i-1} + \mathbf{c}_{i+1}) + \mathbf{A}_2\mathbf{c}_i \\ \qquad \text{for } i = 1, 2, \ldots, n-1 \end{cases} \tag{12}$$

where $\mathbf{I}$ denotes a unit matrix and $\mathbf{0}$ is a zero vector. Moreover, $\mathbf{Q}$ is a matrix:

$$\mathbf{Q} = \frac{1}{a_n h} \sum_{i=0}^{n-1} b_i \mathbf{v}_i \tag{13}$$

and $\mathbf{P}$ is a vector:

$$\mathbf{P} = \frac{1}{a_n h} \sum_{i=0}^{n-1} b_i \mathbf{u}_i \tag{14}$$

where a_n and b_i are scalar coefficients used for n-point gradient approximations [3, p. 66]. Finally, the implicit value $\mathbf{g}'$ of the gradient at $x = 0$ can be expressed in the vector notation as a function of the concentrations $\mathbf{c}'_0$:

$$\mathbf{g}' = \mathbf{P} + \mathbf{Q}\mathbf{c}'_0 \tag{15}$$

where $\mathbf{g}' = [g'_A, g'_B]^T$. The unknown quantities in Eqn. 15 can be $\mathbf{g}'$ and $\mathbf{c}'_0$. They can be determined by combining Eqn. 15 with equations which represent boundary conditions at $x = 0$. Equations 11–15 correspond to the scalar Eqns. 7 and 8 and other Eqns. in p. 89 in Ref. 6.

The Pedersen and Svensmark mechanism, traditional formulation

In a simplified version of this mechanism [14;3, p. 146] four species: A, B, C and D are involved:

$$\left.\begin{array}{lll} A + e^- \rightleftharpoons B & & \\ B + C \longrightarrow A + D & \text{(SET)} & \\ B + D \longrightarrow \text{products} & \text{(fast coupling)} & \end{array}\right\} \tag{16}$$

Only the first three of them require simulation, so that the kinetic PDEs are [14]:

$$\frac{\partial c_A(x,t)}{\partial t} = D\frac{\partial^2 c_A(x,t)}{\partial x^2} + \kappa c_B(x,t)c_C(x,t) \tag{17}$$

$$\frac{\partial c_B(x,t)}{\partial t} = D\frac{\partial^2 c_B(x,t)}{\partial x^2} - 2\kappa c_B(x,t)c_C(x,t) \tag{18}$$

$$\frac{\partial c_C(x,t)}{\partial t} = D\frac{\partial^2 c_C(x,t)}{\partial x^2} - \kappa c_B(x,t)c_C(x,t) \tag{19}$$

where κ is formally a rate constant for the second order homogeneous reaction and equal diffusion coefficients have been assumed. Replacing second order terms with appropriate linearized expressions [3, p. 150], the discrete equations for the Saul'yev LR method can be written:

$$c'_{A_i} - c_{A_i} = \lambda(c'_{A_{i-1}} - c'_{A_i} - c_{A_i} + c_{A_{i+1}}) + \xi\left(\frac{c_{B_i}c'_{C_i} + c'_{B_i}c_{C_i}}{2}\right) \tag{20}$$

$$c'_{B_i} - c_{B_i} = \lambda(c'_{B_{i-1}} - c'_{B_i} - c_{B_i} + c_{B_{i+1}}) - 2\xi\left(\frac{c_{B_i}c'_{C_i} + c'_{B_i}c_{C_i}}{2}\right) \tag{21}$$

$$c'_{C_i} - c_{C_i} = \lambda(c'_{C_{i-1}} - c'_{C_i} - c_{C_i} + c_{C_{i+1}}) - \xi\left(\frac{c_{B_i}c'_{C_i} + c'_{B_i}c_{C_i}}{2}\right) \tag{22}$$

where $\xi = \kappa\delta t$. After introducing coefficients: $a_1 = (1+\lambda)^2$, $a_2 = \xi(1+\lambda)/2$, $a_3 = \xi(1+\lambda)$, $a_4 = \xi\lambda/2$, $a_5 = \lambda(1+\lambda)$, $a_6 = \xi\lambda$, $a_7 = \xi(1-\lambda)/2$, $a_8 = \xi(1-\lambda)$, $a_9 = 1-\lambda^2$ and denoting $d = a_1 + a_2c_{B_i} + a_3c_{C_i}$, the matrices $\mathbf{A}_1$ and $\mathbf{A}_2$ corresponding to Eqns. 20–22 can be written:

$$\mathbf{A}_{1_i} = \begin{bmatrix} \dfrac{\lambda}{1+\lambda} & a_4\dfrac{c_{C_i}}{d} & a_4\dfrac{c_{B_i}}{d} \\ 0 & \dfrac{a_5 + a_4c_{B_i}}{d} & -a_6\dfrac{c_{B_i}}{d} \\ 0 & -a_4\dfrac{c_{C_i}}{d} & \dfrac{a_5 + a_6c_{C_i}}{d} \end{bmatrix} \tag{23}$$

$$\mathbf{A}_{2_i} = \begin{bmatrix} \dfrac{1-\lambda}{1+\lambda} & a_7\dfrac{c_{C_i}}{d} & a_7\dfrac{c_{B_i}}{d} \\ 0 & \dfrac{a_9 + a_7c_{B_i}}{d} & -a_8\dfrac{c_{B_i}}{d} \\ 0 & -a_7\dfrac{c_{C_i}}{d} & \dfrac{a_9 + a_8c_{C_i}}{d} \end{bmatrix} \tag{24}$$

The index "i" has been added to the symbols $\mathbf{A}_1$ and $\mathbf{A}_2$, since this time the matrices depend on the concentrations corresponding to various points x_i at a previous time level. The matrices

23 and 24 can be used for calculations based on Eqns. 6 and 10–15, with the complication that instead of the expression $\mathbf{A}_1^i$ in Eqn. 11 one has a product $\mathbf{A}_{1_i}\mathbf{A}_{1_{i-1}}\cdots\mathbf{A}_{1_1}$. One also has to recalculate the second and third columns of these matrices at every time step and every point x_i. In the ⟨LR,RL⟩ algorithm the matrices 23 and 24 can be calculated on the LR scans and stored to be used for the second time in the RL scan. This reduces the computational time at the expense of additional occupied memory space.

RESULTS AND DISCUSSION

Computations

The computer programs corresponding to the above algorithms (traditional formulation) as well as relevant programs for the classic explicit (EX), 2nd order Runge–Kutta (RK2) and Crank–Nicolson methods with Rudolph's matrix solution technique [8] (CN/R) have been written in the "C" language [17] and compiled using the TURBO C++ compiler (v. 1.01) for an IBM-compatible PC. Most of the calculations have been performed using an IBM compatible PC with an Intel 80386 processor and 80387 math coprocessor, operating at 25 MHz, under MS DOS. Some of the calculations have also been performed on a Digital Equipment VAX 6210 computer, operating under VMS, using Fortran 77.

In the case of the catalytic mechanism 1 two kinds of transients have been simulated: the potential-step transient (CA) under limiting current conditions and the linear potential scan voltammetric transient (LSV), for which the non-dimensional starting potential [3, p. 147] of +6.5 was taken. The reversibility of both reactions in 1 has been assumed in the programs. However, $\kappa_b = 0$ was used as input value in all the simulations. In the CA calculations the non-dimensional time $T = t/\tau$ has been introduced, where τ is an observation time [3, p. 17]. Consequently, the non-dimensional rate constant was $K_f = \kappa_f\tau$. The determined quantity was $G_A/G_A^{anal} - 1$, where G_A was the calculated dimensionless concentration gradient of species A at the electrode and G_A^{anal} was the analytical expression for this gradient, given by Delahay and Stiehl [18]:

$$G_A^{anal} = (\pi T)^{-1/2}\exp(-K_f T) + K_f^{1/2}\mathrm{erf}\left((K_f T)^{1/2}\right) \quad (25)$$

The value of $\log\left|G_A/G_A^{anal} - 1\right|$ corresponding to the non-dimensional time $T = 1$ was considered as a measure of the error involved in the simulations, in a way analogous to that in Ref. 6. The concentrations were normalized by the bulk concentration c_A^0 of A. Thus, the initial concentration values of A were equal to 1 for all the space points except for $x = 0$, where $c_{A_0} = 0$ was assumed. Such a formulation of initial conditions assures a better accuracy in the simulation of potential-step transients [19]. In the LSV calculations the non-dimensional time was $T = Fvt/RT$, as usually defined in the theory of the LSV method [13], where v is the potential scan rate and F, R and T have their usual meaning. Consequently, the non-dimensional rate constant was $K_f = \kappa_f/(Fv/RT)$. As the LSV curves for the catalytic mechanism do not exhibit a peak (except at small κ_f) it was not possible to traditionally discuss the accuracy of the calculations in terms of the peak parameters obtained by various methods. Instead, the value of $\log\left|G_A/G_A^{anal} - 1\right|$ corresponding to the non-dimensional time $T = 16$ was selected as a measure of the error. It was assumed arbitrarily that at this high T value the stationary state, characteristic for the catalytic mechanism [20] is already reached, at least when $K_f \geq 1$, so that, according to [20] one has:

$$G_A^{anal} = K_f^{1/2} \quad (26)$$

In the case of the mechanism 16 the LSV curves were simulated only, using analogous normalizations as for the catalytic mechanism, taking $K = 1$ and the ratio of bulk concentrations $c_C^0/c_A^0 = 3$. The reversible electrode reaction has been assumed. The initial non-dimensional potential [3, p. 49] of +8 was used. Under these conditions the simulated curves exhibited a single peak. The precise calculations reveal [21] that the peak parameters are: $T_p^{acc} = 8.6301$ and $\chi_p^{acc} = 0.4374$, where χ is a non-dimensional current function, defined in a usual way [13]. Therefore, the quan-

tities: $\log|T_p/T_p^{acc}-1|$ and $\log|\chi_p/\chi_p^{acc}-1|$ where T_p and χ_p are simulated peak parameters were used as measures of the error involved in the calculations. These peak parameters were calculated by parabolic interpolation between the three simulated points around the peak.

The non-dimensional space coordinate $X = x(D\tau)^{-1/2}$ was assumed in all the CA calculations. Consequently the non-dimensional space integration step was $H = h(D\tau)^{-1/2}$. The necessary number of integration steps along the x coordinate was calculated, assuming a simulation layer of thickness $6T_{max}^{1/2}$ or $3T_{max}^{1/2}$ for the mechanisms 1 and 16, respectively. The maximal time interval in which the transients were simulated was: $T_{max} = 1$ for the CA transient and mechanism 1, $T_{max} = 16$ for the LSV transient and mechanism 1 and $T_{max} = 10$ for the LSV transient and mechanism 16. In the LSV case $X = x(DRT/\upsilon F)^{-1/2}$ and $H = h(DRT/\upsilon F)^{-1/2}$ were used.

Selection of the parameter λ

The main problem associated with the use of the Saul'yev method is that the parameter λ cannot be too high. Although the method is unconditionally stable (in the von Neumann sense), the accuracy of the solution deteriorates with increasing λ. Also oscillations are anticipated [9]. These properties of the Saul'yev method have been reported in the non-electrochemical literature [22] and the previous applications of this method to electrochemical simulations are consistent with them (see Fig. 3 in Ref. 5 and Figs. 7 and 12 in Ref. 7), although this fact has not been discussed. The above properties apparently result from the asymmetry of the Saul'yev difference formulas [1] (the greater λ the more pronounced is this asymmetry) and can be expressed quantitatively by considering the local truncation error. In the pure diffusion case the principal part of this error is of the order of $\mathcal{O}(\delta T/H - \delta T^2 - H^2)$ and $\mathcal{O}(-\delta T/H - \delta T^2 - H^2)$ for the LR and RL variants of the method, respectively [2,22,23]. The first term becomes dominant when λ increases at constant δT, since H then decreases. On the other hand, when λ decreases, the remaining terms become more important. Intuitively, one

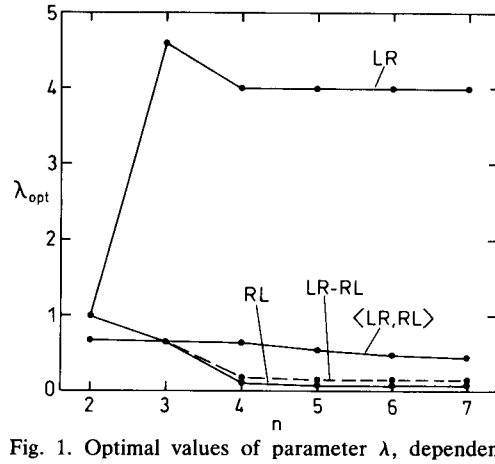

Fig. 1. Optimal values of parameter λ, dependent on the order n of the gradient approximation at $x = 0$. The data refer to the CA simulation in the pure diffusion case.

can expect some compensation or minimization of all these terms to occur for certain λ. In fact, the results [4,5,7] indicate that the error of the simulated current can be significantly minimized or even reduced to zero if a proper, optimal value of λ is chosen. For pure diffusion problems the optimal λ value seems to be independent of δT (see Figs. 7 and 12 in Ref. 7). However, it depends on the order of gradient approximation at $x = 0$ [3, p. 63], as shown in Fig. 1 for the pure diffusion case. In further calculations the five-point gradient approximation was used. This selection corresponds to the plateau of the curves from Fig. 1 for $n > 4$ which allows the neglect of the influence of n on the optimal λ.

The use of the LR–RL or ⟨LR,RL⟩ algorithms results in a reduction of the truncation error, since the term proportional to $\delta T/H$ is cancelled [2,4–7,22,23]. However, according to Lapidus and Pinder [2], the remaining truncation error still has a form $\mathcal{O}((\delta T/H)^2 + \delta T^2 + H^2)$, i.e., the error growth with λ is also expected in that case.

In the presence of homogeneous reactions the optimal λ value depends additionally on the rate constants for these reactions and generally on the considered problem. This can be seen in Fig. 2, where dependencies of the error on λ are presented for various rate constants K_f of the homogeneous reaction in mechanism 1, in the case of

the ⟨LR,RL⟩ algorithm. A similar figure was also obtained for the LR–RL scheme. The position of the error minimum depends on K_f. For $K_f = 10$ the error diminishes with increasing λ in Fig. 2. This does not mean, however, that large λ values are optimal. In that case the errors registered for $T < 1$ increased considerably.

Another difficulty associated with the use of high λ values is that the error reduction is not perfect for the LR–RL scheme, since the terms of the truncation error correspond to different time levels and they do not entirely cancel. This leads to oscillations in the solution, the magnitude of which increases with λ. In the present work such oscillations were observed in almost all the calculations with the LR–RL scheme. Although they were frequently very small, they caused difficulties in the precise determination of the transient curve characteristics (especially in the case of LSV peak position for the Pedersen and Svensmark system). This effect of λ on the simulated transient curves can be most easily demonstrated for LSV simulations, where additional oscillations caused by the discontinuity of the electrode potential at $T = 0$ can be neglected.

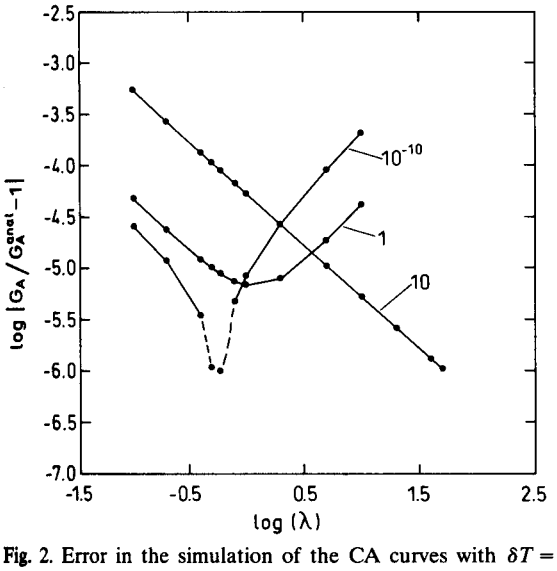

Fig. 2. Error in the simulation of the CA curves with $\delta T = 0.000125$ and $n = 5$ by the ⟨LR,RL⟩ method, as dependent on parameter λ in the case of the catalytic mechanism. Respective values of K_f are indicated in the figure.

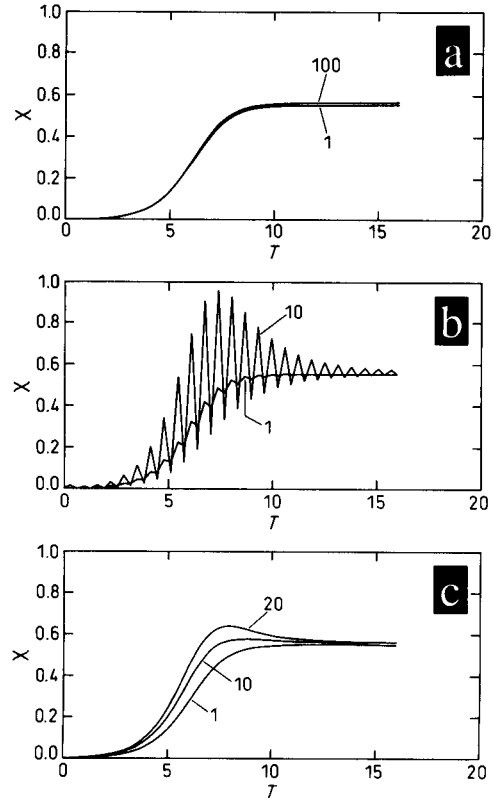

Fig. 3. Simulated LSV transients (current functions vs. non-dimensional time $T = Fvt/RT$) for the catalytic mechanism with $K_f = 1$ and $\delta T = 0.32$. Respective values of λ are indicated in the figure. The simulation methods were: (a) Crank–Nicolson, (b) Saul'yev LR–RL, (c) Saul'yev ⟨LR,RL⟩.

In the CA simulations they are difficult to separate from the above effect of λ. Figure 3 compares LSV curves obtained with the Crank–Nicolson and Saul'yev algorithms. A large integration step $\delta T = 0.32$ has been used in Fig. 3, since the term $\delta T/H$ in the truncation error is then magnified. This also allows the oscillations to be clearly visible along the time axis. It can be seen that in the case of Crank–Nicolson algorithm the λ parameter could be safely increased up to $\lambda = 100$ (in fact, this improved the accuracy, since the truncation error is $\mathcal{O}(\delta T^2 + H^2)$ in that case [2,3]), whereas with the LR–RL method the oscillations occurred already at $\lambda = 1$ and increased with λ. The oscillations were not observed for the ⟨LR,RL⟩ scheme but the error

was considerable, even for $\lambda = 3$. Of course, one would rarely use such high δT in practical calculations. However, similar behaviour was also observed with smaller δT, although for lower δT, oscillations dominating the solution occurred at correspondingly higher λ.

All the above features make the precise determination of optimal λ value very difficult. On the basis of our experience it seems that the arbitrary choice $\lambda = 1$ is the most reasonable and can be recommended, together with the use of δT values as small as possible. The following results have all been obtained with $\lambda = 1$, except for the calculations by the EX and RK2 methods, where $\lambda = 0.4$ was used, because of the von Neumann stability requirements [9].

Efficiency comparisons in the presence of homogeneous reactions

The quality of finite difference methods can be conveniently characterized and compared using efficiency plots, i.e., the dependencies of the error vs. computational time (ct), for various δT and H [3]. Figures 4–7 present efficiency plots obtained in the present work. The computational times refer to the simulation of the respective transient curves in the whole considered intervals of the T variable. It can be seen that the CN/R method is more efficient than the ⟨LR,RL⟩ algorithm in the case of the first order catalytic reaction but the reverse is true in the case of the second order homogeneous reaction. This can be

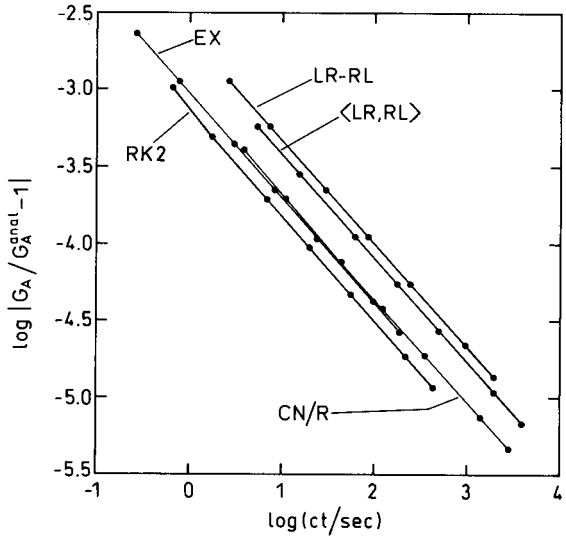

Fig. 4. Efficiency plots for the simulation of CA curves (catalytic mechanism) with $\lambda = 1$ (CN/R, LR–RL and ⟨LR,RL⟩ algorithms) and $\lambda = 0.4$ (EX and RK2). For a given method each point corresponds to different values of δT (and H).

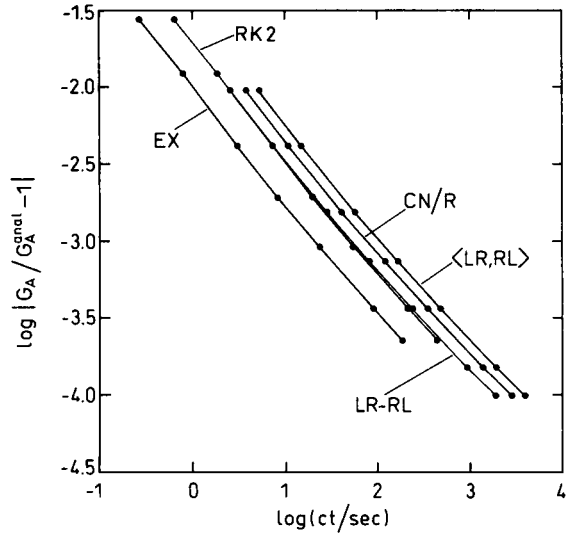

Fig. 5. Efficiency plots for the simulation of LSV curves (catalytic mechanism). Notation as in Fig. 4.

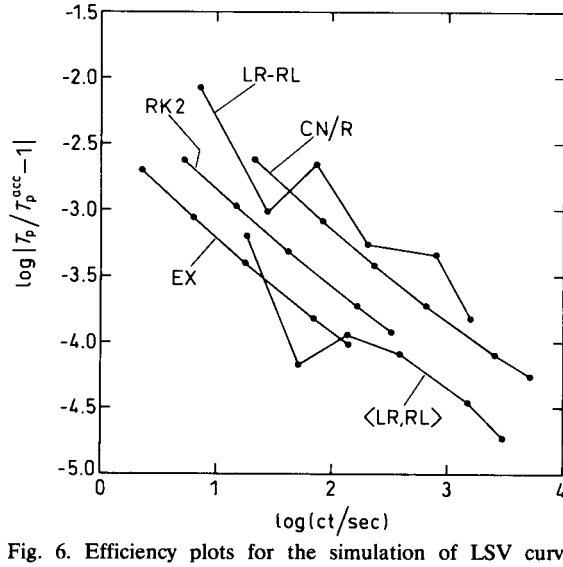

Fig. 6. Efficiency plots for the simulation of LSV curves (Pedersen and Svensmark mechanism). Error of the peak position. Notation as in Fig. 4.

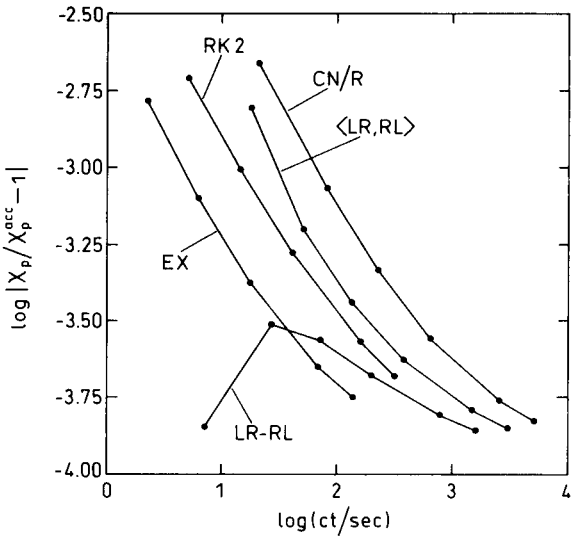

Fig. 7. Efficiency plots for the simulation of LSV curves (Pedersen and Svensmark mechanism). Error of the peak height. Notation as in Fig. 4.

explained by the differences in the total number of operations needed by these algorithms. In the case of the mechanism 1 these numbers of operations are comparable, provided that the calculation of necessary matrices and vectors is done only once and only the backward substitution is repeated in the time loop of the CN/R algorithm [15,21]. However, the accuracy of the CN/R method is better. As opposed to this, second order system 16 requires the inversion of matrices and other calculations to be repeated at every time level in the CN/R algorithm [15,21]. This increases the computational time significantly. The ⟨LR,RL⟩ algorithm requires fewer operations in that case.

Figures 5 and 7 reveal also that the maximal values of the LSV transients, simulated by the LR–RL algorithm are surprisingly accurate, contrary to the CA curves (Fig. 4). This seems to be a fortuitous result, since the accuracy of the LSV peak position is very poor at the same time (Fig. 6).

One should treat Figs. 4–7 with a certain caution. The computer programs corresponding to the relatively complex CN/R or Saul'yev algorithms can be written in many different ways, using various programming languages, various library software and various degree of generality. The efficiency of matrix operations can also be different on various computers, since some of the processors provide vectorized floating point operations. Therefore, one can obtain different relative efficiencies of these methods, depending on the particular implementation. In the present work a set of simple procedures for matrix operations such as addition, multiplication, inversion, substitution, etc., has been written and consequently used in all the CN/R and Saul'yev programs. One can expect a similar approach to be utilized in practical applications of these methods. It was observed, however, that when these procedures were replaced by simpler, direct calculations, without using matrix formulation, excessive loop iterations and function calls, wherever possible, the efficiency plots for the CN/R and Saul'yev algorithms in Fig. 4 shifted downwards in such a way that these algorithms became more efficient than the simple EX or RK2 methods. It was even possible to make the Saul'yev ⟨LR,RL⟩ program a little more efficient than that for the CN/R method, by using all the particular properties of the simulated catalytic mechanism.

In all these comparisons one has to remember that the use of $\lambda > 1$ improves the efficiency of the CN/R method but decreases that of the Saul'yev method. The efficiencies of all the methods from Figs. 4–7 can also be improved by using non-uniform integration steps along the x coordinates [3,24,25].

Limitations on the rate constants

It is well known that the finite difference methods fail in the case of the simulation of very fast homogeneous reactions, whether uniform or non-uniform space integration steps are used [3]. In these cases some of the reactants may form a very thin reaction layer so that unacceptably small integration steps H may be needed to precisely describe concentration profiles. This limits the allowable range of homogeneous rate constant. The other limitation may result from the stability requirements [9]. The Saul'yev algorithms are not free from this drawback. Figure 8 presents de-

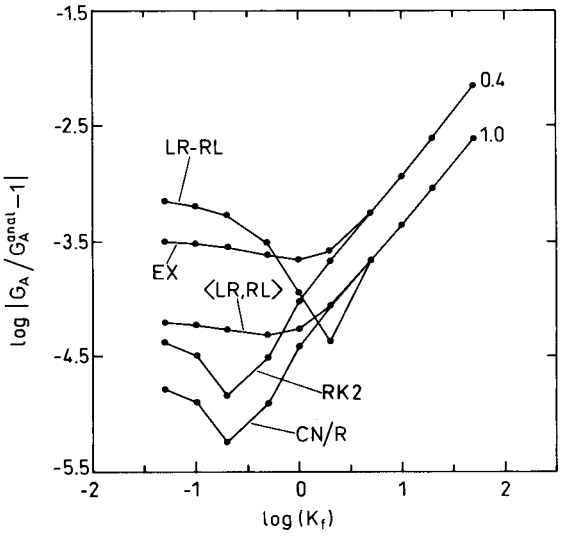

Fig. 8. Errors in the simulation of the CA curves with $\delta T = 0.001$, as dependent on log K_f in the case of the catalytic mechanism. Respective values of λ are indicated in the figure.

pendencies of the simulation error on the rate constant K_f for the catalytic mechanism and potential-step transient. It can be seen that for large K_f ($K_f > 10$ for a particular δT in Fig. 8) the differences in the accuracy of various considered integration methods disappear and all these methods behave equally poorly. In this limit the error seems to depend only on λ and K_f and it increases with K_f.

Conclusions

The successful use of the Saul'yev techniques in the simulation of diffusion/homogeneous reaction problems requires a careful selection of the integration steps h and δt as well as the λ parameter. For typical problems λ close to 1 and maximally small δt values can be recommended.

The alternated LR–RL Saul'yev algorithm is not very attractive within this class of problems, because of its unreliable performance, producing for example oscillations.

The averaged ⟨LR,RL⟩ algorithm can be used with efficiency close to or better than that for the Crank–Nicolson method with the matrix solution technique [8], especially when second order homogeneous reactions are simulated. The main advantage of this scheme is its relative simplicity, as compared with the Crank–Nicolson algorithm. This is particularly important when the traditional, problem-oriented formulation of the simulation algorithms is used.

This work has been done as a part of the Project supported by the Danish Science Research Council Grant No. 11-9311. The authors are grateful to the Danish Research Council for this grant. The authors are grateful to Dr. Ole Østerby of the Datalogisk Institut, Aarhus Universitet, for interesting and helpful comments.

APPENDIX

The method-oriented formulation of the Saul'yev algorithms

The principles of the method-oriented formulation of the algorithms for electrokinetic simulations have been outlined in details in the previous work [15]. Such general Saul'yev algorithms are formulated here. The familiarity of the reader with Ref. 15 is assumed, since notations consistent with that reference (and of necessity not consistent with the main part of the present paper) are used. One has to assume the same conditions as were required for the Crank–Nicolson method [15], in particular that for any one of M species: A, B,..., the expression kin(·) in Eqn. 1 in Ref. 15 is linear with respect to the quantities *dxc*[] and *d2xc*[] as well as homogeneous kinetic terms. Derivative boundary conditions simultaneously at X_0 and X_N are acceptable, however, in the Saul'yev method. Homogeneous kinetic terms of order not higher than 2 will be allowed.

Consider the LR algorithm first. In that case the calculations corresponding to the step FD3 in Ref. 15 start with the step:

(SA1) Calculate boundary concentrations at X_0

which comprises steps BC1 and BC2 [15].

The calculation of bulk concentrations requires a solution of a set of M linear equations:

$$\mathbf{S}\left[C'_{A_i}, C'_{B_i}, \cdots\right]^T = \mathbf{s} \qquad (27)$$

for the vector $[C'_{A_i}, C'_{B_i}, \cdots]^T$ of new concentrations at every space point, where $\mathbf{S}$ is an $M \times M$

matrix and **s** is a vector of M components. The elements of the matrix **S** can be determined, if one defines the following functions in which m denotes a counter which numbers species A, B, $\cdots$:

$$c_{\text{coeff}}(a) = \begin{cases} 1 & \text{if } a = m \\ 0 & \text{if } a \neq m \end{cases} \tag{28}$$

$$cc_{\text{coeff}}(a, b) = \begin{cases} C_{A_i} & \text{if } a \neq b = m \\ C_{B_i} & \text{if } b \neq a = m \\ 2C_{A_i} & \text{if } a = b = m \\ 0 & \text{in other cases} \end{cases} \tag{29}$$

$$d2xc^2_{\text{coeff}}(a) \begin{cases} -2h^{-2} & \text{if } a = m \\ 0 & \text{if } a \neq m \end{cases} \tag{30}$$

$$zero(a) = 0 \tag{31}$$

In Formulas 28–31 the symbolic names a, b, $\cdots$ of the species A, B, $\cdots$ are considered to be equivalent to the serial numbers of these species, in accordance with the rules of the translation of formulas [15]. The functions 28 and 30 are extended versions of functions 13 and 17 from Ref. 15, allowing the kinetic equations to be coupled by homogeneous kinetic terms. Function 29 represents coefficients standing at concentrations for a new time level in the linearized expressions for the second-order homogeneous kinetic terms (compare Eqns. 20–22). The pointer [15] representing second-order concentration operator cc[,] will be denoted by **CC**. Thus, the step of the algorithm, serving to calculate elements S_{jm} of the matrix **S** can be written:

(SA2)** Set pointers: **C** to c_{coeff}, **CC** to cc_{coeff}, **DXC** to *zero* and **D2XC** to $d2xc^2_{\text{coeff}}$ and calculate:
$S_{jm} = \text{kin}(\cdot)_j - 2\delta_{jm}/\delta T$ for $j = 1, 2, \ldots, M$
and $m = 1, 2, \ldots, M$

In this step j numbers the kinetic equations and m is the species counter from Eqns. 28–30. The Kronecker delta is denoted by δ_{jm}.

The place in which the step SA2 needs to occur in the sequence of pointers characteristic for the Saul'yev algorithm depends on the kinetic equations. If expressions kin$(\cdot)$ do not depend on time and space coordinates and there are no second order homogeneous reactions, this step can be performed only once, actually before the step FD1 in Ref. 15. If expressions kin$(\cdot)$ depend explicitly on time but do not depend on the space coordinate and there are no second order homogeneous reactions, step SA2 has to be performed at every time level, within step FD3 but only once at each time level. Otherwise it has to be repeated at every time level and at every discrete space point. When the kinetic expressions kin$(\cdot)$ depend on the space coordinate but not on time and there are no second order homogeneous kinetic terms it might also be possible to calculate a set of matrices **S** (one separate matrix for every space point) before the step FD1 and store them for further use at every time level. Such a solution was not accepted in the present work.

The vector **s** in Eqn. 27 can be calculated if one defines the functions:

$$c_{\text{bulk}}(a) = C_{A_i} \tag{32}$$

$$dxc_{\text{saul}}(a) = (C_{A_{i+1}} - C'_{A_{i-1}})/h \tag{33}$$

$$d2xc_{\text{saul}}(a) = 2(C_{A_{i+1}} - C_{A_i} + C'_{A_{i-1}})/h^2 \tag{34}$$

$$zerozero(a, b) = 0 \tag{35}$$

The step of the algorithm, serving to calculate the components s_A, s_B, $\ldots$, of the vector **s** is:

(SA3) Set pointers: **C** to c_{bulk}, **CC** to *zerozero*, **DXC** to dxc_{saul} and **D2XC** to $d2xc_{\text{saul}}$ and calculate:
$s_A = -2C_{A_i}/\delta T - \text{kin}(\cdot)$, etc. for other species

The following step of the algorithm is:

(SA4) Solve Eqn. 27 numerically for $[C'_{A_i}, C'_{B_i}, \cdots]^T$

In this step various numerical techniques can be utilized, e.g., the LU decomposition method [26] used in the present work. Steps SA3 and SA4 have to be repeated at every time level and at every space point, scanning from the left to the right. Finally, the algorithm is completed by the step:

(SA5)* Calculate boundary concentrations at X_N

which has to be performed only when boundary conditions at X_N depend explicitly on space derivatives or on time.

The algorithm for the RL method is analogous. One difference is that steps SA1 and SA5 are interchanged. There is also a difference in the functions 33 and 34 where $C_{A_{i+1}}$ has to be replaced by $C'_{A_{i+1}}$ and $C'_{A_{i-1}}$ by $C_{A_{i-1}}$. Steps SA3 and SA4 are performed in the order from the right to the left along x coordinate. In the case of the LR–RL algorithm steps SA1–SA5 corresponding to the cases LR and RL have to be used alternately on successive time levels. In the case of the ⟨LR,RL⟩ scheme both the LR and RL algorithms have to be used at each time level and completed with the final step:

(SA6) Average concentrations C'_{A_i} obtained in the LR and RL scans: $C'_{A_i} = (C'_{A_i}(\mathrm{LR}) + C'_{A_i}(\mathrm{RL}))/2$ for $i = 0, 1, \ldots, N$. and every species A, B, $\cdots$

In the calculations of the boundary conditions at X_0 within the LR scan or at X_N within the RL scan, there is a problem of C'_{A_i} concentrations close to the boundary, which are needed for multipoint gradient approximations. These concentrations are not determined yet in the moments when they are needed. A similar difficulty occurs in the Crank–Nicolson method [15]. Therefore, provisory values of these concentrations have to be calculated within the iterative procedures [15] for the steps SA1 or SA5, using procedures for steps SA2–SA4.

The above LR–RL and ⟨LR,RL⟩ algorithms have been implemented in the second version of the "ELSIM" program [27] and an agreement of the simulation results with those for the traditionally formulated Saul'yev algorithms, described in this paper, has been obtained [15].

REFERENCES

1 V.K. Saul'yev, Integration of Equations of Parabolic Type by the Method of Nets, Pergamon Press, Oxford, 1964.
2 L. Lapidus and G.F. Pinder, Numerical Solution of Partial Differential Equations in Science and Engineering, Wiley, New York, 1982; and References cited therein.
3 D. Britz, Digital Simulation in Electrochemistry, Springer, Berlin, Heidelberg, 1988; and References cited therein.
4 B. Marques da Silva, L.A. Avaca and E.R. Gonzáles, J. Electroanal. Chem., 250 (1988) 457.
5 B. Marques da Silva, L.A. Avaca and E.R. Gonzáles, J. Electroanal. Chem., 269 (1989) 1.
6 D. Britz, B. Marques da Silva, L.A. Avaca and E.R. Gonzáles, Anal. Chim. Acta, 239 (1990) 87.
7 D. Britz and M.F. Nielsen, Collect Czech. Chem. Commun., 56 (1991) 20.
8 M. Rudolph, J. Electroanal. Chem., 314 (1991) 13.
9 L.K. Bieniasz, J. Electroanal. Chem., 345 (1993) 13.
10 S.W. Feldberg, in A.J. Bard (Ed.), Electroanalytical Chemistry, Vol. 3, Marcel Dekker, New York, 1969, p. 199.
11 D. Britz, J. Electroanal. Chem., 240 (1988) 17.
12 J. Heinze, M. Störzbach and J. Mortensen, J. Electroanal. Chem., 165 (1984) 61.
13 A.J. Bard and L.R. Faulkner, Electrochemical Methods. Fundamentals and Applications, Wiley, New York, 1980.
14 S.U. Pedersen and B. Svensmark, Acta Chem. Scand., A40 (1986) 607.
15 L.K. Bieniasz, J. Electroanal. Chem., 340 (1992) 19.
16 D. Britz, J. Heinze, J. Mortensen and M. Störzbach, J. Electroanal. Chem., 240 (1988) 27.
17 B.W. Kernighan and D.M. Ritchie, The C programming Language, Prentice-Hall, Englewood Cliffs, NJ, 1978.
18 P. Delahay and G.L. Stiehl, J. Am. Chem. Soc. 74 (1952) 3500.
19 D. Britz, unpublished results.
20 J.M. Savéant and E. Vianello, Electrochim. Acta, 10 (1965) 905.
21 D. Britz, J. Electroanal. Chem., in press.
22 G.M. Birtwistle, Comput. J., 11 (1968) 317.
23 D.J. Evans and A.R.B. Abdullah, Int. J. Comput. Math., 14 (1983) 73.
24 T. Joslin and D. Pletcher, J. Electronanal. Chem., 49 (1974) 171.
25 R. Seeber and S. Stefani, Anal. Chem., 53 (1981) 1011.
26 W.H. Press, B.P. Flannery, S.A. Teukolsky and W.T. Vetterling, Numerical Recipes in C, Cambridge University Press, New York, 1988.
27 L.K. Bieniasz, Comput. Chem., 16 (1992) 11.

Analytica Chimica Acta, 278 (1993) 71–81
Elsevier Science Publishers B.V., Amsterdam

Further studies on the resolution of carboxylic acid enantiomers by liquid chromatography with fluorescence and laser-induced fluorescence detection

Toshimasa Toyo'oka, Mumio Ishibashi and Tadao Terao

Division of Drugs, National Institute of Hygienic Sciences, 1-18-1 Kamiyoga, Setagaya-ku, Tokyo 158 (Japan)

(Received 14th October 1992; revised manuscript received 9th December 1992)

Abstract

The optical purities of chiral derivatization reagents 4-(*N*,*N*-dimethylaminosulphonyl)-7-(3-aminopyrrolidin-1-yl)-2,1,3-benzoxadiazole (DBD-APys), 4-(aminosulphonyl)-7-(3-aminopyrrolidin-1-yl)-2,1,3-benzoxadiazole (ABD-APys) and 4-nitro-7-(3-aminopyrrolidin-1-yl)-2,1,3-benzoxadiazole (NBD-APys) were determined by chromatographic separation with an Ultron ES-PHCD (β-cyclodextrin phenylcarbamate derivative) chiral stationary phase column. With the exception of (+)-4-nitro-7-(3-aminopyrrolidin-1-yl)-2,1,3-benzoxadiazole (D-NBD-APy), which was found to have a purity of 99.5%, the enantiomers were determined to be more than 99.8% pure. The rate of the derivatization reaction for each enantiomer of DBD-APy at room temperature in the presence of the carboxylic acid reaction promoters 2,2′-dipyridyl disulphide (DPDS) and triphenylphosphine (TPP), was essentially the same for each enantiomer of naproxen. The reaction rates at 50°C were comparable at room temperature. When the derivatizations with DBD-APy and NBD-APy were carried out in the presence of diethyl phosphorocyanidate (DEPC) instead of DPDS and TPP quantitative derivatizations were not obtained even after a prolonged reaction time. The diastereomers derived from anti-inflammatory drugs and *N*-acetylamino acid enantiomers were efficiently resolved by both normal-phase (R_s = 2.58–7.60) and reversed-phase (R_s = 1.62–6.96) chromatography. The resolution of carboxylic acid enantiomers by liquid chromatography with laser-induced fluorescence (LIF) detection was also investigated. The minimum detectable levels by reversed-phase chromatography with an argon ion laser at 488 nm were 29 fmol of ABD-APy-Nap, 11 fmol of DBD-APy and 2.9 fmol of NBD-APy. Ibuprofen enantiomers added to rat plasma and human urine were completely separated by an ODS column with water–acetonitrile as eluent without interference from endogenous compounds. Sensitive detection was achieved with a commercially available LIF detector. Negligible mutagenicity of the reagents was observed by the Ames test using *Salmonella typhimurium* strains TA100 and TA98.

Keywords: Fluorimetry; Liquid chromatography; Acetylamino acids; Carboxylic acids; Chiral derivatization; Laser-induced fluorescence; Pharmaceuticals

Most of the recent advances in chiral separation technology have been achieved with liquid chromatography (LC) [1,2]. The enantiomers can be separated chromatographically using a chiral stationary phase (CSP) (direct method) or an achiral stationary phase after conversion of the enantiomers into diastereomeric derivatives (indirect method). Many of the LC methods have been successfully used to separate optical isomers such as non-steroidal anti-inflammatory drugs [3–5]. Although the indirect method [6–9] requires more manipulations than the direct separation

Correspondence to: T. Toyo'oka, Division of Drugs, National Institute of Hygienic Sciences, 1-18-1 Kamiyoga, Setagaya-ku, Tokyo 158 (Japan).

using CSP columns [10–17], it provides greater sensitivity and selectivity for the resolution of trace amount of racemates.

In a previous paper [18], the syntheses of fluorescent chiral derivatization reagents for carboxylic acid functional group, the fluorescence characteristics of the compounds derived from these reagents and the use of the reagents to separate carboxylic acid enantiomers by LC with fluorescence detection were reported. That work included the reagents D- and L-isomers of 4-(*N*,*N*-dimethylaminosulphonyl)-7-(3-aminopyrrolidin-1-yl)-2,1,3-benzoxadiazole (DBD-APy), 4-(aminosulphonyl)-7-(3-aminopyrrolidin-1-yl)-2,1,3-benzoxadiazole (ABD-APy) and 4-nitro-7-(3-aminopyrrolidin-1-yl)-2,1,3-benzoxadiazole (NBD-APy). The diastereomers derived from the enantiomers of drugs and *N*-acetylamino acids were completely separated by an ODS column and detected in the 15–45 fmol range (signal-to-noise ratio = 3). The resulting diastereomers had the attractive feature of excitation and fluorescence at the relatively long wavelengths of 460–480 nm and 530–610 nm, respectively. As the excitation maxima are close to the emission of an argon ion laser at 488 nm, the possibility of trace analysis of racemates with laser-induced fluorescence (LIF) detection was anticipated. Indeed, intensive fluorescence detection in the femtomole to attomole range was possible with the diastereomers derived from NBD-APy [19]. Further, the DBD-APy derivatives were amenable to peroxyoxalate chemiluminescence; therefore, ultratrace detection of DBD-APy diastereomers at the attomole level were achieved with a postcolumn LC reaction with bis[4-nitro-2-(3,6,9-trioxadecyloxy)-phenyl] oxalate (TDPO)–hydrogen peroxide (H_2O_2) and bis(2,4,6-trichlorophenyl) oxalate (TCPO)–H_2O_2 [20].

This paper describes the features of the chiral derivatization reagents (optical purity, mutagenicity and reactivity toward each enantiomer, etc.), and comparison of the resolution of carboxylic acid enantiomers with the chiral derivatization reagents by normal- and reversed-phase LC. DL-Ibuprofen added to rat plasma and human urine was also determined with a commercially available LIF detector.

EXPERIMENTAL

Materials and reagents

The fluorescent derivatization reagents (+)-4-(*N*,*N*-dimethylaminosulphonyl)-7-(3-aminopyrrolidin-1-yl)-2,1,3-benzoxadiazole (D-DBD-APy), (+)-4-(aminosulphonyl)-7-(3-aminopyrrolidin-1-yl)-2,1,3-benzoxadiazole (D-ABD-APy) and (+)-4-nitro-7-(3-aminopyrrolidin-1-yl)-2,1,3-benzoxadiazole (D-NBD-APy) were synthesized as described previously [18]. The syntheses of diastereomers (DBD-APy-Nap, ABD-APy-Nap and NBD-APy-Nap), derived from D-naproxen (Nap) and the fluoresecence reagents (D-DBD-APy, D-ABD-APy and D-NBD-APy), were described previously [18]. 2-(6-Methoxy-2-naphthyl)propionic acid (DL-naproxen), 2-(4-isobutylphenyl)propionic acid (DL-ibuprofen) and 2-[*p*-(2-oxocyclopentylmethyl)phenyl]propionic acid (DL-loxoprofen) were donated by Tokyo Tanabe Pharmaceutical (Tokyo), Kyowa Hakko Kogyo (Tokyo) and Sankyo (Tokyo), respectively. The enantiomers of *N*-acetylamino acids were kindly supplied by Ajinomoto (Tokyo). Diethyl phosphorocyanidate (DEPC) (Wako, Osaka), triphenylphosphine (TPP) (Wako) and 2,2′-dipyridyl disulphide (DPDS) (Tokyo Kasei, Tokyo) were used as received. Trifluoroacetic acid (TFA), acetonitrile, *n*-hexane, ethyl acetate (AcOEt) and water were of LC grade (Wako). All other chemicals were of analytical-reagent grade and were used as received.

LC

The liquid chromatograph consisted of two LC-9A pumps (Shimadzu, Kyoto) and an SCL-6B system controller (Shimadzu). Sample solutions were injected with a SIL-6B auto injector (Shimadzu). A Shimadzu RF-550 fluorescence monitor, equipped with a 12-μl flow cell, was used for the detection. A Tosoh LF-8010 monitor, equipped with a 5-μl flow cell and an interference filter at 540 ± 20 nm, was employed for LIF detection. Figure 1 shows a schematic diagram of the LF-8010 LIF detector. A 15-mW argon ion laser at 488 nm was used.

The analytical columns were Inertsil ODS-2 (150×4.6 mm i.d., 5 μm) for reversed-phase

chromatography and Inertsil SIL (150 × 4.6 mm i.d., 5 μm) (GL Sciences, Tokyo) for normal-phase separations. The columns were maintained at 40°C with a model 655A-52 column oven (Hitachi, Tokyo). The flow-rate of the eluent was fixed at 1.0 ml min^{-1}. The peak areas obtained from the fluorescence and LIF detectors were quantitated with a C-R4A Chromatopac (Shimadzu). All mobile phases were degassed with an on-line DGU-3A degasser (Shimadzu). The signal-to-noise ratios were calculated from the difference between the peak height of each diastereomer and the variation of the baseline noise.

Determination of optical purity of the derivatization reagents with a CSP column

Optical purities of the derivatization reagents were determined with an Ultron ES-PHCD CSP column (150 × 6.0 mm i.d., 5 μm) (Shinwa Chemical Industries, Kyoto). A 2-μl portion of the reagent solution (1000 μg ml^{-1} in CH_3CN) was injected on to the column maintained at 30°C, separated with 20 mM phospate buffer (pH 5.0)–CH_3CN and detected at 220 nm. Buffer solution of pH 5.0 was prepared by mixing 20 mM KH_2PO_4 and 20 mM K_2HPO_4.

Mutagenicity test of the derivatization reagents

Salmonella typhimurium strains TA100 and TA98 were used for the mutation assays with or without metabolic activation by rat S9 mix. Each test sample was dissolved in dimethyl sulphoxide and the mutagenic activity was measured by means of the Ames test with preincubation at 37°C for 20 min. Furylfuramide (AF-2) and 2-aminoanthracene (2AA) were also tested as positive controls. Strain TA100 carries a base-pair substitution mutation in the *his*G gene and responds best to base-pair substitution mutagens, while TA98 carries a frameshift mutation in the *his*D gene and responds best to frameshift mutagens.

Reactivity of D- *and* L-*isomers of DBD-APy to naproxen*

A 0.1-ml volume of 10 mM DBD-APy (D- or L-isomer) in CH_3CN, 0.25 ml of naproxen (5 μM of one enantiomer) in CH_3CN and 0.15 ml of a CH_3CN solution of 10 mM DPDS and 10 mM

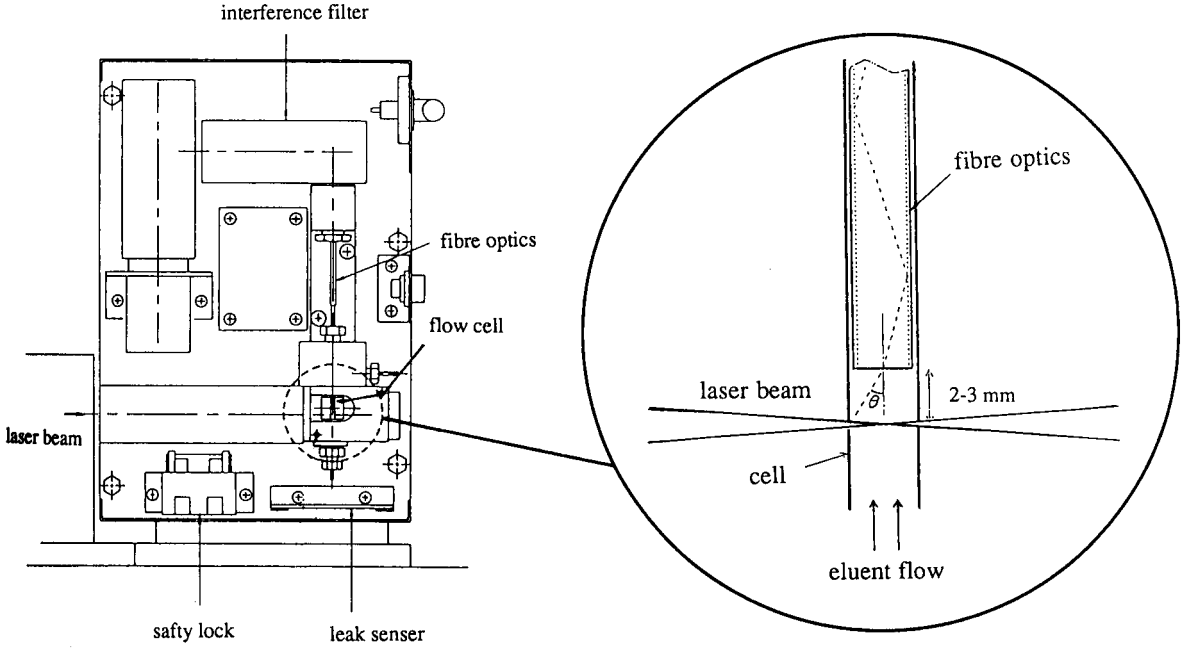

Fig. 1. Schematic diagram of optical block for laser fluorimetric detector.

TPP were mixed in 1.5-ml glass vials. The vials were capped and allowed to stand for 4 h at room temperature or 50°C. At fixed time intervals, an aliquot (20 μl) of the solution was automatically injected into the Inertsil ODS-2 column and the fluorescence peak area of the resulting diastereomer was calculated with an integrator. The reagent blanks without naproxen were treated in the same manner. The yield at each sampling time was calculated from the peak area of the authentic fluorophore.

Derivatization of D-naproxen with D-DBD-APy or D-NBD-APy in the presence of DEPC

The chiral derivatization reagent (2 mM D-DBD-APy or D-NBD-APy) and D-naproxen (5 μM) in 0.5 ml of CH_3CN reacted at room temperature in the presence of 1% DEPC. The reaction solution in the vials was maintained at room temperature for 4 h. After fixed time intervals, an aliquot (5 μl) of the solution was injected into the Inertsil ODS-2 column and the reaction yield determined in the same manner as described above.

LC separation of the diastereomers derived from carboxylic acid enantiomers and D-DBD-APy

Carboxylic acid enantiomers (ca. 1 mg each) were reacted at room temperature with D-DBD-APy (0.25 mM) in 0.5 ml of CH_3CN in the presence of DPDS (2.5 mM) and TPP (2.5 mM). After a 2-h reaction time, an aliquot (5 μl) of the solution was injected into the Inertsil ODS-2 reversed-phase column and Inertsil SIL normal-phase columns.

LIF detection of carboxylic acid enantiomers

Naproxen (1 μM of the racemic mixture) and D-DBD-APy (2 mM) in 1.0 ml of CH_3CN were reacted at room temperature in the presence of DPDS (3 mM) and TPP (3 mM). After a 2-h reaction time, an aliquot (10 μl) of the diluted solution (×100) was injected into the Inertsil ODS-2 column and separated with water–CH_3CN (52 + 48) as eluent.

Determination of carboxylic acid enantiomers in plasma and urine with LIF detection

A 1.0-ml volume of human urine spiked with 8 μl (4 nmol of each enantiomer) of 1 mM DL-ibuprofen was adjusted pH 1–2 with 36% HCl (ca. 10 μl), then 3 ml of 10 mM sodium acetate buffer (pH 2.0) were added to the solution. The acidified urine was applied to a Bond Elut Certify II LRC extraction column (Varian, Harbor City, CA), which was washed with 2 ml of methanol and 2 ml of 10 mM sodium acetate buffer (pH 2.0). The column was washed sequentially with 2 ml of 10 mM sodium acetate buffer (pH 2.0) and 2 ml of 10% acetic acid. The column was dried by drawing air through it for 5 min with a water aspirator. All washings were discarded. DL-Ibuprofen was eluted with 2 ml of 0.1% aqueous TFA–CH_3CN (1 + 1). The eluate was evaporated to dryness and the residue was dissolved in 1.0 ml of CH_3CN (urine extraction sample).

A 0.5-ml volume of rat plasma spiked with 2 μl (1 nmol of each enantiomer) of 1 mM DL-ibuprofen was also adjusted pH 1–2 with 36% HCl (ca. 5 μl), then 3.5 ml of 10 mM sodium acetate buffer (pH 2.0) were added to the solution. The acidified plasma was also applied to the solid-phase column and treated in the same manner as described for the urine sample. The dried eluate containing DL-ibuprofen was dissolved in 0.5 ml of CH_3CN (plasma extraction sample).

A 0.25-ml volume of the prepared urine or plasma extract, 0.1 ml of D-DBD-APy (2 mM) in CH_3CN and 0.15 ml of a mixed solution of DPDS (2 mM) and TPP (2 mM) in CH_3CN were thoroughly mixed in 1.5-ml glass vials. The vials were capped and allowed to stand for 2 h at room temperature (20–30°C). The diluted samples were analysed by reversed-phase LC with LIF detection. A blank urine or plasma sample without D-DBD-APy was also treated in the same manner.

RESULTS AND DISCUSSION

Optical purity and mutagenicity of fluorescence derivatization reagents

The determination of trace amounts of one enantiomer in the presence of a much greater amount of the other enantiomer requires a high level of optical purity for the reagent. Therefore, the optical purities of the chiral derivatization

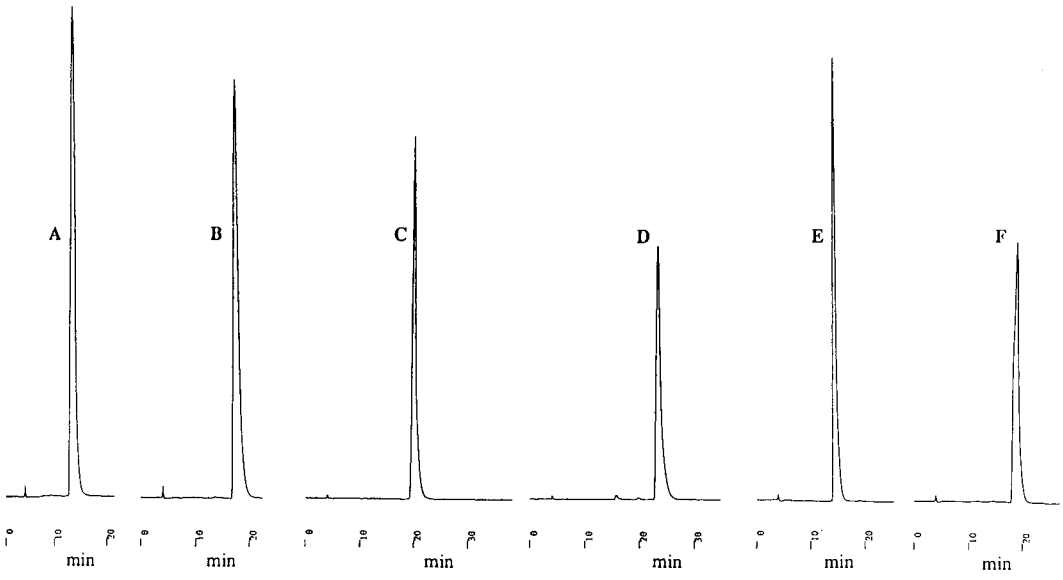

Fig. 2. CSP column separation of enantiomers of chiral derivatization reagents (A) L-ABD-APy; (B) D-ABD-APy; (C) L-NBD-APy; (D) D-NBD-APy; (E) L-DBD-APy; (F) D-DBD-APy. Eluent: (A) 20 mM phosphate buffer (pH 5.0)–CH_3CN (90 + 10) for ABD-APy; (B) 20 mM phosphate buffer (pH 5.0)–CH_3CN (85 + 15) for NBD-APy; (C) 20 mM phosphate buffer (pH 5.0)–CH_3CN (80 + 20) for DBD-APy. For other LC conditions, see Experimental.

reagents were measured using CSP columns, such as ovomucoid [21] and cyclodextrins [22]. The DL-enantiomers of the reagents were not completely separated by some the CSP columns because there was little or no retention owing to the high polarity of the compounds. Only the ES-PHCD (β-cyclodextrin phenylcarbamate derivative) column provided complete separations of all pairs of DBD-APy, NBD-APy and ABD-APy (Fig. 2 and Table 1). No separations of the pairs of the enantiomers were observed with the unmodified β-CD columns. The results suggest that the aromatic ring structure in the CSP is important for the resolution of the enantiomers. The optical purities of the reagents, calculated from peak-area ratios of the two enantiomers, were more than 99.8%, except for D-NBD-APy which had a purity of 99.5%.

According to one report [23], some nitrobenzofurazans exhibit mutagenic activity; therefore, the mutagenicities of the reagents were determined by the Ames test using *Salmonella typhimurium* strains TA100 and TA98 [24]. As shown in Table 2, no mutagenic activities were observed with TA98 with and without activation with the S9 mix. NBD-APys showed slight mutagenic activity with TA100. As no great difference was observed with and without S9 mix (1.5 versus 1), it is

TABLE 1

Resolution of chiral derivatization reagents using a CSP column [a]

Chiral reagent	L-Isomer		D-Isomer		α	R_s	Eluent
	Retention time (min)	k'	Retention time (min)	k'			
ABD-APy	13.31	3.44	17.39	4.80	1.40	2.33	A
NBD-APy	20.01	5.67	23.33	6.78	1.20	2.01	B
DBD-APy	14.46	3.82	18.96	5.32	1.39	2.82	C

[a] LC conditions and detection as in Fig. 2.

obvious that the mutagenicity is independent of metabolic activation. Further, no differences in the mutagenicities of the enantiomers of all three reagents were observed. Judging from the results for positive controls, AF-2 and 2AA, the mutagenicities of these reagents are of a very low order of activity.

Derivatization of naproxen with the chiral reagents

The chiral reagents DBD-APys, ABD-APys and NBD-APys require activation of the carboxylic acid for derivatization. Among the activation agents tested, the combination of DPDS and TPP gave highest reaction yields. However, the reaction with NBD-APy did not go to completion even after a prolonged reaction and the yield was only 65% [18]. Therefore, the derivatization of D-naproxen in the presence of DEPC, one of the activation agents, was subjected to a detailed study. Figure 3 shows the time course of the reactions with D-NBD-APy and D-DBD-APy at room temperature. There was essentially no improvement over activation with DPDS and TPP. Quantitative yields were not obtained (70% with

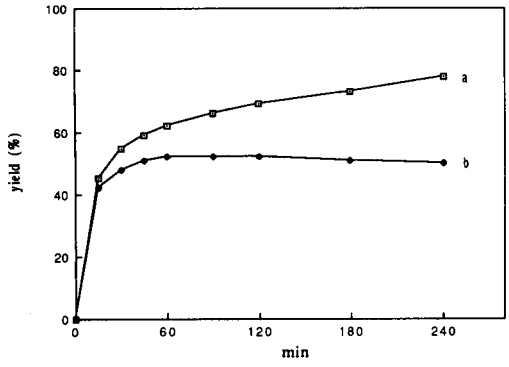

Fig. 3. Derivatization of D-naproxen with chiral reagents in the presence of DEPC, (a) with D-DBD-APy and (b) with D-NBD-APy. Eluent, water–CH_3CN (55+45) for DBD-APy-Nap and water–CH_3CN (60+40) for NBD-APy-Nap; fluorescence detection, 580 nm (excitation at 470 nm) for DBD-APy-Nap and 540 nm (excitation at 470 nm) for NBD-APy-Nap. For other LC conditions, see Experimental.

TABLE 2

Mutagenic activities of chiral derivatization reagents in *Salmonella typhimurium* strains TA100 and TA98

Strain	Concentration (μg per plate)	D-DBD-APy		L-DBD-APy		D-NBD-APy		L-NBD-APy		D-ABD-APy		L-ABD-APy	
		−S9	+S9	−S9	+S9	−S9	+S9	−S9	+S9	−S9	+S9	−S9	+S9
TA100	0	88	170										
	1	90	240	106	204	98	214	146	254	110	246	108	184
	5	112	206	106	210	144	268	156	256	122	238	130	224
	10	56	170	112	220	244	282	184	318	202	280	112	208
	50	98	246	112	222	512	676	434	594	104	272	96	288
	100	106	258	124	202	754	1132	642	798	96	232	114	224
	500	112	240	128	242	1556	2390	1676	2366	106	208	152	240
	1000	130	242	140	200	1376	880	2174	1972	140	208	128	292
Positive control:													
AF-2	0.02	1079											
2AA	2		2021										
TA98	0	22	41										
	1	24	37	27	31	21	33	23	31	17	47	27	37
	5	28	46	29	27	31	43	27	36	22	51	29	40
	10	17	37	27	38	28	30	13	31	23	39	27	46
	50	22	37	28	30	100	75	26	54	14	32	28	47
	100	21	44	18	34	142	89	25	78	28	33	21	31
	500	28	35	16	38	172	132	47	81	37	40	23	42
	1000	17	40	17	54	136	83	50	86	25	45	32	34
Positive control:													
AF-2	0.05	335											
2AA	2		1749										

D-DBD-APy and 50% with D-NBD-APy). Therefore, DBD-APys, in the presence of DPDS and TPP, is the best derivatization reagent for carboxylic acid enantiomers. Consequently, both enantiomers of DBD-APy were used in the following experiments.

It was necessary to test the reactivity of each enantiomer of the reagents toward each enantiomer of the carboxylic acids because differences in reactivity could give mixtures of diastereomers that would not accurately reflect the isomeric composition of the drug. Therefore, the reactivities of D-DBD-APy and L-DBD-APy to naproxen (D- or L-enantiomer) were investigated. Judging from the reaction curves in Fig. 4, the formation of the diastereomers derived from D-DBD-APy and D-naproxen and derived from L-DBD-APy and L-naproxen, is faster than those of diastereomers derived from D-DBD-APy and L-naproxen and derived from L-DBD-APy and D-naproxen. However, the reactivities seem to be comparable for both isomers of DBD-APys. The results were not improved by increasing the reaction temperature to 50°C (data not shown). DBD-APys in the presence of DPDS and TPP can be confidently used for the resolution of carboxylic acid enantiomers.

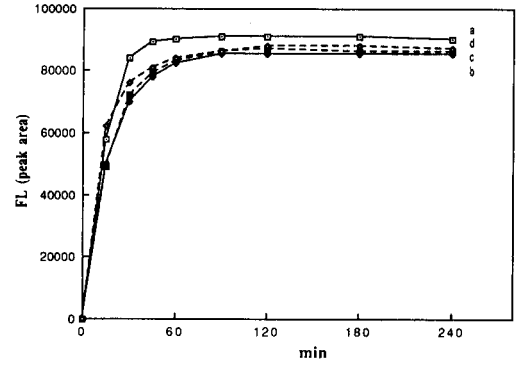

Fig. 4. Time course of derivatization reaction with D-DBD-APy (or L-DBD-APy) in the presence of DPDS and TPP (a) Reaction of D-naproxen with D-DBD-APy; (b) reaction of L-naproxen with D-DBD-APy; (c) reaction of D-naproxen with L-DBD-APy; (d) reaction of L-naproxen with L-DBD-APy. Eluent, water–CH_3CN (55 + 45); fluorescence detection, 580 nm (excitation at 470 nm). For other LC conditions, see Experimental.

TABLE 3

LC separation of diastereomers derived from D-DBD-APy by reversed-phase chromatography [a]

Carboxylic acid	D-isomer		L-isomer		α	R_s	Eluent
	Retention time (min)	k'	Retention time (min)	k'			
Ibuprofen	15.32	9.21	18.49	11.33	1.23	3.53	E
Ibuprofen	26.22	16.48	32.73	20.82	1.26	4.92	D
Naproxen	11.32	6.55	13.35	7.90	1.21	2.70	D
Naproxen	19.49	11.99	24.02	15.01	1.25	4.42	C
Loxoprofen	8.17	4.45	9.10	5.07	1.14	1.63	D
Loxoprofen	13.25	7.83	15.29	9.19	1.17	2.55	C
N-Acetyl-Trp	24.88	15.59	19.34	11.90	1.31	5.04	B
N-Acetyl-Phe	26.45	16.63	18.79	11.53	1.44	6.96	B
N-Acetyl-Tyr	8.79	4.86	7.47	3.98	1.22	2.29	B
N-Acetyl-Tyr	18.03	11.02	14.31	8.54	1.29	4.25	A
N-Acetyl-Leu	21.47	13.31	18.82	11.54	1.15	2.72	B
N-Acetyl-Val	11.83	6.88	11.03	6.35	1.08	1.18	B
N-Acetyl-Val	25.07	15.71	23.13	14.42	1.09	1.62	A
N-Acetyl-Met	12.80	7.54	11.68	6.79	1.11	1.55	B
N-Acetyl-Met	27.65	17.44	24.69	15.46	1.13	2.33	A

[a] Column, Inertsil ODS-2 (150 × 4.6 mm i.d., 5 μm) at 40°C; eluent, (A) water–CH_3CN (75 + 25), (B) water–CH_3CN (70 + 30), (C) water–CH_3CN (55 + 45), (D) water–CH_3CN (50 + 50), (E) water–CH_3CN (45 + 55), flow-rate, 1.0 ml min^{-1}, fluorescence detection, excitation at 470 nm, emission at 580 nm.

Resolution of carboxylic acid enantiomers by reversed- and normal-phase chromatography

The resolution of some carboxylic acid enantiomers by using a reversed-phase column with acidic eluents was reported in a previous paper [18]. Excellent resolution was obtained with anti-inflammatory drugs and *N*-acetylamino acids containing aromatic ring structures. However, the R_s values of some aliphatic *N*-acetylamino acids such as *N*-acetylleucine, -valine and -methionine were marginal with reversed-phase chromatography with acidic elutions. Therefore, the separation was studied with a reversed-phase column with neutral eluents. As shown in Table 3, the resolution of all anti-inflammatory drugs and some of the *N*-acetylamino acids tested was improved with water–CH_3CN eluent systems. However, there was no improvement of the separations of *N*-acetylproline, -alanine and -asparagine. Therefore, the separations were attempted with normal-phase chromatography using an Inertsil SIL column. The R_s values were greater than those obtained with reversed-phase chromatography for all carboxylic acids (Table 4). Further, *N*-acetylproline, -alanine and -aspargine were completely separated with EtOH–AcOEt as the eluent.

Typical chromatograms of the resulting diastereomers with reversed- and normal-phase columns are depicted in Figs. 5 and 6. L-Enantiomers of the drugs elute more rapidly than the D-enantiomers, whereas D-enantiomers of *N*-acetylamino acids elute before the L-enantiomers in normal-phase chromatography (Table 4 and Fig. 6). In contrast, the opposite results were obtained with reversed-phase chromatography (Table 3 and Fig. 5). No exceptions were observed among the pairs of enantiomers. The results described above suggest that the formation of hydrogen bonds between the stationary phases and the amide diastereomers, derived from carboxylic acid enantiomers and the derivatization reagents, play important roles in the separations. Although carboxylic acid enantiomers were well

TABLE 4

LC separation of diastereomers derived from D-DBD-APy by normal-phase chromatography [a]

Carboxylic acid	D-isomer		L-isomer		α	R_s	Eluent
	Retention time (min)	k'	Retention time (min)	k'			
Ibuprofen	13.18	7.79	8.64	4.76	1.64	6.72	A
Ibuprofen	8.03	4.36	5.52	2.68	1.62	4.56	B
Ibuprofen	5.48	2.65	4.02	1.68	1.58	2.90	C
Naproxen	20.56	12.71	13.35	7.90	1.61	7.60	A
Naproxen	11.51	6.67	7.80	4.20	1.59	5.70	B
Naproxen	7.11	3.74	5.08	2.39	1.57	3.86	C
Loxoprofen	26.61	16.74	19.31	11.87	1.41	5.51	A
Loxoprofen	13.92	8.28	10.33	5.89	1.41	4.41	B
Loxoprofen	8.27	4.51	6.33	3.22	1.40	3.37	C
N-Acetyl-Trp	8.21	4.47	11.96	6.97	1.56	5.56	D
N-Acetyl-Phe	6.59	3.40	11.13	6.42	1.89	6.98	D
N-Acetyl-Tyr	7.03	3.68	11.14	6.43	1.74	6.09	D
N-Acetyl-Leu	6.18	3.12	10.48	5.99	1.92	7.48	D
N-Acetyl-Val	7.01	3.68	11.13	6.42	1.75	6.09	D
N-Acetyl-Met	6.78	3.52	11.25	6.50	1.85	6.63	D
N-Acetyl-Ala	13.33	7.89	16.11	9.74	1.24	2.58	D
N-Acetyl-Asn	5.79	3.62	7.77	4.18	1.15	3.88	D
N-Acetyl-Pro	12.17	7.12	15.53	9.35	1.31	2.58	E

[a] Column, Inertsil SIL (150 × 4.6 mm i.d., 5 μm) at 40°C; eluent, (A) *n*-hexane–AcOEt (50 + 50), (B) *n*-hexane–AcOEt (40 + 60), (C) *n*-hexane–AcOEt (30 + 70), (D) EtOH–AcOEt (5 + 95), (E) EtOH–AcOEt (10 + 90); flow-rate, 1.0 ml min^{-1}; fluorescence detection, excitation at 452 nm, emission at 538 nm.

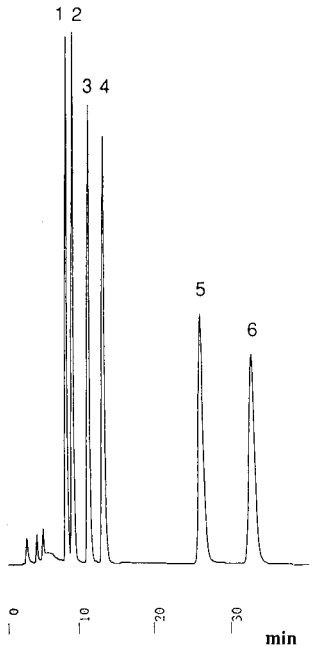

Fig. 5. Chromatograms obtained for separation of profens with a reversed-phase column. Peaks: 1 = D-loxoprofen; 2 = L-loxoprofen; 3 = D-naproxen; 4 = L-naproxen; 5 = D-ibuprofen; 6 = L-ibuprofen; LC conditions are given in Table 3.

resolved by normal-phase chromatography, the use of this technique is unfavourable for determination in biological specimens because of sample handling difficulties and the limited lifetimes of the column. Hence the reversed-phase column was adopted for subsequent experiments.

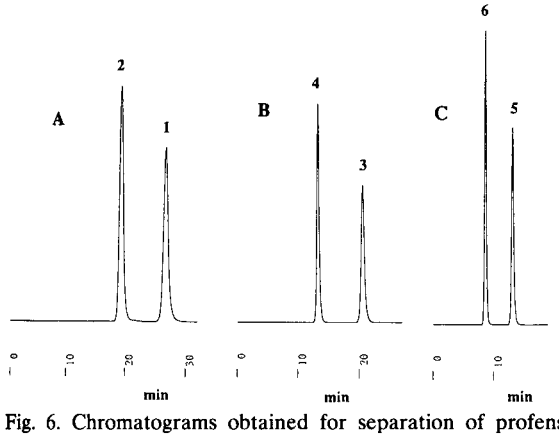

Fig. 6. Chromatograms obtained for separation of profens; with a normal-phase column. Peaks 1–6 as in Fig. 5. LC conditions are given in Table 4.

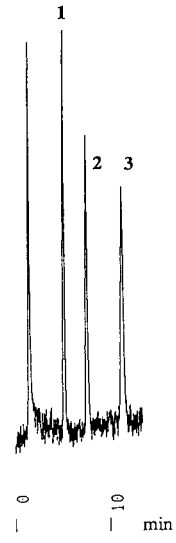

Fig. 7. Chromatograms of authentic diastereomers obtained with LIF detection. Peaks: 1 = ABD-APy-Nap (200 fmol); 2 = NBD-APy-Nap (15 fmol); 3 = DBD-APy-Nap (50 fmol). Eluent, water–CH_3CN (50 + 50). For other LC conditions, see Experimental.

Resolution of diastereomers with LIF detection

In a previous paper [19], the LIF detection of the diastereomers derived from DL-naproxen with ABD-APy, DBD-APy and NBD-APy was described. Figure 7 shows the separation of three authentic diastereomers (200 fmol of ABD-APy-Nap, 50 fmol of DBD-APy-Nap and 15 fmol of NBD-APy-Nap). The detection limits (signal-to-noise ratio of 3) of ABD-APy-Nap, DBD-APy-Nap and NBD-APy-Nap on the chromatogram were 29, 11 and 2.9 fmol, respectively. Among the derivatives, the NBD-APy moiety showed the lowest detection limit. Although the sensitivity of the DBD-APy derivative is one-quarter of that with NBD-APy, DBD-APy was employed in this experiment because of its higher reactivity. The chromatographic separation of DL-naproxen (corresponding to 100 fmol each) derived from D-DBD-APy is shown in Fig. 8. Good separation and highly sensitive detection were obtained with reversed-phase LC with the LIF detector.

Determination of DL-ibuprofen added to biological samples with LIF detection

For the recovery of profens such as naproxen and ibuprofen in biological samples, the solid-

phase extraction method is generally used. It is employed for the chemiluminescence determination described in a previous paper [20]. Therefore, a Bond-Elut Certify II LRC column was employed for the extraction of DL-ibuprofen added to rat plasma and human urine. As shown in Fig. 9, DL-ibuprofen in both samples was separated well; however, the detectability was about half of that of DBD-APy-Nap. This may be due to the difference in the fluorescence quantum yields (ϕ) and/or incomplete recovery of DL-ibuprofen from the solid-phase column.

In conclusion, DBD-APy derivatization reagents seem to be applicable for the resolution of trace amounts of carboxylic acid enantiomers in biological samples because of excellent resolution of the enantiomers, quantitative reaction under mild reaction conditions at room temperature, good fluorescence quantum efficiency and suitability for various detection methods (fluorescence, laser-induced fluorescence, chemiluminescence, etc). The lack of mutagenic activity is an advantage in terms of safety.

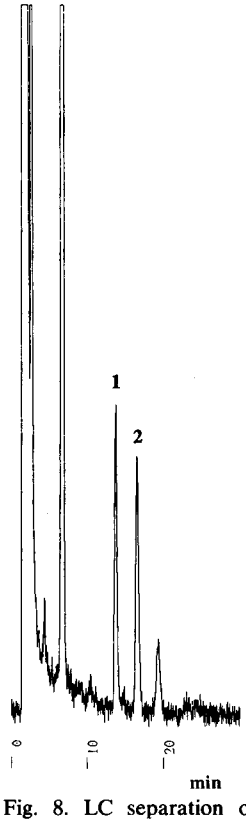

Fig. 8. LC separation of D-DBD-APy derivatives of DL-naproxen. Peaks: 1 = D-naproxen; 2 = L-naproxen. Each peak corresponds to 100 fmol. For conditions, see Experimental.

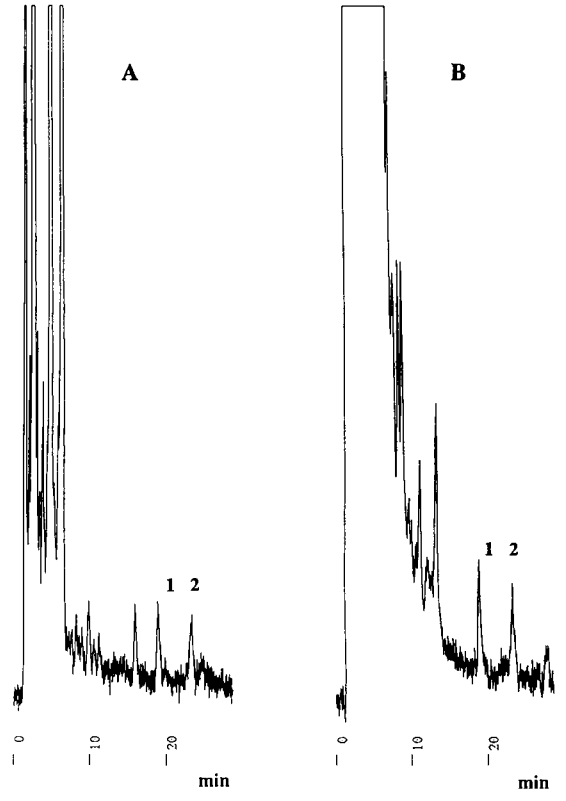

Fig. 9. Chromatograms obtained from rat plasma and human urine with D-DBD-APy. (A) Plasma (50 fmol each); (B) urine (100 fmol each). Peaks: 1 = D-ibuprofen; 2 = L-ibuprofen. Eluent: water–CH_3CN (47+53). For other LC conditions, see Experimental.

The authors thank Drs. T. Nohmi and M. Matsui, National Institute of Hygienic Sciences, for the Ames test. Thanks are also due to Dr. C.R. Warner, Food and Drug Administration, Washington, DC, for reviewing the manuscript, Tosoh for the loan of the LF-8010 LIF detector and Shinwa Chemical Industries for the gift of CSP columns.

REFERENCES

1 T.J. Ward and D.W. Armstrong, M. Zief and L.J. Crane (Eds.), Chromatographic Chiral Separation, Dekker, New York, 1988.
2 V. Davankov and A.M. Krstulovic (Eds.), Chiral Separation by HPLC, Horwood, Chichester, 1989.
3 J. Goto, M. Hasegawa, S. Nakamura, K. Shimada and T. Nambara, J. Chromatogr., 152 (1978) 413.
4 J. Goto, N. Goto, A. Hikichi, T. Nishimaki and T. Nambara, Anal. Chim. Acta, 120 (1980) 187.
5 J. Goto, N. Goto and T. Nambara, J. Chromatogr., 239 (1982) 559.
6 J. Goto, M. Ito, S. Katsuki, N. Saito and T. Nambara, J. Liq. Chromatogr., 9 (1986) 683.
7 N. Nimura and T. Kinoshita, J. Chromatogr., 352 (1986) 169.
8 S. Einarsson, B. Josefsson, P. Moller and D. Sanchez, Anal. Chem., 59 (1987) 1191.
9 J. Goto, N. Goto, G. Shao, M. Ito, A. Hongo, S. Nakamura and T. Nambara, Anal. Sci., 6 (1990) 261.
10 P.E. Hare and E. Gil-Av, Science, 204 (1979) 1226.
11 W.H. Pirkle and R. Dappen, J. Chromatogr., 404 (1987) 107.
12 L. Oliveros and M. Cazau, J. Chromatogr., 409 (1987) 183.
13 G. Gargaro, F. Gasparrini, D. Misiti and C. Villani, Chromatographia, 24 (1987) 505.
14 W.H. Pirkle and T.C. Pochopsky, Chem. Rev., 89 (1989) 347.
15 C. Petterson and C. Gioeli, J. Chromatogr., 398 (1987) 247.
16 K. Iwaki, S. Yoshida, N. Nimura, T. Kinoshita, K. Takeda and H. Ogura, J. Chromatogr., 404 (1987) 117.
17 T. Shinbo, T. Yamaguchi, K. Nishimura and M. Sugiura, J. Chromatogr., 405 (1987) 145.
18 T. Toyo'oka, M. Ishibashi and T. Terao, Analyst, 117 (1992) 727.
19 T. Toyo'oka, M. Ishibashi and T. Terao, J. Chromatogr., 625 (1992) 357.
20 T. Toyo'oka, M. Ishibashi and T. Terao, J. Chromatogr., 627 (1992) 75.
21 J. Haginaka, C. Seyama, H. Yasuda, H. Fujima and H. Wada, J. Chromatogr., 592 (1992) 301.
22 S.H. Lee, A. Berthod and D.W. Armstrong, J. Chromatogr., 603 (1992) 83.
23 D.G. MacPhee, G.P. Robert, B. Ternai, P. Ghosh and R.W. Stephens, Chem. Biol. Interact., 19 (1977) 77.
24 B.N. Ames, J. McCann and E. Yamasaki, Mutat. Res., 31 (1975) 347.

Analytica Chimica Acta, 278 (1993) 83–89
Elsevier Science Publishers B.V., Amsterdam

Comparison of the performance of RP C_{18} on silica and polymeric supports for the liquid chromatographic separation of metal–amino acid complexes with postcolumn derivatization

F. Baffi, M.C. Ianni and E. Magi

Istituto di Chimica Generale, Cattedra di Chimica Analitica, Università di Genova, Viale Benedetto XV 3, 16132 Genova (Italy)

M. Ravera

ITIS A. Gastaldi, Via Milano, 16126 Genova (Italy)

(Received 18th September 1992; revised manuscript received 22nd December 1992)

Abstract

On the basis of previous studies on the behaviour of metal–amino acid complexes with reversed-phase C_{18} stationary phases, which can provide useful information on metal speciation, the performances of different silica and polymeric supports were compared. Both the pH stability of the stationary phase and the presence of free OH groups in the support material, with ion-exchange effects, were considered. To determine amino-acids more rapidly and with higher reproducibility and sensitivity, a postcolumn derivatization procedure is also described. The results indicate that the use of a reversed phase on a non-conventional silica support, with postcolumn derivatization, seems to be necessary to determine metal–amino acid complexes.

Keywords: Liquid chromatography; Amino acids; Copper; Metal complexes

In recent years, reversed-phase liquid chromatography (RPLC) has been used in speciation analysis studies [1,2]. However, many problems related to the stationary phase, such as its influence on the analyte and the effect of the eluent, have still to be studied. Previous results [3] have shown that the RP C_{18} silica phase can retain copper species, which were polar to a higher or lesser extent. In fact, the silica phase shows an ion-exchange mechanism because of the presence of silanol groups. It is possible to recognize the copper–amino acid complexes among the other copper species in the eluted fractions by atomic absorption spectrometry with electrothermal atomization (ETAAS) for copper and by LC, with *o*-phthalaldehyde precolumn derivatization and fluorescence determination, for amino acids. However, the problems related to this kind of procedure are to analyse the fractions for the amino acids more rapidly and to standardize the performance of the RP C_{18} silica.

This paper describes a postcolumn derivatization procedure, carried out with the *o*-phthalaldehyde system, for the direct determination of amino acids, without further injection of the fractions on to the column.

The first part of this work was carried out on the copper–glycine complex, using no column in

Correspondence to: F. Baffi, Istituto di Chimica Generale, Cattedra di Chimica Analitica, Università di Genova, Viale Benedetto XV 3, 16132 Genova (Italy).

the LC postcolumn derivatization scheme. The aim was to check the extent of absorption on the PTFE surface of the mixer, of the delay tube and on all the connecting tubings. Further, a study was performed with several columns and with the copper–glycine complex in order to compare the performances of RP C_{18} supported on various phases. It is intended to study the final procedure for the preconcentration and analysis of metal–amino acid complexes in the near future.

The choice of the support materials was based on the consideration of two crucial problems: the pH stability of the stationary phase when real samples are treated and the presence of free OH groups, due to incomplete coverage of the silica, having an ion-exchange effect; the latter is important if samples at low concentrations are injected on to the column.

EXPERIMENTAL

Instrumentation

The LC system was a Bruker Quaternary Gradient LC 2300 and the data system was an LC-21 Epson QX 10 microcomputer with an FX-85 printer. The temperature control unit for the column was a Violet T 55.

The postcolumn derivatization reaction was performed in a PTFE delay tube (Supelco) immersed in a thermostatic bath. The detector was a Bruker LC 315 fluorescence monitor with a diffraction grating monochromator, a xenon lamp and a 12-μl quartz flow cell. The excitation and emission wavelengths used were 360 and 530 nm, respectively. Glycine and phenylalanine were determined according to a previously described procedure [4]. The fractions were collected with a Frac-200 fraction collector (Pharmacia). The determination of copper in the injected samples and in the eluate fractions, for the mass balance, was carried out by ETAAS using Zeeman-effect background correction (Varian Spectra A3000).

Reagents and materials

Glycine and phenylalanine (Serva), basic copper(II) carbonate, borax and methanol (Carlo Erba, RPE), 85% phosphoric acid and 30% sodium hydroxide solutions (Suprapur), acetonitrile (for chromatography) (Merck) and Fluoraldehyde (*o*-phthalaldehyde reagent solution) (Pierce) were used.

The samples and eluents were prepared using water obtained from a Milli-Q system (Millipore) and filtered with a polycarbonate apparatus (Sartorius, Model SM 165.10) through 0.45 μm Millipore filters. All containers were made of polyethylene to prevent possible copper contamination.

Cleaning procedure

Containers, filtration apparatus, Millipore filters and micropipette tips were treated before use with hydrochloric acid (Carlo Erba, RPE), washed with 1,1,2-trifluoroethane (Carlo Erba, RPE) and stored in polyethylene bags or Petri dishes. All chemical procedures were carried out in a laminar vertical flow hood and polyethylene gloves were worn.

Samples preparation

The complexes of copper with the amino acids glycine and phenylalanine were prepared according to Hirson and Barsily [5]. Solid $CuCO_3 \cdot Cu(OH)_2 \cdot nH_2O$ was added, in excess, to a 10 mM solution of glycine or phenylalanine at 50°C and shaken for a few minutes. After cooling and filtration the sample was prepared for injection by 1 + 9 dilution with methanol–borax buffer (pH 9) (80 + 20). When only glycine or phenylalanine was injected, the 10 mM solution was diluted 1 + 9 just like the sample of the copper complex.

The stability of copper–amino acid complexes with respect to the pH of the eluent was verified by visible light spectrophotometry (625 and 610–630 nm for the complexes with glycine and phenylalanine, respectively), under less suitable conditions, i.e., a large excess of phosphate eluent at pH 7.2, without borax buffer and acetonitrile. The volume of the samples injected was 20 μl.

Chromatographic set-up

A schematic diagram of the main components of the LC system is shown in Fig. 1.

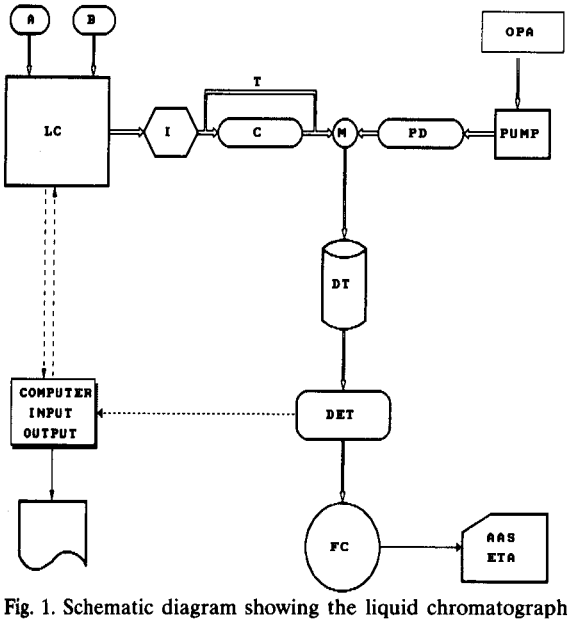

Fig. 1. Schematic diagram showing the liquid chromatograph (LC), the postcolumn derivatization apparatus and the fraction collector. A and B = eluent reservoirs; I = injector; C = column; T = by pass tubing; M = mixer; PD = pulse damper; OPA = *o*-phthalaldehyde reservoir; DT = delay tube; DET = fluorimetric detector; FC = fraction collector.

Columns. The columns used in this study were as follows: Polyspher RP C_{18} (150 mm × 4.6 mm i.d.), average particle diameter 10 μm (Merck); HEMA RP C_{18} (250 mm × 4.6 mm i.d.), particle diameter 10 μm (Alltech); and Superpac-Spherisorb ODS-2 (Dual-Bond) (250 mm × 4 mm i.d.), average particle diameter 5 μm (Pharmacia LKB). These columns had not been previously used.

Eluents. Because of the continuous postcolumn addition of derivatization reagent, which gives problems with regard to the background, high-purity buffers and reagents were used. The eluents prepared by a 12.5 mM phosphate buffer (A) with acetonitrile (AcCN) in various percentages were used under isocratic conditions. The phosphate buffer was prepared by mixing 0.80 ml of 85% H_3PO_4 and 1.95–2.00 ml of 30% NaOH to give a pH of 7.2 and adding Milli-Q-purified water up to 1 l. It is necessary to use eluents with a pH of 7.2 because the maximum pH value permitted when the silica support for RP C_{18} is used is of 7.5.

Final postcolumn derivatization procedure. After many experiments, the optimum conditions were found to be a variable-flow rate from 1 to 1.5 ml min^{-1} for the eluent and 0.5 ml min^{-1} for the derivatization reagent and a temperature of the delay tube of 50°C.

The detection limit of this procedure is 0.1 fmol, which is about ten times lower than previous results obtained with precolumn derivatization [3]. As the limiting step in this work is the sensitivity of the copper determination by ETAAS, the amounts of amino acids injected on to the column are much greater than necessary, which causes elution as large peaks.

Fraction collection. The volumes of the collected fractions, for the subsequent ETAAS determination, varied from 0.50 to 1.00 ml.

RESULTS AND DISCUSSION

Absorption phenomena in postcolumn derivatization

The possible absorption phenomena of copper species, yielded by the derivatization reaction, on the PTFE surface between the column exit and the fraction collector, including the reaction delay tube, were checked and minimized. The chromatographic column was by-passed with a PTFE tube (T in Fig. 1).

The glycine, used as a standard, was first injected in each experiment. The flow of eluent started immediately, up to elution of the glycine. The flow was then stopped, the copper complex sample was injected and the elution restarted. In addition, ionic copper alone was injected in to the apparatus, without a column but with the derivatization reagent, and used as a blank. The fractions for copper determination were also collected.

The eluents used were A–AcCN in the proportions (1) 98 + 2, (2) 95 + 5, (3) 93 + 7, (4) 90 + 10 and (5) 85 + 15. The results obtained for the injection of the complex with the first four eluents are shown in Fig. 2. No significant difference among the eluents was found. There is a maximum at a retention time of about 1 min with a 40–50% recovery. Moreover, there is an over-

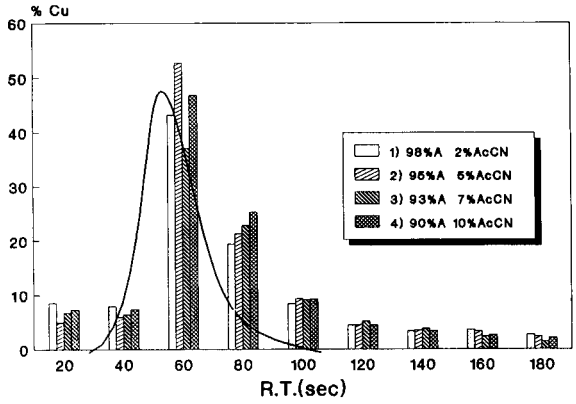

Fig. 2. Recovery of copper in the fractions (0.66 ml) and chromatogram of glycine obtained by injection of the copper–glycine complex, without a column. Isocratic conditions. Eluents 1, 2, 3 and 4, flow-rate, 1.5 ml min; fluorescence detector excitation and emission wavelengs 360 and 530 nm, respectively; flow-rate of derivatization reagent, 0.5 ml min^{-1}; delay tube temperature, 50°C. Amount of copper injected copper and total recovery for each eluent: (1) 400 ng and 92%; (2) 295 ng and 98%; (3) 220 ng and 82%; (4) 400 ng and 100%. Peak area recovery, 100%.

lap, although partial, between the peak of glycine and the band of copper. The cause of incomplete overlap is the dead volume of the PTFE tube between the cell of the fluorimeter and the cup of the fraction collector. The average total recovery of copper is 93%.

The materials and the assembly are satisfactory for postcolumn derivatization without significant absorption phenomena. The chromatographic peak of non-complexed glycine, for eluent 1, is shown in Fig. 3. From a comparison between the areas of the peaks in Figs. 1 and 3 it can be concluded that the derivatization parameters are optimum for complete decomposition of the complex.

The band of copper, injected separately and only with eluent 1, without derivatization, is shown in Fig. 4. The ionic copper can be absorbed more strongly, but there is no problem anyway because the derivatization reaction that binds ionic copper will always be used.

Comparison of the performances of RP C_{18} on different supports

The procedure was carried out with each of the columns fitted in the apparatus shown in Fig.

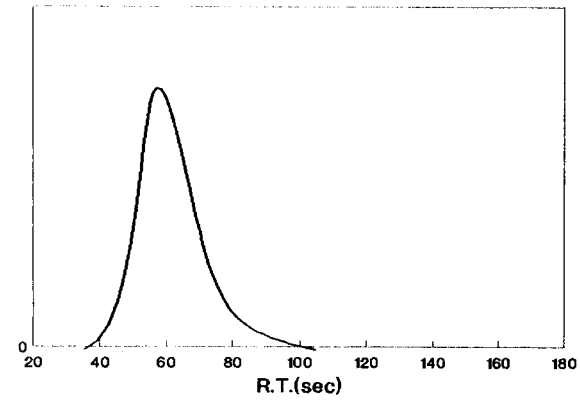

Fig. 3. Chromatogram after injection of non-complexed glycine with eluent 1. Other conditions as in Fig. 2.

1. Three C_{18} materials were used and their properties, provided by the manufacturers, are reported below. As previously indicated, the columns had not been previously used. In practice, the control of the number of chromatographic runs is very important [3].

Polyspher RP C_{18} (Merck). This is the result of a unique preparation process, in which C_{18} groups are covalently bound to a rigid polymeric macroporous matrix. These C_{18} groups shield the analytes from π-orbitals buried deep within the polymeric matrix. This material can be used repeatedly from pH 0 to 14. The mean particle diameter is 10 μm. Two chromatographic runs were car-

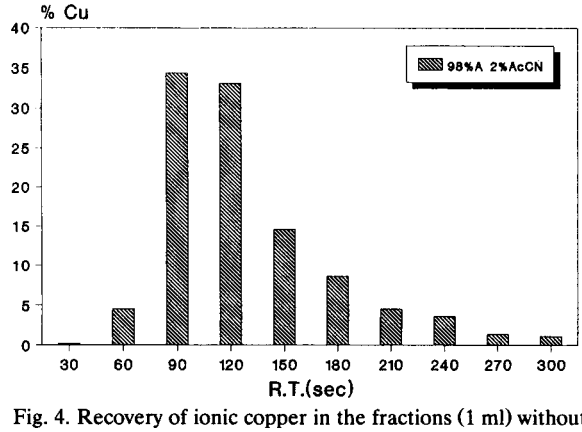

Fig. 4. Recovery of ionic copper in the fractions (1 ml) without column and derivatization, with eluent 1. Flow-rate, 1.5 ml min^{-1}. Amount of copper injected, 430 ng; total recovery, 113%.

ried out with eluents 4 and 5, because this column does not tolerate eluents containing more than 90% of the aqueous component.

No recovery of copper was obtained. It seems that complete decomposition of the complex and a very strong retention of ionic copper occur. Only after flushing the column for several hours, with an eluent containing 70% AcCN was copper found in the eluate. For this reason there are no data available regarding this column, and we consider that it is not useful for this type of study.

HEMA RP C_{18} (Alltech). This material is based on the mechanically rigid and chemically resistant hydroxyethylmethacrylate copolymer. The C_{18} chains were end-capped afterwards. The distribution of the particle diameter is 8–12 μm and the pH operating range is 2–13. The new column was conditioned for 1 h with eluent 1 (flow-rate 1 ml/min). It was kept in AcCN at the end of each run.

Two chromatographic runs were carried out with eluents 1 and 4; the results are shown in Fig. 5. The influence of the reversed phase support, with decomposition of complex, is evident. A difference in retention time of 6 min between the two maxima, even under the best conditions (eluent 4), was found.

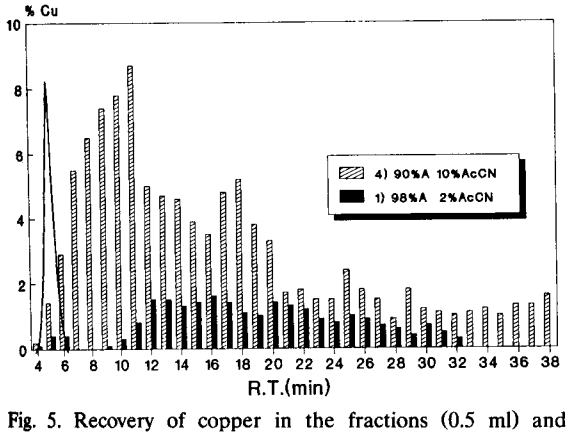

Fig. 5. Recovery of copper in the fractions (0.5 ml) and chromatogram of glycine using eluents 1 and 4 by injection of the copper–glycine complex, with the HEMA RP C_{18} column. Column temperature, 30°C, flow-rate, 1 ml min^{-1}. Amount of copper injected and total recovery for each eluent: (1) 710 ng and 105%, (4) 774 ng and 24%. Peak area recovery, 98%. Other conditions as in Fig. 2.

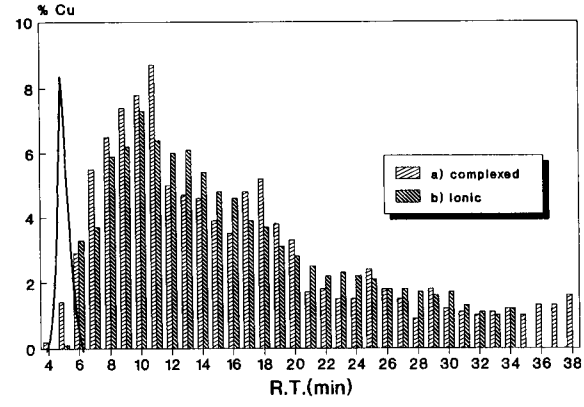

Fig. 6. Comparison between the recovery of copper in the fractions (0.50 ml) obtained by (a) injection of the copper–glycine complex and (b) injection of ionic copper. Column, HEMA RP C_{18}; eluent, 4. Other conditions as in Fig. 2. Amount of copper injected and total recovery: (a) 710 ng and 105%; (b) 397 ng and 98%.

The total recovery (105%) is satisfactory, but the band of copper shows a long tail. The total recovery with the eluent 1 is much lower (24%). Probably the greater percentage of buffer in the eluent makes the ion-exchange effect by OH groups more pronounced.

To confirm the significant influence of the column support, ionic copper was injected, without a derivatization reaction, and the column was eluted with eluent 4. The results obtained are shown in Fig. 6 and compared with the previous results reported in Fig. 5 for the same eluent 4 and the copper–glycine complex, in order to make a direct comparison. The overlap of the copper band confirms the great influence of the reversed-phase support, which also masks the influence of the derivatization reaction on absorption phenomena.

Superpac Dual-Bond (Pharmacia LKB). First the silica surface is precapped with C_2 compounds and then loaded with C_{18} chains. The result is a more efficient coverage of the silica gel surface (25% greater compared with a typical C_{18} gel). The particles have an average diameter of 5 μm and a pH operating range from 2 to 7.5.

Two chromatographic runs were carried out with eluents 2 and 4. From the results of previous experiments (Fig. 5) it turned out that eluent 1

was not suitable for this experiment. The results obtained are shown in Fig. 7. By examining the trend of the copper recovery in the fractions of the eluate, a distribution similar to that in Fig. 2 (without a column) is observed. The band of copper, in fact, for the better eluent 4, is narrow, with a maximum (about 20%) that differs from the maximum of the glycine peak by another 20% with regard to retention time. The total recovery of copper is satisfactory, with an average value of 91%, without the presence of the secondary bands, which were observed in a previous study [3] with conventional RP C_{18}.

A further chromatographic run was carried out with eluent 5, with a higher content of AcCN (15%). The results are also reported in Fig. 7; no improvement was obtained. The optimum eluent composition seems to be A–AcCN (90 + 10) (eluent 4).

This kind of RP C_{18} column is very interesting, taking into account the lack of performance for the Polyspher and HEMA columns. Moreover, the limited separation between the amino acid peak and the narrow band of copper is acceptable. This means that the copper–amino acid complex is not much affected by the support material.

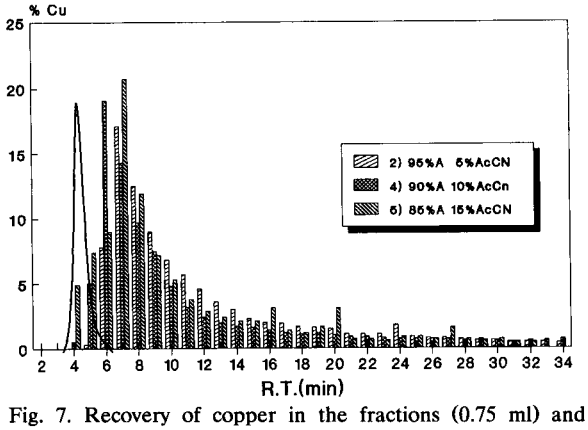

Fig. 7. Recovery of copper in the fractions (0.75 ml) and chromatogram of glycine for eluents 2, 4 and 5 by injection of the copper–glycine complex on the Superpac Dual-Bond C_{18} column. Flow-rate eluents, 1 ml min^{-1}. Amount of copper injected and total recovery for each eluent: (2) 631 ng and 94%, (4) 806 ng and 90%, (5) 470 ng and 90%. Peak area recovery, 96%. Other conditions as in Fig. 2.

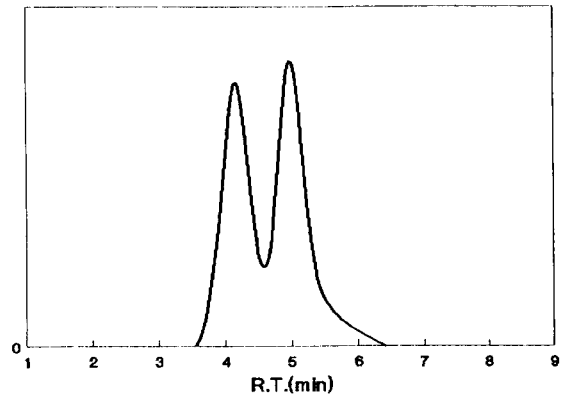

Fig. 8. Chromatogram after injection of non-complexed glycine and phenylalanine with eluent 4, injected on the Superpac Dual-Bond C_{18} column. Other conditions as in Fig. 2.

Subsequently this column was tested with the injection of a sample containing uncomplexed glycine and phenylalanine and using eluent 4. The choice of phenylalanine was based on chromatographic considerations (presence of an aromatic ring) and because of its appreciable abundance in marine matrices, e.g. in phytoplanktonic cells [4] and in humic acid isolated from sediments [6].

The chromatogram obtained is shown in Fig. 8. The two peaks partially overlap. However the amount of the amino acids injected is about 1000 times higher than the detection limit. Moreover, as the band of copper is narrow, it is possible to lower the amounts of copper and amino acids injected, thus lessening the problems for the separation and also for the preconcentration.

A very important consideration is the ageing of the material, which is always accompanied by a decrease in the percentage coverage. With uncontrolled use of the column, the results could be completely different [3].

Conclusions

The postcolumn derivatization procedure reported here, in comparison with the precolumn procedure used previously [3], guarantees, at 50°C, complete decomposition of the complexes. The present procedure has higher reproducibility and sensitivity.

The use of reversed-phase C_{18} material on a silica support seems not to be useful for the separation of the more interesting metal–amino acid complexes, but the use of a reversed phase prepared in a non-conventional mode is recommended. In fact, in this work, satisfactory results were obtained with the Dual-Bond column, and it will be used in a future study of the separation of copper complexes with amino acids in marine ecosystems, after suitable preconcentration at higher contents on the same solid phase. The chromatograms with peaks for amino acids and narrow bands for copper and other metals, although there is not complete overlap, will give useful information for metal speciation.

This work is a contribution of the Gruppo di Ricerca Oceanologica–Genova (GRO–G) and was financially supported by the Ministero Pubblica Istruzione, Fondi 40%, Italy.

REFERENCES

1 G.L. Mills and J.G. Quinn, Mar. Chem., 10 (1981) 93.
2 D.J. Mackey, Mar. Chem., 13 (1983) 169.
3 F. Baffi, M.C. Ianni, A.M. Cardinale, M. Ravera, E. Magi and R. Frache, Anal. Chim. Acta, 260 (1992) 99.
4 F. Baffi, Int. J. Environ. Anal. Chem., 41 (1990) 173.
5 B. Hirson and I. Barsily, Bull. Soc. Chim. Fr., (1957) 1336.
6 E.A. Romankevich, Geochemistry of Organic Matter in the Ocean, Springer, Berlin, 1984, p. 190.

Analytica Chimica Acta, 278 (1993) 91–97
Elsevier Science Publishers B.V., Amsterdam

Role of SCN^- in the liquid–liquid extraction of Pd(II) by Kelex 100 in Toluene from aqueous chloride solutions. The equilibrium approach

E. Anticó, M. Hidalgo, A. Masana and V. Salvadó
Departament de Química, Universitat de Girona, 17071 Girona (Spain)

J. Havel
Katedra Analytické Chemie, Masaryk University, 61137 Brno (Czech Republic)

M. Valiente
Departament de Química, Universitat Autònoma de Barcelona, 08193 Bellaterra, Barcelona (Spain)

(Received 12th September 1992; revised manuscript received 4th January 1993)

Abstract

The liquid–liquid extraction of Pd(II) by 7-(4-ethyl-1-methyloctyl)quinolin-8-ol [Kelex 100 (HL)] in toluene from 1 M aqueous chloride solutions in the presence of SCN^- is described. The investigations included both elucidation of the equilibrium extraction reactions by measurement of the metal distribution and the characterization of extraction kinetics by measuring the Pd(II) extraction rate. In both studies the experimental data were interpreted by chemical models obtained with appropriate numerical calculations by using the programs LETAGROP-DISTR and KILET. In the case of extraction equilibria, it is suggested that the complex species PdL_2 and PdSCNL are formed in the organic phase and PdClL in the aqueous phase to explain the metal distribution observed experimentally. With respect to extraction kinetics, the "best" model was found taking into account the reversible reaction to the formation of aqueous Pd–SCN^-–Cl^- species with the organic extractant Kelex 100. The results obtained for both equilibrium and kinetic data reveal that SCN^- behaves as a catalytic reagent, in agreement with previous results.

Keywords: Extraction; Palladium

The extraction of Pd(II) from chloride media by various common extractants is known to be not very effective. The process is faster from iodide and thiocyanate solutions [1]. As hydrometallurgical processes with palladium are normally carried out in chloride media, several extractants have been developed to treat palladium in this medium. Kelex 100, 7-(1-vinyl-3,3,5,5-tetramethylhexyl)-quinolin-8-ol (pre-1976), appears to be a selective palladium extractant under conditions where most metals cannot be extracted [2], but it has the disadvantage of a slow extraction rate. Later it was found [3] that an important increase in the extraction rate could be realized when a small amount of thiocyanate is added to the aqueous chloride solution. This effect is explained by a "*trans*-effect catalyst" mechanism. The addition of a quaternary ammonium salt to the extractant solution also produced a catalytic effect [4]. Enhancement of the extraction rate has also been

Correspondence to: M. Valiente, Departament de Química, Universitat Autònoma de Barcelona, 08193 Bellaterra, Barcelona (Spain).

reported for other metals [5]; thus, the extraction rate of Co(II) by DEHPA is increased in the presence of carboxylic ligands (acetate, succinate, formate and salicylate) in the aqueous phase. Both effects have been explained in terms of catalytic processes.

The mentioned investigations are related to the kinetics of the liquid–liquid extraction of related metal ions. On the other hand, there is a need for thermodynamic characterization of the extraction reactions including chemical speciation of extracted metals. This knowledge will shed some light on the mechanism of metal extraction to explain the enhancement of the extraction rate. In this respect, some recent studies add new information to the chemistry of Pd(II) extraction by dialkyl sulphides [6] and by trialkylphosphine sulphides [7] in the presence of thiocyanate.

This work examined the extraction equilibrium of Pd(II) by Kelex 100 post-1976 [7-(4-ethyl-1-methyloctyl)quinolin-8-ol] in toluene from aqueous chloride solutions containing small amounts of SCN^-. The study also included a revision of the extraction kinetics.

EXPERIMENTAL

Reagents and solutions

Kelex 100 was kindly supplied by Shering España (Barcelona, Spain) and was purified as described by Al-Bazi and Freiser [3]. Sodium chloride (analytical-reagent grade, Panreac) was purified as described previously [8]. Sodium thiocyanate solutions were standardized by titration with silver nitrate solution, iron(III) ammonium sulphate being used as an indicator.

A 3×10^{-3} M stock solution of Pd(II) was obtained by dissolving the required amount of palladium chloride (Spanish Society of Precious Metals) in 0.1 M hydrochloric acid, and was standardized gravimetrically with dimethylglyoxime [9].

The aqueous phase, containing 3×10^{-5} M Pd(II) and 1.0 M Cl^-, was prepared by dilution of the stock palladium solution by adding the necessary amount of sodium chloride. In these solutions thiocyanate was present in the range 8×10^{-5}–4×10^{-4} M. The H^+ concentration was kept constant in all experiments at 0.01 M to prevent the hydrolysis of palladium.

The organic phase was prepared by dissolving Kelex 100 in toluene (analytical-reagent grade, Panreac), which had been successively washed with 0.5 M sodium hydroxide, distilled water, 0.5 M hydrochloric acid and doubly distilled water before use. The Kelex 100 concentration was varied from 3.83×10^{-5} to 2.14×10^{-4} M. In some experiments trilaurylammonium chloride (TLAHCl) (Merck) was added to the organic solutions.

Apparatus

A Labinco rotary mixer was employed to shake aqueous and organic solutions. A Hitachi U-1100 UV–visible spectrophotometer was used for the measurement of absorbance.

Analyses

The concentration of Pd(II) in the aqueous phase was determined by a spectrophotometric method, measuring the absorbance at 310 nm in excess of thiocyanate [10].

Experiments were carried out to determine thiocyanate content in the organic phase. Negative results were obtained by elemental analyses.

Procedure

The distribution of palladium between equal phase volumes (10 ml) was determined as a function of Kelex 100 and thiocyanate concentrations. The experimental data were expressed in terms of the distribution coefficient, D, defined as

$$D = [\mathrm{Pd(II)}]_{org}/[\mathrm{Pd(II)}]_{aq}$$

The shaking time needed to reach equilibrium was determined previously and was found to be about 600 h. After this time, the mixture was centrifuged and the phases were separated. A 1-ml sample of the aqueous phase was removed and analysed.

For studying the extraction kinetics, the experimental procedure was the same as for studying the extraction equilibrium, but samples were withdrawn at different times until equilibrium

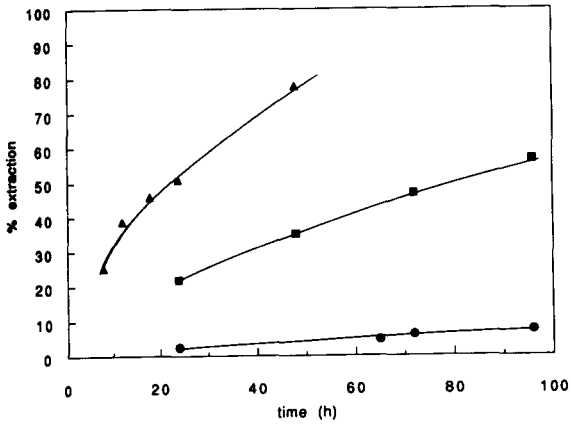

Fig. 1. Effect of aqueous thiocyanate or organic TLAHCl on the extraction rate of palladium. ● = 5×10^{-4} M Kelex 100; ■ = 5×10^{-4} M Kelex 100 + 2×10^{-4} M TLANCl; ▲ = 5×10^{-4} M Kelex 100 + 2×10^{4} M SCN^-.

was reached. The experiments were performed at a controlled room temperature of 22 ± 1°C.

RESULTS AND DISCUSSION

Palladium extraction equilibrium

Figure 1 shows the effect of both aqueous thiocyanate and organic TLAHCl on the extraction rate of palladium. As observed, SCN^- is most effective in enhancing the rate of extraction,

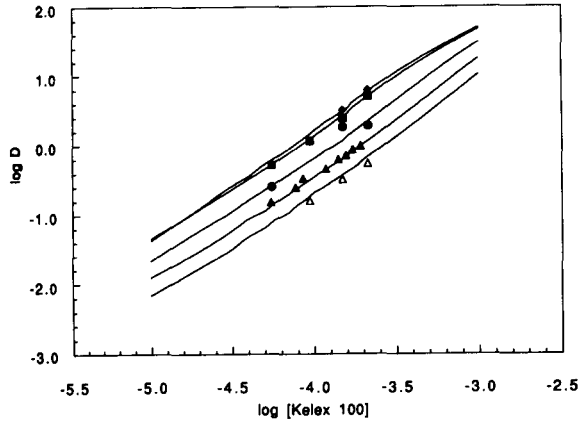

Fig. 2. Distribution coefficient of Pd(II) as a function of Kelex 100 concentration at different levels of SCN^-. Continuous lines are the theoretical curves obtained from model VIII. [SCN^-]: △ = 4×10^{-4}; ▲ = 3×10^{-4}; ● = 2×10^{-4}; ■ = 1×10^{-4}; ♦ = 8×10^{-5} M.

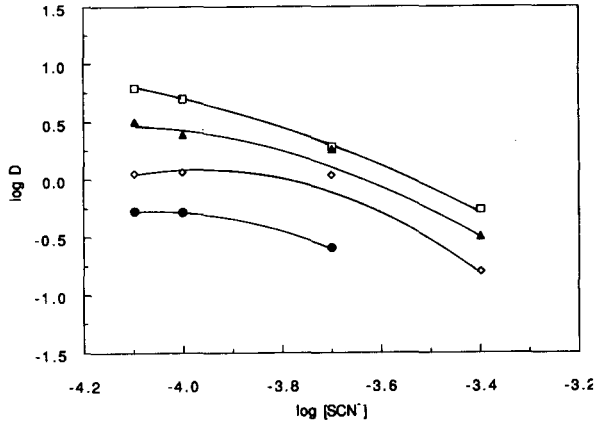

Fig. 3. Effect of thiocyanate on the extraction of Pd(II). [Kelex 100]: □ = 2.14×10^{-4}; ▲ = 1.5×10^{-4}; ◇ = 9.42×10^{-5}; ● = 5.56×10^{-5} M.

so efforts were concentrated on characterizing the reactions in the presence of SCN^-.

Figure 2 shows the experimental values of the distribution coefficient as a function of the Kelex 100 concentration. In Fig. 3 the effect of thiocyanate is shown for the range 8×10^{-5}–4×10^{-4} M. Maximum extraction was found for [SCN^-] = 8×10^{-5} and 1×10^{-4} M.

To analyse the obtained data the following points were considered. Aqueous palladium is present as a tetrachloro complex, $PdCl_4^{2-}$, at chloride concentrations higher than 0.1 M and at a ionic strength of 1.0. In the presence of thiocyanate some mixed species are formed according to the reaction

$$PdCl_4^{2-} + iSCN^- \rightleftharpoons PdCl_{(4-i)}SCN_i^{2-} + iCl^- \quad (1)$$

with $i = 1, 2, 3$ and 4. The values of k_i were obtained from the literature [11].

When this aqueous phase was contacted with an organic solution containing the extractant Kelex 100 in toluene, several reactions occurred which can be described by the following equations, where reaction (2) means the formation of complexes in the organic and reaction (3) in the aqueous phase:

$$PdCl_4^{2-} + nHL_{org} + mSCN^- \rightleftharpoons (PdCl_{4-(m+n)}SCN_mL_n)_{org} + (m+n)Cl^- + nH^+ \quad (2)$$

$$PdCl_4^{2-} + pHL_{org} + qSCN^- \rightleftharpoons PdCl_{4-(p+q)}SCN_pL_q + (p+q)Cl^- + pH^+ \quad (3)$$

It is known from the literature that extraction of Pd(II) with Kelex 100 occurs via a chelating process [2]. The species formed may contain chloride and thiocyanate in addition to one or two molecules of Kelex 100.

In addition to reactions 1–3 other reactions that influence the system must be taken into account. These reactions are the protonation of thiocyanate [12], the distribution of neutral Kelex 100 between the organic and aqueous phases [2] and the protonation of Kelex 100 in the aqueous phase [2]. The dissociation of the phenolic proton of Kelex 100 can be ignored in acidic media as its pK_a value is high [2].

To evaluate the composition of the extracted species and the corresponding formation constants, the experimental data were analysed numerically with both LETAGROP-DISTR [13] and EXLET [14] programs, which are based on the minimization of the error-square sum, U:

$$U = \sum_{i=1}^{N} (\log D_{calc} - \log D_{exp})^2 \quad (4)$$

where D_{exp} are the experimental values of the distribution coefficient, D_{calc} are the corresponding values calculated from the relevant mass-balance equation for a proposed model and N is the total number of experimental points.

The results of the LETAGROP-DISTR calculations for different models tested, based on reactions 2 and 3, are summarized in Table 1. As can be seen, model I with only one complex formed in the organic phase, which contains one molecule of palladium and two molecules of Kelex 100, gives the worst fit. With models II–VI, which include metal–Kelex 100 complexes in the aqueous phase, a considerable improvement of the fit is observed except for model V.

Models VII and VIII include the formation of mixed complexes with chloride and thiocyanate

TABLE 1

Results of the equilibrium study for the different extraction models using the LETAGROP-DISTR and the EXLET program

Model	Species model	Pd, SCN^-, HL	Log k	σ(log D) [a]	U
I	PdL_2(org)	1, 0, 2 (org)	7.05 ± 0.13	0.146	0.450
II	PdL_2(org)	1, 0, 2 (org)	7.21 ± 0.07	0.088	0.164
	PdL_2(aq)	1, 0, 2 (aq)	6.34 ± 0.21		
III	PdL_2(org)	1, 0, 2 (org)	7.23 ± 0.06	0.073	0.113
	PdClL(aq)	1, 0, 1 (aq)	4.46 ± 0.16		
IV	PdL_2(org)	1, 0, 2 (org)	7.46 ± 0.07	0.083	0.145
	PdSCNL(aq)	1, 1, 1 (aq)	9.14 ± 0.11		
V	PdL_2(org)	1, 0, 2 (org)	7.06 ± 0.13	0.146	0.450
	$Pd(SCN)_2L$(aq)	1, 2, 1 (aq)	11.24, max. = 12.48		
VI	PdL_2(org)	1, 0, 2 (org)	7.24 ± 0.06	0.073	0.112
	PdL_2(aq)	1, 0, 2 (aq)	5.57, max. = 6.09		
	PdClL(aq)	1, 0, 1 (aq)	4.40 ± 0.18		
VII	PdL_2(org)	1, 0, 2 (org)	7.22 ± 0.06	0.072	0.110
	PdL_2(aq)	1, 0, 2 (aq)	Max. = 5.95		
	PdClL(aq)	1, 0, 1 (aq)	4.48 ± 0.15		
	PdClL(org)	1, 0, 1 (org)	3.79, max. = 4.29		
VIII	PdL_2(org)	1, 0, 2 (org)	7.14 ± 0.07	0.059	0.077
	PdL_2(aq)	1, 0, 2 (aq)	Max. = 5.88	R = 0.1297	
	PdClL(aq)	1, 0, 1 (aq)	4.37 ± 0.17	χ^2 = 5.64 (12.60)	
	PdSCNL(org)	1, 1, 1 (org)	8.16, max. = 8.44		

[a] σ(log D) is the standard deviation defined as $\sigma(\log D) = [U/(N - N_k)]^{1/2}$, where N_k is the number of constants to be adjusted. The error in the constants is given as $\pm 3\sigma(\log k)$ but for $\sigma(k) > 0.2k$ the "best" value of log k and the maximum value $\{\log[k + 3\sigma(k)]\}$ are given. Goodness of fit for model VIII was calculated by the EXLET(92) program [15].

not only in the aqueous but also in the organic phase. The fit is slightly better than for model VI but, for the complex $PdClL_{org}$, the ratio $k/\sigma(k)$ is less than 2.0, which means that the presence of this species is negligible. This is not the case for $PdSCNL_{org}$.

It can be concluded that model VIII explains the experimental data best. Based on this model, the theoretical curves in Fig. 2, were calculated.

The stoichiometry of metal complexes with respect to Cl^- and H^+ cannot be determined as all the experimental data were obtained at high constant Cl^- and low constant pH values.

The last model was also introduced in the EXLET program. Because of the minimizing routines used, the fit was even better. With this program one can also obtain directly the distribution of the species with respect to the different components; it could be verified that the complex PdL_2 is the major one responsible of the extraction of palladium at a thiocyanate concentration lower than 1×10^{-3} M and that the presence of the species PdSCNL in the organic phase was always less than 3.6% of the total metal concentration (see Fig. 4). These results lead to a lower detection limit of thiocyanate ion in the organic phase. It is also possible with the EXLET program to refine the stoichiometry of some complexes simultaneously with equilibrium constants

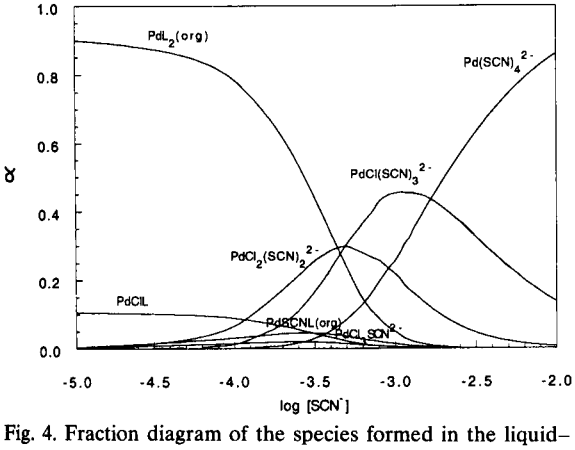

Fig. 4. Fraction diagram of the species formed in the liquid–liquid extraction system Pd(II)–SCN^-–Kelex 100, calculated by using model VIII.

(see model VIII in Table 1); it was obtained for the palladium complex that the metal-to-ligand ratio of 1:2 was correct. Finally, this program offers other statistical criteria to evaluate the goodness of the model. Thus, not only U, the sum of squares of residuals, but also the standard deviation of the response function and four moments of residuals were calculated: arithmetic mean, variance, coefficient of skewness and coefficient of curtosis. Further, Pearson's χ^2 test was applied and the Hamilton R-factor calculated. The statistical parameters were satisfactory. The standard deviation of 0.059 appears to be high but it is less than estimated inaccuracy of the experiments (about 0.075). However, the value of χ^2 is acceptable, because it is less than the theoretical value (12.60).

The equilibrium study by Ma and Freiser [2] in 2.0 M chloride and in the absence of thiocyanate explains the Pd(II) extraction by the equation

$$PdCl_4^{2-} + 2HL_{org} \rightleftharpoons PdL_{2org} + 2H^+ + 4Cl^- \quad (5)$$

with a value for k_{ex} equal to $10^{5.86 \pm 0.06}$. In this work, the value obtained for the extraction constant from 1.0 M Cl^- medium is $10^{7.14 \pm 0.07}$. Taking into account the differences in Cl^- concentration, a corrected value of $k_{ex} = 10^{5.94 \pm 0.07}$ is obtained, which is in good agreement with the value of Ma and Freiser.

From these results, it follows that, although thiocyanate acts as an accelerator of the process, the value of the k_{ex} is not modified by this ion. This agreement also supports the role of thiocyanate as a catalytic agent. On the other hand, a comparison of the present results with those obtained previously with triisobutylphosphine sulphide (TIBPS) [7] or dioctyl sulphide (DOS) [6] instead of Kelex 100 reveals a completely different role of thiocyanate in the extraction mechanism. Thus, whereas in all instances the rate of extraction is enhanced, with TIBPS and DOS, SCN^- also acts as a complexing ligand stabilizing the extracted metal species. It seems that the role of thiocyanate also depends on the type of chemical interaction between the extracting agent and the aqueous metal species. With TIBPS and DOS

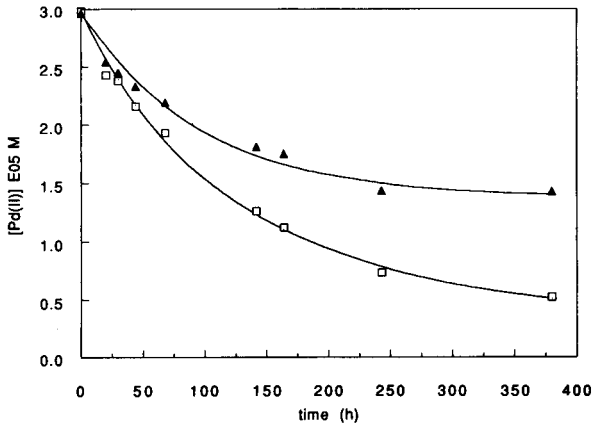

Fig. 5. Extraction rate data represented as aqueous palladium concentration vs. time. Solid lines were calculated by using the kinetic model based on Eqn. 6. $[SCN^-]$: □ = 1×10^{-4}; ▲ = 3×10^{-4} M.

a solvating reaction is assumed, whereas with Kelex 100 it is a chelating interaction.

Palladium extraction kinetics

In order to characterize the extraction rate of the system under study, the decrease in the palladium concentration with time was measured until equilibrium was reached for two different aqueous thiocyanate concentrations (see Fig. 5). It was observed that the presence of thiocyanate not only influences the extraction rate but also the extent of the extraction.

These experimental data were modeled by using the computer program KILET [16], which is a general regression program applying a pit-mapping minimizing method. The aim of the calculations is to find the "best" kinetic model, i.e., the number of reactions, reaction stoichiometry and rate constants. Table 2 gives the results obtained by the KILET program when just a forward first-order reaction is considered. A model including the corresponding reverse reaction (constant rate symbolized by k_r) improves the fit considerably, as shown by the results in the table.

In these two previous models just a first-order reaction with respect to the metal was considered. When the complexity of the system is taken into account, it is reasonable to consider other species taking part in the reaction, i.e., Kelex 100 and thiocyanate. In the studied range of thiocyanate concentration between 8×10^{-5} and 4×10^{-4} M, palladium is present mostly in two forms, $PdCl_2(SCN)_2^{2-}$ and $PdCl(SCN)_3^{2-}$ [3]. Hence it can be assumed that the reaction

$$PdCl_2(SCN)_2^{2-} + 2HL_{org} \rightleftharpoons PdL_{2org} + 2Cl^- + 2SCN^- + 2H^+ \quad (6)$$

or

$$PdCl(SCN)_3^{2-} + 2HL_{org} \rightleftharpoons PdL_{2org} + Cl^- + 3SCN^- + 2H^+ \quad (7)$$

could take place. The results obtained are also given in Table 2.

A comparison of these two models (Eqns. 6 and 7) reveals a better fit for the model described by the latter. Also for this model it is observed that k_f and k_r are similar for the different thio-

TABLE 2

Results obtained for the different models using the KILET program

Equation model	$[SCN^-]_{tot}$ (M)	U [a]	σ [a]	R factor ($\times10^2$)	k_f	k_r
Pd(II)aq → Pd(II)org	1×10^{-4}	1.515×10^{-2}	4.353×10^{-1}	7.6	$(6.04\pm0.38)\times10^{-3}$	–
	3×10^{-4}	6.201×10^{-2}	8.084×10^{-2}	13.0	$(3.02\pm0.43)\times10^{-3}$	–
Pd(II)aq → Pd(II)org	1×10^{-4}	4.761×10^{-3}	2.439×10^{-2}	4.26	$(7.11\pm0.43)\times10^{-3}$	$(1.22\pm0.38)\times10^{-3}$
	3×10^{-4}	5.950×10^{-3}	2.496×10^{-2}	4.02	$(5.95\pm0.29)\times10^{-3}$	$(5.48\pm1.08)\times10^{-3}$
[6]	1×10^{-4}	2.892×10^{-10}	6.013×10^{-7}	3.5	$(2.02\pm0.23)\times10^{5}$	$(1.82\pm1.16)\times10^{4}$
	3×10^{-4}	4.764×10^{-10}	7.717×10^{-7}	3.8	$(1.58\pm0.20)\times10^{5}$	$(3.65\pm0.10)\times10^{4}$
[7]	1×10^{-4}	2.916×10^{-11}	6.037×10^{-7}	3.5	$(2.01\pm0.36)\times10^{5}$	$(8.00\pm0.00)\times10^{7}$
	3×10^{-4}	5.444×10^{-11}	8.249×10^{-7}	4.1	$(1.46\pm0.23)\times10^{5}$	$(8.10\pm0.00)\times10^{7}$

[a] In this case U is the square sum of residuals of aqueous Pd(II) concentration; σ is the standard deviation.

cyanate concentrations. Theoretical [Pd(II)] vs. time curves, obtained from Eqn. 7, are presented in Fig. 5 together with the experimental points. Some other models, including only one molecule of Kelex 100, were tried, but in all instances the fit was much worse than that obtained with Eqn. 7. For these results it must be taken into account that experimental data were recorded during 400 h, which allows not only the contribution of the backward reaction but also the formation of final complex species in the organic phase.

Although the results have to be considered to represent the overall extraction rate process and assuming that the contribution of diffusion is negligible, they agree to some extent with those reported by Al-Bazi and Freiser [3]. They suggested that the homogeneous reaction

$$PdCl(SCN)_3^{2-} + HL \rightarrow Pd(SCN)_3HL^- + Cl^- \quad (8)$$

was the rate-determining step.

The kinetic model assuming Eqns. 6 and 7 also agrees with the results obtained in equilibrium studies where the maximum extraction yield corresponded to the maximum formation of $PdCl_2(SCN)_2^{2-}$ and $PdCl(SCN)_3^{2-}$ aqueous species. The proposed model also supports the role of SCN^- as a catalyst of the extraction process in the sense that the formation of the PdL_2 complex is energetically easier (faster) from mixed chloro–thiocyanate species $PdCl_2(SCN)_2^{2-}$ or $PdCl(SCN)_3^{2-}$ than from the corresponding chloro complex. Also, the confirmation of the formation of an aqueous PdL complex in the equilibrium study supports the stepwise extraction mechanism suggested by Al-Bazi and Freiser.

This work was carried out under a CICYT project (MAT-886/90-C02). CIRIT is also acknowledged for the support given to the acquisition of some of the equipment employed (ref. AR90-3620).

REFERENCES

1 T. Sekine and Y. Hasegawa, Solvent Extraction Chemistry, Dekker, New York, 1977.
2 E. Ma and H. Freiser, Inorg. Chem., 23 (1984) 3344.
3 S.J. Al-Bazi and H. Freiser, Solvent Extr. Ion Exch., 4 (1986) 1121.
4 Q. Rong and H. Freiser, Solvent Extr. Ion Exch., 5 (1987) 923.
5 D.T. Wasan, Z.M. Gu and N.N. Li, Faraday Discuss. Chem. Soc., 77 (1984) 67.
6 G. Cote, K.M. Ganguly and D. Bauer, Hydrometallurgy, 23 (1989) 37.
7 M. Hidalgo, A. Masana, V. Salvadó, M. Muñoz and M. Valiente, Talanta, 38 (1991) 483.
8 Some Laboratory Methods, Inorganic Chemistry, Royal Institute of Technology (KTH), Stockholm, 1959.
9 A.I. Vogel, Textbook of Quantitative Inorganic Analysis, Longman, London, 1978.
10 K.S. De Haas, J. Inorg. Nucl. Chem., 35 (1973) 3231.
11 A.A. Biryukou and V.I. Shelenskaya, Russ. J. Inorg. Chem., 12 (1967) 1362.
12 L.G. Sillén and A.E. Martell, Stability Constants of Metal-Ion Complexes, Supplement No. 1. Chemical Society, House, London, 1964.
13 D.H. Liem, Acta Chem. Scan., 25 (1967) 1521.
14 J. Havel and M. Meloun, in D.J. Leggett (Ed.), Computational Methods for the Determination of Formation Constants, Plenum, New York, 1985, p. 22.
15 J. Havel, M. Aguilar and M. Valiente, Comput. Chem., submitted for publication.
16 J. Havel and J.L. González, Scr. Fac. Sci. Nat. Univ. Purkynianae Brun., 19 (1989) 183.

Analytica Chimica Acta, 278 (1993) 99–113
Elsevier Science Publishers B.V., Amsterdam

Flow-injection sample preparation for organotin speciation analysis of water by capillary gas chromatography–microwave-induced plasma atomic emission spectrometry

Joanna Szpunar-Łobińska, Michiel Ceulemans, Ryszard Łobiński and Freddy C. Adams

Department of Chemistry, University of Antwerp (UIA), Universiteitsplein 1, B-2610 Wilrijk (Belgium)

(Received 20th October 1992; revised manuscript received 5th January 1993)

Abstract

A semi-automated flow-injection system was developed for on-line sample preparation for the determination of mono-, di- and tributyl- and -phenyltin compounds in water. The procedure is based on the preconcentration of ionic organotin compounds by sorption on bonded silica with octadecyl functional groups followed by on-column ethylation using sodium tetraethylborate. The derivatized species are eluted with 250 μl of methanol, separated by gas chromatography and detected with a microwave-induced plasma atomic emission detector. Aliquots of 25 μl of the eluate are introduced on to a capillary column using the cool injection technique. The solvent is vented off in the liner before the temperature of the latter is raised to release the analytes. A 10–50-ml water sample is sufficient for the analysis and a detection limit of 0.1 ng l^{-1} can be obtained. The developed procedure was applied to the determination of organotin compounds in a number of river water samples which were analysed in parallel using a manual liquid–liquid extraction procedure. The results agreed within 10–15% for concentrations of a few ng l^{-1}.

Keywords: Atomic emission spectrometry; Flow injection; Gas chromatography; Sample preparation; Microwave-induced plasma; Organotin; Plasmas; Preconcentration; Solid-phase extraction; Speciation; Waters

The growing awareness of the pollution of the aquatic environment by organotin compounds in recent years has resulted in a steadily increasing number of reports concerning the analytical chemistry of these contaminants. The greatest hazard to biological life is associated with the use of tributyl- (TBT) and triphenyltin (TPT) compounds as biocides, especially in antifouling paints [1–4]. The most affected are waters with intense ship activity such as in harbour docks and estuaries. Once released, organotins can undergo a variety of physico-chemical processes such as biodegradation, biomethylation, sorption on the particulate matter or vaporization [2–4].

As the toxicity of organotin is strongly species dependent, a viable analytical method for monitoring these contaminants should be species selective, allowing for the determination of the target compounds (e.g., TBT and TPT) without interference from other organotin species. At present, the speciation analysis of organotin is usually performed by coupled techniques based on a combination of a chromatographic separation technique with a sensitive and element selective detection method [5–7]. Despite the increasing popularity of liquid chromatography–inductively coupled mass spectrometry [8–10], the coupling of gas chromatography (GC) with atomic absorp-

Correspondence to: F.C. Adams, Department of Chemistry, University of Antwerp (UIA), Universiteitsplein 1, B-2610 Wilrijk (Belgium).

tion spectrometry (AAS) [5,11,12], flame photometric detection (FPD) [4,13,14], microwave-induced plasma atomic emission spectrometry (MIP-AES) [15,16] and mass spectrometry (MS) [14,17] remain the most preferred owing to the good resolution and the availability of sensitive detectors.

Regulations coming to force in many countries have created the need for simple, rapid and easy to automate methods for speciation analysis of organotin at low ng l^{-1} levels in environmental waters. Limitations in the current methods for speciation analysis of organotin are mostly on the sample preparation side. Indeed, the instrumentation is commercially available (GC–FPD, GC–AES) or can be assembled relatively easily in the laboratory (GC–AAS). However, although a comprehensive chromatographic run for organotin species takes less than 15 min, the analytes must first be separated from water, derivatized and often preconcentrated. Procedures based on extraction of organotin chelates with diethyldithiocarbamate or tropolone followed by Grignard derivatization are usually multi-step, tedious and time consuming. Losses of analytes can occur and there is a potential health hazard in handling large amounts of volatile organic solvents. Another approach to sample preparation involves in situ derivatization by hydride generation [18,19] or ethylation with sodium tetraethylborate ($NaBEt_4$) [20–23] followed by purge-and-trap or extraction separation/preconcentration. The analysis time is considerably reduced but some disadvantages still remain. Purge-and-trap methods offer very efficient preconcentration, but suffer from condensation problems in the case of less volatile hydrides such as Bu_3SnH or Ph_3SnH or ethylated organotin compounds. These disadvantages are eliminated in liquid–liquid extraction procedures but the volume of the extract obtained is usually 100–1000 times larger than can be injected on to a GC column. The necessity for a further preconcentration step by evaporation prevents these methods from being automated.

Solid-phase extraction is an attractive approach to the preconcentration of traces of analytes. Its advantages over liquid–liquid extraction include a higher enrichment factor, lower risk of contamination and the ease of application to field sampling and in *on-line* manifolds. These advantages have been widely explored for the preconcentration of ultratraces of metals (chelate sorbents) [24] and organic pollutants (alkyl-bonded sorbents) [25–27], whereas reports on the application of this technique in the analytical chemistry of organometallic compounds are very scanty [13,28–33], seldom leading to viable analytical methods. Different solid phases such as graphitized carbon black [28,29], C_8 [30] and C_{18} [30–33] have been used as sorbents, allowing preconcentration factors of 500–1000 to be achieved. The procedures developed so far have mostly been restricted to individual species and the selectivity was poor. The large sample volumes processed resulted in long sampling times. Considerable amounts of the eluate which needed to be evaporated were usually obtained. Hence, the figures of merit of the analytical methods based on solid-phase extraction of organotin compounds did not match those obtained using liquid–liquid extraction or purge-and-trap procedures. The analysis time was even longer owing to the necessity for off-line derivatization.

This paper presents a comprehensive optimization study of the sorption of mono-, di- and tributyl- and -phenyltin compounds using C_{18} packed microcolumns and extraction discs, followed by in situ heterophase derivatization of ionic species using $NaBEt_4$. A semi-automated system for on-line preconcentration/derivatization of organotin compounds was developed and applied to the analysis of river water samples by capillary GC–AES.

EXPERIMENTAL

Apparatus

The flow-injection manifold consisted of a Minipuls peristaltic pump (Gilson, Viliers le Bel, France) fitted with Tygon (for aqueous solutions) and Viton (for organic solvents) pump tubing (Gilson), two six-way valves (Rheodyne, Cotati, CA), four miniature three-way valves (Hamilton, Darmstadt, Germany) and a C_{18} microcolumn

(Perkin-Elmer, Überlingen, Germany). The flow system was assembled of 0.5 mm i.d. PTFE tubing and connectors. Filter holders (diameter 25 mm) obtained from Schleicher and Schüll (Dassel, Germany) were used to house extraction discs.

Ethylated organotin species were separated on an HP-1 capillary column (25 m × 0.32 mm i.d., 0.17 μm film thickness) using a Model 5890 Series II gas chromatograph (Hewlett-Packard, Avondale, PA) and detected by means of an HP Model 5921A atomic emission detector. The gas chromatograph was equipped with a KAS 503 temperature-programmed cooled injection system (Gerstel, Mülheim, Germany). Injections were made manually using a Hamilton 701RN syringe equipped with a needle (0.64 mm o.d.) with a polished finish (Gerstel) to fit the septumless injection head. Smooth finished glass vaporization tubes filled with a 2-cm plug of Tenax (80–100 mesh) (Hewlett-Packard) were used.

Materials

Analytical-reagent grade chemicals obtained from Merck (Darmstadt, Germany) were used unless stated otherwise. Deionized water, further purified in a Millipore Milli-Q system, was used throughout.

Bu_4Sn (93%), Bu_3SnCl (96%), Bu_2SnCl_2 (95%), $BuSnCl_3$ (95%), Ph_3SnCl (95%), Ph_2SnCl_2 (96%) and $PhSnCl_3$ (98%) were obtained from Aldrich (Milwaukee, WI). Stock solutions were prepared by dissolving the appropriate amount of the organotin salt in ethanol–water (96 + 4, v/v) to yield a theoretical concentration of 0.5 mg ml^{-1} (as Sn) and were stored at 4°C in the dark. The exact concentration was determined by flame AAS after conversion of organotin into tin by means of sulphuric acid, nitric acid and hydrogen peroxide [11]. The chromatographic purity of the standards with respect to other organotin compounds was checked by GC–AES after ethylation and liquid–liquid extraction. Working standard solutions were prepared daily by appropriate dilution of the stock solution with 0.01 M hydrochloric acid.

Sodium tetraethylborate ($NaBEt_4$) was obtained from Strem Chemicals (Bischheim, France). A 0.3% (w/v) aqueous solution was prepared daily.

Citric acid–phosphate buffer solution (pH 5.0)

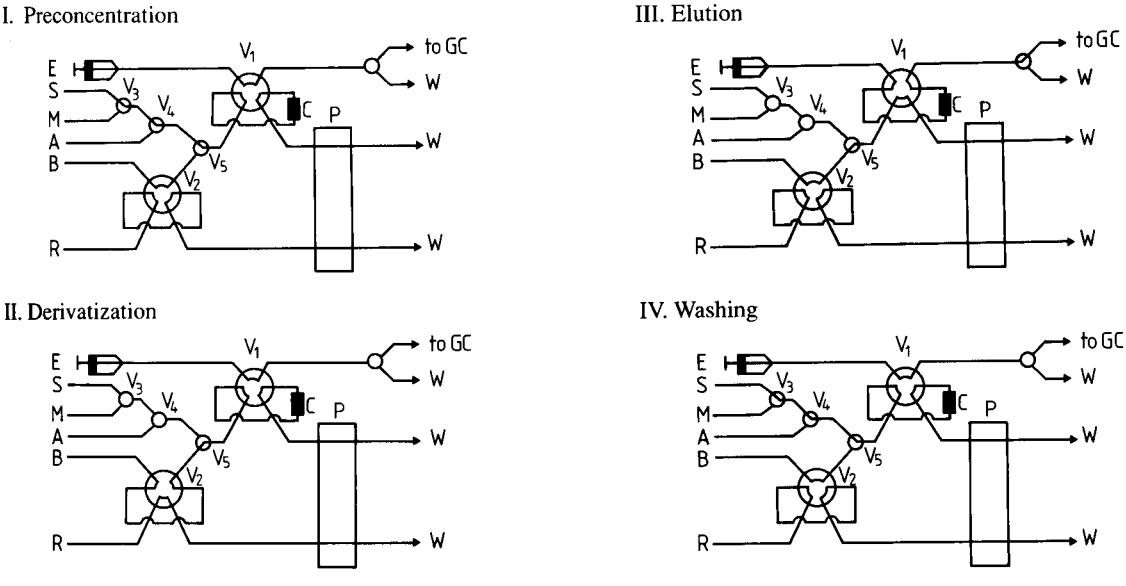

Fig. 1. Flow manifold used in on-line preconcentration–derivatization of organotin compounds. B = Buffer; E = eluent; S = sample; R = derivatizing reagent; M = methanol; A = air, P = peristaltic pump; V_1, V_2 = six-way valves; V_3–V_6 = three-way valves; C = preconcentration microcolumn; D = to detector; W = to waste.

was prepared by dissolving 10.3 g of citric acid monohydrate and 18.156 g of sodium dihydrogenphosphate dihydrate in 1 l of water. Ammonia–citrate buffer solution (pH 9.0) was prepared by dissolving 20.6 g of sodium citrate in 1 l of water and adjusting the pH with concentrated ammonia.

Empore extraction discs (diameter 25 mm) with Bakerbond C_{18} were obtained from J.T. Baker (Deventer, Netherlands). After installation in the filter holder, the discs were prewashed with 10 ml of methanol followed by 10 ml of water.

Liquid–liquid extraction was done in custom-designed 60-ml bottle-like vessels with a thin neck (9 mm i.d.). The design of the vessels allowed easy recovery of the organic phase and made cleaning them easier compared with a separating funnel. Extraction vessels were cleaned by boiling in concentrated HNO_3 solution. Sampling bottles and glassware were cleaned with a common detergent, thoroughly rinsed with deionized water, soaked in 10% hydrochloric acid, and rinsed with deionized water just before use.

Off-line recovery experiments

A 100-ml volume of water was spiked with a known concentration of six organotin compounds added as a mixed standard solution. Then pH was adjusted by adding 10 ml of buffer and the sample was drawn by pumping through a 25-mm Empore extraction disc (5 ml min^{-1}) or the C_{18} microcolumn (2 ml min^{-1}). Organotin compounds were determined in the eluate using the liquid–liquid extraction procedure described below. In order to determine the organotin retained on the membrane, the latter was immersed in a buffer solution (pH 5) containing 0.3% $NaBEt_4$ and treated ultrasonically for 5 min on addition

TABLE 1

Sequence of operation of the *on-line* preconcentration–derivatization system

Operation	Step	Duration (min)	Function	Medium pumped	Valve position [a]					
					V_1	V_2	V_3	V_4	V_5	V_6
Preconcentration	1	5 [b]	Sample loading Filling injection loop with reagent	Sample Reagent	1	1	1	1	1	– [c]
Derivatization	2	2.5	pH adjustment	Buffer	1	1	–	–	0	–
	3	1	Derivatization	Buffer	1	0	–	–	0	–
Elution	4	0.5	Drying the column	Air	0	–	–	–	–	0
	5	0.5	Elution	Eluent	0	–	–	–	–	1
Washing	6	2.5	Washing of the column and sample delivery tubing	Methanol	0	–	0	1	1	0
	7	1.5	Conditioning the column	0.01 M HCl	0	–	–	0	1	0

[a] Six-way valves:

Position 1 Position 0

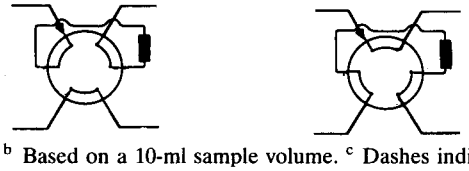

Three-way valves:

Position 1 Position 0

[b] Based on a 10-ml sample volume. [c] Dashes indicate not important.

of 2 ml of hexane to the system. After separation of phases the organic phase was analysed for organotin by GC–AES.

Solid phase extraction–derivatization procedure

The flow-injection manifold for *on-line* integrated preconcentration/derivatization of ionic butyltin and phenyltin species in different operation modes is shown in Fig. 1. A detailed sequence of operations is given in Table 1 together with the corresponding positions of the valves.

Four principal operations can be distinguished in each cycle:

Preconcentration. A 10–50-ml sample (S) was drawn through a C_{18} microcolumn (C) fitted in the injection loop of the Rheodyne six-way valve (V_1) by pumping at a flow-rate of 2.0 ml min^{-1}. The injection loop of the valve V_2 was filled with the $NaBEt_4$ solution (R).

Derivatization. The column was washed with 5 ml of citrate–ammonia buffer solution (B) (pH 9.0) and then the V_2 valve was switched allowing the derivatizing agent to enter the column. Then the column was dried by pumping air.

Elution. The derivatized organotin species were eluted from the column with 250 μl of methanol (E) by means of an all glass syringe. A 5-μl volume of tetrabutyltin (TeBT) in methanol was added as an internal standard.

Washing. The sample-delivery channel of the manifold and the column were washed with 5 ml of methanol.

The eluate was analysed by GC–AES. Calibration was done using a five-point (including the

TABLE 2

GC–AES operating parameters

Injector parameters:	
Injection volume	25 μl
Injection temperature	15°C
1st heat-up rate	2°C s^{-1}
1st retention temperature	25°C
1st retention period	60 s
2nd heat-up rate	12°C s^{-1}
2nd retention temperature	260°C
2nd retention period	60 s
GC parameters:	
Column	HP-1 (25 m × 320 μm i.d., 0.17 μm film thickness)
Column head pressure	130 kPa He
Oven programme:	
Initial temperature	45°C, held for 2 min
Ramp rate	20°C min^{-1}
Final temperature	280°C, held for 1 min
Interface parameters:	
Transfer line	HP-1 column
Transfer line temperature	280°C
AES parameters:	
Wavelength	303.419 nm
He make-up flow-rate	240 ml min^{-1}
Scavenger gases:	
H_2 pressure	3.5 atm
O_2 pressure	1.4 atm
Spectrometer purge flow-rate	2 l min^{-1} N_2
Solvent vent off-time	4.5 min
Column–detector coupling	Column to cavity
Cavity temperature	280°C

blank) graph obtained by analysing a mixed solution of ionic butyl- and phenyltin compounds at the 0, 5, 20, 50 and 100 ng l^{-1} levels.

Liquid–liquid extraction procedure

A 50-ml volume of a water sample to be analysed was placed in an extraction vessel, 0.5 g of sodium acetate was added and the pH was adjusted to 5 with acetic acid. Then 1 ml of a 0.3% (w/v) aqueous $NaBEt_4$ solution and 1 ml of hexane, containing TeBT as internal standard, were added. The mixture was shaken manually for 5 min. After phase separation (5 min), the hexane phase was collected by means of an Eppendorf pipette and transferred into a conical vial. Calibration was done by the method of standard additions. An amount of the mixed standard containing the concentrations of organotin species approximately equal to those in the sample was added.

Preparation of real samples

River water samples were filtered through a 0.45 μm filter (Millipore) and acidified to pH 2 with concentrated Suprapur hydrochloric acid. All samples were stored in the dark at ambient temperature and the analyses were completed within 1 week after sampling.

GC–AED measurements

The injector, gas chromatograph and atomic emission detector operating conditions are summarized in Table 2. The signals were measured in the peak-height mode, which was found to give lower detection limits [16].

RESULTS AND DISCUSSION

The method for sample preparation for organotin speciation analysis proposed in this work consists of three steps: preconcentration of ionic organotin by retention on a solid-phase sorbent, in situ derivatization of the compounds retained and elution of the derivatized species. Each of these steps needed to be optimized in detail to obtain the maximum yield. A successful design of a manifold for automated analysis must ensure that these three steps be realized in the same set-up while only different solutions are pumped. The optimization of the whole system was aimed at maximizing the sample throughput and bringing the detection limits down to the sub-ng l^{-1} level. This required reducing both the sample and the eluate volumes while maintaining quantitative efficiency of all the processes involved.

Choice of packing material

Disposable, tropolone-loaded C_{18} silica cartridges proved to offer a viable approach to *off-line* preconcentration of ionic organotin compounds, giving recoveries between 71 and 98% [13]. However, chelating agents are easily washed out of the solid phase support by organic solvents, preventing the use of such columns for multiple analyses without reloading them with the reagent. On the other hand, the use of an aqueous solution for elution would lead to a non-gas chromatographable eluate. Therefore, to meet the objectives of this work it was necessary to find a sorbent both capable of withstanding a large number of preconcentration–elution cycles (more than 100) and neutral to the derivatizing agent. Bonded silica with octadecyl functional groups (C_{18}), found to be promising by other workers [30,31,33], was investigated here in detail. This choice was further supported by the commercial availability of microcolumns (15 mm^3) filled with this sorbent, which had already proved very successful in *on-line* preconcentration of many metals [34–36]. The feasibility of using bonded silica with octadecyl functional groups in the form of extraction discs was also studied.

Retention of organotin compounds on C_{18} sorbents

In order to investigate the effect of pH on the retention of butyl- and phenyltin compounds on a C_{18} packing, a solution containing a known amount of the six respective species in dilute HCl or a buffer at pH 2–12 was pumped through the microcolumn or the extraction disc. The amount of organotin not retained was determined in the effluent using the liquid–liquid extraction–derivatization procedure described under *Experimental*.

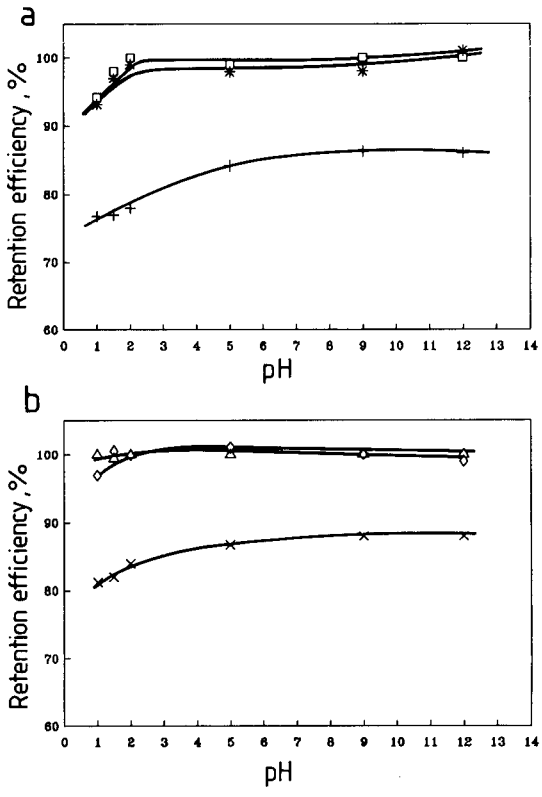

Fig. 2. Effect of pH on the efficiency of the retention of (a) butyltin and (b) phenyltin compounds on a C_{18} microcolumn. + = monobutyltin; * = dibutyltin; □ = tributyltin; × = monophenyltin; ◇ = diphenyltin; △ = triphenyltin.

Microcolumns. The dependence of the pH on the organotin sorption efficiency is shown in Fig. 2. Tributyl- and triphenyltin are quantitatively retained over the whole pH range investigated. The sorption efficiency of disubstituted organotins is slightly influenced by pH but only a small proportion (< 5%) of the spike is found in the eluate. The recoveries of monosubstituted organotins are substantially lower (80–90%), probably owing to decreasing retention efficiency of a C_{18} column with an increase in the polarity and ionic character of the analytes. The recoveries increase slightly with increasing pH but at higher pH values significant (up to 15%) and variable losses of di- and trisubstituted organotin compounds on the walls of the sample container and tubing may occur. Therefore, lower pH values were preferred. In practice, acidified filtered water samples (pH ≈ 2) were passed through the column.

The sample flow-rate has no effect on the retention efficiency in the range 0.5–3.5 ml min^{-1}, although high sampling flow-rates have been reported to affect negatively the performance of some solid sorbents [37]. The maximum allowable loading flow rate was limited by the flow resistance of the packing material, which increased with the lifetime of the column. As there is a direct relationship between the loading flow-rate and the sampling frequency, the highest possible flow-rates were always applied to achieve a high sample throughput. The breakthrough volume was not determined, but as much as 50 ml of relatively dirty harbour water with a load up to 1 μg of organotin did not result in breakthrough.

Extraction discs. The microcolumns used in this study suffer from some disadvantages such as relatively high cost and low flow-rates. C_{18} extraction discs have been reported to offer a promising alternative [31] and were examined in detail. The maximum allowable sample flow-rate through an extraction membrane is proportional to the disc size. However, the dead volume also increases with increasing size of the extraction cell, resulting in larger volumes of the eluting solvent. Membranes with a diameter of 25 mm were chosen as a compromise. The dependence of pH on the sorption efficiency follows a similar curve to those in Fig. 2 but considerably lower recoveries are observed for all the species except TBT and TPT. Only about 75% of DBT and DPT and 10–20% of the monosubstituted organotin species are retained. A remedy could be the addition of a chelating agent or using two membranes in series, but then other problems (reagent washout and flow restriction) are expected to occur.

Derivatization of organotin compounds

The application of Grignard reagents in an *on-line* system is difficult owing to their high reactivity, low stability and the necessity for their post-derivatization decomposition. These drawbacks are eliminated by the use of $NaBEt_4$. Two approaches to the derivatization of organotin are possible unless an extra extraction module is in-

corporated in the system. They are based either on elution of the retained ionic organotin compounds followed by mixing the eluate with $NaBEt_4$ solution and homogenous reaction, or on heterogenous derivatization of the analytes on the column itself. The first approach resulted in a relatively high content of salt ($NaBEt_4$ or products of its decomposition) in the gas chromatographed solution and was the cause of rapid clogging of the liner and contamination of the capillary column. *On-column* ethylation was first proposed by Ashby and Craig [20,21]. They used a packed injection liner doped with an ethanolic solution of the reagent prior to the injection of a solution containing ionic organotin species. However, little success was achieved with tributyltin species, which required high injection temperatures at which the borate decomposed. Because similar, if not more pronounced, problems were expected for phenyltin compounds, a novel approach to *on-column* derivatization was adopted in this work. A stream of the $NaBEt_4$ aqueous solution was passed through the microcolumn containing the ionic organotin species. In this way, the derivatization reaction is carried out at room temperature, the ionic organotin compounds on the C_{18} column always come into contact with a fresh portion of the reagent and the build-up of the borate on the column, which could otherwise lead to its clogging, is avoided.

The effects of operational variables such as pH, $NaBEt_4$ concentration and flow-rate were studied in order to find conditions for quantitative *on-column* derivatization of organotin compounds.

Effect of pH. pH was found to have a large effect on the ethylation of organotin by $NaBEt_4$ in aqueous media and the efficiency of the liquid–liquid extraction [22]. In order to study the influence of pH on the *on-column* derivatization, known amounts of butyl- and phenyltin compounds were retained on the column from 0.01 M HCl. Then the pH of the column was adjusted by pumping buffer (pH 1–12) through the sorbent, which was followed by injection of 0.5 ml of 0.3% $NaBEt_4$ solution into the buffer carrier stream. The derivatized organotins were eluted with 250 μl of methanol and gas chromatographed. The

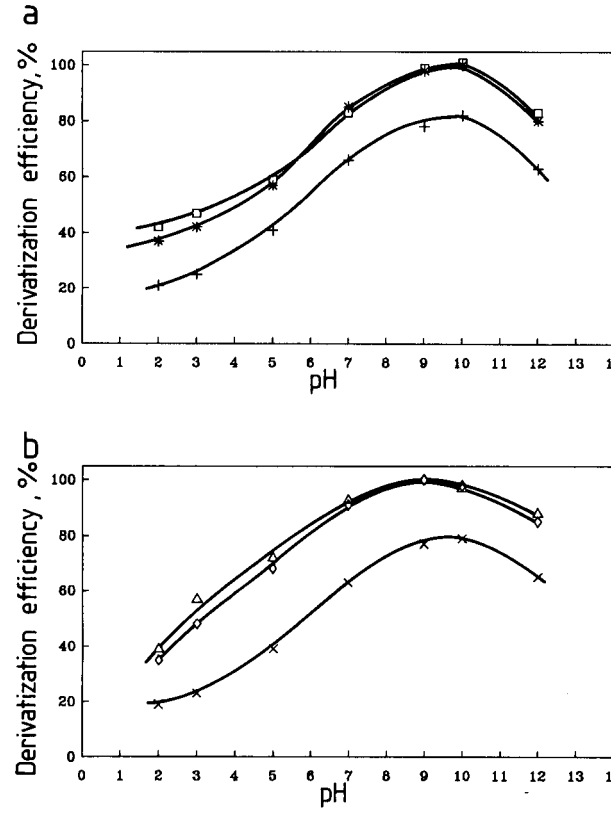

Fig. 3. Effect of pH on the efficiency of the *on-column* derivatization of (a) butyltin and (b) phenyltin compounds. Symbols as in Fig. 2.

effect of pH on the derivatization yield is showed in Fig. 3. A strong influence of pH is observed with a similar shape for all the compounds examined. The optimum acidity range is narrow (pH 9–10) and corresponds to the pH of the $NaBEt_4$ solution. Hydrolysis of organotin compounds starts to occur at pH > 10, resulting in a decrease in the derivatization efficiency.

Effect of $NaBEt_4$ concentration. The concentration of the derivatizing reagent was optimized in the range 0.05–1.5%. Figure 4 shows the results, which were corrected for the retention efficiency so they apply to the derivatization yield only. For di- and trisubstituted organotin compounds the maximum derivatization yield ($> 96\%$) was observed for an $NaBEt_4$ concentration of 0.3% and remained constant at higher concentrations. For monosubstituted compounds the maxi-

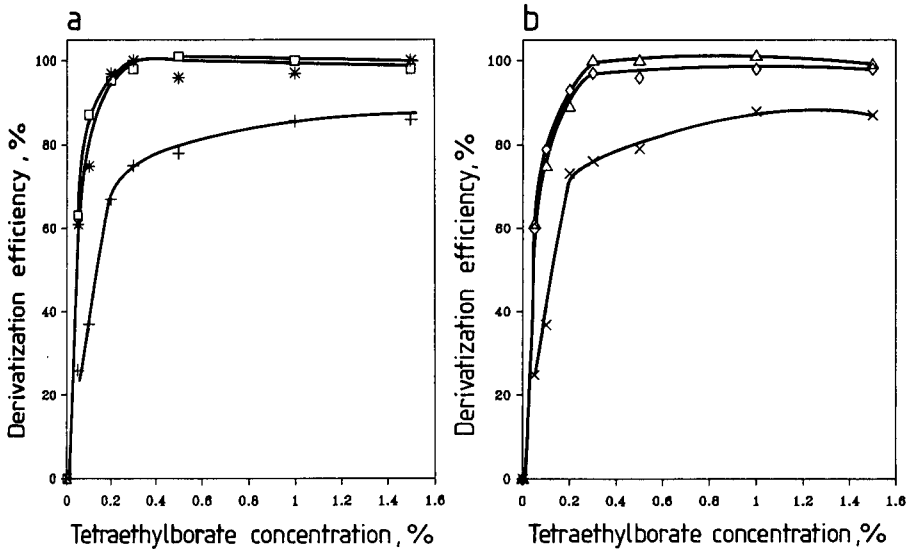

Fig. 4. Effect of the $NaBEt_4$ concentration on the efficiency of the *on-column* derivatization of (a) butyltin and (b) phenyltin compounds. Symbols as in Fig. 2.

mum was reached only at a reagent concentration of 1% but no quantitative derivatization was obtained. The greater amount of $NaBEt_4$ necessary for the derivatization of $BuSn^{3+}$ and $PhSn^{3+}$ may be partly explained by the stoichiometry of the reaction, i.e., 3 mol of $NaBEt_4$ are required for the derivatization of 1 mol of $BuSn^{3+}$ compared with 1 mol required for Bu_3Sn^+. Also, applying $NaBEt_4$ at such a high concentration led to a very rapid deterioration of the column. Therefore, the lowest possible value, i.e., 0.3%, was chosen and some more losses of monosubstituted compounds were accepted. A reagent volume of 0.5 ml is sufficient to achieve reproducible results and its increase has no effect on the signal height. The flow-rate of the reagent-carrying buffer

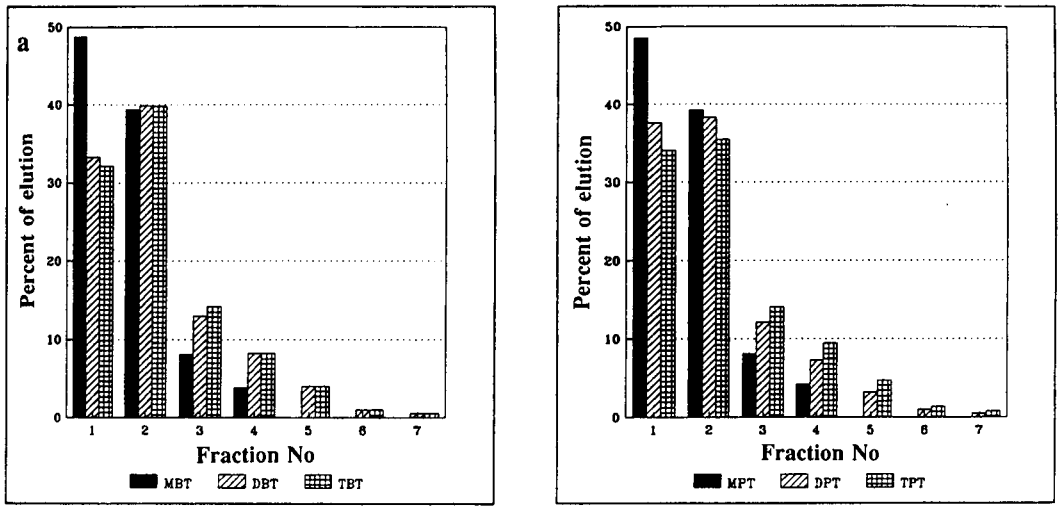

Fig. 5. Elution of the ethylated (a) butyltin and (b) phenyltin compounds from a C_{18} column (fraction volume ca. 25 μl). MBT = monobutyltin; DBT = dibutyltin; TBT = tributyltin; MPT = monophenyltin; DPT = diphenyltin; TPT = triphenyltin.

stream has no effect on the derivatization efficiency in the range 0.5–3.5 ml min^{-1}.

Derivatization of organotin on extraction discs. Owing to the large volume of the extraction cell comparing with that of the column, a larger volume of the derivatizing agent is necessary to moisten the whole membrane. Even then, however, the derivatization yields obtained did not exceed 50% for either of the compounds. Considering also the lower sorption efficiency, the use of membranes in the flow manifold was abandoned, although they may be useful for *off-line* preconcentration of TBT.

Elution

A suitable solvent should ensure rapid and quantitative elution of the derivatized analytes from the column and cause no interferences in the subsequent GC–AES determination using the *in-liner* preconcentration mode [38]. The latter condition eliminates solvents with boiling points higher than ca. 70°C owing to difficulties in selective removal of the solvent by venting it off from the injection liner without losses of the analytes. On the other hand, the more volatile the solvent, the less reproducibly its small volumes can be handled, affecting the accuracy of the analysis. Methanol, hexane and dichloromethane were examined. The last solvent was found occasionally to produce artefacts in the GC of ethylated organotin species. The elution was faster with methanol than with hexane, so methanol was chosen.

For elution, a syringe was filled with about 1 ml of methanol, which was pushed through the column. The elution curves are shown in Fig. 5. The volume of the elution solvent should be kept as small as possible to avoid unnecessary dilution of the gas chromatographed solution. A 250-μl volume of methanol is sufficient to achieve more than 90% elution of the derivatized analytes. Initially, the eluate was collected in a small flask with a 250-μl mark. However, this method resulted in very poor precision (ca. 30%), probably for the following reasons. First, evaporation losses were considerable owing to the large surface-to-volume ratio of effluent droplets. Also, the mark on the flask could only be matched with difficulty

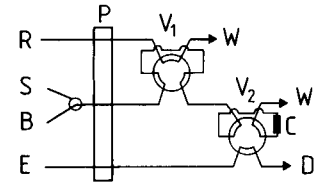

Fig. 6. Flow manifold used in on-line preconcentration–derivatization of organotin compounds. B = Buffer; E = eluent; S = sample; R = derivatizing reagent; P = peristaltic pump; V_1, V_2 = six-way valves; C = preconcentration microcolumn; D = to detector; W = to waste.

as the volume of the drop was irreproducible and could constitute as much as 10% of the collected eluate. Therefore, addition of an internal standard is essential. Tetrabutyltin was chosen for this purpose.

Design of the flow-injection manifold

Solid-phase extraction procedures can be affected by interferences which can originate from commercially available columns and cartridges [37]. The elution solvent may extract these compounds from the polypropylene housing and the C_{18}-bonded porous silica during the elution step. The tubing used for assembling of the flow manifold must be chosen with care to avoid contamination from organotin compounds, which are sometimes used as stabilizers of plastics. Easily cleanable all-glass syringes were preferred to the disposable type to avoid contamination, especially from the rubber plunger.

In the initial phase of the experiments, the manifold shown in Fig. 6 was used. It offered good performance but sorption of ionic organotin on the pump tubing caused problems even in acidic media. In addition, the system required an operator's attention owing to a possibility of leaks arising in the initial phase of derivatization resulting from the flow resistance of the column. These drawbacks were eliminated by designing a manifold in which the sample was not pumped through the column but sucked (Fig. 1) as a consequence of the underpressure yielded by the peristaltic pump. The tubing between the sample container and the microcolumn was shortened to a few cm and contact of the sample with the Tygon tubing was eliminated. In addition, any temporary in-

crease in flow resistance of the column did not result in leaks but only in intrusion of air into the system. A disposable filter with a 0.45-μm pore size was installed between the column and the sample container to eliminate the particulate fraction from environmental waters which could otherwise clog the preconcentration column.

A complete cycle of preconcentration–derivatization consisting of four stages took about 15 min with a loading period of 5 min corresponding to 10 ml of sample. The lifetime of the column was about 150–200 cycles.

GC–AES conditions

The low sample capacity of the capillary column was circumvented by removal of the solvent in the injector liner before the sample is transferred on to the column [38]. The principle of operation consists in injecting 25 μl of the analytes solution at a low temperature (15–25°C) on to a Tenax trap which is purged with helium. Under these conditions the solvent is vented off while the higher boiling organotin compounds are retained in the liner. After the solvent has been removed, the temperature of the liner is increased and the analytes are released on to the column. Larger volumes can be introduced by multiple injection but then problems associated with the blank value and interferences arise.

The detector operating conditions were adapted from previous work [16]. The switch-on and -off times of the purge valve needed to be adjusted to match the injection programme (Table 2). It must be emphasized that in contrast to other methods using $NaBEt_4$ for organotin speciation analysis, in this work the metal ions are not co-extracted. This is important in the analysis of real samples that contain ubiquitously present high levels of Pb^{2+} and other metals. Large amounts of Et_4Pb formed during ethylation of inorganic lead entering the discharge tube reduce its lifetime, resulting in a decrease in sensitivity and peak tailing. The GC column was kept at the end of each run for 1 min at 280°C to remove any high-boiling contaminants.

Determination of organotin compounds in standard solutions

A typical chromatogram of a mixed standard solution containing approximately equal amounts of ionic butyl- and phenyltin compounds analysed according to the flow-injection procedure is shown in Fig. 7.

The chromatogram shows a number of unidentified peaks. Examination of the emission spectrum taken at their apices leads to the conclusion that they are due to tin-containing compounds. The retention times of these compounds are dif-

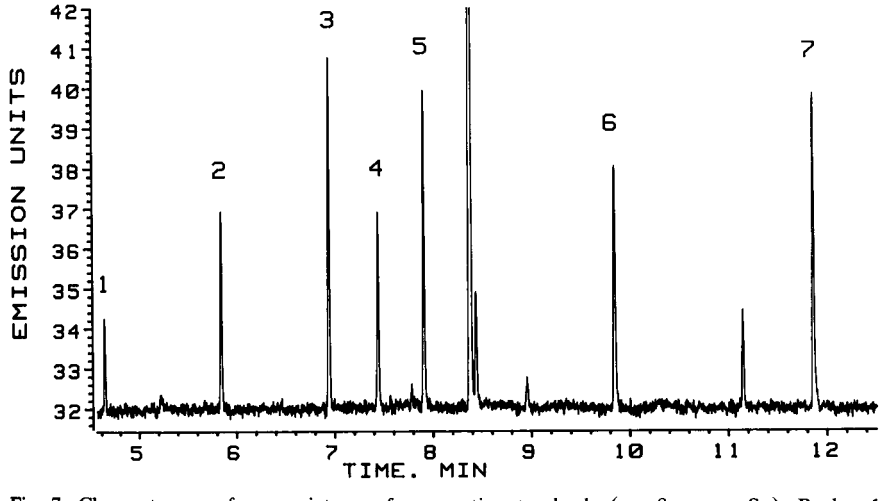

Fig. 7. Chromatogram for a mixture of organotin standards (ca. 8 pg as Sn). Peaks: 1 = inorganic tin; 2 = monobutyltin; 3 = dibutyltin; 4 = monophenyltin; 5 = tributyltin; 6 = diphenyltin; 7 = triphenyltin.

TABLE 3

Calibration data and detection limits for ionic butyl- and phenyltin compounds

Compound determined	Sensitivity [a] (e.u. pg^{-1}) [b]	y-Intercept (e.u. $\times 10^2$) [b]	Correlation coefficient	Detection limit ($ng\ l^{-1}$) [c]	R.S.D. (%) [d]
MBT	0.72	+0.09	0.9995	0.17	9.2
DBT	1.33	−0.06	0.9997	0.10	5.1
TBT	1.33	+0.09	0.9998	0.10	4.9
MPT	0.74	+0.04	0.9995	0.17	8.8
DPT	0.94	−0.13	0.9996	0.12	6.6
TPT	1.31	+0.04	0.9998	0.10	4.3

[a] The recovery is taken into account. [b] e.u. = Emission units. [c] Based on 20 ml of sample. [d] Estimated for five measurements.

TABLE 4

Comparison of solid-phase extraction procedures for preconcentration of organotin compounds

Sorbent	Compounds determined	Sample volume	Sorption conditions	Elution solvent (volume)	Detection	Detection limit ($ng\ l^{-1}$)	Recovery (%)	Ref.
Carbopack, LC_{18}	MBT + DBT, TBT	1000 ml (Carbopack), 250 ml (LC_{18})		MeOH–tropolone (2 ml) and MeOH (2 ml)	GFAAS	10	92–97 90–91	30
Carbopack, LC_{18}	MBT, DBT, TBT	1000 ml (Carbopack), 250 ml (LC_{18})		MeOH–tropolone	GC–FPD	2	98–100 94–102	30
Bakerbond C_{18}, Empore discs	TBT	100 ml	pH 4.5	Ethyl acetate ($2 \times 250\ \mu l$)	GC–ECD	Not given	91–104	31
Graphitized carbon black	TBT, TPrT, TPT	1000 ml	pH ≈ 8	MeOH–CH_2Cl_2 (2 ml)	LC–FPD	20	Not given	29
Graphitized carbon black	TBT, TPT	Up to a few l	5 ml HNO_3 per 1 l	MeOH–CH_2Cl_2 (2 ml)	LC–AAS	0.7–0.8	≤ 95	28
Bond Elut C_{18}	DPT, TPT, MMT, DMT, TMT, MBT, DBT, TBT	1000 ml	Not given	THF–acetic acid–tropolone	LC–AAS	30	63–96	32
Tropolone–Sep-Pak C_{18}	MBT, DBT, TBT, TeBT, MPT, DPT, TPT, MCyHT, DCyHT, TCyHT	100–500 ml	pH 2–3	Et_2O (3 ml)	GC–FPD	Not given	71–98	13
C_{18}	TBT	100 ml	pH 2–4.5	Ethyl acetate	GC–ECD		93	33
C_{18}	MBT, DBT, TBT, MPT, DPT, TPT	10–50 ml	pH 2	MeOH ($250\ \mu l$)	GC–MIP-AES	0.1–0.2 [a]	80–100	This work

[a] Species dependent, for 20 ml of sample.

ferent from those of the analytes so they do not interfere in the analysis. These unidentified peaks also occur in the blank value and increase in height with increasing concentration of the borate. The number and the height of the unidentified signals were found to be strongly dependent on the batch of the reagent used.

Calibration graphs. Calibration graphs were established by using mixed standard solutions in the range 0–100 ng l^{-1}. The regression equations, given in Table 3, show good linearity but different response factors with respect to the analyte, which is due to the non-quantitative recovery of mono-substituted organotins.

Precision and accuracy. Table 3 also shows the precision of the procedure at various concentration levels for the determination of butyl- and phenyltin standards. The precision is similar for all the organotin compounds studied and is comparable to that for the method based on liquid–liquid extraction–derivatization [22].

Detection limits. Instrumental detection limits calculated as three times the standard deviation of the noise were about 0.15–0.2 pg, which was worse than initially reported for the same instrument [16] but comparable to those in later work [39]. Experimental detection limits taking into account the recoveries are given in Table 3. The blank values were a problem only for MBT, reaching 0.5 pg (as Sn). They could be minimized by careful cleaning of the sample containers and washing of the system with methanol after the analysis cycle is completed.

Table 4 summarizes the experimental conditions and figures of merit available in the literature on the application of solid-phase extraction in the speciation analysis of organotin. Apart from eliminating the necessity for *off-line* derivatization, the method developed in this work reduces considerably the amount of sample necessary for analysis while in the same time offering at least an order of magnitude better detection limits. Detection limits of 0.1 ng l^{-1} can be obtained routinely and only up to 50 ml of sample are required. The same characteristics are likely to be obtained using a much cheaper FPD instrument as the instrumental detection limits are comparable (0.15 pg for AES, 0.2 pg FPD [22]).

Determination of organotin compounds in real samples

The applicability of the method to the determination of organotin species in real samples was demonstrated by the analysis of fifteen river water samples from the river Scheldt estuary. Organotin compounds were detected in all the samples analysed at concentrations in the ranges 10–140, 8–67 and 4–11 ng l^{-1} for mono-, di- and

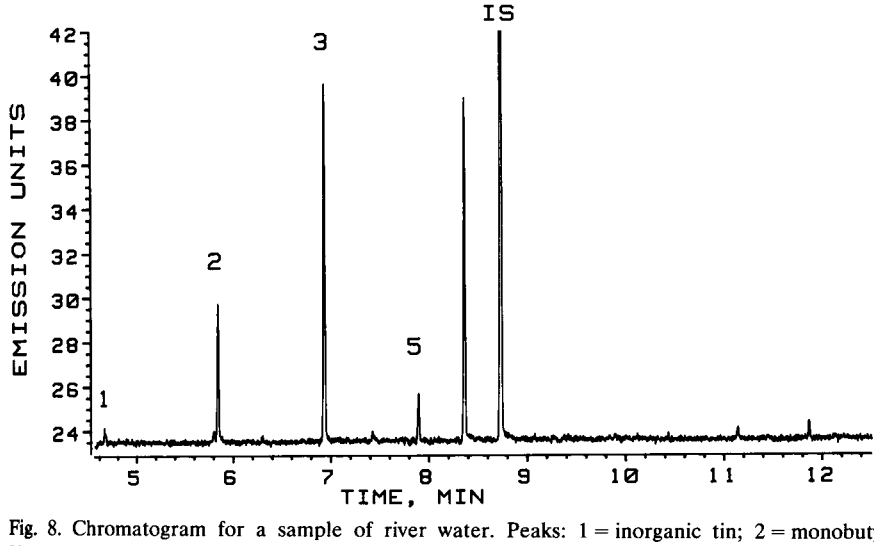

Fig. 8. Chromatogram for a sample of river water. Peaks: 1 = inorganic tin; 2 = monobutyltin; 3 = dibutyltin; 5 = tributyltin; IS = internal standard (tetrabutyltin).

tributyltin in the dissolved phase, respectively. A typical chromatogram of a river water sample is shown in Fig. 8. To verify the accuracy of the method, all the samples were analysed independently by a liquid–liquid extraction method involving ethylation of ionic organotin in the aqueous phase with $NaBEt_4$ followed by extraction of the derivatized species into hexane. The comparison of the results is shown in Fig. 9. The results obtained by the flow-injection and extraction methods agreed to within less than 15% for all the samples. The largest differences were observed for MBT. The reasons for this discrepancy include the non-quantitative recovery of this species in either of the methods and also possible blank contributions.

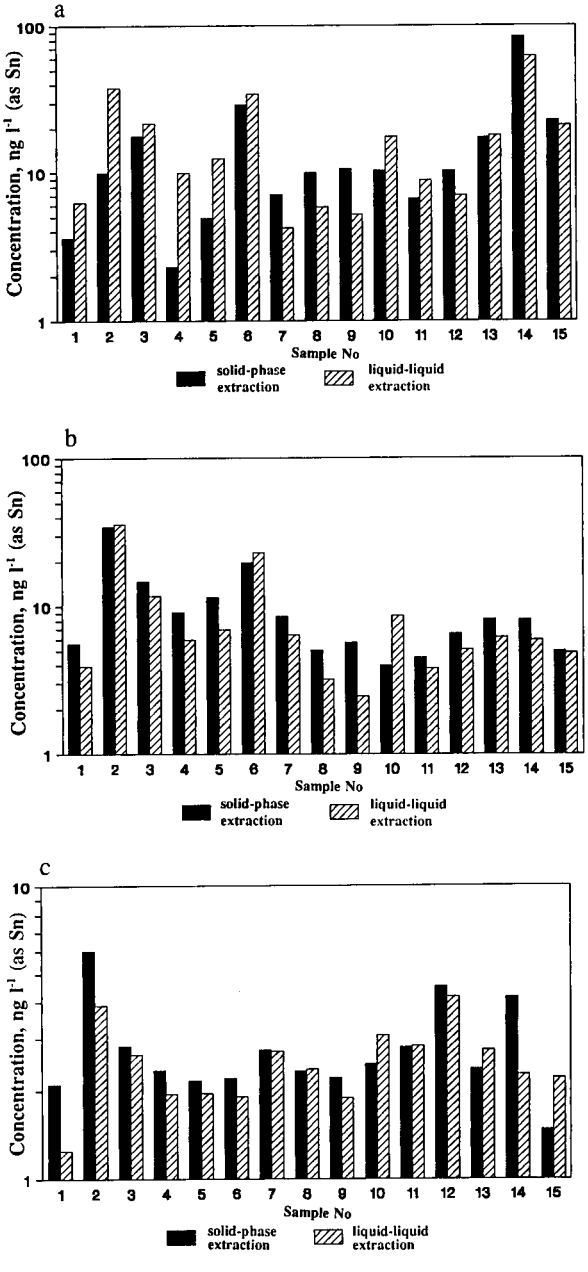

Fig. 9. Comparison of the results of the determination of organotin compounds in river water samples: (a) monobutyltin; (b) dibutyltin; (c) tributyltin.

The characteristics obtained so far are sufficient for the determination of organotin in water at levels of interest from the environmental point of view. A further increase in the experimental detection limits is possible by the use of larger sample volumes, which would result, however, in longer loading periods.

Conclusion

The procedure developed offers numerous advantages over the hitherto reported methods owing to a combination of simplicity and very high sensitivity. They result from increasing the preconcentration factor by using the solid-phase instead of the liquid–liquid extraction separation, integration of the separation and derivatization steps which is possible by optimization of the ethylation of organotin on a solid-phase support, automated *in-liner* preconcentration of the analytes in the extract which permits an injection of 25 μl on to a capillary column and the use of a sensitive and selective detector. The method is readily applicable in field analysis. Thus it eliminates the necessity for the storage of large volumes of untreated water samples, which is not only cumbersome but may also result in losses and changes in speciation due to degradation processes. Full automation of the procedure requires interfacing of the sample preparation manifold developed here with a gas chromatograph. Such interfaces have recently been reported for the determination of organic contaminants in water [40].

Research grants to J.S.Ł. and M.C. by the Belgian Science Policy Office and NFWO (Bel-

gium), respectively, are gratefully acknowledged. This work was financially supported by the IGBP Global Change (GC/06/006) programme.

REFERENCES

1 R.J. Maguire, Appl. Organomet. Chem., 1 (1987) 475.
2 M.J. Waldock, J.E. Thain and M.E. Waite, Appl. Organomet. Chem., 1 (1987) 287.
3 R.J. Huggett, M.A. Unger, P.F. Seligman and A.O. Valkirs, Sci. Total Environ., 26 (1992) 232.
4 K. Fent and J. Hunn, Environ. Sci. Technol., 25 (1991) 221.
5 O.F.X. Donard and R. Pinel, in R. Harrison and S. Rapsomanikis (Eds.), Environmental Analysis Using Gas Chromatography Interfaced with Atomic Spectroscopy, Horwood, Chichester, 1989, pp. 189–222.
6 O.F.X. Donard and F.M. Martin, Trends Anal. Chem., 11 (1992) 17.
7 Y.K. Chau, Analyst, 117 (1992) 571.
8 J.W. MacLaren, K.W.M. Siu, J.W. Lam, S.N. Willie, P.S. Maxwell, A. Palepu, M. Koether and S.S. Berman, Fresenius' J. Anal. Chem., 337 (1990) 721.
9 H. Suyani, J. Creed, T. Davidson and J. Caruso, J. Chromatogr. Sci., 27 (1989) 139.
10 S. Branch, L. Ebdon, S. Hill and P. O'Neill, Anal. Proc., 26 (1989) 401.
11 W.M.R. Dirkx, W.E. Van Mol, R.J.A. Van Cleuvenbergen and F.C. Adams, Fresenius' Z. Anal. Chem., 335 (1989) 769.
12 D.S. Forsyth, Sci. Total Environ., 89 (1989) 299.
13 M.D. Müller, Anal. Chem., 59 (1987) 617.
14 I. Tolosa, J.M. Bayona, J. Albaigés, L.F. Alencastro and J. Tarradellas, Fresenius' J. Anal. Chem., 339 (1991) 646.
15 B.F. Scott, Y.K. Chau and A. Rais-Firouz, Appl. Organomet. Chem., 5 (1991) 151.
16 R. Łobiński, W.M.R. Dirkx, M. Ceulemans and F.C. Adams, Anal.Chem., 64 (1992) 159.
17 H. Suyani, J. Creed, J. Caruso and R.D. Satzger, J. Anal. At. Spectrom., 4 (1989) 777.
18 O.F.X. Donard, in B. Weltz (Ed.), 5th Colloquium Atomspektrometrische Spureanalytik, Überlingen, 1989, pp. 395–417.
19 M.J. Waldock, M.E. Waite, D. Miller, D.J. Smith and R.J. Law, Aquatic Environment Protection: Analytical Methods, MAFF Directorate of Fisheries Research, Lowestoft, 1989.
20 J.R. Ashby and P.J. Craig, Appl. Organomet. Chem., 5 (1991) 173.
21 J.R. Ashby and P.J. Craig, Sci. Total Environ., 78 (1989) 219.
22 P. Michel and B. Averty, Appl. Organomet. Chem., 5 (1991) 393.
23 J.R. Ashby, S. Clark and P.J. Craig, J. Anal. At. Spectrom., 3 (1988) 735.
24 Y.A. Zolotov and N.M. Kuz'min, Preconcentration of Trace Elements, Elsevier, Amsterdam, 1990.
25 T.A. Bellar and W.L. Budde, Anal. Chem., 60 (1988) 2076.
26 G.A. Junk and J.J. Richard, Anal. Chem., 60 (1988) 451.
27 E.J. Poziomek and G.A. Elceman, Environ. Sci. Technol., 26 (1992) 1313.
28 T. Ferri, E. Candarelli and B.M. Petronio, Talanta, 36 (1989) 513.
29 S. Chiavarini, C. Cremisini, T. Ferri, R. Morabito and A. Perini, Sci. Total Environ., 101 (1991) 217.
30 S. Chiavarini, C. Cremisini, T. Ferri, R. Morabito and C. Ubaldi, Appl. Organomet. Chem., 6 (1992) 147.
31 O. Evans, B.J. Jacobs and A.L. Cohen, Analyst, 116 (1991) 15.
32 K. Kadokami, T., Uehiro, M. Morita and K. Fuwa, J. Anal. At. Spectrom., 3 (1988) 187.
33 G.A. Junk and J.J. Richard, Chemosphere, 16 (1987) 61.
34 M. Sperling, X. Yin and B. Weltz, J. Anal. At. Spectrom., 6 (1991) 295 and 615.
35 Z. Fang, M. Sperling and B. Weltz, J. Anal. At. Spectrom., 5 (1990) 639.
36 S. Xu, L. Sun and Z. Fang, Anal. Chim. Acta, 245 (1991) 7.
37 G.A. Junk, M.J. Avery and J.J. Richard, Anal. Chem., 60 (1988) 1347.
38 R. Łobiński and F.C. Adams, J. Anal. At. Spectrom., 7 (1992) 987.
39 W.M.R. Dirkx, R. Łobiński, M. Ceulemans and F.C. Adams, Sci. Total Environ., in press.
40 G.R. van den Hoff, S.M. Gort, R.A. Baumann, P. van Zoonen and U.A.Th. Brinkman, J. High Resolut. Chromatogr., 14 (1991) 465.

Analytica Chimica Acta, 278 (1993) 115–123
Elsevier Science Publishers B.V., Amsterdam

Liquid desorption of organic solvents from industrial sludges [1]

Luciano Ceccon

Dipartimento di Economia e Merceologia delle Risorse Naturali e della Produzione, Università di Trieste, Via Valerio 6, 34127 Trieste (Italy)

Alessandro Turello, Graziella Mocellin and Luigi Colugnati

Chemio srl, Via Cussignacco 39, 33040 Pradamano, Udine (Italy)

(Received 10th June 1992; revised manuscript received 4th January 1993)

Abstract

Analysis of organic solvent residues in industrial sludges is usually based on preliminary extraction from the matrix, followed by gas chromatographic determination. Liquid desorption with carbon disulphide is one of the most frequently used methods of recovery. As a large number of variables can affect desorption efficiencies, recoveries from two wastes with different physico-chemical characteristics were evaluated. The loading of solvents affected the desorption efficiencies particularly of polar compounds: the recoveries increased with increased loading. The analyte composition played an important role: recoveries of polar solvents were generally higher in the presence of other polar compounds. The desorption efficiencies of almost all the solvents examined increased on decreasing the waste/desorbing agent ratio.

Keywords: Extraction; Desorption; Industrial sludges; Organic solvents

In a previous paper some of the parameters that can affect the desorption efficiencies of organic solvents from industrial sludges when carbon disulphide (CS_2) is employed as the desorbing agent were examined [1]. In particular, the influence of the physico-chemical characteristics of the matrix, the loading of solvents and the extraction time were taken into account. The organic carbon content and pH of the matrix are known to play important roles in determining the recoveries of organic compounds in environmental samples [2,3]. The desorption efficiencies of organic solvents adsorbed on activated carbons are dependent on loading [4–9]. Other important factors that were shown to influence recoveries are the analyte composition and the sample/desorbing agent ratio. Several workers have demonstrated that desorption efficiencies are dependent on the presence of other compounds, at least for polar solvents [4–6,10–12]. In general, an increase in recoveries with increasing desorption volume (for a constant weight of sample) was observed [5,13]. This study was therefore undertaken to monitor the possible effects of other variables on the desorption of organic solvents from industrial sludges, namely the analyte composition and the sludge/desorbing agent ratio. Further, the effect of the solvent loading was evaluated over a wider range of concentrations.

Correspondence to: L. Ceccon, Dipartimento di Economia e Merceologia delle Risorse Naturali e della Produzione, Università di Trieste, Via Valerio 6, 34127 Trieste (Italy).

[1] **Note 2.**

EXPERIMENTAL

Matrix selection and preparation

Two matrices were selected from waste streams of two different production units, namely a painting unit employing polyurethane and polyester enamels and a painting unit employing essentially polyurethane enamels together with small amounts of polyester and nitrocellulose enamels. Both production units consisted of a spray-painting cabin supplied with an air exhauster to a scrubber. The former unit was provided with a dry scrubber and the latter with a wet scrubber. The material from the paint not utilized and gathered at the bottom of the scrubber, was collected in large amounts and used in the present study. These two wastes were selected on the basis of their different physico-chemical characteristics (pH and organic carbon).

Approximately 100-g portions of each matrix were finely ground using a ZK 1 blade homogenizer (Braun). Both wastes were freed from solvents and water in a VV 2000 rotary vacuum evaporator (Heidolph, Kronberg, Germany) at 60°C to minimize possible structural modifications. Before recovery studies were performed, both matrices were screened to 1 mm and kept in a desiccator over phosphorus pentoxide.

pH measurement

pH measurement of both wastes was performed according to the ASTM method [14] using an S 202 digital pH meter (SEAC) supplied with an Orion RX 91-56 electrode.

Residual moisture determination

Residual moisture in the two dried matrices was determined by Karl Fischer titration using an automatic ABU 93 triburette, a VIT 90 video titrator and a SAM 90 sample station (Radiometer, Copenhagen, Denmark).

Organic carbon determination

The organic carbon content in the two dried matrices was determined by a modification of the method of Springer and Klee for compost [15]: about 0.1 g of waste was oxidized at 160°C with 0.167 M $K_2Cr_2O_7$ in acidic medium (concentrated H_2SO_4), and excess of $K_2Cr_2O_7$ was back-titrated with Mohr's salt [iron(II) ammonium sulphate].

Ash determination

The ash content in the two dried matrices was determined by weighing the residue obtained after treatment for 24 h at 660°C in a muffle oven.

Preparation of standard mixtures of solvents

All solvents were commercially available compounds of the highest purity.

Approximately 2 g each of ethyl acetate, methyl isobutyl ketone, isobutanol, toluene, *n*-butyl acetate, *p*-xylene, 2-ethoxyethyl acetate and cyclohexanone were accurately transferred into a 25-ml glass-stoppered volumetric flask (standard mixture 1).

Approximately 2 g each of dichloromethane, methyl ethyl ketone, isobutanol, isobutyl acetate, *n*-butanol, 2-ethoxyethanol, *p*-xylene and *o*-xylene were accurately transferred into a 25-ml glass-stoppered volumetric flask (standard mixture 2).

Approximately 200 mg each of dichloromethane, methyl ethyl ketone, ethyl acetate, methyl isobutyl ketone, isobutanol, isobutyl acetate, toluene, *n*-butanol, *n*-butyl acetate, 2-ethoxyethanol, *p*-xylene, *o*-xylene, 2-ethoxyethyl acetate and cyclohexanone were accurately transferred into a 10-ml glass-stoppered volumetric flask (standard mixture 3).

Approximately 1.5 g each of *n*-butanol and *p*-xylene were accurately transferred into a 10-ml glass-stoppered volumetric flask (*n*-butanol–*p*-xylene mixture).

Approximately 1.5 g each of 2-ethoxyethanol and toluene were accurately transferred into a 10-ml glass-stoppered volumetric flask (2-ethoxyethanol–toluene mixture).

Preparation of standard solutions

A stock standard solution containing 2000 mg l^{-1} each of solvents was prepared by dissolving an aliquot of standard mixture 3 in CS_2 (J.T. Baker). (**Caution**: CS_2 is very toxic.) By successive dilutions with CS_2, working standard solutions containing 20, 10 and 5 mg l^{-1} each of the solvents were prepared.

A stock standard solution containing 10 000 mg l^{-1} each of *n*-butanol and *p*-xylene was prepared in CS_2. By dilution with CS_2, working standard solutions containing 1000 and 10 mg l^{-1} each of *n*-butanol and *p*-xylene were prepared.

A stock standard solution containing 10 000 mg l^{-1} each of 2-ethoxyethanol and toluene and working standard solutions containing 1000 and 10 mg l^{-1} each of 2-ethoxyethanol and toluene were likewise prepared.

Blank test

For both wastes, 2 g of dried matrix were weighed in a 40-ml screw-capped glass vial with a PTFE septum (Supelco), 20 ml of CS_2 were added and the waste–solvent mixture was occasionally shaken by hand for 1 h. After the solids had settled (within 1–2 min), an aliquot (about 1 ml) of clear supernatant liquid was transferred into a 15-ml screw-capped glass vial with a PTFE septum (Supelco) over anhydrous sodium sulphate to eliminate traces of water and 1 μl was injected immediately into the gas chromatograph.

Recovery tests

Standard mixtures of solvents. For a 100 000 μg g^{-1} loading, 0.6 g of dried matrix was weighed in a 40-ml screw-capped glass vial with a PTFE septum and 1.6 g of standard mixture 1 or 2 was added to produce a 2-g amount of waste. The vial was occasionally shaken by hand for 1 h and left aside for 24 h. CS_2 (20 ml) was added and the vial was shaken by hand for either 5 min or occasionally for 24 h. At the end of the equilibration time, solids settled (within 1–2 min). An aliquot (about 1 ml) of the clear supernatant liquid was transferred into a 15-ml screw-capped glass vial with a PTFE septum over anhydrous sodium sulphate, and 0.2 μl was injected immediately into the gas chromatograph.

A 1.6-g amount of standard mixture 1 or 2 was dissolved in 20 ml of CS_2. An aliquot (about 1 ml) was transferred into a 15-ml screw-capped glass vial with a PTFE septum over anhydrous sodium sulphate, and 0.2 μl was injected immediately into the gas chromatograph.

For a 10 000 μg g^{-1} loading, 1.74 g of dried matrix were likewise mixed with 0.28 g of standard mixture 3 to produce a 2-g amount of waste. The vial was occasionally shaken by hand for 1 h and left aside for 24 h. Either 40 or 10 ml of CS_2 were added and the vial was shaken by hand for 5 min. After solids had settled, an aliquot of the clear supernatant liquid was processed as described for the 100 000 μg g^{-1} loading, and 1 μl was injected immediately into the gas chromatograph.

An aliquot (about 1 ml) of stock standard solution containing 2000 mg l^{-1} each of solvents was likewise processed as described for the 100 000 μg g^{-1} loading, and 0.5 μl was injected immediately into the gas chromatograph.

For a 100 μg g^{-1} loading, 2 g of dried matrix were mixed with either 40 ml of standard solution containing 5 mg l^{-1} each of solvents, or 20 ml of standard solution containing 10 mg l^{-1} each of solvents or 10 ml of standard solution containing 20 mg l^{-1} each of solvents. The waste–solvent mixture was processed as described for the 10 000 μg g^{-1} loading, and 2.5–5 μl were injected immediately into the gas chromatograph.

An aliquot (about 1 ml) of working standard solution containing 5, 10 or 20 mg l^{-1} each of solvents was processed as described for the 100 000 μg g^{-1} loading, and 2.5–5 μl were injected immediately into the gas chromatograph.

n-Butanol or 2-ethoxyethanol. For the 100 000 μg g^{-1} loading, 1.8 g of dried matrix were weighed in a 40-ml vial and 0.4 g of either *n*-butanol–*p*-xylene mixture or 2-ethoxyethanol–toluene mixture was added to produce a 2-g amount of waste. The vial was occasionally shaken by hand for 1 h and left aside for 24 h. Either 40, 20 or 10 ml of CS_2 were added and the vial was shaken by hand for 5 min. After solids had settled, an aliquot of the clear supernatant liquid was transferred into a 15-ml vial over anhydrous sodium sulphate, and 0.2 μl was injected immediately into the gas chromatograph.

An aliquot (about 1 ml) of stock standard solution containing 10 000 mg l^{-1} each of either *n*-butanol and *p*-xylene, or 2-ethoxyethanol and toluene, was transferred into a 15-ml vial over anhydrous sodium sulphate, and 0.2 μl was injected immediately into the gas chromatograph.

For the 10 000 μg g^{-1} loading, 2 g of dried

matrix were weighed in a 40-ml vial and 20 ml of working standard solution containing 1000 mg l^{-1} each of either *n*-butanol and *p*-xylene, or 2-ethoxyethanol and toluene, were added. The waste–solvent mixture was processed as described for the 100 000 $\mu g\ g^{-1}$ loading, and 1 μl was injected immediately into the gas chromatograph.

An aliquot (about 1 ml) of working standard solution containing 1000 mg l^{-1} each of either *n*-butanol and *p*-xylene, or 2-ethoxyethanol and toluene, was processed as described for the 100 000 $\mu g\ g^{-1}$ loading, and 1 μl was injected immediately into the gas chromatograph.

For the 100 $\mu g\ g^{-1}$ loading, to 2 g of dried matrix were added 20 ml of working standard solution containing 10 mg l^{-1} each of either *n*-butanol and *p*-xylene, or 2-ethoxyethanol and toluene. The waste–solvent mixture was processed as described for the 100 000 $\mu g\ g^{-1}$ loading, and 2.5–3 μl were injected immediately into the gas chromatograph.

An aliquot (about 1 ml) or working standard solution containing 10 mg l^{-1} each of either *n*-butanol and *p*-xylene, or 2-ethoxyethanol and toluene, was processed as described for the 100 000 $\mu g\ g^{-1}$ loading, and 2.5–3 μl were injected immediately into the gas chromatograph.

Duplicate extractions were performed in all instances; each analysis was performed in triplicate. All tests were carried out at room temperature (22 ± 2°C).

Gas chromatography

A Dani 6800 gas chromatograph, equipped with a stainless-steel column and flame ionization detector, was used. A 2 m × 2 mm i.d. column, packed with 15% Ucon LB 550X on 80–100-mesh Chromosorb W AW (Supelco), was employed. Operating conditions for standard mixtures of solvents were as follows: column temperature, programmed from 60°C (maintained for 5 min) to 150°C at 5°C/min, the final temperature being maintained for 5 min; injector and detector temperatures, 170°C; nitrogen carrier gas flow-rate, 23 ml min^{-1} (set at 60°C); hydrogen flow-rate, 23 ml min^{-1}; and air-flow-rate, 200 ml min^{-1}. Separation of *n*-butanol and *p*-xylene was achieved at 140°C (isothermal) and that of 2-ethoxyethanol and toluene at 130°C (isothermal).

Peak areas were determined with a Shimadzu C-R3A integrator.

Statistical analysis

A Student *t*-test was used to determine if differences existed among recoveries obtained under different experimental conditions.

RESULTS AND DISCUSSION

Effect of solvent loading

The same two wastes as considered in a previous study [1] were used. The two wastes were selected with physico-chemical characteristics as different as possible (wastes A and B). The main characteristics of the two matrices are shown in Table 1.

To eliminate water and sample interferences, the two wastes were first dried and freed from retained solvents. After extraction with CS_2, the two dried matrixes (see *Blank test*) produced

TABLE 1

Main characteristics of the wastes examined

Characteristic	Waste A	Waste B
Origin	Spray-painting cabin with dry scrubber	Spray-painting cabin with wet scrubber
Type of matrix	Solid waste consisting of polyurethane and polyester enamels	Sludge from essentially polyurethane enamels
pH	5.86	8.51
Organic carbon content (%) [a]	24.4	18.2
Ash content (%) [a]	7.38	28.86

[a] Dry weight.

TABLE 2

Recoveries (%) of industrial solvents from dried waste A as a function of equilibration time with carbon disulphide and of loading of solvents [a]

Solvent	Loading of solvent ($\mu g\ g^{-1}$)						
	100 000				10 000 [b]	1000 [b]	100
	Standard mixture 1		Standard mixture 2				
	5 min [c]	24 h [c]	5 min [c]	24 h [c]	5 min [c]	5 min [c]	5 min [c]
Dichloromethane			89.4 ± 6.3	98.3 ± 5.7	93.7 ± 0.9	94.2 ± 1.1	90.7 ± 12.6
Methyl ethyl ketone			94.8 ± 2.5	98.3 ± 1.7	89.4 ± 3.2	87.7 ± 2.6	85.8 ± 6.1
Ethyl acetate	96.5 ± 2.0	92.4 ± 2.0			91.5 ± 4.2	96.7 ± 1.1	87.0 ± 4.2
Methyl isobutyl ketone	99.1 ± 1.2	97.3 ± 1.9			97.3 ± 0.7	97.7 ± 2.2	92.2 ± 4.7
Isobutanol	95.4 ± 2.0	92.2 ± 2.5	94.5 ± 1.4	96.2 ± 1.0	80.0 ± 1.2	79.1 ± 1.3	74.0 ± 6.6
Isobutyl acetate			99.4 ± 1.1	99.2 ± 2.2	97.2 ± 1.7	97.3 ± 0.2	94.2 ± 6.6
Toluene	99.9 ± 1.1	98.6 ± 1.5			102.0 ± 0.8	101.7 ± 1.7	103.2 ± 2.0
n-Butanol			94.9 ± 0.6	95.4 ± 0.5	80.0 ± 1.5	74.9 ± 3.2	79.5 ± 8.0
n-Butyl acetate	99.7 ± 1.7	98.7 ± 1.8			98.4 ± 1.1	98.7 ± 1.1	93.9 ± 3.3
2-Ethoxyethanol			94.6 ± 3.0	96.1 ± 1.6	81.1 ± 1.1	72.6 ± 2.8	66.5 ± 8.1
o-Xylene			100.2 ± 1.4	100.4 ± 1.4	102.1 ± 0.4	100.8 ± 3.2	108.5 ± 5.6
2-Ethoxyethyl acetate	99.7 ± 3.7	100.1 ± 4.5			94.7 ± 1.0	93.0 ± 1.8	94.0 ± 5.2
Cyclohexanone	99.1 ± 2.1	98.5 ± 1.4			95.0 ± 0.9	91.6 ± 0.5	90.3 ± 4.1

[a] Average percentage recovery for six determinations ± standard deviation. Waste/carbon disulphide ratio, 2 g/20 ml. [b] From [1]. [c] Equilibration time.

chromatograms free of detectable levels of solvents originally incorporated in the sample. Removal of water was almost quantitative; the residual moisture was 0.3 and 0.4% in wastes A and B, respectively.

The desorption efficiencies of organic solvents

TABLE 3

Recoveries (%) of industrial solvents from dried waste B as a function of equilibration time with carbon disulphide and of loading of solvents [a]

Solvent	Loading of solvent ($\mu g\ g^{-1}$)						
	100 000				10 000 [b]	1000 [b]	100
	Standard mixture 1		Standard mixture 2				
	5 min [c]	24 h [c]	5 min [c]	24 h [c]	5 min [c]	5 min [c]	5 min [c]
Dichloromethane			93.6 ± 5.7	96.1 ± 4.9	93.6 ± 6.1	97.0 ± 0.4	95.8 ± 6.1
Methyl ethyl ketone			97.7 ± 2.0	98.1 ± 1.9	94.7 ± 1.3	93.4 ± 3.0	91.9 ± 5.0
Ethyl acetate	96.6 ± 3.3	97.4 ± 2.3			93.3 ± 1.5	95.7 ± 2.1	89.4 ± 5.3
Methyl isobutyl ketone	99.5 ± 2.1	99.0 ± 1.4			97.7 ± 0.1	96.5 ± 0.7	94.7 ± 4.1
Isobutanol	95.3 ± 4.2	94.7 ± 2.3	97.2 ± 1.7	96.7 ± 0.8	84.5 ± 1.2	80.8 ± 1.3	78.1 ± 4.9
Isobutyl acetate			99.6 ± 1.4	99.2 ± 1.1	98.8 ± 1.5	96.5 ± 1.5	94.8 ± 4.2
Toluene	99.8 ± 1.9	99.6 ± 1.4			101.9 ± 1.5	100.3 ± 0.3	100.8 ± 3.0
n-Butanol			97.3 ± 1.6	96.1 ± 0.5	84.4 ± 0.5	80.2 ± 1.7	82.6 ± 4.9
n-Butyl acetate	99.5 ± 2.0	99.4 ± 1.7			98.5 ± 0.7	97.2 ± 2.6	96.2 ± 3.2
2-Ethoxyethanol			98.0 ± 4.9	97.3 ± 0.9	87.2 ± 1.8	77.8 ± 2.9	79.7 ± 9.5
o-Xylene			99.7 ± 1.1	100.7 ± 1.2	102.1 ± 0.7	97.9 ± 0.4	105.3 ± 5.0
2-Ethoxyethyl acetate	100.1 ± 2.9	99.2 ± 2.9			99.0 ± 3.7	96.5 ± 1.7	93.8 ± 7.9
Cyclohexanone	98.5 ± 1.1	98.9 ± 1.0			96.2 ± 1.6	95.2 ± 1.7	89.1 ± 6.2

[a–c] See Table 2.

adsorbed on activated carbons increase with increasing loading [4–9]. For this reason, recoveries from the two wastes were examined at the highest possible loadings, corresponding to sludges with a 70% solvent content, that is, distillation residues. Recoveries at a loading lower than that considered previously [1] were also examined. At a loading of 100000 $\mu g\ g^{-1}$ of each solvent, the kinetics of recovery was taken into account by carrying out extractions for 5 min and 24 h. These two times were selected as recoveries from the same two wastes were demonstrated to be not significantly different after 5 min, 1 h and 24 h for loadings of 10000, 1000 and 200 $\mu g\ g^{-1}$ [1]. For a loading of 100 $\mu g\ g^{-1}$, recoveries were evaluated only after 5 min.

For a loading of 100000 $\mu g\ g^{-1}$, two standard mixtures were used. Standard mixture 1 consisted of seven solvents belonging to several classes of organic compounds usually found in industrial sludges (acetates, ketones, alcohols, aromatic hydrocarbons), in addition to *p*-xylene as the internal standard. Standard mixture 2 consisted of seven solvents representing all the various classes of compounds more frequently present (chlorinated hydrocarbons, ketones, acetates, alcohols, aromatic hydrocarbons, glycol ethers), in addition to *p*-xylene as the internal standard. Isobutanol was present in both standard mixtures 1 and 2.

For handling simplicity, the spike technique was used at 100000 and 10000 $\mu g\ g^{-1}$ loadings and desorption from solution [1] at a 100 $\mu g\ g^{-1}$ loading. Desorption from solution was carried out with *p*-xylene as the internal standard.

Percentage recoveries were determined by comparison of the peak area of each solvent with the peak area of the internal standard in the solution obtained after equilibration with waste and in a similar solution without addition of waste.

The results obtained are given in Tables 2 and 3. For comparison, the data relating to 10000 and 1000 $\mu g\ g^{-1}$ loadings, already reported previously [1], are also given.

As can be seen, at a 100000 $\mu g\ g^{-1}$ loading the differences in recoveries after 5 min and 24 h were not significant at the 1% level. The only exception was ethyl acetate in waste A, for which a significant decrease in recovery was observed after 24 h. However, this difference may probably be considered as a random variation. The composition of the solvent mixture had little effect on the recovery of isobutanol; the recovery was slightly lower from standard mixture 1, but the difference was significant at the 1% level only for waste A after 24 h.

The results obtained confirmed our previous observation [1] that specific adsorption phenomena occur not only for strongly polar solvents even at the highest concentrations, but also for weakly polar analytes at the lowest concentrations. Only aromatic hydrocarbons showed quantitative recoveries over the entire range of concentrations examined. Two main parameters may be hypothesized to play an important role in determining these adsorption effects: the number and chemical nature of the adsorption sites (possibly surface oxides present on the matrix) and

TABLE 4

Recoveries (%) of industrial solvents from dried wastes A and B as a function of loading of solvents and of analyte composition [a]

Waste	Solvent	Loading of solvent ($\mu g\ g^{-1}$)					
		100000		10000		100	
		Alone [b]	Mixture [b]	Alone [b]	Mixture [b,c]	Alone [b]	Mixture [b]
A	*n*-Butanol	79.1 ± 2.9	94.9 ± 0.6	75.0 ± 2.6	80.0 ± 1.5	74.2 ± 7.8	79.5 ± 8.0
	2-Ethoxyethanol	81.7 ± 3.7	94.6 ± 3.0	80.2 ± 3.9	81.1 ± 1.1	76.5 ± 6.1	66.5 ± 8.1
B	*n*-Butanol	81.7 ± 1.7	97.3 ± 1.6	79.0 ± 1.9	84.4 ± 0.5	77.1 ± 6.8	82.6 ± 4.9
	2-Ethoxyethanol	83.2 ± 3.3	98.0 ± 4.9	82.6 ± 1.1	87.2 ± 1.8	73.2 ± 7.9	79.7 ± 9.5

[a] Average percentage recovery for six determinations ± standard deviation. Equilibration time, 5 min; waste/carbon disulphide ratio, 2 g/20 ml. [b] Alone, when present alone; mixture, when present in a mixture of 13 solvents. [c] From [1].

the properties of the desorbing agent (CS_2 may be a poor competitor with polar solvents for polar adsorption sites). A similar explanation has been given for adsorption phenomena of solvents retained on activated carbons [6,8,9,12].

Effect of analyte composition

The recoveries of polar solvents from activated carbons depend on the presence or absence of other polar compounds [4–6,10–12]. In this work, the effect of analyte composition was evaluated by determining the recoveries of *n*-butanol and 2-ethoxyethanol from the two wastes under two different conditions: when present alone and in a mixture of thirteen solvents. *n*-Butanol and 2-ethoxyethanol were selected as alcohols and glycol monoethers previously showed the strongest specific adsorption [1]. The recovery of *n*-butanol when alone was evaluated by employing *p*-xylene as the internal standard and that of 2-ethoxyethanol by employing toluene. The results obtained are presented in Table 4.

The analyte composition was found to affect the recoveries considerably at a 100000 $\mu g\ g^{-1}$ loading. The recoveries of solvents when present in mixtures proved to be notably and significantly ($p < 0.01$) higher than the recoveries of the same solvents when present alone at this loading. However, it seems important to highlight the fact that under these extreme conditions the weight of dry waste differs considerably in the two cases. Dry waste represents only 30% of the total weight for the solvents present in mixtures, but 90% for the solvent present alone.

At lower loadings the recoveries were generally slightly higher for solvents when present in mixtures, even if the differences were not significant ($p < 0.01$) for 2-ethoxyethanol from waste A at a 10000 $\mu g\ g^{-1}$ loading, and for both tested solvents from both wastes at a 100 $\mu g\ g^{-1}$ loading.

The observed results may be explained by two types of effects: strong interactive forces between polar analytes in the non-polar solvent CS_2, and/or non-equilibrium phenomena such as the irreversible adsorption of an amount of analyte on the matrix. These two types of effects were hypothesized to explain the dependence of des-

TABLE 5

Recoveries (%) of industrial solvents from dried waste A as a function of loading of solvents and of waste/carbon disulphide ratio [a]

Solvent	Loading of solvent ($\mu g\ g^{-1}$)								
	100000			10000			100		
	2:40 [b]	2:20 [b]	2:10 [b]	2:40 [b]	2:20 [b,c]	2:10 [b]	2:40 [b]	2:20 [b]	2:10 [b]
Dichloromethane				97.9 ± 4.8	93.7 ± 0.9	87.5 ± 5.7	94.2 ± 8.2	90.7 ± 12.6	78.4 ± 5.1
Methyl ethyl ketone				97.1 ± 2.3	89.4 ± 3.2	85.8 ± 2.7	90.5 ± 8.3	85.8 ± 6.1	79.8 ± 4.8
Ethyl acetate				98.5 ± 4.2	91.5 ± 4.2	90.3 ± 2.6	96.3 ± 7.2	87.0 ± 4.2	85.1 ± 5.6
Methyl isobutyl ketone				100.2 ± 2.3	97.3 ± 0.7	94.0 ± 2.5	99.7 ± 5.9	92.2 ± 4.7	91.9 ± 6.1
Isobutanol				90.1 ± 5.3	80.0 ± 1.2	71.0 ± 4.2	81.8 ± 7.4	74.0 ± 6.6	62.4 ± 4.3
Isobutyl acetate				98.2 ± 2.4	97.2 ± 1.7	96.1 ± 2.3	100.5 ± 3.6	94.2 ± 6.6	95.8 ± 5.0
Toluene				100.4 ± 3.1	102.0 ± 0.8	99.5 ± 1.4	98.6 ± 3.4	103.2 ± 2.0	98.0 ± 1.6
n-Butanol	92.5 ± 2.6	79.1 ± 2.9	75.8 ± 1.9	89.7 ± 4.8	80.0 ± 1.5	69.3 ± 3.2	83.3 ± 4.4	79.5 ± 8.0	58.9 ± 5.6
n-Butyl acetate				94.3 ± 4.5	98.4 ± 1.1	95.6 ± 1.6	94.5 ± 5.5	93.9 ± 3.3	89.2 ± 3.0
2-Ethoxyethanol	90.5 ± 4.6	81.7 ± 3.7	75.6 ± 2.2	87.7 ± 3.6	81.1 ± 1.1	68.8 ± 4.1	61.8 ± 10.1	66.5 ± 8.1	62.6 ± 5.5
o-Xylene				98.8 ± 1.6	102.1 ± 0.4	99.4 ± 1.6	101.0 ± 4.6	108.5 ± 5.6	97.3 ± 2.3
2-Ethoxyethyl acetate				97.6 ± 4.3	94.7 ± 1.0	88.7 ± 2.6	89.5 ± 8.1	94.0 ± 5.2	91.0 ± 5.2
Cyclohexanone				97.0 ± 2.9	95.0 ± 0.9	87.2 ± 2.8	83.4 ± 4.3	90.3 ± 4.1	86.6 ± 6.2

[a] Average percentage recovery for six determinations ± standard deviation. Equilibration time, 5 min. [b] Waste/carbon disulphide ratio (w/v). [c] From [1].

orption efficiency of polar compounds on the presence or absence of other polar compounds in activated carbons [4,5,10].

Effect of waste / desorbing agent ratio

The matrix/desorbing agent ratio may affect the recoveries of analytes from activated carbons [5,13] and also from solid wastes [14]. In general, an increase in desorption efficiency with increasing desorption volume (at constant weight of sample) is observed. Here, the effect of waste/desorbing agent ratio on recoveries was evaluated by determining the recoveries from both matrices, under the same solvent loading and at a constant weight of waste, at three different ratios, 2:40, 2:20 and 2:10 (w/v). The results obtained are given in Tables 5 and 6.

As can be seen, generally higher recoveries were obtained by employing a 2:40 ratio, particularly for waste A. The recoveries were lower by employing a 2:20 ratio, and even lower employing a 2:10 ratio. The differences in recoveries were significant at the 5% level for both wastes at a 100 000 $\mu g\ g^{-1}$ loading. At lower loadings, the differences were not always significant ($p < 0.05$), particularly for waste B at a 10 000 $\mu g\ g^{-1}$ loading, and for both wastes at a 100 $\mu g\ g^{-1}$ loading. The recoveries of aromatic hydrocarbons remained virtually quantitative on varying the waste/desorbing agent ratio. The best compromise between recovery, dilution of the solution to be injected and consumption of CS_2 may therefore be a 2:20 ratio.

Conclusion

The results obtained in this study and those already published allow some conclusions to be drawn. Desorption efficiencies were evaluated in two wastes for solvents belonging to all the various classes of compounds usually found in industrial sludges. The organic carbon content and pH of the matrix did not significantly affect recoveries. The desorption efficiencies of all the solvents studied except aromatic hydrocarbons increased with increasing loading. The water content of the matrix had little effect on the recoveries of all the compounds except 2-ethoxyethanol. The presence of other polar solvents notably increased the recoveries of polar solvents at a 100 000 $\mu g\ g^{-1}$ loading; at lower loadings this effect was generally smaller. The recoveries increased on decreasing waste/desorbing agent ratio; only the recov-

TABLE 6

Recovery (%) of industrial solvents from dried waste B as a function of loading of solvents and of waste/carbon disulphide ratio [a]

Solvent	Loading of solvent ($\mu g\ g^{-1}$)								
	100 000			10 000			100		
	2:40 [b]	2:20 [b]	2:10 [b]	2:40 [b]	2:20 [b,c]	2:10 [b]	2:40 [b]	2:20 [b]	2:10 [b]
Dichloromethane				94.7 ± 3.5	93.6 ± 6.1	93.6 ± 3.7	91.5 ± 8.4	95.8 ± 6.1	78.2 ± 7.1
Methyl ethyl ketone				93.9 ± 4.1	94.7 ± 1.3	92.2 ± 3.3	92.7 ± 6.6	91.9 ± 5.0	84.7 ± 4.7
Ethyl acetate				96.1 ± 3.6	93.3 ± 1.5	94.2 ± 3.7	98.8 ± 7.6	89.4 ± 5.3	92.1 ± 4.7
Methyl isobutyl ketone				96.6 ± 2.8	97.7 ± 0.1	95.2 ± 3.1	99.9 ± 3.1	94.7 ± 4.1	92.8 ± 3.1
Isobutanol				86.3 ± 4.7	84.5 ± 1.2	75.5 ± 4.5	89.0 ± 2.3	78.1 ± 4.9	69.7 ± 5.7
Isobutyl acetate				97.1 ± 3.8	98.8 ± 1.5	96.1 ± 3.5	99.8 ± 2.8	94.8 ± 4.2	96.6 ± 3.5
Toluene				98.5 ± 2.4	101.9 ± 1.5	99.2 ± 1.7	99.5 ± 2.2	100.8 ± 3.0	99.6 ± 3.5
n-Butanol	91.5 ± 2.5	81.7 ± 1.7	74.8 ± 1.8	88.3 ± 3.3	84.4 ± 0.5	72.8 ± 2.0	75.0 ± 2.9	82.6 ± 4.9	65.6 ± 3.5
n-Butyl acetate				99.4 ± 1.0	98.5 ± 0.7	96.4 ± 2.6	99.1 ± 2.3	96.2 ± 3.2	86.8 ± 4.3
2-Ethoxyethanol	90.2 ± 1.1	83.2 ± 3.3	77.0 ± 3.0	87.0 ± 2.8	87.2 ± 1.8	74.4 ± 2.4	74.3 ± 4.9	79.7 ± 9.5	67.9 ± 4.6
o-Xylene				98.8 ± 1.6	102.1 ± 0.7	100.1 ± 1.5	100.7 ± 4.0	105.3 ± 5.0	100.0 ± 2.4
2-Ethoxyethyl acetate				98.6 ± 3.3	99.0 ± 3.7	92.6 ± 3.1	93.2 ± 7.4	93.8 ± 7.9	87.8 ± 4.3
Cyclohexanone				97.9 ± 1.4	96.2 ± 1.6	91.6 ± 1.7	93.5 ± 7.0	89.1 ± 6.2	90.8 ± 5.6

[a–c] See Table 5.

eries of aromatic hydrocarbons were not affected by this parameter. The study of the kinetics of desorption demonstrated that equilibrium was reached within 5 min in all instances.

The authors thank Roberta Antonutti for technical assistance and Rossana Levi for typing the manuscript.

REFERENCES

1 L. Ceccon, A. Turello, G. Mocellin and L. Colugnati, J. Assoc. Off. Anal. Chem., 72 (1989) 1010.
2 M.P. Coover, R.C. Sims and W. Doucette, J. Assoc. Off. Anal. Chem., 70 (1987) 1018.
3 D.A. Dzombak and R.G. Luthy, Soil Sci., 137 (1984) 292.
4 J.C. Posner and J.R. Okenfuss, Am. Ind. Hyg. Assoc. J., 42 (1981) 643.
5 J.C. Posner, Am. Ind. Hyg. Assoc. J., 42 (1981) 647.
6 J. Rudling, Appl. Ind. Hyg., 2 (1987) 170.
7 R.G. Melcher, R.R. Langner and R.O. Kagel, Am. Ind. Hyg. Assoc. J., 39 (1978) 349.
8 J. Rudling and E. Björkholm, Am. Ind. Hyg. Assoc. J., 47 (1986) 615.
9 J. Rudling and E. Björkholm, J. Chromatogr., 392 (1987) 239.
10 F.X. Mueller and J.A. Miller, Am. Ind. Hyg. Assoc. J., 40 (1979) 380.
11 M. Fracchia, L. Pierce, R. Graul and R. Stanley, Am. Ind. Hyg. Assoc. J., 38 (1977) 144.
12 J. Rudling, Am. Ind. Hyg. Assoc. J., 49 (1988) 95.
13 R.A. Dommer and R.G. Melcher, Am. Ind. Hyg. Assoc. J., 39 (1978) 240.
14 American Society for Testing and Materials, Annual Book of ASTM Standards, ASTM, Philadelphia, PA, 1986, Sect. 11, Vol. 11.04, Method D 3987-85.
15 U. Springer and J. Klee, Z. Pflanzenernähr. Düng., Bodenk., 64 (1954) 1.

Analytica Chimica Acta, 278 (1993) 125–136
Elsevier Science Publishers B.V., Amsterdam

Effects of fusion charge composition on the determination of platinum group elements using collection into a minimized nickel sulphide button

Tomáš Paukert and Ivan Rubeška

Czech Geological Survey, Malostranské náměstí 19, 118 21 Prague 1 (Czech Republic)

(Received 16th September 1992; revised manuscript received 5th January 1993)

Abstract

For characterizing fire assay fusion and the collection of platinum group elements (PGE) into a NiS button, two parameters referring to the charge before fusion were defined. One is the extraction ratio E, expressed as the mass ratio of the sample plus flux to the collector (Ni + S) and the other is the sulphur content in the collector S_c, expressed as a percentage. Using graphite furnace atomic absorption spectrometry after fire assay into a minimized NiS button, the PGE recoveries were investigated when varying these two parameters. The experimental data show that for an acceptable recovery, S_c may vary in a fairly broad range, namely 30–50%. Any excess of sulphur seems to be easily removed during fusion by oxidation with atmospheric oxygen. For full recovery, an extraction ratio $E \geqslant 30$ is admissible. However, at high extraction ratios the sample composition, particularly its sulphur content, becomes highly critical and sulphur must be taken into account when preparing the fusion charge. The precision and accuracy of the recommended procedure were tested on ten reference materials. The comparison of the results with those of SARM-7, which is used by most analysts, was favourable. There is a need for many more analysts to report their results before "usable values" can be established for other reference materials and statistical tests can be done.

Keywords: Atomic absorption spectrometry; Fire assay; Nickel sulphide button; Platinum group metals

The determination of platinum group elements (PGE) in geological materials still relies primarily on fire assay fusion as the first step towards extracting PGE from the silicate matrix. Acid digestion is applicable only for Pt and Pd, and has been used mainly as a an inexpensive alternative for sample screening [1].

The extension of gold fire assay to PGE and their collection into a lead button is satisfactory only for Pt, Pd and Rh. The other elements, i.e., Ru, Os and Ir, are not soluble in lead; they are only "wetted", and because of their high density they sink into the molten lead and become mechanically fixed [2].

In the presence of Au and Ag in amounts in excess of fifteen times the mass of PGE, the lead button may be treated by cupellation. During this process, however, Os and Ru are lost. Iridium does not alloy readily with either Au or Ag but forms a black deposit clinging to the bottom of the bead. Attempts to use other metals in place of lead as collectors, such as Sn, In, Cu or Cu + Fe, were not particularly successful when applied to geological materials.

A more comprehensive fire assay procedure (FA) including all the PGE and Au uses collection into nickel sulphide (NiS-FA). Artificial sulphides formed during fusion in the presence of

Correspondence to: T. Paukert, Czech Geological Survey, Malostranské náměstí 19, 118 21 Prague 1 (Czech Republic).

sulphur in the fusion charge are called mattes. They are highly insoluble in the siliceous slag and are excellent collectors of PGE. They were first proposed by Williamson and Savage [3] for collecting Os and Ir. Although Cu and Fe sulphides are equally efficient as collectors, Ni sulphide has the advantage that it can be dissolved in HCl and thus separated from the PGE, which should remain as the insoluble residue of PGE sulphides. Iron sulphides are more difficult to dissolve completely and to separate.

The NiS-FA procedure was later successfully applied to all PGE [4] and became virtually a standard procedure. Although Williamson and Savage [3] did not elaborate on how the fusion charge composition was derived, most subsequent workers used the same composition of the flux ($Na_2CO_3 + Na_2B_4O_7$) and the collector (Ni + S). The original procedure uses substantial amounts of Ni and S and the resulting button is fairly massive (20–30 g). This, of course, increases requirements with respect to the purity of the nickel used and makes the dissolution of the button a lengthy procedure. Only recently have studies been made of the efficiency of collection when the button mass is decreased [5–7].

BASIC CONSIDERATIONS

The fusion charge for FA has two main components: the flux, which secures a low melting point so that at furnace temperature (ca. 1000°C) the slag is sufficiently fluid, and the collector, into which the PGE are extracted. However, limited information is available on how the fusion charge should react to a changing composition of the sample. Robert et al. [4] suggested a flux to sample ratio of 1:1, and for a 90-g flux they recommended 20 g of NiO and 10 g of S. For 32 g of $NiCO_3$, not more than 15 g of sulphur is acceptable.

The standard procedures used at the Norilsk plant [8] require that the collector amounts to 5–7% of the charge (sample + flux) and that the S to Ni mass ratio be between 0.38 and 0.51. The copper present is taken into account in the following way: for each gram of Cu in the sample, 0.2–0.25 g of S is added; this amount is not included in the above-mentioned S to Ni ratio.

An Australian procedure asserts that the ratio of nickel plus base metals to sulphur should be 1.26:1, and that for a full recovery refusion of the slag is necessary [9].

In this study, attempts were made to acquire a better insight into the processes and parameters controlling the formation of the button and the collection of PGE. The main aim was to minimize the button mass and thus reduce possible blank values.

The NiS-FA may be considered as an extraction step of PGE by an immiscible liquid phase of nickel sulphide from a silicate melt. Thus, the controlling parameters should include the following.

The first parameter is the extraction ratio E, which can be defined as the mass ratio of the siliceous slag and the sulphide phase. As both undergo changes during the fusion, as a first approximation the expression

$$E = (m_{\text{sample}} + m_{\text{flux}})/(m_{\text{Ni}} + m_{\text{S}}) \quad (1)$$

where m is the mass of the component indicated by the subscript, was used. In addition to soda and borax, the m_{flux} may also include any silica added to the charge. The sulphide phase formed during FA naturally includes not only the nickel and sulphur added to the charge, but also any sulphur, Ni and possibly Fe, Cu and other metals present in the sample. On the other hand, an unknown amount of sulphur is lost during fusion, owing to oxidation by higher valence oxides (Fe_2O_3) and by atmospheric oxygen. Likewise, part of the Ni is bound to the siliceous slag. All these factors introduce a level of uncertainty. Therefore, the simple Eqn. (1) was used.

The second controlling parameter is the sulphur content in the collector, expressed as a percentage, or

$$S_c = m_S \times 100/(m_S + m_{Ni}) \quad (2)$$

It was expected that S_c would control the composition of the artificial sulphides formed during the fusion, but this does not seem to be the case. With a higher sulphur content, simply more metals from the sample, mainly iron, are bound into the sulphide phase.

The third controlling factor is the partition coefficient between the sulphide and siliceous phases. As its value is evidently very high, the effects should be negligible in comparison with the effects of the first two parameters, and were not considered further.

In Table 1 the fusion charges used by different workers are compared and the two controlling parameters, E and S_c, as calculated are given. Most workers kept S_c below 45% and E between 5 and 7. In this study, these two parameters were varied over greater ranges. Other experimental conditions, such as fusion temperature, fusion time and preparation of the sample solutions from the buttons, were kept constant as far as possible.

EXPERIMENTAL

Equipment

An LK 112.11 muffle furnace (MLW, Bad Frankenhausen) with a controlled temperature range of 20–1200°C, a Perkin-Elmer Model 4000 atomic absorption spectrometer with an HGA 500 graphite furnace and chart recorder, a Plattner mortar, vacuum filtration apparatus, fritted glass crucibles (10–16 μm porosity) and fire assay crucibles (250 ml volume) were used.

Reagents

All reagents were of analytical-reagent grade. PGE stock standard solutions were prepared from the purest chemicals commercially available. Nickel powder was obtained from Inco Metals.

Procedure

Weigh a 20-g sample into a crucible and mix thoroughly with 24 g of $Na_2B_4O_7$, 12 g of Na_2CO_3, 1.9 g of nickel powder and 1.8 g of sulphur powder. Any sulphur present in the sample is subtracted from the 1.8 g of sulphur added. If the sulphur content in the sample is $> 9\%$, SiO_2 is added.

Place the crucibles in a preheated furnace at 600°C and set the temperature to 1000°C. When the temperature has reached 1000°C, leave it for 60 min, then set it to 1100°C and leave it for another 20 min. After the fusion is completed, remove the crucibles from the furnace and allow them to cool.

Separate the button mechanically from the slag, then crush it in a Plattner mortar and transfer it to a 250-ml beaker covered with a watch-

TABLE 1

Composition of the fire assay into NiS used by various workers

Ref.	FA mass to be weighed (g)						FA parameters	
	Borax	Soda	Ni [a]	S	SiO_2	Sample	E	S_c
4	60	30	32 $NiCO_3$	12.5	–	5–25	3.4–5.0	44.2
8 [b]	210 (b)		20 NiO	4.5–6.5	–	100	14.0–15.4	22.3–29.3
8 [c]	100 (c)		15 NiO	5.5	–	20	7.0	31.9
11	38	65	20 NiS		15	50–100	8.4–10.9	35.3
12	60	30	32 $NiCO_3$	12.5	–	5–25	3.4–4.1	44.2
13	60	30	32 $NiCO_3$	12.5	–	30–50	4.2–5.0	44.2
14	60	30	32 $NiCO_3$	12.5	–	20–50	3.9–5.0	44.2
15 [d]	8	12	6 NiO	3	2.5	5–10	3.6–4.2	39.0
15 [b]	8	18	6 NiO	3	3	5–10	4.4–5.0	39.0
16	60	30	32 $NiCO_3$	12.5	5	20–30	4.1–4.4	44.2
17	20	10	5	3	3	15	6.0	37.5
18	60	30	16	10	0–10	50	5.4–5.8	38.5
19	36	18	3.2	3	20	10	13.5	48.4
5	50 [f]	25	0.5–10	0.35–7	5	25	6.2–123	41.2
6	70	35	5.4 $NiCO_3$	1.83	20 [g]	10–30	30.2–34.7	40.9
This work	24	12	1.9	1.8	–	20	15.1	48.6

[a] Ni metal powder, except where given otherwise. [b] Generalized for ores (b) mixture soda–borax–crushed glass (4 + 2 + 1). [c] concentrates (c) soda–borax–crushed glass (2 + 1 + 1). [d] Ores. [e] Concentrates. [f] $Li_2B_4O_7$ instead of $Na_2B_4O_7$. [g] 10 g SiO_2 + 10 g MgO.

glass. Dissolve the pulverized button in 50 ml of concentrated HCl on a hot-plate at 80–90°C. Filter the solution through a fritted glass crucible. Wash the undissolved residue on the frit once with concentrated HCl and four times with distilled water.

Dissolve the residue directly on the frit with a mixture of 100 ml of concentrated HCl and H_2O_2 (1 + 1) with three repetitions, collecting the solution into the original beaker in which the dissolution of the button took place. Evaporate the solution to wet salts and transfer the latter into a 10-ml volumetric flask with 1 M HCl. The solution is then ready to be measured by either graphite furnace atomic absorption spectrometry (GFAAS) or inductively coupled plasma mass, spectrometry (ICP-MS).

Measurement by GFAAS

The conditions for the GFAAS measurement are summarized in Table 2. Background correction, sampling volume 20 μl and integrated absorbance with a 4-s integration time were used. Values close to the limits of detection were evaluated from peak-height readings on the chart recorder. The calibration solutions were 200, 100, 50, 20, 10 and 0 ng PGE ml^{-1} in 1 M HCl with 10 μg Ni ml^{-1} added.

RESULTS AND DISCUSSION

Procedure

Grinding. The button is crushed in a Plattner mortar of hardened steel. The powdered material is fine enough to dissolve within about 4 h, hence pulverization may be avoided. Nevertheless, for buttons above 5 g, pulverization was necessary. When using the vibrating mill, no significant losses were observed. When using a shatter-box, Boisvert et al. [19] found losses of up to 20%.

Dissolution. Crushed buttons (< 3 g) are dissolved in 50 ml of concentrated HCl. For each additional gram of button mass, 25 ml of concentrated HCl are added. The resulting solutions are usually bright green; in some solutions, particularly for buttons resulting from fusion charges with $S_c > 50\%$, a slight turbidity may be observed. This turbidity did not seem to influence the recovery of PGE.

An attempt was made to speed up the dissolution by using a closed system in a microwave oven (Model MDS-81D; CEM, Matthews, NC). The dissolution was much faster, lasting less than 1 h, but no PGE were found. Probably the PGE sulphides were also dissolved and passed into the filtrate.

Kuznetsov et al. [11] suggested concentrated H_2SO_4 for the dissolution of NiS buttons. Although the dissolution is rapid, almost all the copper and other heavy metals remain undissolved, causing serious interferences during the following steps. Particularly sulphates interfere in the determination by GFAAS [20].

Filtration. The solutions were filtered through glass crucibles with a frit. Filtration with paper filters requires the same amount of time as with fritted glass, but the filter paper partly disintegrates and the cellulose fibres cause problems in the following steps. To avoid this, a PTFE filter was tried. However, its porosity (0.45 μm) was too low and the filtration time too long, resulting in 30–50% lower values of the PGE found. This was probably caused by the oxidation of PGE

TABLE 2

GFAAS measurement conditions

Element	Line (nm)	Slit (nm)	Temperature (°C)/ramp + hold time (s)			
			Drying	Pyrolysis	Atomization	Cleaning
Pt	265.9	0.7	110/1 + 14	1200/10 + 2	2700/0 + 4	2700/1 + 1
Pd	340.5	0.7	110/1 + 14	900/10 + 2	2500/0 + 4	2500/1 + 1
Ru	349.9	0.2	110/1 + 14	1200/10 + 2	2700/0 + 4	2700/1 + 1
Rh	369.2	0.2	110/1 + 14	1200/10 + 2	2600/0 + 4	2600/1 + 1
Ir	264.0	0.7	110/1 + 14	1200/10 + 2	2700/0 + 4	2700/1 + 1

sulphides by air and their subsequent loss in the filtrate. In a radiochemical study, Parry et al. [21] reported losses of 29% Au, 26% Pt, 10% Ru and 7% Ir during the filtration step.

Interferences with the GFAAS measurement. The most sensitive Rh line at 343.489 nm is flanked on both sides by Ni lines at 343.356 nm (lower energy level 207 cm^{-1}) and 343.728 nm (resonance line), which cause an overcorrection when using a deuterium lamp background corrector. The Rh line used has a three times lower sensitivity but is free from this interference.

The Pd line used is only fourth in sensitivity, but the resulting calibration graph is linear. It was selected because the limits of detection of Pd are not critical and are mostly limited by blank values.

The Ir line at 264.038 nm is second in sensitivity, but allows the use of a wider slit, achieves a better signal-to-noise ratio and gives less curved calibration graphs. The sensitivities of both Ir and Ru depend greatly on the quality of the tube surface and decrease markedly with the number of firings.

Mutual interferences of PGE occur when the interferent-to-analyte ratios are high [10,20]. In the analysis of geological samples, this generally does not cause any serious errors because in the final solution nickel, iron and copper are present in considerably higher concentrations than the individual PGE. Using the above-described procedure for the button dissolution, the following concentrations were typically found by flame AAS for buttons weighing 1 g or more: 1–500 mg Ni l^{-1}; 0.1–5 mg Fe l^{-1} and 0.01–1 mg Cu l^{-1}.

The effects of Ni, Fe and Cu as sulphates in these particular concentration ranges were therefore tested. The influence of Fe and Cu was found to be negligible. With the minimized button, the concentrations of these elements were kept < 1 mg l^{-1} in the final solution. More serious problems are caused by the presence of Ni [19,20]. Measurements were made with synthetic solutions containing all the PGE, except Os, at the same concentration and Ni added as $NiSO_4$. The most significant interferences were observed for Pd and Ir, as shown in Fig 1. For real samples and buttons < 3 g, the concentra-

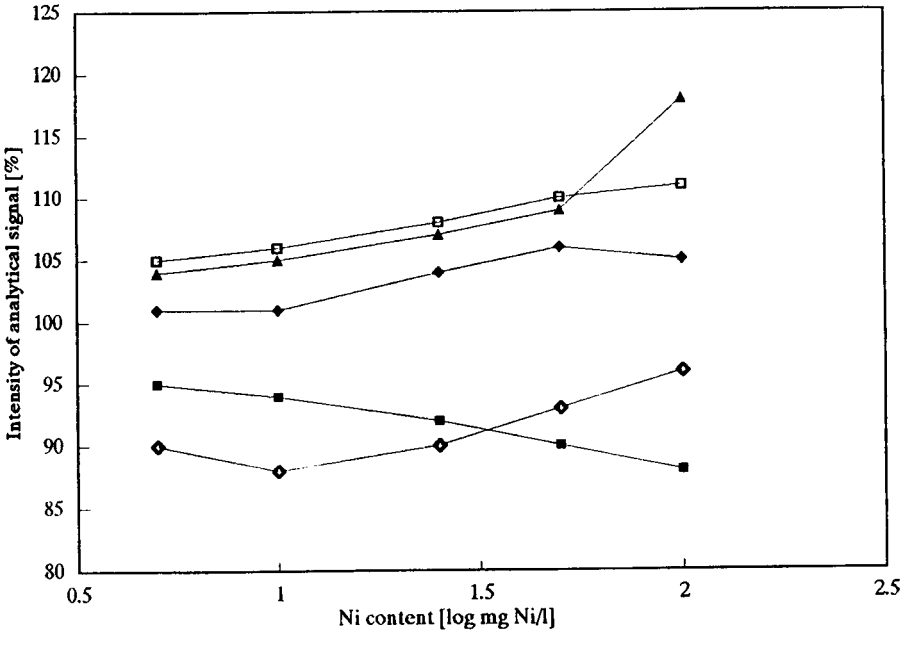

Fig. 1. Effect of $NiSO_4$ on the intensity of the analytical signal of PGE measured by GFAAS. ■ = Ru; ♦ = Rh; ▲ = Pd; □ = Ir; ◇ = Pt.

tion of Ni in the final solution was usually well below 20 mg l^{-1}.

Therefore, in all sample solutions, first the Ni content was measured by flame AAS and, for the PGE measurement, calibration solutions spiked with the appropriate amount of nickel sulphate were used. Generally, calibration solutions containing 10 mg Ni l^{-1} are used. A similar approach has been utilized by other workers [19].

Button composition

Nickel forms four natural sulphides, namely the subsulphide Ni_3S_2 (heazlewoodite), NiS (millerite), Ni_3S_4 (polydymite) and NiS_2 (vaesite). Of the four, only millerite is considered to be soluble in HCl [22]; the other three require nitric acid. Nevertheless, nickel may form artificial sulphides, such as Ni_7S_6 or $Ni_{3-x}S_2$, which are not stable to attack by HCl.

In their pioneering work, Williamson and Savage [3] found that the composition of the button was 69.3% Ni and 27.9% S. This corresponds to a eutectic point between Ni_3S_2 and Ni_6S_5. The composition of the button remains close to these values even when the sulphur content in the charge varies. For S_c values between 39 and 46%, 25.9–28.2% S was found in the resulting button. Excess of sulphur was evidently lost by oxidation during fusion.

Oxidation is fairly intensive even after the fusion has been completed and the sulphide phase has settled at the bottom of the crucible. Bubbles of the SO_2 formed on the surface of the button induce a convective flow of the slag upwards in the middle and downwards along the walls of the crucible. Thus, the sulphide phase is permanently in contact with an oxygen-saturated slag. This convective flow of the slag is a characteristic feature of the NiS-FA and makes the button mass much more dependent on the fusion conditions (temperature, time, oxygen concentration in the furnace atmosphere) than those of Pb-FA. The convective slag circulation also probably improves the efficiency of the extraction and collection.

If present, other heavy metals (Cu, Fe) enter the sulphide phase, and the increase in the button mass with the corresponding increase in S_c values is much more pronounced. In the presence of iron, pentlandite [$(Fe, Ni)_9S_8$] and violarite ($FeNi_2S_4$) have been identified by x-ray diffractography. If the S_c value in such samples is higher than 50%, the button becomes very massive, it gradually disintegrates in air and is only partly dissolved in HCl. The filtrated residue reacts vigorously even with H_2O_2 itself. The resulting sample solution thus contains large amounts of Ni, Fe, Cu and sulphates which interfere with the PGE measurement by GFAAS. As Fe and Cu sulphides are also effective collectors

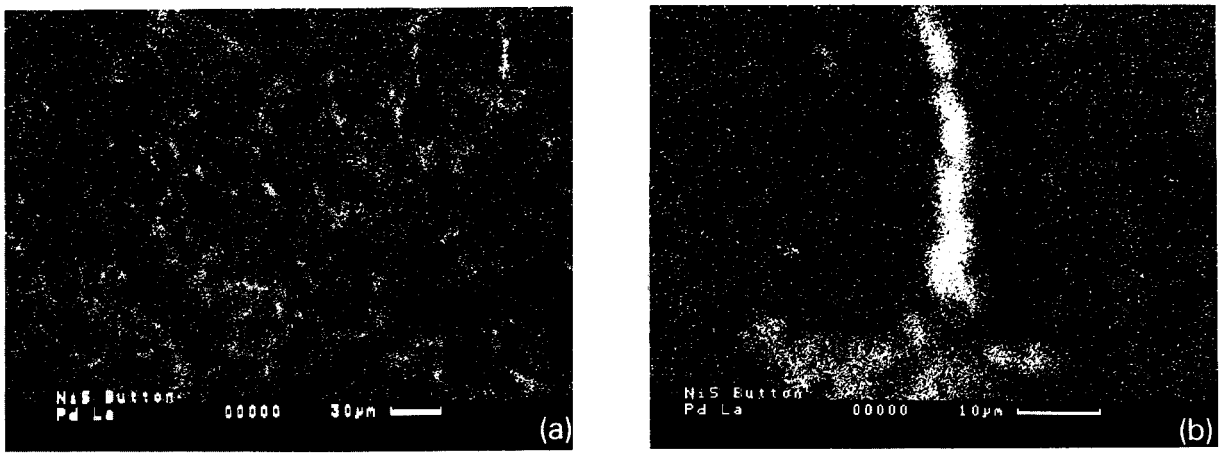

Fig. 2. (a) X-ray microprobe scan of Pd in the NiS button. (b) Magnification of the top right corner (courtesy of J. Fryda, CGS Prague).

of the PGE, this does not affect the collection, but only the ease with which the buttons can be dissolved and measured.

The button mass is a suitable indicator of the correct fusion conditions. This mass depends mainly on the amount of Ni + S added and on the time and temperature of FA. Increased S added to a "blank" granite sample caused a negligible difference in the button size (from 1.8 up to 1.9 g). If base metals that can form sulphides are present, the button mass will increase up to 100%. A large button mass therefore indicates that the S content of a sample has been underestimated. Hence the S content in a sample is necessary for calculating the correct FA charge. Oxidative compounds in the sample reduce the final button mass. Their presence is revealed by a white layer of alkaline sulphates on the surface of the cool slag.

To learn more about the PGE distribution in the NiS button itself an investigation was carried out using an x-ray microprobe (Cambridge Scanning, Link EXL, Microspec WDX-3PC). For this study a sample containing 0.4% of Pd was assayed. A 5-g portion of sample resulted in an approximate concentration of 1% of Pd in a 2-g button. The record of an angle scan at wavelengths from 400 up to 445 pm of Pd on the button studied is shown in Fig. 2a. The micrograph illustrates that palladium was not distributed homogeneously throughout the button mass. Pulse counts per second measured at various places in the button indicated large differences, from 50 up to 2500. Palladium formed randomly scattered spots of either alloys with nickel and other PGE or sulphides, which are represented by light dots in the photograph. The magnification of a concentrated spot of Pd is shown seen in Fig. 2b. Other PGE are probably present in similar clusters. This would unfortu-

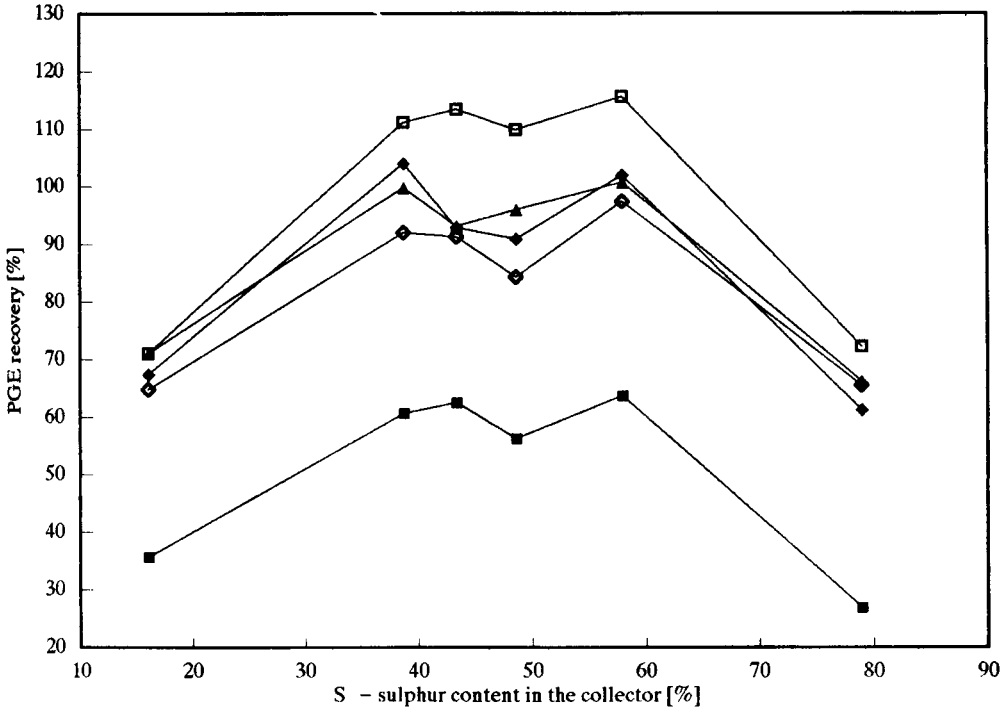

Fig. 3. PGE recovery for sulphur content S_c = 16–79%. Symbols as in Fig. 1.

nately cause severe bias of the results if the analysis of PGE by laser ablation (LA–ICP-MS) directly from the NiS button was utilized.

Effect of S_c and E on PGE results

For the experimental work, the reference material (RM) UMT-1 was chosen. For each particular parameter S_c or E, 20-g sample aliquots were fused and analysed in duplicate. The PGE data obtained on changing S_c and E are presented in Tables 3 and 4, respectively. The recovery of PGE is expressed as a percentage of the recommended values (RVs).

As seen in Fig. 3, except for the extreme values $S_c = 16\%$ and 79%, for which the recoveries were low, the results did not show any clear dependence. As the results for all the PGE are closely correlated, it is possible that the variations observed were caused by losses during the dissolution of the button and separation of PGE rather than by the collection. The conditions of the dissolution could not be kept constant because of the difficulties in dissolving buttons from charges with high S_c values. Even though the RVs of UMT-1 have not yet been certified, the low recovery of Ru (up to 60%) indicated its loss during the analytical procedure.

TABLE 3

Analyses of UMT-1 with various E and S_c factors

E	S_c	m (g) [a]	Concentration (ng g^{-1})				
			Ru	Rh	Pd	Ir	Pt
5	79.0	5.3	4.3	6.05	69	6.3	84
10	58.0	4.6	10.2	10.0	105	10.1	125
13	43.4	3.6	10	9.1	97	9.9	117
15	48.6	3.3	9.0	8.9	100	9.6	108
18	38.7	2.6	9.7	10.2	104	9.7	118
20	16.1	1.3	5.7	6.6	74	6.2	83
RV [23]			16	9.8	104.2	8.73	128.3

[a] m = Mass of a button.

The differences in the PGE results for $E = 15$ and $S_c = 48.6$ in Tables 3 and 4 can be ascribed to the accuracy of the GFAAS measurements. The data also include a reproducibility factor. The FA conditions recommended in this paper

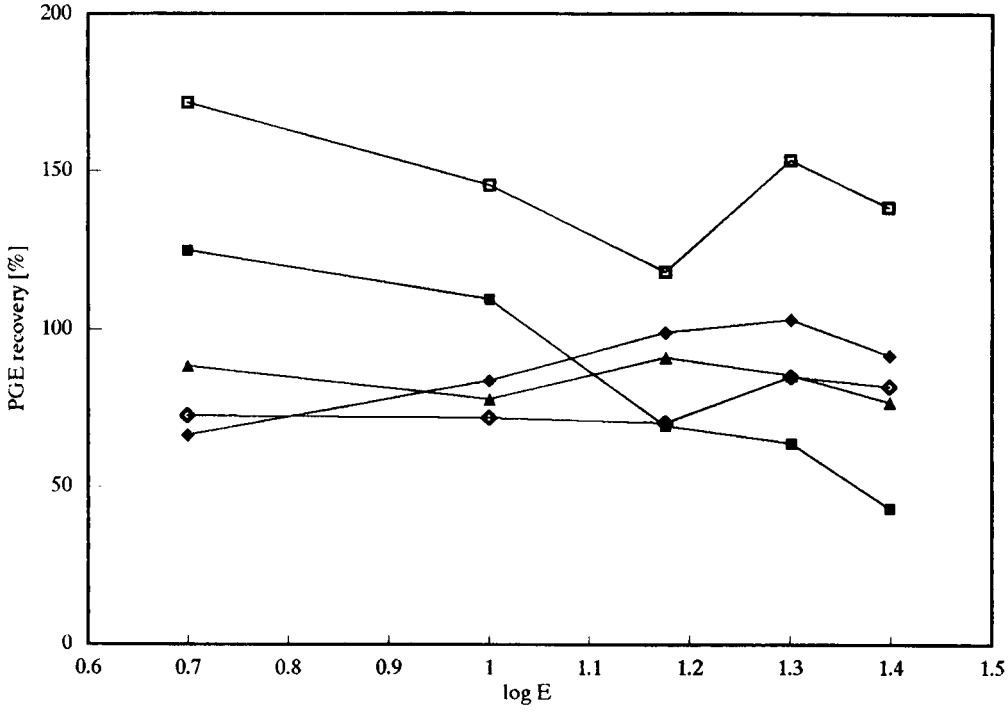

Fig. 4. PGE recovery with a constant sulphur content of $S_c = 46–48\%$ and a changing E factor ($E = 5–25$). Symbols as in Fig. 1

TABLE 4

Analyses of UMT-1 with various E and constant S_c

E	S_c	m (g) [a]	Concentration (ng g^{-1})				
			Ru	Rh	Pd	Ir	Pt
5	48.2	7.6	22	6.5	92	19.1	93
10	48.2	2.8	17.5	8.2	81	12.7	92
15	48.6	1.4	11.1	9.7	95	10.3	90
20	48.6	0.9	10.2	10.1	89	13.4	109
25	48.6	0.6	6.9	9	80	12.1	105

[a] m = Mass of a button.

were sufficient for the virtually complete collection of the PGE. The investigation of the PGE recovery showed no serious losses into slag because the second FA using the slag from the first fusion as a sample did not find any PGE concentrations above the detection limits of GFAAS.

Nevertheless, there are other important points that must be addressed with great care. In particular, unnecessary treatment of dissolved buttons may cause interruption of evolution of H_2S, coprecipitation of solid sulphur and dissolution of certain parts of the PGE, which pass into the filtrate. Solid sulphur interferes with the subsequent dissolution of the PGE sulphides by HCl + H_2O_2. From this reason, it is recommended to saturate solutions during dissolution of NiS buttons with H_2S from an external apparatus. Hence the PGE sulphides do not dissolve and are kept on a filter. Some investigators[17] also used coprecipitation on Te, which may prevent the loss of the PGE after the dissolution of a button.

If the S_c values in the FA charge are kept within the range 45–55% and only the extraction factor is varied from $E = 5$ to 25, any differences observed are not statistically significant. There is also no, or little, correlation between the results for the individual PGE, as can be seen in Figs. 3 and 4.

These results indicate that the efficiency of the extraction of the PGE metals does not depend critically on the S_c values of the fusion charge and that an extraction ratio of up to 30 is acceptable. This is in agreement with the findings of Robert et al. [4], who with $E = 5$ found no significant differences for S_c values between 24 and 52%.

Asif and Parry [5] tested extraction ratios of up to 123 and considered even this ratio to be acceptable. Too high extraction ratios are, however, unsuitable for routine analyses because the sample composition becomes highly critical. Any S, Ni, Cu and Fe present in the sample will strongly affect the button resulting from the fusion. A too high sulphur content in the presence of base metals and iron produces buttons that are difficult to dissolve and, during dissolution and filtration, losses of PGE may easily occur [21].

For routine analyses compromise conditions were therefore selected, recommending $E = 15$ and $S_c = 48\%$. Under these conditions, the sample composition must be taken into consideration only if the sulphur content is $> 0.2\%$.

Precision and accuracy

The precision and accuracy of the procedure were tested by analysing several RMs. The best analysed RM, SARM-7 from Mintek [24], has an exceptional high content of PGE, and therefore

TABLE 5

Results for SARM-7

Element	Concentration (ng g^{-1})							
	This work		Asif and Parry [5]		Haines and Robert [20]		RV [24]	
	Found	s [a]	Found	s [a]	Found	s [a]	Value	s [a]
Ru	391	53.6	540	99	450	50	430	57
Rh	201	25.6	240	28	220	20	240	13
Pd	1498	83.9	1350	270	1460	50	1530	32
Ir	68	14.0	88	11	61	4	74	12
Pt	3237	602	3240	210	3750	120	3740	45

[a] s = Standard deviation.

TABLE 6

Analyses of PTC-1, UMT-1 and Su-1a

Element	Concentration (ng g^{-1})								
	PTC-1			UMT-1			Su-1a		
	Found	s [a]	RV [23]	Found	s [a]	RV [23]	Found	s [a]	RV [23]
Ru	419	26.7	–	11.1	2.1	–	44.4	6.1	–
Rh	586	11.1	620	9.5	0.7	9.8	59.2	2.6	80
Pd	10273	653	12700	98.8	5.0	104.2	367	13.0	370
Ir	145	6.9	–	9.7	1.0	8.73	24.2	2.2	–
Pt	2775	311	3000	115	11.9	128.3	420	60.2	410

[a] s = Standard deviation.

only 5-g aliquots were taken; these were made-up to 20 g with an in-house reference granite sample. The results of the analyses with the proposed method (five repetitions) and those of several other workers are summarized in Table 5. Almost all of the present results lie within the tolerance of the RV [24] if limits at the 95% confidence level are considered (see Table 5). Only the results of Pt suffer from a higher error, which may be explained by the low sample masses (5 g) that were taken for the analysis. Haines and Robert's data [20] were based on large buttons processed, whereas our and Asif and Parry's data [5] were obtained from the analyses of minimized buttons.

In Table 6, analyses of three RMs are summarized together with the RVs, where available. The data were derived from four separate analyses of 5-g sample aliquots for PTC-1, five results on 20-g sample aliquots for UMT-1 and ten results on 20-g sample aliquots for Su-1a.

Silica was added to the flux for PTC-1 to accommodate a larger part of the base metals in the slag. Because of the high sulphur content in Su-1a, the sample was first roasted at 620°C for 6 h. Although during roasting part of the Ru may have been lost by oxidation and volatilization [25],

TABLE 7

Analyses of reference materials for the PGE

Element	Concentration (ng g^{-1})								
	TDB-1			WGB-1			WPR-1		
	Found	s [a]	s_{rel} (%) [a]	Found	s [a]	s_{rel} (%) [a]	Found	s [a]	s_{rel} (%) [a]
Ru	< 2	–	–	4.6	1.4	30.4	23.4	1.8	7.7
Rh	< 0.5	–	–	< 0.5	–	–	14.0	1.3	9.3
Pd	24.3	0.5	2.1	10.9	2.2	20.2	241	11.0	4.6
Ir	< 3	–	–	3.3	0.2	6.1	16.8	1.5	8.9
Pt	6.7	2.4	35.8	5.5	1.7	30.9	299	34.0	11.4
	WMG-1			WMS-1			NIES No.8		
	Found	s [a]	s_{rel} (%) [a]	Found	s [a]	s_{rel} (%) [a]	Found	s [a]	s_{rel} (%) [a]
Ru	50.0	7.0	14.0	82.8	12.6	15.2	13.3	2.1	15.8
Rh	24.8	1.7	6.9	251	30.9	12.3	23.9	3.3	13.8
Pd	397	18.7	4.7	1176	115	9.8	180	27.7	15.4
Ir	38.9	2.4	6.2	169	43.0	25.4	38.9	21.1	54.2
Pt	880	198	22.5	1468	161	11.0	185	14.3	7.7

[a] s = Standard deviation; s_{rel} = relative standard deviation.

it was considered that owing to the highly reducing environment the losses were not excessive. This assumption, however, will have to be verified further.

In Table 7, analyses of 5 RMs recently released by CANMET (not yet certified) and one RM released by NIES, Japan (No. 8, vehicle exhaust particulates) are presented to indicate the degree of precision achieved with this procedure. Each sample was analysed five times; 20-g portions of TDB-1, WGB-1 and WPR-1, 10-g portions of WMG-1 and WMS-1 and 2-g portions of NIES No. 8 were taken.

The relative standard deviations (s_{rel}) given in Table 7 were within the range for routine ultra-trace PGE analyses. The s_{rel} was high (> 20%) when the concentration was close to the determination limits. The problem of the high s_{rel} for Ir in NIES No. 8 may be ascribed to the inhomogeneity of the sample, as only 2-g sample aliquots were treated. The differences for other RMs are difficult to compare because only RVs, without any confidence levels are available, if at all. Although ten international RMs were analysed, the RVs for all the PGE and their confidence levels have only been published for SARM-7. Therefore, the results for the other RMs analysed in this work cannot be statistically evaluated. However, they will be useful for the derivation of the RVs of the PGE for these RMs.

The blank values for all the reagents were lower than the limits of determination of the PGE determined. These were established from ten measurements of a blank solution as $10s$. The limits of determination were Ru < 3, Rh < 0.5, Pd < 1, Ir < 5 and Pt < 3 ng g^{-1}.

Conclusion

To characterize the fusion charges for NiS-FA, two important parameters should be considered: the extraction ratio E, defined as the ratio of the sample plus flux to the collector, (Ni + S) and the sulphur content, S_c, expressed as a percentage of sulphur in the collector. Any sulphur present in the sample must, however, be included in the S_c value.

For efficient NiS-FA collection, both parameters may vary over fairly broad ranges. E values of up to 30 and possibly higher [5] have been found to be adequate. Nevertheless, with higher E values, the S_c value becomes more critical, particularly if the sample contains base metals and iron. For such samples it is advisable to keep the S_c values below 50%, otherwise the base metals will enter the sulphide phase and the dissolution of the button and proper separation of PGE will become difficult. During this step marked PGE losses may occur.

With an extraction ratio of $E = 13$ and an 8% iron content in the sample, S_c values of up to 50% were found to be admissible. For samples with very high iron and base metal contents, it is advisable to add silica in order to accommodate these metals in the siliceous slag.

In our laboratory we use compromise conditions characterized by $E = 15$ and $S_c = 45$–48%. Under these conditions, any sulphur content in the sample below 0.2% may be disregarded. When analysing chromitite samples, silica amounting to as much as three times the sample mass must, however, be added in order to accommodate Fe and Cr in the slag.

It is believed that minimizing the mass of the NiS button does not substantially influence the recovery of PGE and may be applied in routine work. Moreover, such a procedure decreases the consumption of reagents, in particular toxic nickel, and minimizes high blank problems. Hence this procedure is more expeditious than when using large buttons.

REFERENCES

1 J.B. Gowing and P.J. Potts, Analyst, 116 (1991) 773.
2 O.C. Shepard and W.F. Dietrich, Fire Assaying, Met-Chem Research, Boulder, CO, 1989, p. 206.
3 J.E. Williamson and J.A. Savage, J. S. Afr. Inst. Min. Metall., (1965) 343.
4 R.V.D. Robert, E. Van Wyk and R. Palmer, Rep. Natl. Inst. Metall., S. Afr., No. 1371 (1971).
5 M. Asif and S.J. Parry, Analyst, 114 (1989) 1057.
6 D. Rice, Abstracts of Geoanalysis 90 Conference, Huntsville, Ont., June 1990.
7 I. Rubeška and T. Paukert, Abstracts of the 3rd Czechoslovak Conference on Atomic Spectroscopy, Smolenice, March 1990, p. 55.

8 Fire Assay Concentration of PGE, Au and Ag using Ni Button Collector, Plant Standard Procedure 0401-35-141-79, Norilsk, 1979.
9 D.P. Herring, B.D. Price and W.P. Staunton, Aust. Inst. Geosci. Bull., No. 8 (1988) 87.
10 R.V.D. Robert and E. Van Wyk, Rep. Natl. Inst. Metall. S. Afr., No. 1705 (1975).
11 A.P. Kuznetsov, J.N. Kukushkin and D.F. Makarov, Zh. Anal. Khim., 29 (1974) 2155.
12 A. Diamantatos, Anal. Chim. Acta, 94 (1977) 49.
13 E.L. Hoffman, A.J. Naldrett, J.C. Van Loon, R.G.V. Hancock and A. Mason, Anal. Chim. Acta, 102 (1978) 157.
14 I. Shazali, L. Van't Dack and R. Gijbels, Anal. Chim. Acta, 196 (1987) 49.
15 A.I. Kvasov, Geokhimiya, No. 7 (1987) 1045.
16 A.R. Date, A.E. Davis and Y.Y. Cheung, Analyst, 112 (1987) 1217.
17 S.E. Jackson, B.J. Fryer, W. Gosse, D.C. Healey, H.P. Longerich and D.F. Strong, Chem. Geol., 83 (1990) 119.
18 P.J. Potts, A Handbook of Silicate Rock Analysis, Blackie, Glasgow, 1987, p. 491.
19 R. Boisvert, M. Bergeron and J. Turcotte, Anal. Chim. Acta, 246 (1991) 365.
20 J. Haines and R.V.D. Robert, Rep. Natl. Inst. Metall. S. Afr., No. M34 (1982).
21 S.J. Parry, M. Asif and I.W. Sinclair, J. Radioanal. Nucl. Chem., 123 (1988) 593.
22 R.C. Weast (Ed.), CRC Handbook of Chemistry and Physics, Chemical Rubber Clevelend, OH, 51st edn., 1970–71, p. B114.
23 W.S. Bowman, Certified Reference Materials, CCRMP 90–1E, CANMET, Ottawa, 1992.
24 T.W. Steele, J. Levin and I. Copelowitz, Rep. Natl. Inst. Metall. S. Afr., No. 1696 (1975).
25 P.E. Moloughney, Assay Methods Used in CANMET for the Determination of Precious Metals, SP86-1E, CANMET, Ottawa, 1986.

Analytica Chimica Acta, 278 (1993) 137–147
Elsevier Science Publishers B.V., Amsterdam

Large scale evaluation of a pattern recognition/expert system for mass spectral molecular weight estimation

Donald R. Scott

Atmospheric Research and Exposure Assessment Laboratory, U.S. Environmental Protection Agency, Research Triangle Park, NC 27711 (USA)

A. Levitsky and S.E. Stein

Chemical Kinetics and Thermodynamics Division, National Institute of Standards and Technology, Gaithersburg, MD 20899 (USA)

(Received 15th September 1992; revised manuscript received 12th November 1992)

Abstract

A previously developed fast, personal-computer based method of estimating molecular weights of organic compounds from low resolution mass spectra has been thoroughly evaluated. The method is based on a rule-based pattern recognition/expert system approach which uses empirical linear corrections which are iteratively applied to two mass spectral features to yield estimates. This technique has been extensively evaluated with 400 spectra of volatile and nonvolatile compounds of pharmaceutical interest and with 31378 high quality NIST spectra of compounds of molecular weight 30–500. Subsets of the NIST spectra were evaluated including a 23989 spectra volatile set. The overall median and average absolute deviations from the true molecular weights of the 400 spectra were 1.5 and 13 daltons. For the large NIST set and volatile subset the overall median and average absolute deviations were 1.8–2.0 and 13–17 daltons. In both sets of spectra the best results were obtained with the nonhalobenzene and unknown classes. Due to misclassification errors better results were obtained by bypassing the classifier. Median errors with spectra with the molecular ion present were ca. twenty times lower than those without the molecular ion. The present system can rapidly produce molecular weight estimates with median absolute errors of 2 (average 15) daltons.

Keywords: Mass spectrometry; Pattern recognition; Expert systems; Molecular weight estimation

Molecular weight estimates can be helpful in the identification of organic compounds from gas chromatographic–mass spectrometric (GC–MS) data of both simple and complex samples, e.g. environmental samples, which may contain a large number of unknown and sometimes unresolved compounds. In library search techniques the molecular weight can be used as a screening variable to increase the search speed. In manual or computer-assisted interpretation of spectra a molecular weight estimate can provide partial identification information, even with some mixtures, and eliminate potential candidate compounds.

In conjunction with the development of a pattern recognition/expert system for classification and identification of toxic and related volatile organic compounds from GC–MS data [1,2], a rapid and simple method for estimating molecular weights has been developed [3], improved [4,5] and evaluated. This method uses a set of empirical rules which were developed by and imple-

Correspondence to: D.R. Scott, Atmospheric Research and Exposure Assessment Lab., U.S. Environmental Protection Agency, Research Triangle Park, NC 27711 (USA).

mented with an inductive rule-based expert system. It is based on the direct linear relationship of two easily determined mass spectral features, MAXMASS (the largest mass with an intensity of at least 5%) and HIMAX1 (the largest mass with at least an intensity of 1%), with the true average molecular weight. Previous evaluations of the technique used 32 test spectra of possible volatile air pollutants, 99 reference spectra of randomly selected volatile compounds and 100 GC–MS ambient air field spectra. Results of these evaluation studies showed that the validity of the procedures greatly exceeded the domain of the original training set. The present study describes the results of an extensive evaluation of the latest version of the system [5] with a set of 400 spectra of primarily pharmaceutical interest and a set of 31 378 high quality reference spectra from the NIST (National Institute of Standards and Technology)/EPA/MSDC Database. Various subsets of the NIST spectra were also used in the evaluation.

METHODS

The 400 pharmaceutical spectra were obtained from J.T. Clerc and S. Heuerding of the Institute of Pharmacy, University of Bern and came from the OCETH Database at ETH Zurich. These 400 organic compounds were composed of only the elements carbon, hydrogen, nitrogen and oxygen. The number of carbon atoms in a compound ranged from 3 to 36 and the molecular weights were from 58 to 578. The general types of chemical structures found in this set are summarized in Table 1. The other reference spectra used to test the algorithms were from the NIST/EPA/MSDC Database, personal computer Version 3. All spectral intensities were ternary encoded when testing the molecular weight predictor. Intensities (relative to the base peak intensity of 100%) of 0 to 4.99% were assigned values of 0, those of 5 to 49.9%, values of 0.5 and those of 50 to 100%, values of 1.0. Values of the masses for MAXMASS and HIMAX1 were input in response to the queries from the expert system. The pharmaceutical spectral data were manually input into the molecular weight prediction system. The large NIST sets of spectra were batch processed with routines written to access the mass spectral database and the expert system algorithms. Development and evaluation of the expert system were performed on DOS-based personal computers.

TABLE 1

Composition of 400 pharmaceutical spectra

Type	Range of formula	Number of spectra
Hydrocarbons	C_7H_{14} to $C_{36}H_{26}$	58
Hydrocarbons with oxygen	$C_3H_4O_2$ to $C_{35}H_{70}O_1$	182
Hydrocarbons with nitrogen	$C_5H_{14}N_2$ to $C_{27}H_{21}N_1$	45
Hydrocarbons with oxygen and nitrogen	$C_4H_9N_1O_2$ to $C_{32}H_{38}N_2O_8$	115

APPROACH

In a recent study [3] it was shown that there are definite linear relationships between the experimental mass spectral feature, MAXMASS, and the true molecular weights of 400 randomly selected volatile organic compounds from the NIST mass spectral database. The molecular weight referred to here is the one computed with average isotopic compositions. MAXMASS is defined to be the highest observed mass with an intensity of 5%, or greater, of the base peak in a low resolution mass spectrum. This feature provides an accurate lower limit to and directly predicts the actual molecular weights to within a few mass units for 72% of the 400 randomly selected reference spectra studied previously [3]. An illustration of the relationship between the molecular weight and MAXMASS within the set of 400 pharmaceutical spectra is given in Fig. 1. Note that three spectra have MAXMASS values greater than their average molecular weights. This is due to isotope peaks and one contaminated spectrum.

The algorithms in the molecular weight expert system operate by applying linear corrections to

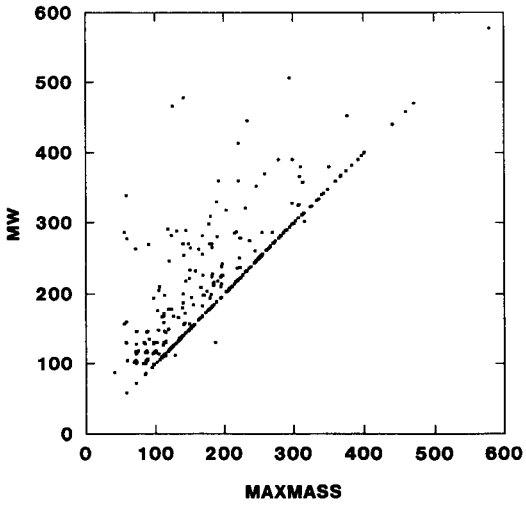

Fig. 1. Linear relationship between MAXMASS and true molecular weight (58–578 daltons) for 400 pharmaceutical mass spectra. Note the three spectra below the 1:1 diagonal line.

either MAXMASS, for all classes except for the unknown one, or to HIMAX1, for the unknown class, to provide molecular weight estimates. HIMAX1 is defined to be the highest observed mass with an intensity of 1%, or greater. There are six separate modules with molecular weight prediction rules, one for each class. The linear corrections for each module were empirically determined by the rule-based expert system from training spectra and then edited by the developer [3–5]. For the unknown class only one iteration of corrections to HIMAX1 gives very good results, but both MAXMASS and HIMAX1 are used in the rules [5]. For all other classes two iterations of corrections to MAXMASS were used [4]. MAXMASS is assumed to be the first approximation to the molecular weight, MW(0). The first iteration of rules adds, or subtracts, an empirical correction term to yield a better molecular weight estimate, MW(1). This second estimate then is used with the second set of empirical rules which apply more corrections to MW(1) to yield the final estimate, MW(2). Further details are given in Refs. 4 and 5.

The empirically derived linear corrections are commonly related to neutral losses in the spectra which prevent the use of the experimental spectral reference points, MAXMASS or HIMAX1, directly from yielding the correct molecular ion mass. In other cases they are smaller corrections which must be applied to these reference points to yield accurate molecular ion masses. MAXMASS and HIMAX1 themselves are very efficient indicators of the molecular ion mass. For example in the set of 400 pharmaceutical spectra, MAXMASS, without corrections, is equal to the mass of the molecular ion 27.5% of the time and within one dalton of the molecular ion mass another 27.5% of the time. HIMAX1 is directly equal to the molecular ion mass 16.2% of the time and within one dalton another 39.3%. MAXMASS and HIMAX1 are equal 24% of the time.

The basic design of the expert system is sequential and is based on "divide and conquer" strategy. A pattern recognition-based classifier is followed by molecular weight estimator modules for each class, one for each iteration of corrections to MAXMASS. The classifier provides partial identification information and directs the spectrum to a specific class route including the unknown class. The classifier and molecular weight rules were derived from a training set of 106 NIST reference spectra of compounds whose structures are listed in Table 2.

The classes determined by the classifier were: nonhalobenzenes, chlorobenzenes, bromo- and bromochloroalkanes/alkenes, mono- and dichloroalkanes/alkenes, tri-, tetra- and pentachloroalkanes/alkenes, and unknown (all others). These were previously determined from the training set data using SIMCA unsupervised pattern recognition [6,7] and shown with cross validation to be statistically valid. The training spectra used to derive the rules for the classification module consisted of the spectra of the 75 member target set and an additional 31 spectra in the unknown class. The set of masses used in deriving the rules were selected from the original 151 masses of the training set by using those with high Shannon information content and high peak intensity. Peaks with intensities of 50% of the base peaks or greater were used as much as possible. From an original set of 31 high intensity masses, fourteen were used in the final rules. All peak inten-

TABLE 2

Structures in training set

Class	Structure	Number in Set
Nonhaloben-zenes	Benzene	1
	Alkylbenzenes	10
	Alkenylbenzenes	1
	Phenylketones	1
	Phenylaldehydes	1
	Benzonitriles	1
Chlorobenzenes	Chlorobenzenes	4
	Alkylchlorobenzenes	3
	Alkenylchlorobenzenes	1
Mono- and dichloro-alkanes/ alkenes	Monochloroalkanes	4
	Monochloroalkenes	1
	Dichloroalkanes	8
	Dichloroalkenes	3
	Monochloroepoxyalkane	1
	Monochlorooxyalkene	1
Tri-, tetra- and penta-chloro-alkanes/ alkenes	Trichloroalkanes	5
	Trichloroalkenes	1
	Tetrachloroalkanes	6
	Tetrachloroalkenes	1
	Pentachloroalkanes	1
Bromo- and bromochloro-alkanes/ alkenes	Monobromoalkanes	4
	Dibromoalkanes	7
	Tribromoalkanes	1
	Monobromoalkenes	2
	Monobromomono-chloroalkanes	3
	Monobromodichloro-alkanes	1
	Monobromotrichloro-alkanes	1
	Dibromomonochloro-alkanes	1
Unknown	Cyclic ethers	3
	Acyclic hydrocarbons	13
	Cyclic hydrocarbons	3
	Unsaturated hydro-carbons	3
	Aldehydes	3
	Ketones	3
	Alcohols	2
	Acids	1

sities were ternary encoded to introduce some fuzziness into the rules and to reduce the use of low intensity masses in the resulting rules. The names of the specific training compounds are given elsewhere [4] and further details concerning the classifier have been published [2].

OPERATION OF THE SYSTEM

Communications between the user and the system occur via screen messages and the keyboard. Questions are asked of the user about certain mass peak intensities and the values of MAXMASS and HIMAX1. A typical session for caffeine (1,3,7-trimethyl-2,6-dioxopurine), which has a molecular weight of 194, is shown below. The error listed is a probable error determined with a robust statistic from previous evaluation tests [5]. The average of (MAXMASS and HIMAX1) less 5 daltons was used as the lower limit. This entire session, including looking for peak intensities and manual input of responses, took less than one minute. The first five responses are necessary to classify the spectrum and the last two are needed to determine the molecular weight and its lower limit.

Query	*Response*
What is the intensity of mass peak 42? (Enter 0, 0.5 or 1.)	0.5
What is the intensity of mass peak 63?	0
What is the intensity of mass peak 122?	0
What is the intensity of mass peak 49?	0
What is the intensity of mass peak 93?	0
What is the value of MAXMASS?	195
What is the value of HIMAX1?	195

EXPERT SYSTEM MESSAGE

THE CLASS OF THIS COMPOUND IS UNKNOWN, BUT ITS ESTIMATED MOLECULAR WEIGHT IS 194.5 ± 5.0. A LOWER LIMIT TO ITS MOLECULAR WEIGHT IS 190.

RESULTS AND DISCUSSION

Rule-based expert systems, e.g. the molecular weight estimator, are normally valid only within a specific domain which is defined by the training set used to derive the rules. In the present case the original system should perform well within the five main classes and to a lessor extent within the very large unknown class. Expert systems are

hardly ever evaluated outside of their training domain. However, previous tests [2–5] with a variety of reference and field GC–MS spectra have shown that the system yields very useful results, not only for the volatile training set, but also for a wide variety of volatile and other compounds.

In the present study the figures of merit used for the various tests are the median absolute deviation and the average absolute deviation of predicted values from the true values. Absolute deviations are used since a predicted value is incorrect whether it is positive or negative. One reason for using these particular figures of merit, rather than the standard deviation from the mean, is to allow comparison with the previously reported evaluation data, where they were used. However, the major rationale for the use of these measures is the fact that the distributions of deviations are not normally distributed and that a few very large deviations occur, due to systematic errors. What is required is a robust measure of central tendancy. The median absolute deviation is empolyed to minimize the undue influence of the large deviations. The average absolute deviation, which is influenced by the larger deviations, is also reported for those more familiar with that measure. The median absolute deviation also can be used through the Shapiro-Wilks relationship to provide robust estimates of probable errors which have been used in the messages from the expert system as shown above.

The latest results [5] for the 106 training spectra, which establish an optimum figure of merit for the system, were only 0.0 daltons (median absolute deviation from true values) and 0.6 daltons (average absolute deviation). The system also was tested with a variety of other spectra of compounds none of which had been used to derive the rules for molecular weight prediction. These included a set of 32 spectra of potential air pollutants and other compounds [4]. The median and average absolute deviations for this set were 0.5 and 6.3 daltons. In an extreme test of robustness, 99 NIST reference spectra [4] of compounds with molecular weights less than 350 were randomly selected and used to evaluate the system. The types of compounds included were various hydrocarbons, oxygenated hydrocarbons, nitrogen and sulfur containing compounds, chloro-, bromo- and other halogen substituted hydrocarbons, pyridines and pyrazines, and various substituted benzenes. For this set the median and average absolute deviations were 1.5 and 8.3 daltons. For 39 GC–MS spectra from field ambient air samples the median and average absolute deviations were 0.5 and 3.9 daltons. The set of randomly selected spectra probably establishes the base line for worst performance of the system, which is still very useful.

TABLE 3

Results of molecular weight predictions with pharmaceutical spectra of molecular weight 58–578

Apparent class [a]	Number	Absolute deviation	
		Median	Average
All classes	400	1.5	13
Nonhalobenzenes	65	1.0	8.5
Unknown	283	1.5	11
Chlorobenzenes	14	3.0	20
Mono- and dichloro-alkanes/alkenes	16	4.0	22
Bromo- and bromo-chloro alkanes/alkenes	22	5.0	32

[a] From classifier module.

Evaluation with pharmaceutical spectra

The results of the evaluations given above indicate median absolute deviations of 1.5 daltons can be attained with the system, even outside of the original domain. Further tests are warranted to firmly establish the boundaries of the domain of validity of the system. As part of a method comparison, 400 mass spectra of primarily pharmaceutical interest were used to evaluate the present system [8]. The organic compounds were comprised only of carbon, hydrogen, nitrogen and oxygen and their molecular weights were from 58 to 578. The average molecular weight of these compounds was 207 (median 188). A very wide variety of structures of volatile and nonvolatile compounds were included in this set. The number of carbon atoms in these compounds ranged from 3 to 36 and the formulas from $C_3H_4O_2$ for acrylic acid to $C_{32}H_{38}N_2O_8$ for 11-demethoxyre-

serpine. The general types of chemical composition and empirical formulas are summarized in Table 1.

Forty percent of these spectra were incomplete at masses below 55. Since the classifier module requires information in the mass range below 55 to determine the specific class route for the spectrum, the classifier will not work properly with them. Usually the classifier incorrectly designated these incomplete spectra as due to chloro or bromo compounds. These spectra were run as if they were members of the unknown class. The results of the evaluation of the entire set and of the apparent classes given by the classifier are listed in Table 3. Only one major class, nonhalobenzenes, was actually present in the spectral set. The overall median and average absolute deviations of the predicted molecular weights from the true values were 1.5 and 13 daltons. These results are close to the previous ones for 99 random NIST spectra mentioned above. Even with the misclassification problems the overall results were very good.

As judged by the median deviations, the best results by apparent class were obtained for the nonhalobenzenes (1.0 dalton) and unknown (1.5 daltons) classes. The nonhalobenzenes represent a class of compounds that were actually found in 79 of the 400 spectra and the results reflect the accuracy of the rules for this class. The halogen containing classes were the worst with median deviations of 3 to 5 daltons. Since none of the 400 compounds contained any halogens, the deviations for these 52 compounds were obviously caused by misclassification and subsequent application of incorrect rules. Some of the corrections imbedded in the rules for the bromo- and chloroalkanes/alkenes are very large and their incorrect application causes very large errors. One way to reduce this problem is to run the apparent halo compounds as members of the unknown class. This was done and greatly reduced the deviations from the true molecular weights. For example, the set of 22 apparent bromo compounds had an median absolute deviation of 5 daltons (average 32); but when this set was run as members of the unknown class, the median absolute deviation was reduced to 0.5 daltons (average 5.5).

There were eleven compounds which had ab-

TABLE 4

Molecular weight predictions with all NIST spectra [a]

Number of spectra	MW range	Molecular ion	Classified	Absolute deviation	
				Median	Average
All spectra					
24 464	30–500	Yes	From spectra	1.5	7.7
6914	30–500	No	From spectra	34	50
31 378	30–500	Both	From spectra	2.0	17
24 464	30–500	Yes	As unknown	0.5	1.4
6914	30–500	No	As unknown	31	42
31 378	30–500	Both	As unknown	1.5	10
No Cl or Br spectra					
27 033	30–500	Both	From spectra	1.8	16
Only Cl or Br spectra					
4345	30–500	Both	From spectra	3.5	22
Volatile compound spectra					
23 989	30–300	Both	From spectra	1.8	13
23 989	30–300	Both	As unknown	0.5	8.0

[a] All spectra have quality indicies of 0.6 or greater.

solute deviations greater than 100 daltons. Four of these were due to misclassification problems mentioned above. When run as unknowns, all four deviations decreased to 0.5 daltons except one, α-(1-hydroxycyclopentyl)-benzene acetic acid, 2-(dimethylamino)ethyl ester, which was reduced by 0.5 to 85 daltons. In one case, Darvon metabolite 1, the spectrum was obviously contaminated by high mass ions at the 1% intensity level at a mass which was 104 daltons above the mass of the molecular ion. The other six compounds were bis-(2-dimethylaminoethyl) ether, 2-methylbenzylhydrogenphthalate, 2-nitro-2-nitroxymethyl-1,3-dipropanediol dinitrate, dioctyl phthalate, dioctyl adipate, and narcotine. These latter compounds include ethers, nitro compounds, phthalates and long alkyl groups which heavily fragment and do not leave ions near the molecular ion mass. The rules in the present system handle these latter cases poorly. Despite these problems with the system, these evaluation results show that the system can produce very useful molecular weight estimates with pharmaceutical related spectra.

TABLE 5

Results of molecular weight predictions of all NIST spectra by pattern recognition class [a]

Apparent class	Number	Absolute deviation	
		Median	Average
Nonhalobenzenes	5626	1.0	11
Training set	15	0.0	0.0
Chlorobenzenes	5323	3.0	19
Training set	8	0.0	0.0
Bromo- and bromo-chloroalkanes/alkenes	4095	2.1	22
Training set	20	0.0	0.0
Mono- and dichloro-alkanes/alkenes	1822	4.0	21
Training set	18	0.0	0.2
Tri-, tetra- and pentachloro-alkanes/alkenes	1880	32	33
Training set	14	0.0	0.1
Unknown	12632	1.5	14
Training set	31	0.5	1.7

[a] All NIST spectra have quality indicies of 0.6 or greater.

Evaluation with NIST database spectra

In connection with the translation of the expert system from the shell prototype into a stand-alone version in C, routines were written to access the personal computer version of the NIST mass spectral database (version 3) and run the spectra through the algorithms for the expert system. In order to minimize problems with low quality spectra, only those spectra with quality indices [9,10] of 0.6 or greater were used in these evaluations. The quality index is a general measure of the quality of the spectrum and has a maximum of 1.0. The main set of these spectra consisted of 31378 spectra of compounds with molecular weights of 30 to 500 daltons and an average of 229. This set obviously contained a wide variety of compounds of every structural type in the database including volatile and non-volatile organic and organometallic compounds. An indication of the composition of this set can be obtained from data published on version 1 of the NIST data base [11] where combinations of the four elements (carbon, hydrogen, oxygen and nitrogen) accounted for only 64% of the spectra. A "volatile" subset of these spectra, constrained to compounds of molecular weights of 30–300 daltons (average 191), consisted of 23989 spectra and also was evaluated. Various other subsets of the spectra were used to determine the main sources of errors in the molecular weight procedures. The results are given in Tables 4 and 5 and in Fig. 2.

The distribution of signed deviations from true molecular weights for the entire set of all spectra is shown in Fig. 2. A logarithmic scale was used for N, the number of occurrences, which over emphasizes the relatively small number of large deviations but allows details to be seen. The signed deviations for this set ranged from −75 to 245 daltons with the mode and median for the distribution slightly on the positive side of zero, i.e. under estimation. The average was 12 daltons. Most of the errors were due to under estimating the molecular weights, but the negative deviations show some over estimations, probably due to misclassification problems. The data in Table 4

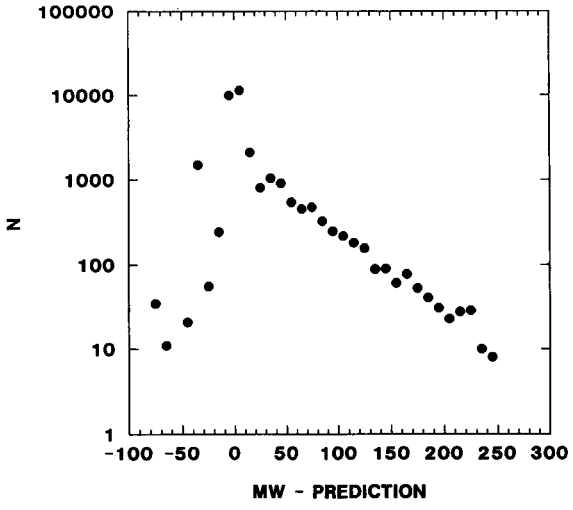

Fig. 2. Distribution of errors in predicted molecular weights for 31378 high quality NIST reference spectra with range of molecular weights 30–500 daltons.

provide more details of the evaluation of the entire data set. The overall median and average absolute deviations were 2.0 and 17 daltons, respectively. These performance data are similar to those for the set of pharmaceutical spectra, but the average absolute deviation is larger.

If the 31378 spectra were divided into two sets, one with the molecular ion present at the 1% intensity level and one without; quite striking results were obtained. When the molecular ion was present, as it was in 78% of these spectra; the median absolute deviation was only 1.5 daltons with a average absolute deviation of 7.7 daltons. However, for the 22% of the spectra where the molecular ion was not present; the median absolute deviation was 34 daltons with an average absolute deviation of 50 daltons. The present procedure works very well when the molecular ion is present and not very well when it is not. Since most spectra in this set had the molecular ion present, the overall performance was still very good.

To determine if the higher molecular weight compounds were distorting the test results, the "volatile" subset of 23989 spectra of compounds with molecular weights of 30–300 daltons was tested. The resulting median absolute deviation of 1.8 vs. 2.0 daltons (average 13 vs. 17) for the entire set showed a small reduction in accuracy of the system due to the higher molecular weight compounds. Since the rules in the system were obtained from spectra of compounds with molecular weights of about 300 or less, this is not unexpected. To see if the 4345 chloro and bromo compounds included in the 31378 spectra were causing problems, the set of 27033 spectra without these compounds was tested. As the results in Table 4 show, there was no appreciable difference of these test results, which produced median and average absolute deviations of 1.8 and 16 daltons, from the results with the entire set of spectra. The 4345 spectra of chloro and bromo compounds was analyzed separately and gave a higher median and average absolute deviation of 3.5 and 22 daltons, indicating some problems with these particular spectra.

In a surprising result, it was found that running all spectra, or the two molecular ion subsets, as members of the unknown class gave better performance than runs using the classifier. For example, the overall median and average absolute deviations for the unknown runs were 1.5 and 10 vs. 2.0 and 17 daltons for the classifier runs. The median absolute deviation for the subset with molecular ion present was a very low 0.5 vs. 1.5 daltons for the classifier runs. For the volatile set the overall median absolute deviation for runs with all spectra as unknowns was 0.5 vs. 1.8 daltons with the classifier. The distribution curve of the signed deviations with all compounds set as unknown was essentially the same shape as illustrated in Fig. 2, but with lower numbers of occurrences at each deviation, except at the mode near zero. These evaluation results show that, for this very large set of compounds which are essentially all of unknown class, it is better to initially designate them as unknowns than to chance misclassification and the application of wrong rules.

The results for the entire set of spectra also were analyzed by apparent class to determine the origin of the misclassification problems. The data for the six classes and for the training set of 106 spectra, which represent the optimum performance for the system, are listed in Table 5. The median absolute deviations for all training classes were 0–0.5 (average 0–1.7) daltons. For the large

test set the best results occurred with the non-halobenzene and unknown classes giving median absolute deviations of 1.0 and 1.5 (average 11 and 14) daltons, respectively. These median results are the same as those for the pharmaceutical spectra, but the average deviations are about 3 daltons higher. The chloro and bromo classes generally gave median absolute deviations of 2 to 4 (averages 19–22) daltons which are very close to the same measures for the pharmaceutical spectra.

However, the results for the 1880 spectra classified as tri-, tetra- and pentachloro-alkane/alkene, which never occurred in the pharmaceutical set, were much worse with median and average absolute deviations of 32 and 33 daltons. The median signed deviation for this apparent class was ca. −30 daltons. This signed deviation was the largest over estimation of all classes run. The over estimation problem is due to the application of large corrections in the rules for this particular class to spectra which should receive much smaller unknown class corrections. Since there were only 732 compounds of all structural types in the database containing three, four or five chloro groups, this set of 1880 spectra obviously has a large number of misclassified spectra.

These latter results, as well as those mentioned above, indicate that most of the problems come from misclassification of spectra as apparent chloro and bromo classes. The classifier was originally developed with a small training set to classify volatile toxic and related compounds and works very well for that purpose [2]. It was never intended to handle such a great variety of structures as are found in the entire database. Since misclassification occurs mainly with apparent halogen classes, the user can check the spectrum for appropriate isotopic clusters to see if it really is a bromo or chloro compound. If it is not, then the molecular weight should be estimated using the unknown class. A message is included in the present expert system for each halogen class to warn the user of this potential problem.

The overall results of the evaluation of the system with all of the previous and present test sets and using the classifier are presented in Fig. 3. The median and average absolute deviations

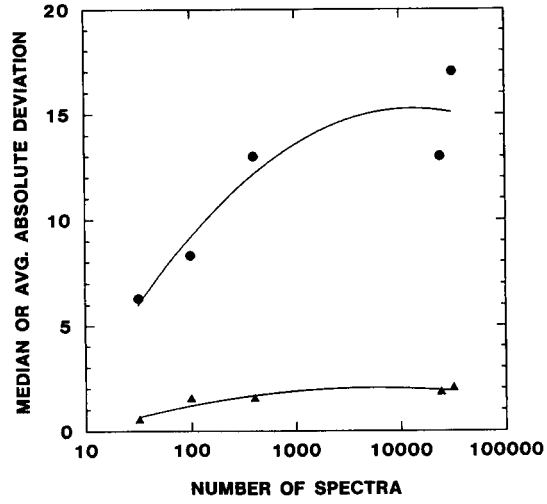

Fig. 3. The median (lower curve) and average (upper curve) absolute deviation of results as a function of the number of spectra in the evaluation set. Results were obtained by using the classifier. Fitted curves are distance weighted least squares.

are plotted as a function of the number of test spectra in the respective set. The sets were 32 spectra of volatile compounds; 99 spectra of randomly selected NIST spectra; the 400 pharmaceutical spectra; the 23 989 NIST spectra of volatile compounds; and the 31 378 NIST spectra. The fitted curves are distance weighted least squares determined. The results with the median deviation (lower curve) show that even a set of 100 randomly selected NIST spectra gives a good estimate of the extrapolated median of about 2 daltons. The curve for the average shows that this performance measure, which is not as robust as the median, is much more sensitive to the number of spectra in the test set. It appears that at least 400 spectra are necessary to get an estimate of the extrapolated average of about 15 daltons.

Conclusions

The empirical pattern recognition/expert system approach for estimating molecular weights based on the two experimental spectral features, MAXMASS and HIMAX1, has been subjected to very extensive and severe testing with spectra from a wide variety of chemical structures. This rule-based system was developed from a set of 106 training spectra originally selected to repre-

sent volatile air pollutants. Previous tests with randomly selected NIST reference spectra showed that the rules were valid beyond the original domain of the training set despite misclassification problems. Results from the present evaluation with two different sources of reference spectra have verified the general validity and accuracy of this approach.

The results of the evaluation with 400 pharmaceutical spectra of both volatile and semi-volatile compounds, some of which are structurally similar to the nonhalobenzene training compounds, showed that the rules were valid for this set. The overall median and average absolute deviations from the true molecular weights were 1.5 and 13 daltons. 13% of the spectra which were misclassified as apparent bromo or chloro compounds produced the worst errors with median absolute deviations of 3–5 daltons (average 20–32).

More extensive tests with 31 378 high quality NIST spectra of compounds with molecular weights of 30–500 and with various subsets have shown the validity of these molecular weight estimation rules. The overall median and average absolute deviations for the total set of spectra were 2.0 and 17 daltons. Generally the true molecular weights were under estimated. For spectra of a volatile subset of compounds of molecular weight 30–300, which is the range of the training compounds used to derive the rules, these same performance measures were 1.8 and 13 daltons. Even better results were obtained by running all spectra as unknown rather than through the classifier. As unknowns the median and average absolute deviations for the total set were 1.5 and 10 daltons and for the volatile set, 0.5 and 8.0 daltons. These latter results reflect the influence of misclassification and subsequent application of the wrong rules. Other evaluation tests showed that the main misclassification problems result in apparent bromo and chloro compounds, particularly with the tri-, tetra- or pentachloroalkane/alkene class. These misclassification problems are due to the limited validity of the pattern recognition classifier which was never intended to cover such a wide range of chemical structures.

It was also found that results obtained with sets of spectra where the molecular ion was present were more accurate than those from sets where the molecular ion was absent. Median absolute deviations for sets where the molecular ion was absent were approximately twenty times those for sets where the molecular ion was present. There are three general types of mass spectra to consider for molecular weight estimation: (a) those where MAXMASS, with corrections, provides very good estimates; (b) those where HIMAX1, with corrections, provides better estimates; and (c) those where neither provides very good estimates. The first group includes the original training set and similar compounds in all classes except the unknown class. The second group includes a wide variety of compounds in the unknown class, as shown in this and previous studies. The last group includes those compounds that fragment and leave essentially no detectable masses near the original molecular ion mass. Some of these latter compounds are included in the target set and are actually correctable. Other examples are some phthalates, nitro compounds and alkanes, which were included in the pharmaceutical spectra. These compounds will cause problems with this technique and probably with other types of molecular weight estimation. It is probably impossible to derive a set of very accurate rules for all compounds.

Despite these problems, the present system can be a very useful method of providing partial identification information for unknown spectra or as a constraint for more rapid and accurate library searches. If the user knows, or suspects, that the spectra are similar to those in the training set, then the classifier should be used. If not, then the spectra should be run as unknowns by inputing zero's in response to each classifier query. A logical strategy for reducing the misclassification problems is to check the spectra denoted by the classifier as apparent chloro or bromo compounds for relevant isotopic clusters. If these are not detected, then the spectrum should be run as a member of the unknown class. Another strategy is to run all suspect cases both through the classifier and as unknowns.

This method also will give a molecular weight estimate for mixtures since the values of MAX-

MASS and HIMAX1 are the only data required when a spectrum is run as a unknown class member. The estimate for mixtures will be that for the component with the highest HIMAX1 value, which is usually the component with the highest molecular weight. An example of the performance with a mixture is given in Ref. 2 where an unknown class spectrum from field GC–MS data is predicted to have a molecular weight of 223. SIMCA pattern recognition classified this as a hydrocarbon. Manual inspection of this spectrum indicates that it is a mixture of a hydrocarbon and the internal standard, 1-fluoro-4-iodobenzene, which has a molecular weight of 222. If the mixtures consist of very high molecular weight contaminants added to the main component, then the molecular weight estimate will not be useful.

The information in this document has been funded in part by the United States Environmental Protection Agency under Interagency Agreement DW 13934923 to the National Institute of Standards and Technology. It has been subjected to Agency review. The mention of trade names or commercial products does not constitute endorsement or recommendation for use.

A copy of the molecular weight estimator employing manual data input can be obtained from the senior author (D.R.S.) by sending a 5.25 or 3.5 inch floppy disk to the address given.

REFERENCES

1 D.R. Scott, Anal. Chim. Acta, 223 (1989) 105.
2 D.R. Scott, Anal. Chim. Acta, 265 (1992) 43.
3 D.R. Scott, Anal. Chim. Acta, 246 (1991) 391.
4 D.R. Scott, Chemom. Intell. Lab. Syst., 12 (1991) 189.
5 D.R. Scott, Chemom. Intell. Lab. Syst., 16 (1992) 193.
6 D.R. Scott, Anal. Chem., 58 (1986) 881.
7 D.R. Scott, Anal. Chim. Acta, 211 (1988) 11.
8 S. Heuerding and J.T. Clerc, Chemom. Intell. Lab. Syst., (1992) submitted for publication.
9 G.W.A. Milne, W.L. Budde, S.R. Heller, D.P. Martinsen, and R.G. Oldham, Org. Mass Spectrom, 17 (1982) 547.
10 D.T. Terwilliger A.L. Behbehani, J.C. Ireland, and W.L. Budde, Biomed. Environ. Mass Spectrom., 14 (1987) 263.
11 D.R. Scott, Anal. Chim. Acta, 228 (1990) 177.

Analytica Chimica Acta, 278 (1993) 149–158
Elsevier Science Publishers B.V., Amsterdam

Cross-peak classification in two-dimensional nuclear magnetic resonance spectra using a two-layer neural network

Simon A. Corne, Julie Fisher, A. Peter Johnson and William R. Newell

School of Chemistry, University of Leeds, Leeds LS2 9JT (UK)

(Received 3rd September 1992; revised manuscript received 21st December 1992)

Abstract

A two-layer simulated neural network has been trained to classify cross-peaks in two-dimensional nuclear magnetic resonance spectra. Examples of peaks for both network training and testing were selected by an experienced spectroscopist. The trained network has been used to classify previously unseen data. Spectral artefacts and authentic cross-peaks are distinguished. Peaks whose shapes have been modified, for example by overlap, are classified correctly. A spectrum for phoratoxin B, a protein of 46 amino acid residues, is used to illustrate the training and performance of the network.

Keywords: Nuclear magnetic resonance spectrometry; Crosspeak classification; Neural networks; Two-layer neural network

Chemists have made increasing use of artificial neural networks in recent years [1]. Applications cover such diverse areas as fault prediction in chemical processes [2] and the prediction of protein secondary structure [e.g., 3]. In spectroscopy, uses of neural networks include peak verification and recognition in infrared spectra [4], quantitative x-ray fluorescence [5], recognition of the proton nuclear magnetic resonance (NMR) spectra of saccharides [6], identification of cross-peaks in NMR spectra from two-dimensional (2D) correlated spectroscopy (COSY) experiments [7] and 2D nuclear Overhauser effect spectroscopy (NOESY) experiments [8]. Three-layer feedforward networks, employing the backpropagation training algorithm [9], have been used in each of these cases. The only significant differences between the application of these networks are in the scaling and transformation of spectral data for input and the presentation of output. In this paper we report the classification of cross-peaks in 2D NOESY spectra using a two-layer artificial neural network.

Analysis of biomolecular NMR spectra is hindered by the large amount of data. Overlap of peaks and artefacts, such as t_1 noise, may alter the shape of peaks in such spectra. Multidimensional experiments can alleviate some of the problems of overlap. Artefacts not only introduce spurious data having intensities comparable to real peaks, but also may be responsible for the corruption of genuine data (for example, "bleaching" due to presaturation of water). In the early stages of analysing a multidimensional spectrum, the NMR spectroscopist makes use of heuristics to recognise artefacts: e.g., (i) genuine cross-peaks have roughly elliptical section, (ii) noise peaks usually have low intensity, (iii) solvent presatura-

Correspondence to: S.A. Corne, School of Chemistry, University of Leeds, Leeds LS2 9JT (UK).

tion artefacts appear in bands parallel to the ω_2 axis, (iv) t_1 noise appears in bands which are not symmetrical about the spectrum's diagonal. There have been several attempts to encode some of these rules of thumb in computer programs. For example, early computer programs for peak-picking used an intensity threshold to distinguish peaks from noise [10]. More sophisticated computer software for data abstraction, increasingly a requirement for the biomolecular spectroscopist, can now distinguish and eliminate high-intensity artefacts as well as lower intensity noise with some success [11,12].

We have identified and characterised some cross-peaks from spectra using STELLA, a component of the NMR processing software, TRITON [12]. STELLA locates local maxima in spectra and classifies them as GENUINE or SPURIOUS by comparing them to preselected examples of each type. These exemplars are selected by the spectroscopist, using the module LEARN2. Here, we report the training of a neural network using these examples and compare the network's ability to classify peaks with that of a three-layer back-propagation network [8].

The aim of this work is to train the network on a variety of peaks observed in different NMR spectra and to use this "knowledge" in order to classify peaks in a variety of spectra from the same types of experiment. Here, we present the results of applying the method to 2D NOESY spectra.

THEORY

The network implemented in this work has a two-layer (input-layer and output-layer) feedforward architecture [13]. Each node in the input layer has a weighted connection to each node in the output layer. Considering a single output node, the output value (y) is calculated by applying a thresholding function to the sum of the products of input node values (x_i) and connection weights (w_i):

$$y = \mathrm{f_h}\left[\sum_{i=0}^{n} w_i x_i\right]$$

where the so-called Heaviside function, f_h, is given by:

$$\mathrm{f_h}(x) = 1,\ x > 0$$

$$\mathrm{f_h}(x) = 0,\ x \leq 0$$

Node 0, the bias, always takes the input value of +1 [14]. The connection weight between this node and the output node is equivalent to the threshold of the output node, $-\theta$.

During supervised training, patterns are presented to the network with the desired output (the target) and weights are adjusted until there are no differences between desired and actual outputs. For this type of network, a suitable method for the modification of weights is the α-LMS algorithm, also known as the Widrow-Hoff delta rule [15]. The equation describing the modification of weights during training is:

$$w_{i,k+1} = w_{i,k} + \eta\left[\epsilon_{i,k} x_{i,k} / |\mathbf{x}|^2\right]$$

where k is a time or training cycle index, $w_{i,k+1}$ is the next value of weight i, $w_{i,k}$ is the present weight, $\mathbf{x}_k$ is the present input pattern vector and ϵ_k is the linear error given by the difference between actual and target outputs. The choice of η controls stability and the rate of convergence [15]; a practical range is 0.1 to 1.0 [16]. Networks of this type are called ADAptive Linear NEurons or ADALINEs. Networks with more than one such ADALINE, i.e., with more than one output node, are called many-ADALINEs or MADALINEs.

PROGRAM DEVELOPMENT

The configuration, the number of processing nodes in each of the layers, is variable to allow experimentation and application to a variety of problems. Several parameters and features of the network are under the control of the user: (i) the number of nodes in the input and output layers; (ii) the training parameters η and w_m; (iii) random noise may be added to the input patterns; (iv) a program mode permits the variation of a training or configuration parameter to evaluate efficiency; (v) training exercises may be repeated,

in which case the weights written to file represent the arithmetic means over the number of exercises.

The input layer for the network which classifies cross-peaks has been set to 121 nodes, corresponding to the maximum number of points in a peak located by LEARN2. The number of nodes in the output layer (n_0) has been fixed at two. The network is thus a MADALINE comprising two ADALINEs. The first ADALINE corresponds to the SPURIOUS class, the second to the GENUINE class. The network output is expected to be (1 0) for a SPURIOUS cross-peak or (0 1) for a GENUINE cross-peak. A bias node has been added to the input layer [14].

The TRITON module LEARN2 creates a peak definition computer file containing records for each selected peak. A peak record comprises the dimensions of the peak, its class, and a matrix of intensities scaled into the range $[-1;+1]$, with the local maximum at the centre of the matrix. To form input vectors for the MADALINE, these data are processed further: each intensity matrix is enlarged, if necessary, to the maximum dimension expected by STELLA (11×11) by centring the matrices on the local maximum element and padding the matrix with elements of zero intensity; the matrix is then decomposed into a vector of 121 elements. The peak class is written as a vector, to form the target output for the network.

For a complete spectrum whose peaks have not yet been classified, the STELLA module SMART2 is used to extract the local maxima constrained only by a set of thresholds. A version of LEARN2, modified to process peaks read from a file, is then used to convert the resultant peak file into one containing descriptions of all local maxima including the peak intensity matrices. The peak matrix file is then processed further as described above, except that the peak class vector is not written.

The MADALINE simulator and peak preprocessor have been written in standard C on a VAX 6310 running VMS 5.5; versions for the IBM PC, Sun and Silicon Graphics workstations require no modification to the source code. Pattern and weights files may be written and read in ASCII or binary formats. A typical spectrum file contains ca. 3×10^5 floating point numbers. The simulator and associated programs are still under development; further details are available upon request.

EXPERIMENTAL

Peak examples were taken from a 2D NOESY spectrum for phoratoxin B, a protein of 46 amino acids, supplied by Professor Kaptein (State University of Utrecht). The initial training set was created using LEARN2 with thirty-six examples of each of the two peak classes. Some of the peaks selected for the training set are shown in Fig. 1. A further set was created with twenty examples of each of the two classes to test the performance of the trained network.

Training

Connection weights were initialised to random values in the range $[-w_m; +w_m]$, where w_m (weight maximum) was set by the user. The training set was then read from a computer file. The order of the training set was randomised at the start of each training step (epoch) to minimise large changes in the individual weights and to reduce the risk of the network settling into a local minimum. A single stage in training consists of calculating the network outputs and modifying the connection weights [9]. Following the modification of weights, the next pattern in the randomised set is presented to the network. An epoch ends when all patterns have been presented. Training is an iterative procedure, ended when the number of output/target errors is reduced to zero or the user-specified maximum number of epochs is reached. The weights are written to a computer file following the completion of training.

Classification of patterns

In order to classify patterns corresponding to peaks observed in 2D NMR spectra, the network uses weights, written to file after a training session, to calculate the output vectors for the previously unseen input vectors. The output vectors give the classification of the input patterns. For

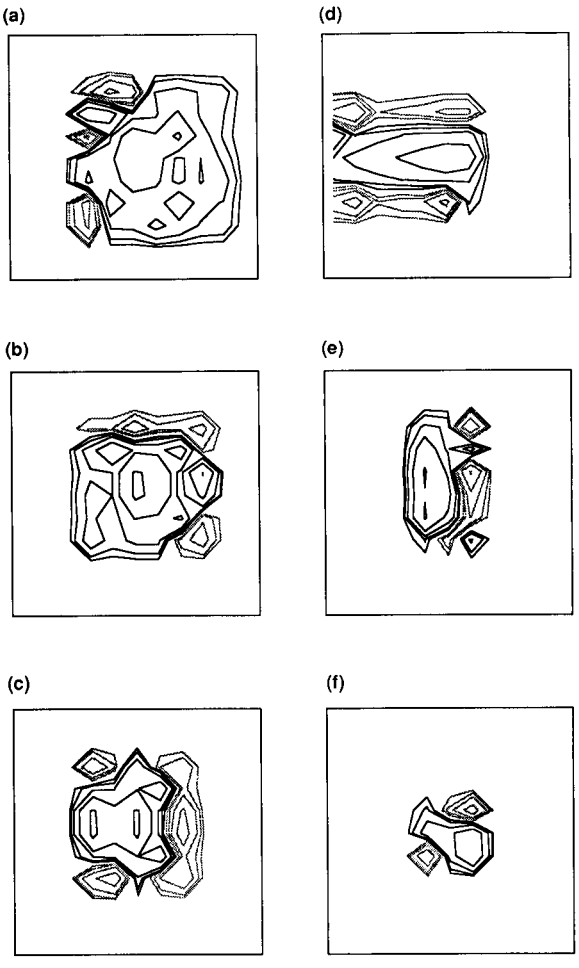

Fig. 1. Example cross-peaks used for training. The peaks were abstracted from the phoratoxin B NOESY spectrum, using the TRITON module LEARN2. Bold lines represent positive intensity, faint lines represent negative intensity. (a–c) GENUINE (peak c is one of an overlapping pair); (d) SPURIOUS, intense solvent presaturation artefact; (e) SPURIOUS, intense t_1 noise artefact; (f) SPURIOUS, low intensity noise.

the target vectors, the output vectors are expected to contain only one non-zero element, which has the value one. Inconclusive states may occur: all elements of the output vector are zero or more than one element has the value one. Patterns causing either of these states are called UNCLASSIFIED. The classifications of all the peaks were recorded in computer files. These are used to refer to the original spectrum, by indexing the peak file generated by the STELLA module SMART2. A separate peak file is created for each classification. The peak file index program has been implemented using standard C on a VAX 6310 running VMS 5.5. The peak files are then used with further TRITON modules for plotting and analysis.

The UNCLASSIFIED data provide valuable feedback for data abstraction. Such patterns are likely to fall into two categories: those with no close training patterns and those that a spectroscopist might find difficult to classify. Patterns in the first category could be added to the training set, with the appropriate classification supplied by the spectroscopist. The second case emphasises the importance of data abstraction incorporating context and rules.

RESULTS AND DISCUSSION

Optimisation of the rate of training

The training rate of networks is affected by the gain (η) and maximum initial weight (w_m) [17]. Values or ranges for gain are quoted in some texts [16,18] but may vary from problem to problem. The effect of varying these parameters on the processing time taken on a VAX 6310 to complete training is shown in Fig. 2.

Both parameters have an effect upon the accuracy of classification (see Tables 1 and 2) of SPURIOUS patterns; all twenty GENUINE peaks in the test set were classified correctly. Therefore, the values of weight maximum and gain used for subsequent work (0.75 and 0.82, respectively) represent the optima not for the rate of training, but for efficient training with optimum accuracy of classification.

Optimisation of accuracy

Repeated training, with the averaging of weights, was found to improve the accuracy of the SPURIOUS peak classification, as shown in Table 3; again, all twenty GENUINE peaks were classified correctly. This enhancement was evident with increasing repetition up to 16 exercises; thereafter, no improvement was observed for this particular classification set. The vectors for each ADALINE were reformatted as matrices corre-

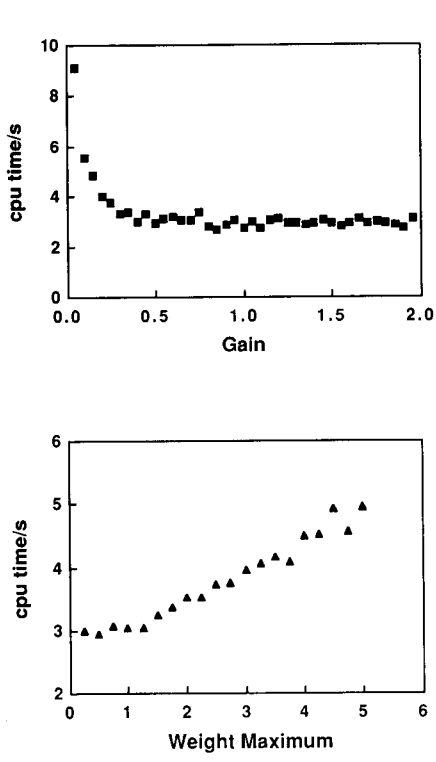

Fig. 2. Variation of CPU time used on a VAX 6310 to complete training. (a) Dependency upon gain; (b) Dependency upon the initial weight maximum, w_m.

TABLE 1

Effect of gain (η) on classification accuracy for the twenty SPURIOUS patterns in the classification set

η	Number of peaks classified		
	Correct	Incorrect	Inconclusive
0.10	18	1	1
0.20	18	1	1
0.30	17	2	1
0.40	17	2	1
0.50	18	1	1
0.60	18	2	0
0.70	18	0	2
0.80	18	0	2
0.82	19	0	1
0.84	18	0	2
0.86	18	0	2
0.88	18	1	1
0.90	18	0	2

TABLE 2

Effect of initial weight maximum (w_m) on classification accuracy for the twenty SPURIOUS patterns in the classification set

w_m	Number of peaks classified		
	Correct	Incorrect	Inconclusive
0.25	19	1	0
0.50	19	1	0
0.75	19	0	1
1.00	19	1	0
1.25	19	1	0
1.50	18	0	2
1.75	18	0	2
2.00	18	0	2
2.25	18	1	1
2.50	18	0	2
2.75	18	0	2
3.00	18	1	1
3.25	18	0	2
3.50	18	0	2
3.75	18	0	2

sponding to the size of the original peak matrices. When plotted, as in Figs. 3 and 4, the refinement of weights with increasing repetition of training is apparent. It is also interesting to note the complementary nature of the weight matrices for the GENUINE and SPURIOUS ADALINEs.

Classification of peaks in a complete spectrum

Local maxima for the phoratoxin NOESY spectrum were extracted using the TRITON module SMART2, constraining the abstraction using absolute and relative intensity thresholds. The peak list produced was processed into a classification set.

TABLE 3

Effect of averaging weights over training cycles on classification accuracy for the twenty SPURIOUS patterns in the classification set

Cycles	CPU time (s)	Number of peaks classified		
		Correct	Incorrect	Inconclusive
1	3.25	18	1	1
4	12.60	18	1	1
16	49.18	19	0	1
64	193.9	19	0	1
256	783.4	19	0	1
1024	3164	19	0	1

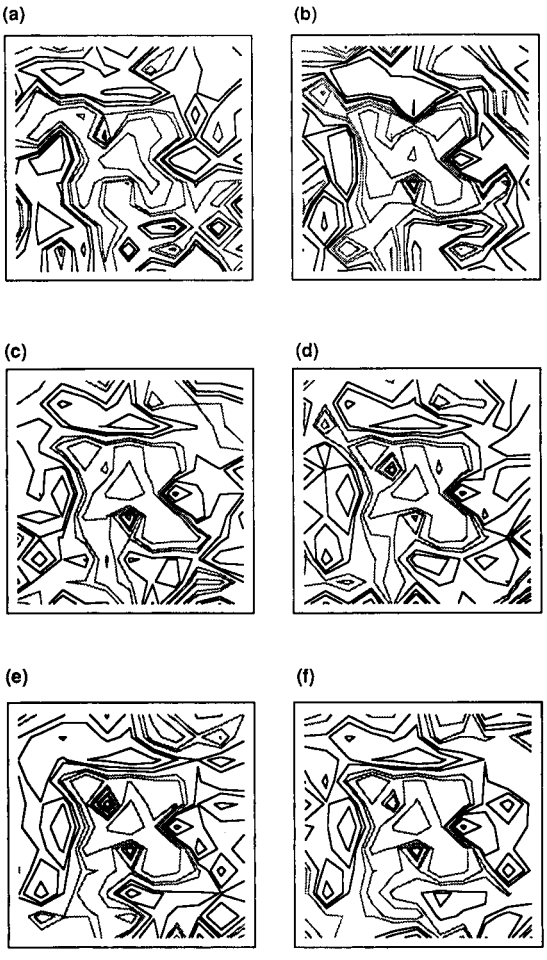

Fig. 3. Refinement of weights matrices for the SPURIOUS ADALINE with increasing number of training cycles. Bold lines represent positive intensity, faint lines represent negative intensity. (a) 1 cycle. (b) 4 cycles. (c) 16 cycles. (d) 64 cycles. (e) 256 cycles. (f) 1024 cycles.

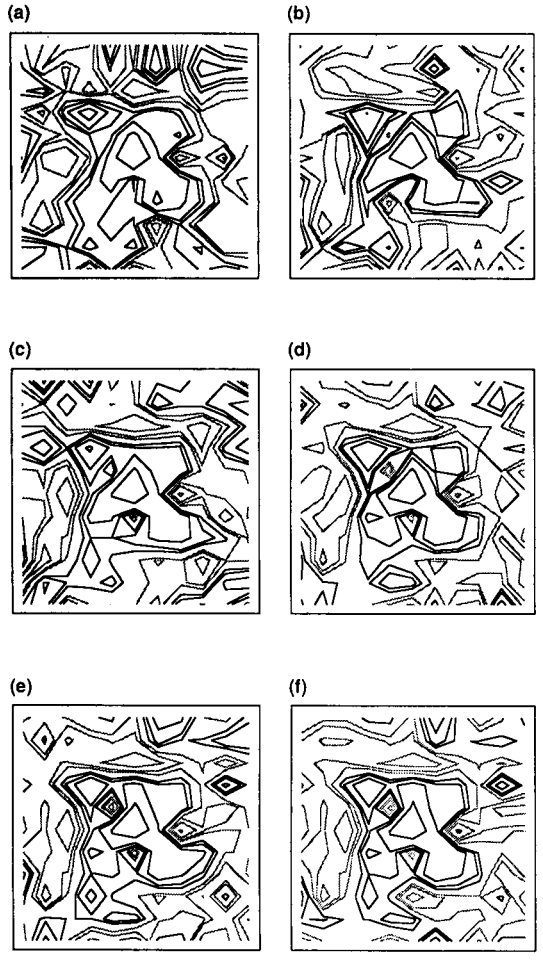

Fig. 4. Refinement of weights matrices for the GENUINE ADALINE with increasing number of training cycles. Bold lines represent positive intensity, faint lines represent negative intensity. (a) 1 cycle. (b) 4 cycles. (c) 16 cycles. (d) 64 cycles. (e) 256 cycles. (f) 1024 cycles.

The network was trained using the optimal values described above. The classification set comprised 2371 patterns. The results of classification are summarised in Table 4. The major differences between the MADALINE and the backpropagation network are the number of peaks identified as SPURIOUS and the number UNCLASSIFIED. False classification of a SPURIOUS peak as GENUINE causes errors throughout any subsequent analysis of a spectrum. Close examination of the spectrum identified 36 false GENUINE peaks for the MADALINE and 50

TABLE 4

Comparison of the MADALINE, backpropagation network and STELLA on peak classification in a NOESY spectrum

Classification	Number of peaks classified		
	STEL-LA	MADA-LINE	Backprop-agation
GENUINE	1484	1178	1183
SPURIOUS	488	1177	905
UNCLASSIFIED	399	16	283

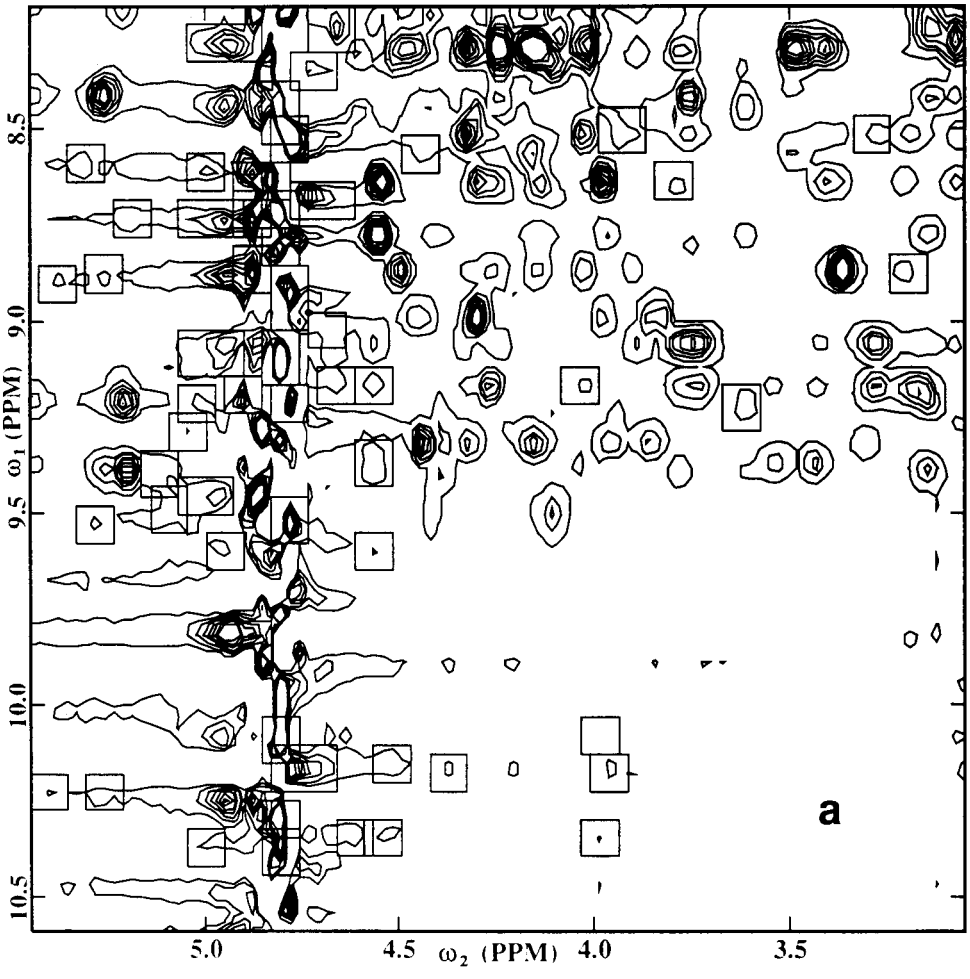

Fig. 5. Peaks classified by the network following data abstraction using SMART2. The figures, showing a small region of the NOESY spectrum for the protein phoratoxin B, were created using the TRITON module INSP. The boxes were added to the basic figure using the TRITON module PPMAN2. (a) Peaks classified as SPURIOUS; (b) peaks classified as GENUINE; (c) local maxima identified by SMART2 that produce inconclusive network outputs.

TABLE 5

CPU time used by the neural networks and associated programs in training (72 peaks) and classification (2371 peaks) on a VAX 6310

Process	MADALINE		Backpropagation network [a]	
	Overall	Mean per pattern	Overall	Mean per pattern
16 Training exercises	49.18	0.683	655.2	9.10
Mean training exercise	3.07 ± 0.7	0.043	41.0 ± 4	0.569
Preprocessing	271.5 ± 2	0.115	271.5 ± 2	0.115
Classification [b]	19.1 ± 0.3	0.008	38.9 ± 2	0.016
Filtering	32.3 ± 0.2	0.014	32.3 ± 0.2	0.014

[a] Configuration and training parameters as per reference [8]. [b] Data from ten separate exercises.

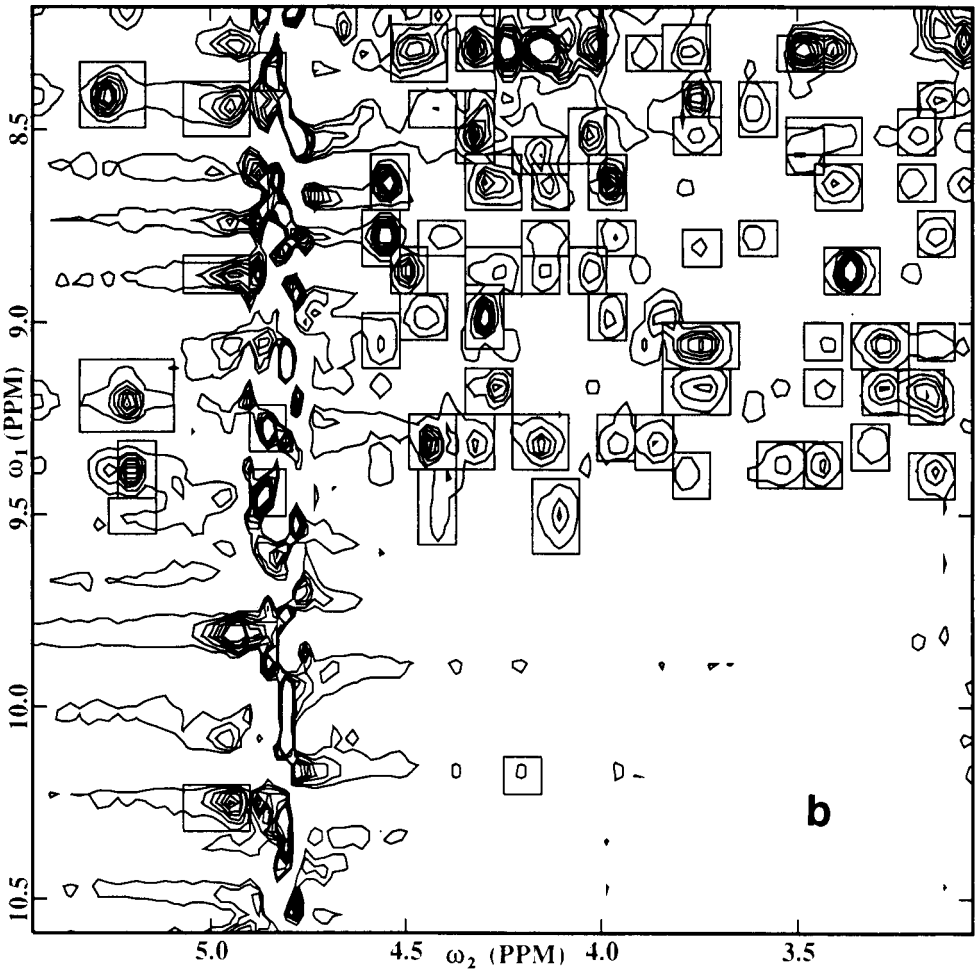

Fig. 5 (continued).

for the backpropagation network. Peaks classified by the MADALINE for a small region of the spectrum are shown in Fig. 5. Figure 5c illustrates a peak in the same region of the spectrum that gave inconclusive network outputs. The timings, given in Table 5, include the input and output of files as well as the time required for calculations (averaged over 16 exercises).

The ability of a two-layer feed-forward network with Widrow-Hoff supervised training to classify cross-peaks in 2D NOESY spectra has been demonstrated. The accuracy with which it performed the classification has been compared with a backpropagation network. The MADALINE achieves greater accuracy. The network can be used to classify peaks in new spectra, without further training. At present the network does not incorporate an explicit notion of context (for example, the presence or absence of a symmetry-related cross-peak, noise bands and solvent signals). A general data abstraction program based upon network classification and incorporating both rules and context is under development.

We thank the Maxwell Foundation for its financial support. We would like to thank David W. Corne of Edinburgh University for his help with neural network issues. We would also like to

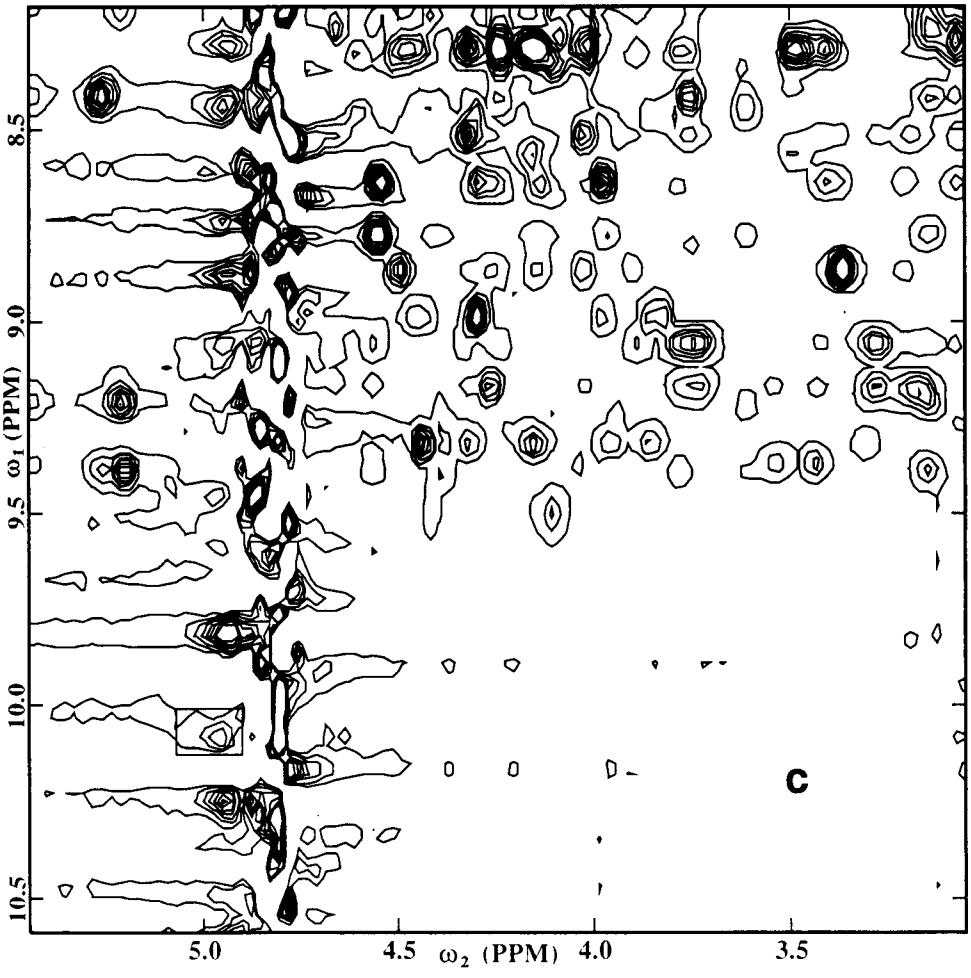

Fig. 5 (continued).

acknowledge Professor R. Kaptein, Dr. R. Boelens and Dr. G.J. Kleywegt for their assistance in the modification of parts of the TRITON software and for permission to use the phoratoxin spectrum.

REFERENCES

1 J. Zupan and J. Gasteiger, Anal. Chim. Acta, 248 (1991) 1.
2 V. Venkatasubramanian, R. Vaidyanathan and Y. Yamamoto, Comp. Chem. Eng., 14 (1990) 699.
3 N. Qian and T.J. Sejnowski, J. Mol. Biol., 202 (1988) 865.
4 B.J. Wythoff, S.P. Levine and S.A. Tomellini, Anal. Chem., 62 (1990) 2702.
5 M. Bos and H.T. Weber, Anal. Chim. Acta, 247 (1991) 97.
6 J.U. Thomsen and B. Meyer, J. Magn. Reson., 84 (1989) 212.
7 M. Kjaer and F.M. Poulsen, J. Magn. Reson., 94 (1991) 659.
8 S.A. Corne, A.P. Johnson and J. Fisher, J. Magn. Reson., 100 (1992) 256.
9 J.L. McClelland and D.E. Rumelhart, Parallel Distributed Processing, Vol. 1, MIT Bradford Press, Cambridge, 1986.
10 K.P. Neidig, H. Bodenmüller and H.R. Kalbitzer, Biochem. Biophys. Res. Commun., 125 (1984) 1143.
11 S. Glaser and H.R. Kalbitzer, J. Magn. Reson., 74 (1987) 450.
12 G.J. Kleywegt, R. Boelens and R. Kaptein, J. Magn. Reson., 88 (1990) 601.
13 R. Beale and T. Jackson, Neural Computing: An Introduction, Adam Hilger, Bristol, 1990.

14 P.D. Wasserman, Neural Computing: Theory and Practice, Van Nostrand Reinhold, New York, 1989.
15 B. Widrow and S.D. Stearns, Adaptive Signal Processing, Prentice Hall, Englewood Cliffs, NJ, 1985.
16 B. Widrow and M.A. Lehr, Proc. IEEE, 78 (1990) 1415.
17 S.-B. Cho and J.H. Kim, Pattern Recognition Lett., 13 (1992) 309.
18 J.E. Dayhoff, Neural Network Architectures, an Introduction, Van Nostrand Reinhold, New York, 1990.

Analytica Chimica Acta, 278 (1993) 159–176
Elsevier Science Publishers B.V., Amsterdam

Source input elucidation in aquatic systems by factor and principal component analysis of molecular marker data

Joan O. Grimalt and Joaquim Olivé

Department of Environmental Chemistry (CID–CSIC), Jordi Girona 18, 08034 Barcelona, Catalonia (Spain)

(Received 17th July 1992; revised manuscript received 4th January 1993)

Abstract

The usefulness of principal component analysis (PCA) and factor analysis (FA) for source input elucidation in environmental studies using molecular markers for sample description was evaluated. A case study involving the determination of aliphatic and chlorinated hydrocarbons, fatty acids, alcohols, chlorophylls and some detergent indicators in water particulates from a deltaic system was selected as a representative testing dataset. PCA afforded useful results to differentiate between major groups of samples but not between geochemical sources. In contrast, FA provided a direct correspondence between factor loadings and marker groups defining geochemically consistent organic matter contributions. For autochthonous compounds, FA has allowed an even more precise characterization of input sources than that obtained by the common "qualitative" molecular marker approach. These results were obtained despite the unsuitable dimensions of the dataset describing the system [102 compounds (variables) × 40 samples]. No improved results were obtained from the application of FA or PCA to subgroups of the data involving smaller number of compounds. This is consistent with the hypothesis that a limited number of sources is responsible for the occurrence of these lipid markers in the delta waters.

Keywords: Environmental analysis; Factor analysis; Molecular markers; Principal component analysis; Waters

A major recent advance in environmental sciences has been the use of molecular markers for the identification of organic inputs in aquatic systems. Molecular markers are in principle defined as compounds, usually lipid molecules, whose structure can be related to specific sources. This concept has proved to be very useful in petroleum exploration and palaeoenvironmental geochemistry [1] where organic molecules (biomarkers) are used as tracers of the originally sedimented biogenic materials. The application of this concept to recent depositional systems also involves the consideration of pollution sources. Thus, long-chain alkylbenzenes [2,3] or trialkylamines [4] can be related to contributions from anionic or cationic detergents respectively, in a similar way that 4α,23,24-trimethyl-5α(H)-cholest-22(E)-en-3β-ol is associated with dinoflagellate inputs [5].

However, few lipid molecules can be unambigously related to specific sources. The geochemical reassessment of several widely used markers (e.g., β-sitosterol [6] and coprostanol [7]) has shown that the correct interpretation of the information contained in the lipid signature cannot usually rely on single compounds, but requires the joint consideration of groups of molecules. On the other hand, very relevant information is contained in the distribution patterns of diverse linear lipid compounds (e.g., n-alkanes [8], n-alcohols [9], n-aldehydes [10]), although the occurrence of the individual homo-

Correspondence to: J.O. Grimalt, Department of Environmental Chemistry (CID–CSIC), Jordi Girona 18, 08034-Barcelona, Catalonia (Spain).

logues may have low or no environmental significance. All these aspects compel to the use of multivariate methods, namely principal component analysis (PCA) and factor analysis (FA), as a systematic way of handling, unravelling and understanding the lipid data generated in these environmental studies. Their application may allow the avoidance of biased interpretations and also provide additional information beyond that a priori expected from the background geochemical knowledge.

Unfortunately, the application of multivariate methods in environmental lipid studies is not straightforward. Database shape represents one major problem because the independent variables (determined compounds) may considerably outnumber the samples. The molecular analysis of the lipid fraction in waters or sediments is usually achieved by solvent extraction, column chromatographic fractionation and gas chromatography (GC). The overall analytical procedure is elaborate and time consuming, which restricts the number of samples that can be analysed. However, a wealth of information is obtained from each sample because the use of capillary GC columns and mass spectrometric detection (GC–MS) affords the identification and determination of large numbers of molecules. The determination of a smaller number of compounds in exchange of the analysis of a larger number of samples is not a realistic approach. Usually it does not avoid the complex analytical procedures, merely involving the generation of less information from approximately the same amount of work.

Previous applications of multivariate methods to organic geochemical studies [11–21] have involved databases with variable numbers ranging between 10 and 35, reaching up to 70 in some instances. However, modern analytical instrumentation combined with automated data acquisition systems affords the identification and determination of larger numbers of compounds, e.g., > 100, and this is a routine activity in many environmental organic geochemical studies. The extrapolation of these previous studies to datasets of such variable sizes is not straightforward. Hence, the first objective of this was concerned with the feasibility of PCA and FA for the characterization of organic input sources in environmental systems described with large numbers of compounds. The resulting PCs or Fs are evaluated in terms of their consistency with the background geochemical knowledge.

The application of multivariate methods to molecular marker studies has sometimes been addressed by preselection of the compounds to be included in the datasets using the already available geochemical information. Besides problems of bias and loss of information, this approach may easily result in multivariate analysis outputs merely reflecting the information purposely included in the database at the stage of compound choice. An alternative approach to this type of application is database splitting into compound subgroups and, subsequently, independent multivariate analysis. Bias is avoided by subgroup definition according to general criteria. The feasibility of this type of application to provide useful results in environmental studies con-

TABLE 1

List of samples of water particulate material collected in the Ebre Delta

Sampling site [a]	March 86	May 86	July 86	Sept. 86	Nov. 86	Jan. 87	March 87	May 87
F	F1	F2	F3	F4	F5	F6	F7	F8
F′	F′1	F′2	F′3	F′4	F′5	F′6	F′7	F′8
A		A2	A3	A4	A5	A6	A7	
A′		A′2	A′3	A′4	A′5	A′6	A′7	
R	R1	R2	R3	R4	R5	R6	R7	R8
I		I2	I3	I4	I5			I8
D		D2	D3	D4	D5			D8

[a] Sampling sites refer to Fig. 1.

cerns the second objective of this work. Thus, the total dataset was divided between biogenic and anthropogenic markers and each group was evaluated with PCA and FA. The results obtained with this alternative method were compared with those corresponding to the direct analysis of the whole dataset.

In a previous study [22], the first objective was addressed from the multivariate analysis of sedimentary hydrocarbons in a coastal environment. Here, the two objectives were investigated in a case of higher complexity encompassing a wide range of lipids (hydrocarbons, fatty acids, alcohols), pigments (chlorophylls) and pollutants (polychlorobiphenyls, alkylamines). The resulting database involves up to 130 compounds, which are used for the description of 40 water particulate samples. These samples were collected within a current research programme in the Ebre Delta [23–27] and correspond to regular sampling over a period of 18 months (see Table 1).

EXPERIMENTAL

A detailed description of the water sampling system is given elsewhere [28]. The water particulates were collected on a microfibre filter (rated pore size 0.5 μm). Collection of particles larger than 1 mm was prevented by placing a stainless-steel grid at the inlet of the pumping tube. Volumes of about 100 l were collected for each sample at a flow-rate of 500 ml min^{-1}. Filters were changed whenever the rates dropped below 50% of normal.

The procedures for the isolation and analysis of the compounds listed in Table 2 were described in detail elsewhere [26,29]. Briefly, filters were Soxhlet extracted with methanol–dichloromethane (1 + 2), the extracts were hydrolysed with 6% KOH–MeOH and the neutral and acidic fractions were successively recovered by *n*-hexane extraction, the latter after acidification (pH 2) with 6 M HCl. The acidic fractions (compounds 26–42 and g–t in Table 2) were esterified with a solution of BF_3 in methanol. The neutral species were fractionated by column chromatography. A column filled with 8 g each of 5% water-deactivated alumina (70–230 mesh) (Merck) (top) and silica (70–230 mesh) (Merck) (bottom) was used. The following fractions were collected: (I) 20 ml of *n*-hexane (compounds 1–24, 102 and a–f), (II) 20 ml of dichloromethane–*n*-hexane (1 + 9) (compounds 89–100), (III) 40 ml of dichloromethane–*n*-hexane (2 + 8) (compounds 25, 101) and (IV) 40 ml of dichloromethane–*n*-hexane (7.5 + 2.5) and 40 ml of methanol–dichloromethane (1 + 9) (compounds 43–83 and u-β). Fraction IV was silylated prior to instrumental analysis.

Capillary GC (SE-54 column) with flame ionization detection (FID) and GC–MS were used for the qualitative and quantitative analysis of compounds 1–83 and a–β. GC with electron-capture detection (ECD) was used for the determination of compounds 89–102. The detailed instrumental conditions are given elsewhere [26,28, 29].

Pigments were determined on acetone extracts of the filter aliquots following the phaeopigment [30] and the trichromatic [31] methods.

Principal component analysis and factor analysis were performed using laboratory-made Fortran 77 routines dedicated to the handling and calculation of large-dimension datasets. The programs were run either on 8200 VAX or HP 900/835 minicomputers, the operating systems were VMS 5.1 and HP-UNIX, respectively.

RESULTS AND DISCUSSION

Sampling sites and lipid and pigment composition

According to previous experience in the area [23,27], seven sampling sites were selected for study of the water-dissolved and particulate lipid molecules. These included (see Fig. 1) the main river flow, one adjacent channel for irrigation, one channel draining into Alfacs Bay (the largest) and two bays where surface and bottom waters (ca. 3 m deep) were collected for the study of their stratified water columns. Sampling was carried out every 2 months covering a period of 18 months. Table 1 provides a list of the water particulate samples collected during this period.

TABLE 2

List of compounds determined in the particulate fraction of the waters of the Ebre Delta with ranges of variation, means and standard deviations for the whole sample population and for the bay and river + channel sample groups (concentrations in ng l^{-1}; 0 = below 0.1 ng l^{-1} for fatty acids and alcohols, below 0.01 ng l^{-1} for hydrocarbons and below 0.0001 ng l^{-1} for the chlorinated compounds)

No.	Compound	All samples				Bay samples				River + channel samples			
		Mean	S.D.	Min.	Max.	Mean	S.D.	Min.	Max.	Mean	S.D.	Min.	Max.
a	*n*-Tetradecane	0.017	0.059	0	0.30	0	–	0	0	0.039	0.085	0	0.30
b	*n*-Pentadecane	0.14	0.57	0	3.1	0.14	0.66	0	3.1	0.14	0.45	0	1.9
c	*n*-Hexadecane	0.11	0.31	0	1.5	0.0091	0.029	0	0.10	0.23	0.43	0	1.5
d	Norpristane	0.03	0.097	0	0.5	0.0045	0.021	0	0.10	0.061	0.14	0	0.50
1	*n*-Heptadecane	6.9	19	0	93	0.21	0.39	0	1.5	15	26	0.30	93
2	Pristane	0.57	0.85	0	3.0	0.11	0.21	0	0.90	1.1	1.0	0.20	3.0
3	*n*-Octadecane	1.4	2.2	0	12	0.18	0.22	0	0.70	2.8	2.7	0.50	12
4	Phytane	0.68	1.0	0	4.7	0.13	0.17	0	0.60	1.4	1.2	0.20	4.7
5	*n*-Nonadecane	2.1	3.6	0	18	0.26	0.28	0	0.90	4.3	4.4	0.70	18
6	*n*-Eicosane	2.6	4.3	0	23	0.40	0.38	0	1.5	5.3	5.3	1.0	23
7	*n*-Heneicosane	6.5	15	0	92	1.8	3.1	0	13	12	21	0.90	92
8	*n*-Docosane	3.4	4.3	0	22	1.5	2.3	0	11	5.8	5.0	0.80	22
9	*n*-Tricosane	7.6	12	0	72	3.3	6.4	0	31	13	16	1.7	72
10	*n*-Tetracosane	6.5	9.8	0.20	58	5.0	12	0.20	58	8.4	5.9	0.60	25
11	*n*-Pentacosane	8.6	9.9	0.30	54	5.5	11	0.30	54	12	6.5	2.5	26
12	*n*-Hexacosane	6.4	7.9	0.40	44	5.2	9.7	0.40	44	7.9	4.7	1.2	16
13	*n*-Heptacosane	14	16	0.50	64	6.9	12	0.50	55	23	17	2.8	64
14	*n*-Octacosane	5.6	7.3	0.50	42	4.6	9.0	0.50	42	6.8	4.2	0.70	16
15	*n*-Nonacosane	29	43	2.1	170	11	26	2.1	125	51	50	2.6	170
16	*n*-Triacontane	4.6	5.9	0.30	31	3.2	6.3	0.40	31	6.3	5.1	0.30	21
17	*n*-Hentriacontane	15	20	1.8	100	6.9	12	1.8	59	26	23	2.1	100
18	*n*-Dotriacontane	2.7	3.1	0.30	16	1.9	3.1	0.30	16	3.7	2.9	0.60	13
19	*n*-Tritiacontane	4.6	4.5	0.30	19	2.6	3.9	0.30	19	7.1	4.0	0.90	14
20	*n*-Tetratriacontane	2.5	5.1	0	31	1.1	1.7	0	8.7	4.1	7.1	0.20	31
21	*n*-Pentatriacontane	1.5	1.6	0	6.2	0.76	1.1	0	5.3	2.3	1.7	0	6.2
22	*n*-Hexatriacontane	0.82	1.3	0	5.7	0.53	0.70	0	2.8	1.2	1.8	0	5.7
e	*n*-Heptatriacontane	0.19	0.32	0	1.2	0.12	0.17	0	0.5	0.28	0.43	0	1.2
23	UCM [a]	210	280	0	1200	64	36	0	140	400	340	0	1200
24	Phthalate	6.0	6.8	0.2	32	3.0	2.8	0.20	11	9.6	8.4	1.5	32
25	Squalene	2.0	3.6	0	18	2.5	4.7	0	18	1.3	1.2	0	4.0
f	Long-chain alkylbenzenes	0.82	4.1	0	25	0	–	0	0	1.8	6.1	0	25
26	Isotetradecanoic acid [b]	61	74	0	260	31	46	0	200	98	86	0	260
g	*n*-Tetradecenoic acid	28	65	0	300	22	36	0	150	34	89	0	300
27	*n*-Tetradecanoic acid	2600	4000	88	16000	1400	2000	160	9200	4100	5200	88	16000
28	Isopentadecanoic acid	290	240	0	830	145	100	10	410	470	240	0	830
29	Anteisopentadecanoic acid	150	130	0	650	85	54	0	195	230	160	0	650
30	*n*-Pentadecanoic acid	340	810	1.0	4950	100	99	1.0	420	630	1200	10	4950
31	Iso-Hexadecanoic acid	500	970	0	4100	54	68	0	280	1000	1300	0	4100
32	Total *n*-hexadecenoic acids	6200	12000	170	60000	1400	960	170	4600	12000	16000	590	60000

33	*n*-Hexadecanoic acid	7300	11000	250	50000	3050	3700	250	18000	12000	14000	760	50000
h	Isoheptadecanoic acid	13	36	0	180	4.3	14	0	55	24	51	0	180
i	Anteisoheptadecanoic acid	18	53	0	250	5.9	28	0	130	34	72	0	250
34	*n*-Heptadecanoic acid	100	280	0	1700	30	46	0	180	190	400	0	1700
35	Total-*n*-octadecatrienoic acids	1100	1500	15	6600	550	460	15	1800	1700	2000	20	6600
36	*n*-octadecadienoic acid	620	670	15	2700	310	350	15	1400	1000	770	66	2700
37	*n*-octadec-9-enoic acid	2800	3400	64	17000	1400	1900	65	8800	4600	4100	250	17000
38	*n*-octadec-11-enoic acid	1100	620	61	2800	830	420	61	1700	1400	690	88	2800
39	*n*-octadecanoic acid	740	910	22	5100	400	510	22	1900	1100	1100	46	5100
j	*n*-Nonadecanoic acid	44	120	0	645	13	35	0	150	82	170	0	645
40	*n*-cosapentaenoic acid	1800	3400	40	16000	450	490	40	1800	3400	4700	79	16000
k	*n*-Eicosanoic acid	45	180	0	1100	13	50	0	230	84	250	0	1100
l	*n*-Heneicosanoic acid	35	100	0	440	13	35	0	140	61	140	0	440
41	*n*-Docosahexaenoic acid	680	1100	0	4200	640	1100	0	4200	710	1100	0	3900
m	*n*-Docosanoic acid	94	204	0	1000	17	38	0	120	190	280	0	1000
n	*n*-Tricosanoic acid	39	100	0	610	12	40	0	170	73	140	0	610
42	*n*-Tetracosanoic acid	270	290	0	1200	150	190	0	650	430	320	120	1200
o	*n*-Pentacosanoic acid	20	57	0	340	14	26	0	68	27	82	0	340
p	*n*-Hexacosanoic acid	32	88	0	500	2.2	10	0	49	69	120	0	500
q	*n*-Heptacosanoic acid	2.7	11	0	62	29.8	13	0	62	2.6	8.5	0	35
r	*n*-Octacosanoic acid	22	77	0	435	0	–	0	0	50	110	0	435
s	*n*-Nonacosanoic acid	1.2	5.7	0	34	1.5	7.2	0	34	0.72	3.1	0	13
t	*n*-Triacontanoic acid	5.4	18	0	79	0	–	0	0	12	25	0	79
43	*n*-Hexadecan-1-ol [c]	21	26	0	130	13	18	0	71	31	30	0	130
44	*n*-Octadecan-1-ol	20	26	0	100	8.0	14	1.0	64	35	29	0	100
45	Phytol	480	690	2.1	3500	91	130	2.1	610	950	800	6.0	3500
46	Isoeicosan-1-ol	9.6	13	0	59	3.3	4.0	0	14	17	16	0	59
47	*n*-Eicosan-1-ol	50	76	0	350	15	22	0	66	94	95	6.2	350
48	*n*-Heneicosan-1-ol	5.1	8.8	0	37	0.8	1.7	0	6.0	10	11	0	37
49	*n*-Docosan-1-ol	38	52	0	220	16	34	0	150	64	58	0	220
u	24,25,26,27-Tetranorcholest-5-en-3β-ol	4.1	11	0	50	0.69	1.1	0	3.3	8.3	16	0	50
50	*n*-Tetracosan-1-ol	27	39	0	180	6.7	15	0	73	51	45	2.1	180
51	*n*-Petacosan-1-ol	22	34	0	180	10	15	0	60	37	45	0	180
52	24-Norcholesta-5,22-dien-3β-ol	23	44	0	180	5.9	8.8	0	41	44	60	0	180
53	*n*-Hexacosan-1-ol	44	87	0	470	7.1	8.1	0	26	90	115	0	470
54	5β(*H*)-Cholestan-3β-ol	75	120	0	500	8.4	10	0	40	160	140	14	500
v	27-Nor-24-methyl-5β(*H*)-cholestan-3β-ol	5.3	19	0	110	1.6	4.4	0	16	9.8	28	0	110
55	5β(*H*)-Cholestan-3α-ol	12	16	0	62	4.5	5.9	0	21	20	20	0	62
56	Unknown	43	72	0	430	20	20	0	63	70	100	0	430
57	27-Nor-24-methylcholesta-5,22(*E*)-dien-3β-ol	21	27	0	110	15	21	0	84	28	33	0	110
58	Cholesta-5,22(*Z*)-dien-3β-ol	51	67	0	380	34	38	0	140	72	87	0	380
59	5α(*H*)-Cholest-22(*E*)-en-3β-ol	8.5	21	0	120	3.7	4.9	0	22	14	31	0	120
60	Cholest-5-en-3β-ol	270	340	0	1500	100	93	0	380	480	410	24	1500

(Continued on p. 164)

TABLE 2 (continued)

No.	Compound	All samples				Bay samples				River + channel samples			
		Mean	S.D.	Min.	Max.	Mean	S.D.	Min.	Max.	Mean	S.D.	Min.	Max.
61	5α(*H*)-Cholestan-3β-ol	98	130	0	570	35	35	0	140	170	170	8.4	570
62	*n*-Octacosan-1-ol	63	100	0	470	12	15	0	61	120	120	21	470
63	24-Methylcholesta-5,22(*E*)-dien-3β-ol	145	270	0	1700	75	67	0	210	230	380	0	1700
64	24-Methyl-5α(*H*)-cholest-22(*E*)-en-3β-ol	72	92	0	310	34	62	0	210	120	100	0	310
65	5α(*H*)-Cholest-7-en-3β-ol	34	55	0	230	18	29	0	110	54	71	0	230
66	24-Methylcholesta-5,24(28)-dien-3β-ol	260	490	2.0	2900	52	42	2.0	160	520	650	9.6	2900
w	24-Methyl-5α(*H*)-cholest-24(28)-en-3β-ol	79	220	0	1000	3.6	8.3	0	29	170	300	0	1000
67	24-Methylcholest-5-en-3β-ol	104	210	0	970	14	19	0	91	210	280	0	970
68	24-Methyl-5α(*H*)-cholestan-3β-ol	30	78	0	480	5.0	6.0	0	19	60	110	0	480
69	*n*-Nonacosan-1-ol	7.8	11	0	34	4.8	8.4	0	33	12	12	0	34
x	23,24-Dimethylcholesta-5,22(*E*)-dien-3β-ol	15	46	0	280	5.0	11	0	43	26	67	0	280
70	24-Ethylcholesta-5,22(*E*)-dien-3β-ol	110	120	0.40	570	56	72	0.40	240	170	140	3.6	570
y	24-Ethyl-5α(*H*)-cholest-22(*E*)-en-3β-ol	10	22	0	110	6.8	13	0	32	14	30	0	110
z	4α,24-Dimethyl-5α(*H*)-cholest-22(*E*)-en-3β-ol	9.0	25	0	130	5.6	17	0	69	13	33	0	130
71	24-Methyl-5α(*H*)-cholesta-7,22(*E*)-dien-3β-ol	34	66	0	290	6.9	8.2	0	26	67	89	0	290
72	24-Methyl-5α(*H*)-cholest-7-en-3β-ol	25	60	0	280	3.9	5.6	0	18	51	83	0	280
73	23,24-Dimethylcholest-5-en-3β-ol	12	20	0	81	4.2	5.0	0	17	22	26	0	81
α	23,24-Dimethyl-5α(*H*)-cholestan-3β-ol	6.6	13	0	68	2.6	4.3	0	14.5	12	19	0	68
74	24-Ethylcholest-5-en-3β-ol	240	280	0	950	77	110	0	520	440	290	20	950
75	24-Ethyl-5α(*H*)-cholestan-3β-ol	120	200	0	930	58	110	0	530	200	250	3.6	930
76	*n*-Triacontan-1-ol	86	120	0	570	42	40	0	160	140	160	11	570
77	4α,23,24-Trimethyl-5α(*H*)-cholest-22(*E*)-en-3β-ol	15	19	0	83	17	22	0	83	14	16	0	48

78	24-Ethyl-5α(*H*)-cholest-7-en-3β-ol	32	60	0	260	2.5	4.1	0	19	69	76	1.8	260
79	24-Ethylcholesta-5,24(28*Z*)-dien-3β-ol	11	14	0	67	5.7	6.5	0	26	17	18	0	67
80	4α,23,24-Trimethyl-5α(*H*)-cholestan-3β-ol	14	18	0	72	3.1	4.0	0	19	28	19	0	72
81	*N*-Hexadecyl-*N*-methyl-*N*-octadecylamine	5.4	6.5	0	20	3.0	4.1	0	15	8.3	7.7	0	20
82	*n*-Dotriacontan-1-ol	10	13	0	53	4.7	8.4	0	40	17	14	0	53
83	*N*,*N*-Dioctadecyl-*N*-methylamine	9.0	39	0	250	0.44	0.84	0	3.6	19	57	0	250
β	24-Propylcholesta-5,24(28*Z*)-dien-3β-ol	0.19	0.8	0	5.0	0.086	0.26	0	1.2	0.32	1.2	0	5.0
84	Chlorophyll *a* [d]	2600	3400	40	12000	400	380	40	1500	4900	3800	500	12000
85	Phaeophorbide *a*	1700	2300	100	12000	460	340	100	1300	3100	2800	600	12000
86	Chlorophyll *a*	3500	4600	200	20000	785	530	200	2200	6400	5200	900	20000
87	Chlorophyll *b*	310	370	0	1700	120	88	0	400	520	440	50	1700
88	Chlorophyll *c*	530	660	30	2800	150	120	30	500	950	750	80	2800
89	2,2′,5,5′-Tetrachlorobiphenyl (No. 52) [e]	0.14	0.21	0	0.89	0.022	0.027	0	0.10	0.28	0.24	0	0.89
90	2,2′,4,5,5′-Pentachlorobiphenyl (No. 101)	0.15	0.22	0	1.1	0.031	0.043	0	0.17	0.30	0.26	0.044	1.1
91	2,3′,4,4′,5-Pentachlorobiphenyl (No. 118)	0.13	0.21	0	0.86	0.021	0.023	0	0.092	0.27	0.25	0.055	0.86
92	2,2′,4,4′,5,5′-Hexachlorobiphenyl (No. 153)	0.24	0.36	0	1.6	0.041	0.033	0	0.14	0.49	0.43	0.046	1.6
93	2,2′,3,4,4′,5′-Hexachlorobiphenyl (No. 138)	0.26	0.36	0	1.7	0.050	0.055	0	0.23	0.52	0.41	0.062	1.7
94	2,2′,3,4,4′,5,5′-Heptachlorobiphenyl (No. 180)	0.23	0.33	0	1.2	0.039	0.036	0	0.16	0.46	0.39	0.026	1.2
95	Arochlor 1254	1.1	1.6	0	7.9	0.20	0.21	0	0.79	2.2	1.8	0.41	7.9
96	Arochlor 1260 [f]	1.7	2.3	0	9.7	0.32	0.32	0	1.4	3.4	2.6	0.51	9.7
97	Arochlor 1260 [f]	2.0	2.5	0	10	0.44	0.44	0	2.0	3.9	2.7	0.94	10
98	Aldrin	0.047	0.055	0	0.25	0.019	0.010	0.005	0.048	0.082	0.068	0	0.25
99	*o*,*p*′-DDE	0.26	0.32	0	1.2	0.057	0.060	0.021	0.240	0.52	0.34	0.099	1.2
100	*p*,*p*′-DDE	0.20	0.28	0	1.1	0.033	0.037	0	0.16	0.41	0.30	0.047	1.1
101	*p*,*p*′-DDT	0.19	0.26	0	1.3	0.067	0.098	0	0.36	0.35	0.30	0	1.3
102	Hexachlorobenzene	0.24	0.52	0	2.2	0.021	0.035	0	0.15	0.51	0.69	0	2.2

[a] Unresolved complex mixture of hydrocarbons. [b] Nos. 26–t analysed as methyl esters. [c] Nos. 43–80, 82 and β analysed as trimethylsilyl ethers. [d] Nos. 84 and 85 determined by the phaeopigment method [30] and Nos. 86–88 by the trichromatic method [31]. [e] The IUPAC congener numbers [51] corresponding to the isomers are indicated. [f] Nos. 95 and 96 determined with respect to eleven polychlorobiphenyl congeners, No. 97 determined with respect to polychlorobiphenyl congener No. 170.

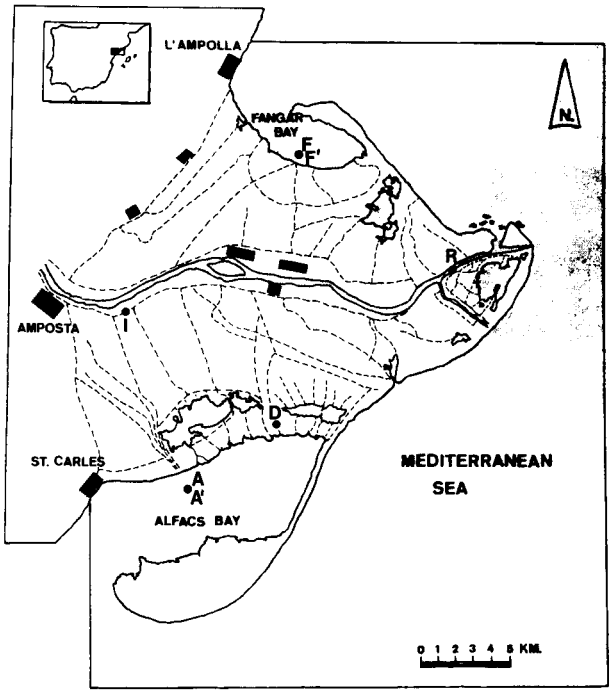

Fig. 1. Map showing the location of the sampling sites selected in the Ebre Delta. F = Fangar Bay, surface water; F′ = Fangar Bay, 3-m deep water; A = Alfacs Bay, surface water; A′ = Alfacs Bay, 3-m deep water; R = River Bed; I = Irrrigation channel; D = drainage channel.

GC and GC–MS of the hydrocarbon, alcohol and fatty acid fractions allowed the identification and determination of 122 compounds and two standard industrial mixtures of polychlorobiphenyls (Aroclor 1254 and 1260). Chlorophyll pigments and phaeophorbide were determined by UV spectrophotometry. The resulting list of 130 water particulate parameters is given in Table 2, where the concentration ranges, means and standard deviations are indicated. The *n*-alkanes, UCM and sterols are in the same order as those found in previous studies (1982–83) in the same area [27,32]. The concentrations of hydrocarbons, fatty acids, sterols and chlorophylls reported in Table 2 are also of the same order of magnitude as those found in other coastal zones [6,33–41].

One major feature of the distribution of lipids, pigments and pollutants in the Ebre delta is the high concentrations of these compounds in the river and channel system compared with the bay water levels. This corresponds to a situation in which most of the allochthonous sources (natural and anthropogenic) and nutrients enter the area by means of the river and their associated irrigation channels [14,23,26]. The allochthonous compounds may only reach the bays after passage

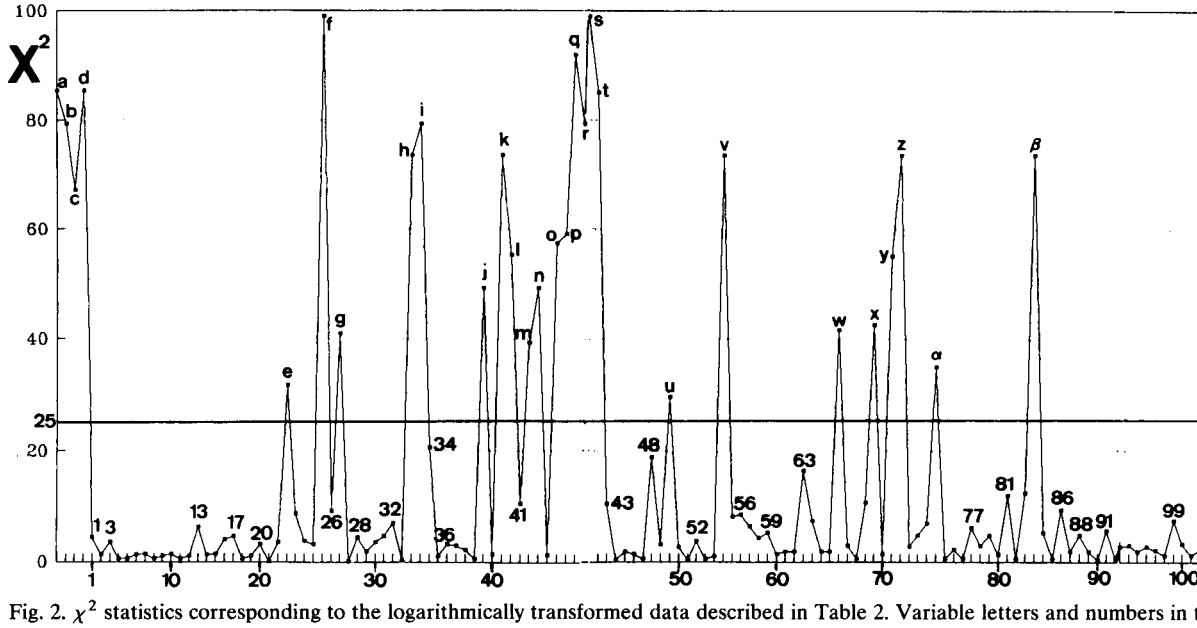

Fig. 2. χ^2 statistics corresponding to the logarithmically transformed data described in Table 2. Variable letters and numbers in the abscissa and marked peaks refer to Table 2. All lettered variables have been rejected for multivariate analysis.

through the rice fields, where they are retained in significant proportion. Likewise, a substantial amount of nutrients, both those originating from river and those from agricultural activities, is retained in the rice fields. Dilution is another aspect determining the final nutrient concentration in the bays, being more significant in Alfacs Bay. In consequence, primary productivity, and hence algal lipids and chlorophylls, are higher in the river and channel waters than in the bays.

Variable tests

An additional significant feature of the data in Table 2 is the diverse concentration ranges of the water constituents. This required autoscaling; each component concentration set was subtracted from the mean and divided by the standard deviation. Therefore, only correlation matrices were considered for multivariate analysis.

However, spurious correlation with strongly censored variables must be avoided. For this purpose, the statistical χ^2 test was applied to logarithmically transformed data as developed in a previous study on sedimentary hydrocarbons [22]; this test allows the easy identification of strongly censored variables. The results corresponding to the application of this test to the database described in Table 2 are shown in Fig. 2. The group

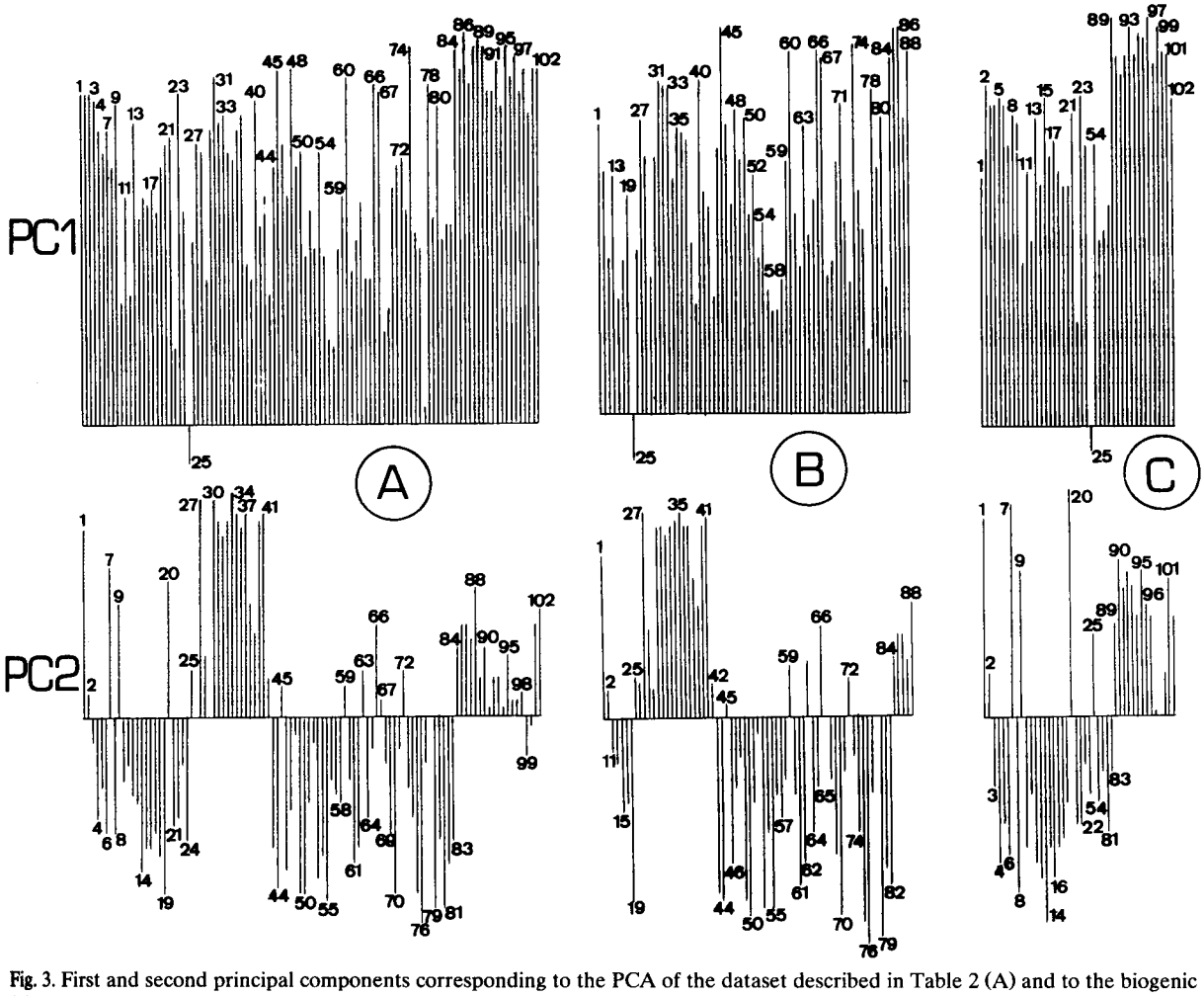

Fig. 3. First and second principal components corresponding to the PCA of the dataset described in Table 2 (A) and to the biogenic (B) and pollution (C) subgroups. Numbers refer to Table 2.

of compounds strongly affected by detection limit thresholds, a–β, exhibit χ^2 values higher than 25. These compounds were not included in the multivariate calculations.

Principal component analysis

The main PCA results corresponding to the Table 2 dataset are reported in Fig. 3A, where the two first eigenvectors are shown. These PCs are represented individually by means of histograms in which the contributions of the variables are proportional to the heights of vertical bars. These plots afford a more detailed examination of the contributions of the variables in the PC/Fs than the traditional two-dimensional charts. This improvement is particularly important when the main objective of the multivariate analysis is concerned with source input elucidation.

PC1 involves 34% of the variance and corresponds to a mixture of compounds originating from various sources: algae [i.e., *n*-heptadecane (1), phytol (45), cholest-5-en-3β-ol (60), chlorophyll *a* (84, 86)], microorganisms [i.e., iso- (28) and anteiso- (29) pentadecanoic acids], higher plants [i.e., *n*-heptacosane (13)], petroleum residues [i.e., UCM (23)], pesticides [i.e., aldrin (98), *p,p*-DDE (100), *p,p'*-DDT (101)], and industrial products [i.e., polychlorobiphenyls (89–99), hexachlorobenzene (102)]. This PC does not reflect a size effect because the calculations were done on autoscaled variables. It indicates that there is a concurrence of biogenic and anthropogenic inputs, which is not suprising because one major geographical source, the river, determines their distribution in the deltaic area.

PC2 involves 14% of the variance and is also constituted by a complex distribution of compounds represented by positive and negative contributions, an aspect that complicates further the interpretation of its environmental significance. The scores corresponding to these PCs are represented in Fig. 4A. They indicate that PC1 and PC2 define major features of the data in Table 2 despite their complexity. Thus, PC1 scores afford a clear differentiation between the bay and the river and channel samples and PC2 scores sepa-

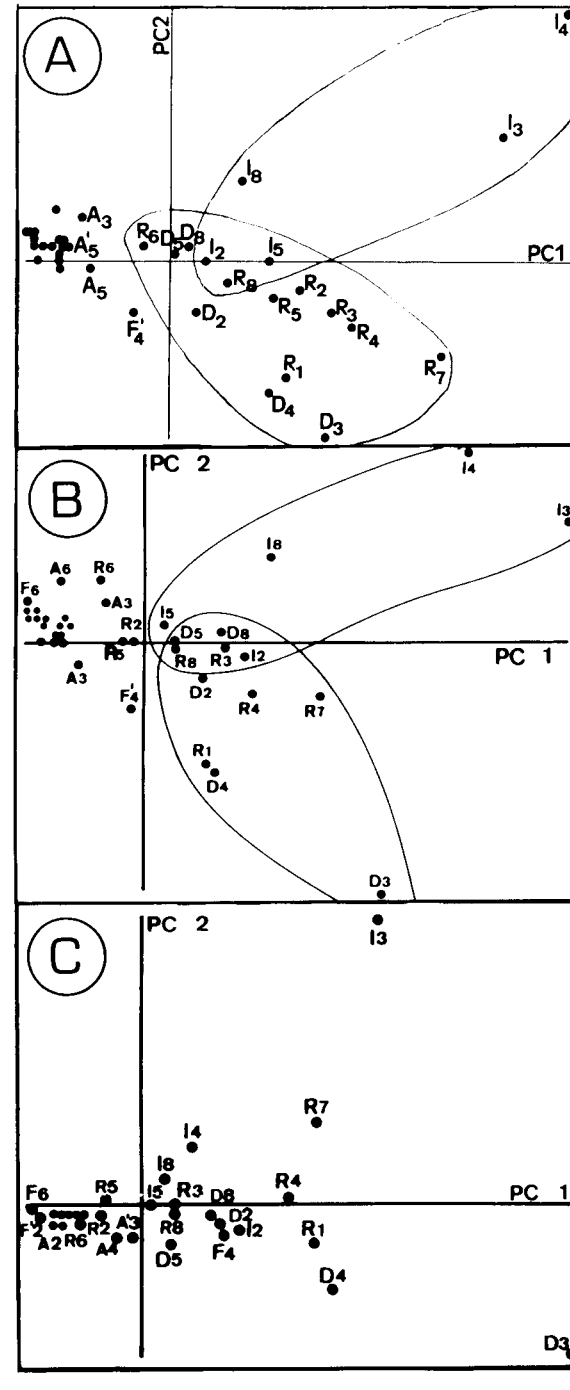

Fig. 4. PC1 and PC2 scores corresponding to the PCA of the dataset described in Table 2 (A) and to the biogenic (B) and pollution (C) subgroups. Sample descriptions refer to Table 1.

rate the irrigation channel samples from those of the river and discharge channel.

The results corresponding to the biogenic and anthropogenic database subgroups indicated above are also represented in Figs. 3 and 4. The compounds that a priori can be attributed to biogenic sources encompass Nos. 1, 2, 11, 13, 15, 17, 19, 25, 26–80, 82, 84 and 88. However, some compounds may originate both from anthropogenic and biogenic sources so that they must be included in both pollutant and biogenic groups.

The main results corresponding to the biogenic subgroup are illustrated in Fig. 3 by representation of PC1 and PC2 that involve 35% and 17% of the total variance, respectively. With the exception of the compounds that have been purposely excluded, these two main PCs parallel those obtained in the previous calculation. Thus, PC1 corresponds to a mixture of algal (i.e., Nos. 1, 45, 60, 84, 86), microbial (i.e., 28, 29) and terrestrial (i.e., 13) sources, and PC2 is also composed of positive and negative contributions. Therefore, the reduction of the data in Table 2 to the subgroup of biogenic compounds (from a total number of 102 to 69) does not involve a higher PC definition of geochemical sources. In terms of scores, similar plots are obtained in the calculations corresponding to the total database and the biogenic subgroup, Fig. 4A and B, respectively. The biogenic PC2 scores also distinguish between the irrigation channel and the river + discharge channel samples.

Forty-three of the compounds included in Table 2 can a priori be related to pollution inputs (Nos. 1–25, 54, 55, 81, 83, 89–102). PCA of the dataset formed by this subgroup results in the PCs described in Fig. 3C where the eigenvalues of the two first principal components represent 48% (first) and 15% (second) of the total variance. A mixture of inputs is again reflected in PC1. This encompasses petroleum residues [i.e., UCM (23)], sewage [i.e., coprostanol (54)], pesticides [i.e., aldrin (98), *p,p'*-DDE (100)] and industrial products [i.e., polychlorobiphenyls (89–97), hexachlorobenzene (102)]. In addition to these, higher plant remains are also represented by *n*-heptacosane (13), *n*-nonacosane (15) and *n*-hentriacontane (17). PC2 also exhibits a combination of positive and negative contributions and is of complex geochemical significance. The scores corresponding to PC1 show again a differentiation between bay and river + channel samples (Fig. 4C), although these two groups are not so well differentiated as in Fig. 4A and B. The PC2 scores essentially enhance the differences between the samples from the river and the irrigation channel, although the resolution is poorer than in the previous calculations.

An additional feature of these PCA calculations is the large number of principal components required for the description of a high proportion of the variance (between eleven and seventeen for 95%). This is a consequence of the high variability of molecular markers in environmental samples, especially in water samples. The dispersion of the total variance among so many components is currently observed provided that a reasonable number of samples is included in the calculations. Studies involving small sample numbers have resulted in descriptions of high percentages of the total variance with a limited number of principal components, but in these cases the results are not representative of the system under study. This dispersion effect and the lack of correspondence between principal components and single geochemical sources require efforts to be focused on the portion of the total variance that is shared by the variables.

Factor analysis

FA was performed in an iterative way. In each cycle, the diagonal elements of the correlation matrix were replaced by the squared communalities obtained from the factor loadings. Then, the new matrix was used to obtain new factor loadings which provided new communality values for the next iteration cycle. The process was repeated until the differences in the traces of two successive correlation matrices were smaller than a threshold. The initial communality values were obtained from a subset of the principal components resulting from the original correlation matrix (diagonal elements equal to unity) [42]. After convergence of the iterative calculation, the factor loadings were VARIMAX rotated.

The factor loadings corresponding to the Table 2 dataset are presented in Fig. 5. Repeated calculations of different factor size models and examination of the loadings for geochemical sense allowed nine factors to be identified as the most reasonable estimate for these data.

Factor 1 is loaded by a series of algal markers encompassing *n*-alkanes (No. 1), fatty acids (Nos. 27, 31–33, 35, 40, 41), alcohols (Nos. 45, 52, 59, 60, 63, 66, 67, 71) and chlorophylls (Nos. 84–88). Most of these loadings are unspecific [i.e., *n*-hexadecanoic acid (No. 33), phytol (No. 45)], and some of them are even used as primary productivity indicators [i.e. chlorophyll *a* (Nos. 84,86)]. However, other compounds can be specifically related to diatom inputs [43,44] [i.e., 24-methylcholesta-5,22(*E*)-dien-3β-ol (No. 63), 24-methylcholesta-5,24(28)-dien-3β-ol (No. 66)]. The con-

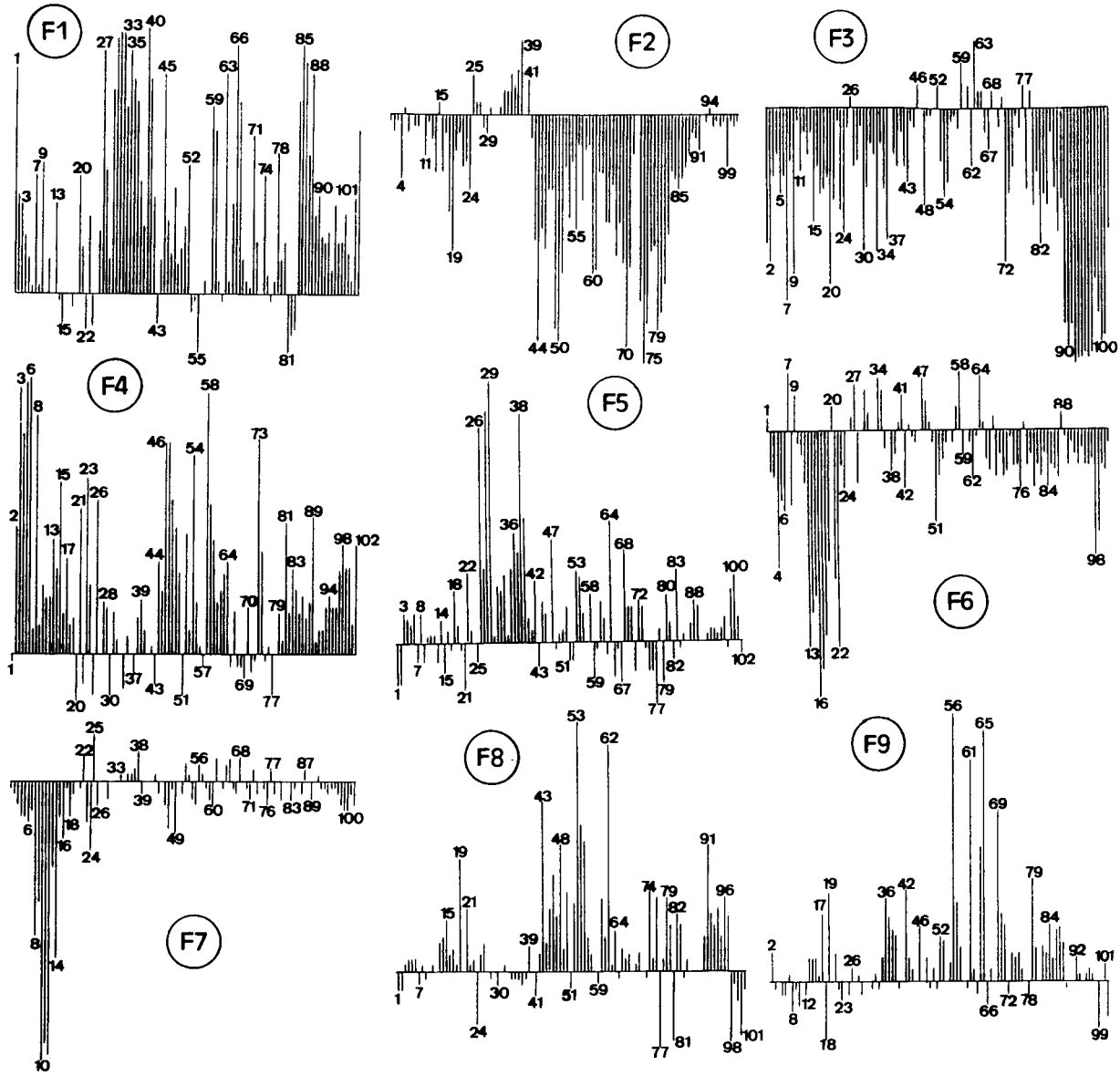

Fig. 5. Factor loadings resulting from FA of the dataset described in Table 2. Numbers refer to Table 2.

currence of primary productivity indicators and diatom markers points to the dominance of this species in the delta waters.

Factor 2 is loaded on several alkan-1-ols (Nos. 44, 49, 50, 76) and sterols (Nos. 60, 61, 70, 71, 74, 75, 79, 80). The dominance of 24-ethylcholest-5,22(*E*)-dien-3β-ol (No. 70) and 24-ethylcholesta-5,24(28*Z*)-dien-3β-ol (No. 106) corresponds to green algal inputs (Chlorophyceae and Prasinophyceae) [6,45]. 24-methyl-5α(*H*)-cholesta-7,22(*E*)-dien-3β-ol (No. 71) is also characteristic of Chlorophyceae. In contrast, 4α,23,24-trimethyl-5α(H)-cholest-22(E)-en-3β-ol (No. 80) is a known marker of dinoflagellates [5]. These two algal sources are also consistent with the loading of 24-ethylcholest-5-en-3β-ol (No. 74) and 24-ethyl-5α(*H*)-cholestan-3β-ol (No. 75) and the C_{16}–C_{24} *n*-alkan-1-ols (Nos. 44, 49, 50, 53). The absence of primary productivity indicators in this factor suggest that flagellates and green algae are minor organic matter producers in the Ebre Delta waters.

Factor 3 is loaded by the chlorinated compounds, namely the polychlorobiphenyls (Nos. 89–97) and *p,p'*-DDT (No. 101), some *n*-alkanes (Nos. 7, 9, 20) and some *n*-alkanoic acids (Nos. 30, 34). The dominance of polychlorobiphenyls indicates that this factor essentially represents industrial residues. However, the concurrence of other chlorinated compounds such as the DDTs (Nos. 99–101) or hexachlorobenzene (No. 102) indicates that in the delta waters these chlorinated species exhibit a distribution behaviour that is roughly independent on source origin. In this respect, the comparison of Figs. 3 and 5 indicates that the differentiation between chlorinated pesticides and industrial species is better afforded by FA than PCA. In addition to the chlorinated species, other compounds significantly load on this factor representing non-pollutant [i.e., *n*-heneicosane (No. 7)] inputs.

Factor 4 is also loaded by several known pollution markers such as the UCM (No. 23), 5β(*H*)-cholestan-3β-ol (No. 54) and *N*-hexadecyl-*N*-methyl-*N*-octadecylamine (No. 81), which can be related to petroleum residues, sewage [7] and detergents [4], respectively, a group of pollutant inputs of likely concurrence in the delta. The loading of C_{18}, C_{19}, C_{20} and C_{22} *n*-alkanes is also in agreement with a petrogenic influence. Some other compounds [e.g., cholesta-5,22(*Z*)-dien-3β-ol (No. 58) or 23,24-dimethylcholest-5-en-3β-ol (No. 73)] that cannot be directly attributed to these pollution sources are also loading in this factor.

The dominant loadings of factor 5, iso- (No. 28) and anteiso- (No. 29) pentadecanoic acids, correspond to microbial inputs [46], a source that is also consistent with the loading of iso-tetradecanoic acid (No. 26) and *n*-octadec-11-enoic acid (No. 47).

Factor 6 is mainly loaded by a distribution of C_{27}–C_{35} *n*-alkanes with odd carbon number preference that is indicative of contributions from higher plants [8]. The presence of some chlorinated compounds [i.e., Aldrin (No. 98), *o,p'*-DDE (No. 99)] as minor significant loadings suggests the concurrence of higher plant (natural allochthonous) and pollutant sources in the delta. This concurrence is also observed in factor 8 that is loaded by sewage indicators [7] [coprostanol (No. 54), epicoprostanol (No. 55)] along with some higher plant markers [9] [*n*-hexacosan-1-ol (No. 53) and *n*-octacosan-1-ol (No. 62)].

Factor 7 is loaded by a modal mixture of C_{22}–C_{28} *n*-alkanes (Nos. 8–14). *n*-Alkane distributions lacking odd-to-even carbon number preference in this range may be produced by bacterial activity [47–49] although in some instances they correspond to specific petroleum spillages [50]. In this respect, the load of the UCM (No. 23) supports a bacterial origin for these *n*-alkanes and represents an important contrast with respect to factor 4 where petroleum sources are represented.

Finally, factor 9 loadings are dominated by 24,25,26,27-tetranorcholest-5-en-3β-ol (No. 61), cholest-7-en-3β-ol (No. 65) and a compound (No. 56) whose structure has not yet been determined. These compounds define an input source that still has to be identified.

As is evidenced in the above discussion, source inputs are better differentiated with FA than with PCA. However, it may again be questioned whether source input elucidation can be improved by reduction of the compounds included

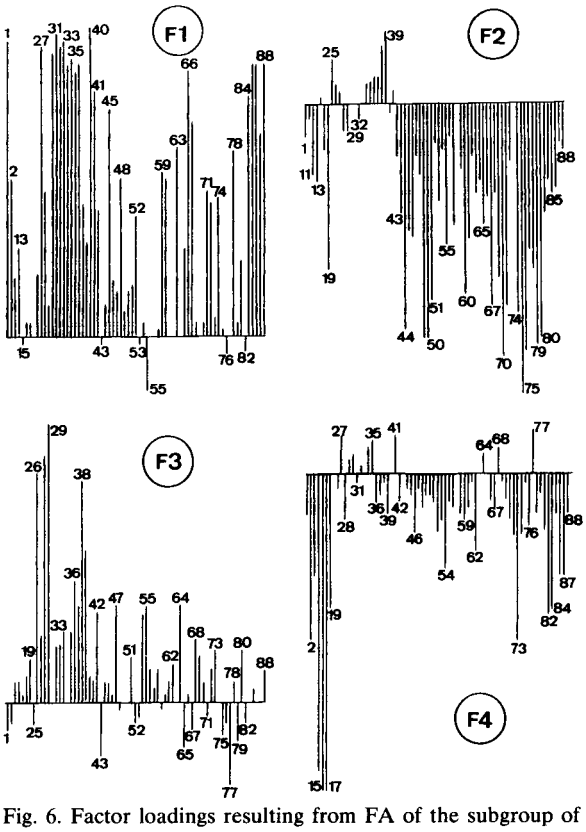

Fig. 6. Factor loadings resulting from FA of the subgroup of biogenic compounds from Table 2 dataset. Numbers refer to Table 2.

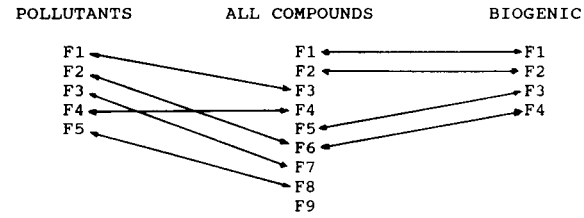

Fig. 7. Correspondence between the factor loadings resulting from FA of the dataset described in Table 2 and its corresponding subgroups of biogenic and pollutant marker compounds.

in the calculations. Therefore, the same subgroups considered in the PCA section were analysed by FA.

The factor loadings corresponding to the 'biogenic' subgroup of compounds are represented in Fig. 6. Repeated calculations using a variable number of factors together with the evaluation of the geochemical significance of the results have allowed four factors to be determined as the most likely estimate for this reduced dataset. The loadings of these factors are very similar to those obtained in the previous calculation (see Figs. 5 and 6). Thus, the two main "biogenic" factors correspond to algal origins, the first related to diatom sources and the second to green algae and

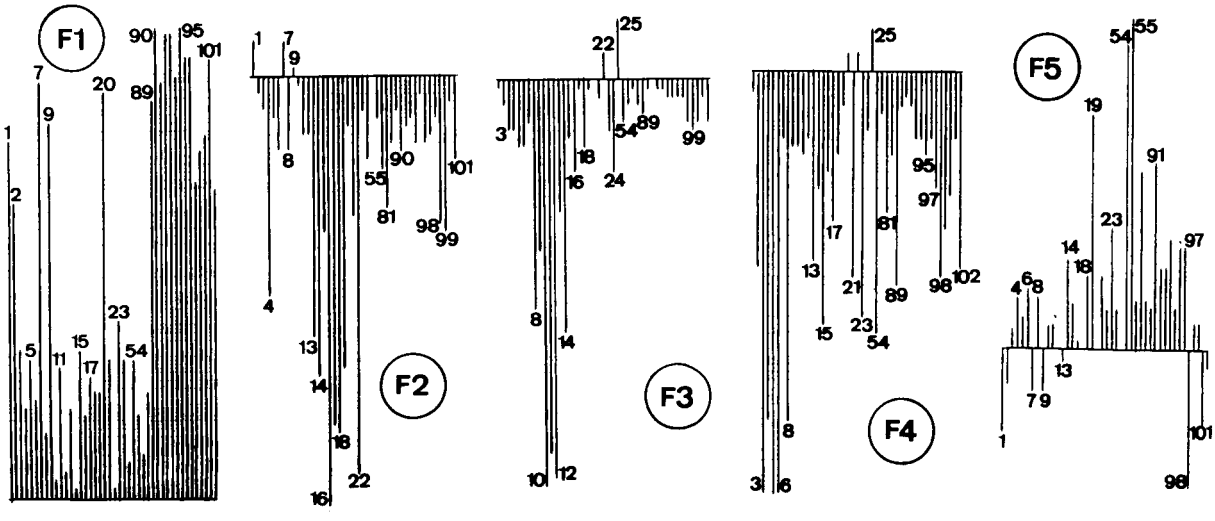

Fig. 8. Factor loadings resulting from FA of the subgroup of pollution markers from Table 2 dataset. Numbers refer to Table 2.

dinoflagellates. Despite the smaller number of compounds included in the calculation the contributions corresponding to these two latter algal species are not resolved in two distinct factors. Factor 3 is related to microbial inputs and factor 4 is loaded by the C_{27}–C_{35} *n*-alkanes of higher plant origin.

The comparison of Figs. 5 and 6 indicates that their factor loadings are in direct correspondence. The differences among the loadings are so significant that the specific correspondences can be determined by simple visual inspection. These are represented in Fig. 7. Similarly to that observed in the PCA calculations, the joint evaluation of Figs. 5–7 shows that data reduction does not generally improve source input elucidation. Except for the contributions initially eliminated from the dataset (the pollutant compounds), equivalent source input mixtures are observed in both types of factors [i.e., microbial and higher plant inputs in factor 3 (Fig. 6) and factor 5 (Fig. 5)].

The reduction of the data in Table 2 to the group of compounds that can be related to pollution inputs also gives rise to five factors upon FA. Again, the decrease in the number of compounds with respect to samples does not result in an improvement of FA for source input elucidation. Thus mixed contributions are observed in factors 1, 4 and 5 (see Fig. 8), corresponding to the same combinations of pollutant compounds found in factors 3, 4 and 8, respectively, in Fig. 5.

Further understanding of the relationships between the factor loadings of the three FA calculations can be obtained from their corresponding communalities (see Fig. 9). In all three cases, the values range between 0.8 and 1 (often between 0.9 and 1) for most variables, indicating that the selected number of factors was adequate. Squalene (No. 25) is the compound showing the lowest communality values (ca. 0.1) and therefore the compound whose variance is less represented by the factor loads. The fragmentation of the database into biogenic and pollutant compounds does not involve any major communality increase with respect to the calculation with the global set of data. This is consistent with the good correspondence between the factor loadings resulting from the three calculations (see Fig. 7) and indicates that no significant improvement in database description is obtained from the independent FA of the biogenic and pollution variable subgroups. In fact, the consideration of only one of these subgroups gives rise to strong decreases in the communality values of compounds such as *n*-heneicosane (No. 11) that may be introduced by both biogenic and pollutant sources.

An important feature resulting from the application of FA to the whole Table 2 dataset is the well defined correspondence between factors and autochthonous inputs. As indicated above, algal inputs are represented by factors 1 and 2, which correspond to diatoms and green algae + dinoflagellates, respectively, and microbial contribu-

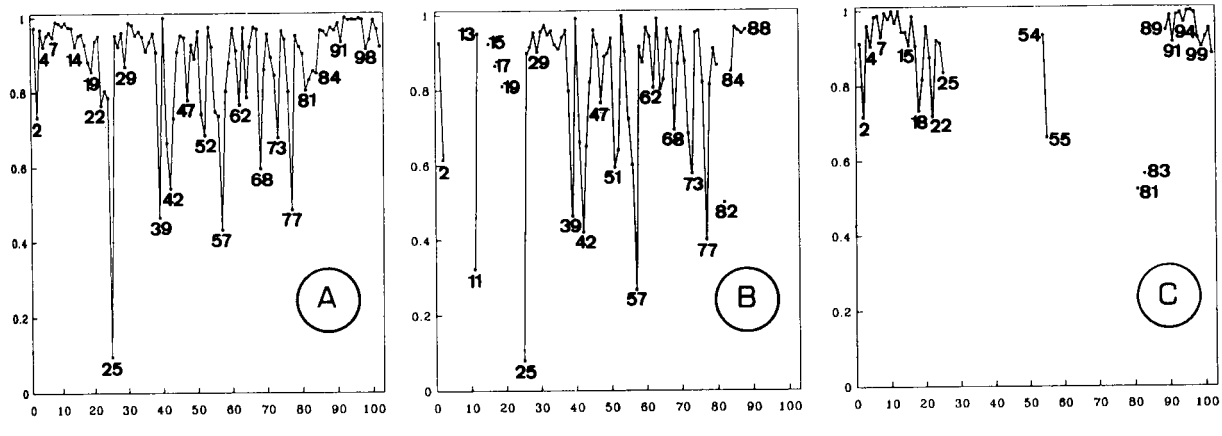

Fig. 9. Communalities corresponding to the FAs represented in Figs. 5A, 6B and 8C. Variable numbers refer to Table 2.

tions are represented by factors 5 and 7. The differentiation between these types of algal and microbial inputs is very difficult, not possible in practical terms, from the classical way of application of the molecular marker concept in which multivariate analysis is not considered. The combined use of FA and molecular markers has therefore afforded a considerable improvement in the capacity of source input elucidation in the delta waters.

In contrast, the characterization of allochthonous inputs, both natural and anthropogenic, is more difficult. The higher plant indicators are distributed among several factors: 2 (24-ethylsterols), 6 (*n*-alkanes) and 8 (*n*-alkanols), which constitutes a complex situation in terms of

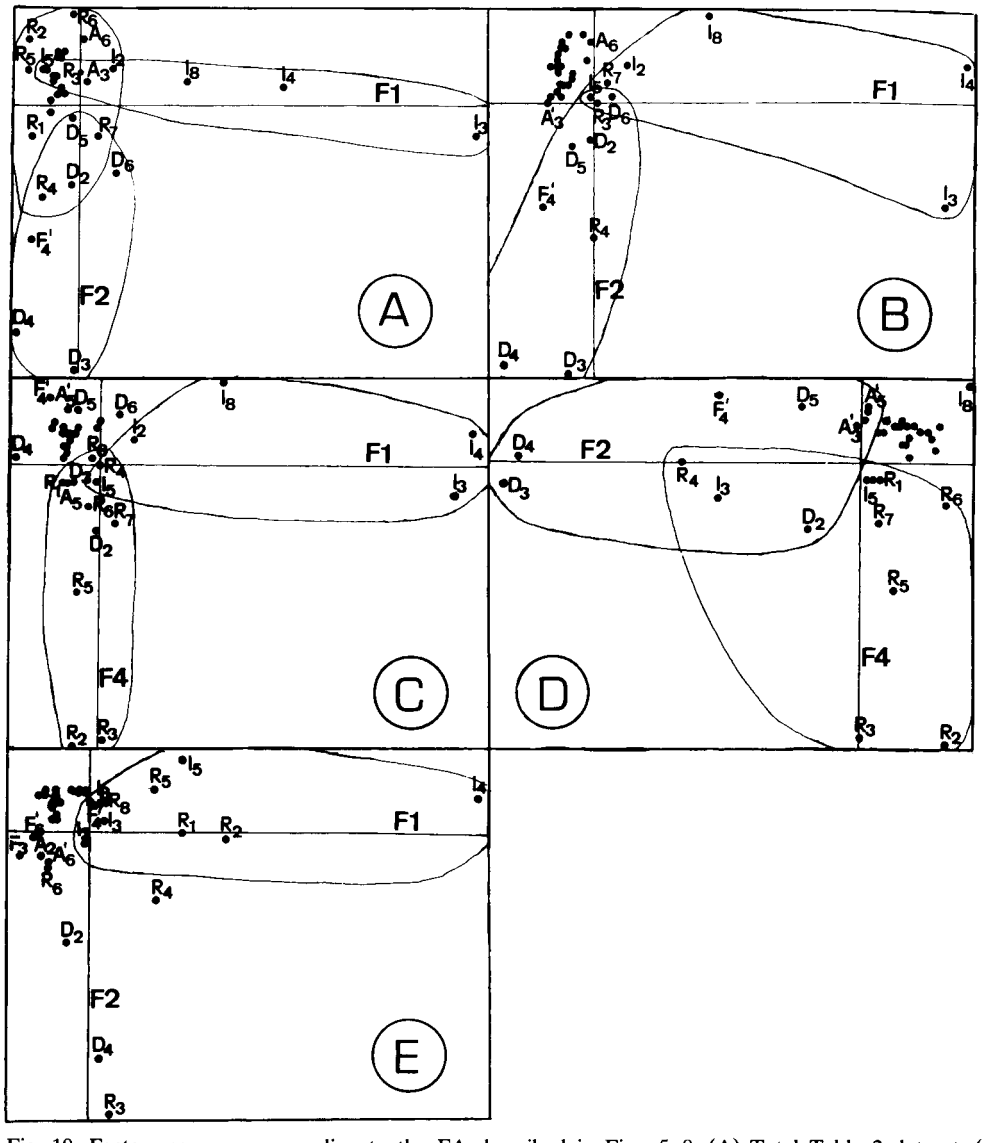

Fig. 10. Factor scores corresponding to the FA described in Figs. 5–8. (A) Total Table 2 dataset; (B), (C) and (D) biogenic subgroup; (E) pollutant markers subgroup. Sample descriptions refers to Table 1.

geochemical sense. The anthropogenic compounds are essentially loading in factor 3 (polychlorobiphenyls, DDTs, hexachlorobenzene) and factor 4 (UCM, coprostanol, *N*-hexadecyl-*N*-methyl-*N*-octadecylamine, *N*,*N*-dioctadecyl-*N*-methylamine), again representing a complex situation. Detergent indicators appear in factor 4 being concurrent with sewage markers. This situation is likely a reflection of the diversity of pollutant discharge sites in the delta. Most industrial spills probably originate from one discharge point [24] but petroleum, detergents and sewage may be introduced from diverse locations. The distribution patterns of the allochthonous contributions may therefore be more complex than those of the autochthonous inputs, and this is reflected in the FA results.

The main factor scores corresponding to the FA calculation described in Figs. 5, 6 and 8 are represented in Fig. 10. The calculations involving the whole Table 2 dataset and the "biogenic subset" are represented in Fig. 10A and B; their factor 1 and 2 scores essentially differentiate the irrigation and the discharge channel samples, respectively. In addition, the biogenic scores factors 1 and 4 differentiate between river and irrigation channel samples (Fig. 10C). Therefore, the representation of the factor 2 and factor 4 scores of this calculation (Fig. 10D) affords a differentiation between river and discharge channel samples. In contrast, the factor 1 and 2 scores corresponding to the "pollution subgroup" (Fig. 10E) are not so directly interpretable in terms of sample location.

In short, according to the calculations in which 'biogenic' compounds are involved, the main features of the molecular marker composition of the irrigation and the discharge channel are represented by diatom and green algae + dino-flagellate inputs, respectively. On the other hand, the best differentiation of the river samples is obtained with score factor 4 (see Fig. 10C and D), which corresponds to the higher plant contributions described by the *n*-alkanes.

Conclusions

FA is an adequate method for source input elucidation in environmental studies using molecular markers for sample description. The application of this method results in a direct correspondence between factor loadings and marker groups defining geochemically consistent organic matter contributions to the system. In many instances, namely autochthonous matter, FA allows an even more precise characterization of input sources than that corresponding to the common "qualitative" molecular marker approach.

This method affords geochemically significant results despite the fact that the molecular marker datasets are currently constituted by a larger number of compounds (variables) than samples. In fact, repeated FA applications to dataset subgroups encompassing the selection of a limited number of compounds has not afforded any improvement with respect to the results obtained from the analysis of the global set of data. This is consistent with the current assumptions of most environmental geochemical studies in which the global population of lipid markers is attributed to a limited number of sources.

In contrast with FA, the use of PCA for the study of this type of data allows a differentiation between major groups of samples but not between geochemically defined source inputs.

The dataset considered in this study was compiled from the results provided by Ruben Llop and Josep Ignasi Gomez-Belinchon, who collected and analysed the water samples, and their cooperation is gratefully acknowledged. The authors are also grateful to Joan Albaigés for useful discussions. Financial support from the Eros-2000 Project is acknowledged.

REFERENCES

1 R.P. Philp and J.N. Oung, Anal. Chem., 60 (1988) 887A.
2 R. Ishiwatari, H. Takada, S. Yun and E. Matsumoto, Nature, 301 (1983) 599.
3 R.P. Eganhouse, D.L. Blumfield and I.R. Kaplan, Environ. Sci. Technol., 17 (1983) 523.
4 M. Valls, J.M. Bayona and J. Albaigés, Nature, 337 (1989) 722.
5 M. Robinson, G. Eglinton, S.C. Brassell and P.A. Cranwell, Nature, 308 (1984) 439.
6 J.K. Volkman, Org. Geochem., 9 (1986) 83.

7 J.O. Grimalt, P. Fernandez, J.M. Bayona and J. Albaigés, Environ. Sci. Technol., 24 (1990) 357.
8 G. Eglinton and H.J. Hamilton, Science, 156 (1967) 1322.
9 P.E. Kolattukudy, Lipids, 5 (1970) 259.
10 F.G. Prahl and L.A. Pinto, Geochim. Cosmochim. Acta, 51 (1987) 1573.
11 P.M. Shaw and R.B. Johns, Org. Geochem., 10 (1986) 951.
12 P.M. Shaw and R.B. Johns, Org. Geochem., 9 (1986) 237.
13 M.A. Sicre, J.L. Paillasseur, J.C. Marty and A. Saliot, Org. Geochem., 12 (1988) 281.
14 J.O. Grimalt, J. Olivé and J.I. Gomez-Belinchon, Int. J. Environ. Anal. Chem., 38 (1990) 305.
15 P.W. Kwan and R.C. Clarck, Jr., Anal. Chim. Acta, 133 (1981) 151.
16 E. Oberrauch, T. Salvatori, L. Novelli and S. Clementi, Chemometr. Intell. Lab. Syst., 2 (1987) 137.
17 O.H.J. Christie, K. Esbensen, T. Meyer and S. Wold, Org. Geochem., 6 (1984) 885.
18 O.M. Kvalheim, Chemometr. Intell. Lab. Syst., 2 (1987) 127.
19 I. Lysyj and P.R. Newton, Anal. Chem., 44 (1972) 2385.
20 H.A. Clark and P.C. Jurs, Anal. Chem., 51 (1979) 616.
21 O.M. Kvalheim, K. Oygard and D. Grahl-Nielsen, Anal. Chim. Acta, 150 (1983) 145.
22 J.O. Grimalt, L. Canton and J. Olivé, Chemometr. Intell. Lab. Syst., 18 (1993) 93.
23 J.I. Gomez Belinchon, R. Llop, J.O. Grimalt and J. Albaigés, Mar. Chem., 25 (1988) 325.
24 J.M. Gonzalez, J. Grimalt and J. Albaigés, Mar. Chem., 14 (1983) 61.
25 R.W. Risebrough, B.W. de Lappe, W. Walker II, B.R.T. Simoneit, J. Grimalt and J. Albaigés, Mar. Pollut. Bull., 14 (1983) 181.
26 J.O. Grimalt, J.I. Gomez Belinchon, R. Llop and J. Albaigés, Chemosphere, 17 (1988) 1893.
27 J. Albaigés, J. Grimalt, J.M. Bayona, R. Risebrough, B. de Lappe and W. Walker, II, Org. Geochem., 6 (1984) 237.
28 J.I. Gomez Belinchon, J.O. Grimalt and J. Albaigés, Environ. Sci. Technol., 22 (1988) 677
29 J.O. Grimalt and J. Albaigés, Mar. Geol., 95 (1990) 207.
30 S. W. Jeffrey and G.F. Humprei, Biochem. Physiol. Pflanzen, 167 (1975) 191.
31 C.J. Lorenzen, Limnol. Oceanogr., 12 (1967) 343.
32 J.M. Bayona, A. Farrán and J. Albaigés, Mar. Chem., 27 (1989) 79.
33 Chr. Osterroht and G. Petrick, Mar. Chem., 11 (1982) 55.
34 K.A. Burns and J.P. Villeneuve, Geochim. Cosmochim. Acta, 47 (1983) 995.
35 S.A. Macko, J.K. Winters and P.L. Parker, Mar. Pollut. Bull., 13 (1982) 174.
36 B.W. de Lappe, R.W. Risebrough and W. Walker, II, Can. J. Fish. Aquat. Sci., 40 (1983) 322.
37 G. Kattner, G. Gercken and K. Eberlein, Mar. Chem., 14 (1983) 149.
38 G. Kattner, G. Gercken and K.O. Hammer, Mar. Chem., 14 (1983) 163.
39 A.P. Murray, C.F. Gibbs, A.R. Longmore and D.J. Flett, Mar. Chem., 19 (1986) 211.
40 J. Neveux and G. de Billy, Deep-Sea Res., 33 (1986) 1.
41 M.E.Q. Pilson, J. Mar. Res., 43 (1985) 849.
42 W.R. Dillon and M. Goldstein, Multivariate Analysis. Methods and Applications, Wiley, New York, 1984.
43 J.A. Ballantine, A. Lavis and J.C. Roberts, Phytochemistry, 18 (1979) 1495.
44 M. Kates, P. Tremblay, R. Anderson and B.E. Volcani, Lipids, 13 (1977) 34.
45 G.W. Patterson, Lipids, 6 (1970) 120.
46 G.J. Perry, J.K. Volkman, R.B. Johns and H.J. Bavor, Jr., Geochim. Cosmochim. Acta, 43 (1979) 1715.
47 R.W. Johnson and J.A. Calder, Geochim. Cosmochim. Acta, 37 (1973) 1943.
48 J. Grimalt, J. Albaigés, A.A.Z. Douabul and H.T. Al-Saad, Naturwissenschaften, 72 (1985) 35.
49 J. Grimalt, E. Torras and J. Albaigés, Org. Geochem., 13 (1988) 741.
50 C. Lee, S.G. Wakeham and J.W. Farrington, Mar. Chem., 13 (1983) 181.
51 K. Ballschmitter and M. Zell, Fresenius' Z. Anal. Chem., 302 (1980) 20.

Analytica Chimica Acta, 278 (1993) 177–187
Elsevier Science Publishers B.V., Amsterdam

Non-linear robust regression procedure for calibration in flame atomic absorption spectrometry

Paweł Kościelniak

Department of Analytical Chemistry, Jagiellonian University, 30 060 Krakow (Poland)

(Received 20th October 1992; revised manuscript received 4th January 1993)

Abstract

Robust regression methods based on the median, namely the single median and the repeated median methods, were developed to adapt them to those cases occurring in flame atomic absorption spectrometry (FAAS) when non-linear calibration relationships are encountered. All essential features of the median methods were preserved owing to the modification suggested and the regression procedures are simple and easy to apply, allowing outliers to be detected and rejected. The resistance of the methods considered to the effect of outliers is discussed. The effectiveness of the median approaches and some advantages over the least-squares non-linear regression method are revealed in examples with both hypothetical data and real calibration data obtained from FAAS.

Keywords: Atomic absorption spectrometry; Calibration; Regression

Analytical calibration, identified generally as the experimental procedure giving rise to conversion of instrumental response into chemical information, is a very significant stage of analysis irrespective of the instrumental techniques applied. The use of a proper means of calibration is important especially when an interference effect is suspected, creating a source of systematic errors in determination. In flame atomic absorption spectrometry (FAAS), the correction for interference effects is commonly accomplished by matching the composition of a set of standard solutions to the sample. In some instances, especially when the sample is completely unknown, the standard additions method is applied. It was shown recently that these modifications of the above calibration methods which are based on a dilution process, e.g., the dilution method [1], the addition and successive dilution method [2] and the gradient ratio calibration method [3], are also effective for particular analytical systems.

Using each of the calibration methods mentioned, the analyte concentration in a sample is calculated by means of either interpolation or extrapolation of a selected mathematical model following the acquisition of a set of experimental data. A well known statistical technique commonly used for the construction of such a calibration line is that of least squares (LS). It consists of minimizing the sum of squares of the residuals around the estimated regression line in the direction of a dependent variable (i.e., instrumental response or its function). For the LS technique it is assumed that the noise in the responses has a normal distribution over the concentration range and that the noise terms are independent of each other. In analytical practice, however, the experimental data obtained may not satisfy these assumptions. An especially important case is frequently met when one or more calibration points give significantly large residuals, relative to the

Correspondence to: P. Kościelniak, Department of Analytical Chemistry, Jagiellonian University, 30 060 Krakow (Poland).

level of noise. The existence of such points, called outliers, violates the assumption of normality of errors. As a consequent, erroneous evaluation of the parameters of a calibration line is obtained using the LS technique and incorrect final analytical results are achieved.

Some methods of robust regression are known that provide protection against a non-normal error distribution. One group is based on calculation of the median, either of the parameters of the calibration line, i.e., the single median [4] and repeated median [5] methods, or the squared residuals, i.e., the least median of squares method [6,7]. It has been demonstrated [8–12] that they are resistant to the effect of outliers so these points can be detected and rejected and then an acceptable calibration line can be constructed. In addition, they also offer a possibility of carrying out LS, after rejection of outliers, with a small error [11].

In all of the papers cited the linear robust regression was considered, i.e., two parameters a_0 and a_1 were estimated in the following model:

$$Y(y) = a_0 + a_1 X(x) \quad (1)$$

where X and Y denote the independent and dependent variables and x and y are input and output experimental data, respectively. This means that only the linear relationship between y and x data or, at most, the linear relationship between the non-parametric functions of them {e.g., $y = a_0 \exp(-a_1 x)$ [8]} could be taken into account in the calibration procedure. However, it is widely known that more complex non-linear calibration dependences may occur in FAAS in some cases at least, e.g., if the observations in a relatively wide range of concentrations of an analyte are made, or if an interference effect taking place in the analytical system assayed is out of proportion to the analyte concentrations or if procedures based on a dilution process [1–3] are used for calibration.

In this work the simple robust methods, namely the single median and repeated median methods, were extended to adapt some non-linear three-parametric models of more versatile form than that of the model in Eqn. 1. The resistance of the methods considered to the presence of outliers is shown on the basis of an example of hypothetical data and calibration data obtained in practice in the cases of non-linearity mentioned above. The efficiency and practical advantages of the approach proposed are presented and discussed.

METHODOLOGY

Functions

The functions accepted for the robust regression procedures proposed here are all three-parametric functions F:

$$y = F(x; a_0, a_1, a_2) \quad (2)$$

which can be transformed into the following general form:

$$Y(x, y) = A_0 + A_1 X(x, A_2) \quad (3)$$

where the parameters A_0, A_1 and A_2, depend-

TABLE 1

Non-linear calibration models for robust regression

$y = F(x; a_0, a_1, a_2)$	$Y(x, y)$	A_0	A_1	A_2	$Y = A_0 + A_1 X(x, A_2)$	
$y = a_0 + a_1 x + a_2 x^2$	y	a_0	a_1	$\frac{a_2}{a_1}$	$Y = A_0 + A_1(x + A_2 x^2)$	(a)
$y = a_0 \exp\left[-\left(\frac{a_1 - x}{a_2}\right)^2\right]$	$\ln y$	$\ln\left(a_0 - \frac{a_1^2}{a_2^2}\right)$	$\frac{2a_1}{a_2^2}$	$-\frac{1}{2a_1}$	$Y = A_0 + A_1(x + A_2 x^2)$	(b)
$y = \frac{a_0 + a_1 x}{1 + a_2 x}$	y	a_0	$a_1 - a_0 a_2$	a_2	$Y = A_0 + A_1\left(\frac{x}{1 + A_2 x}\right)$	(c)
$y = \frac{a_0 x + a_1 x^2}{a_2 x - 1}$	$\frac{y}{x}$	$-a_0$	$-a_1 - a_0 a_2$	$-a_2$	$Y = A_0 + A_1\left(\frac{x}{1 + A_2 x}\right)$	(d)

ing on a_0, a_1 and a_2 only, are estimators of the intercept, the slope of the regression line in the coordinate system Y vs. X and the curvature of this line in the coordinate system y vs. x, respectively.

Some examples of the model in Eqn. 2 are presented in Table 1; all of them are frequently used for calibration purposes in AAS. The most popular function is that of a simple parabolic form [(a) in Table 1]. The hyperbolic model in the form (c) has been used [1,13] because it is able to reflect the calibration dependences most accurately, especially when they are distorted by an interference effect. A more complex function (d) has been included in the calibration algorithms of Perkin-Elmer spectrometers [14].

The characteristic propriety of the model in Eqn. 3 is the creation of the possibility of calculating the parameters A_0, A_1 and A_2 successively one after another on the basis of experimental data x and y. The parameter A_2 can be calculated for every three different data points (x_i, y_i), (x_j, y_j) and (x_k, y_k) from the equation

$$\frac{X_k[x_k, (A_2)_{ijk}] - X_i[x_i, (A_2)_{ijk}]}{X_j[x_j, (A_2)_{ijk}] - X_i[x_i, (A_2)_{ijk}]} = \frac{Y(x_k, y_k) - Y(x_i, y_i)}{Y(x_j, y_j) - Y(x_i, y_i)} \quad (4)$$

which is a particular form of Eqn. 3. For instance, for the pairs of functions (a), (b) and (c), (d) given in Table 1, the parameter A_2 is defined respectively as

$$(A_2)_{ijk} = \frac{S_{ijk}(x_j - x_i) - (x_k - x_i)}{(x_k^2 - x_i^2) - S_{ijk}(x_j^2 - x_i^2)} \quad (5)$$

$$(A_2)_{ijk} = \frac{S_{ijk}(x_j - x_i) - (x_k - x_i)}{x_j(x_k - x_i) - S_{ijk}x_k(x_j - x_i)} \quad (6)$$

where $S_{ijk} = (Y_k - Y_i)/(Y_j - Y_i)$. Having estimated the value of A_2, the parameter A_1 can be calculated for every pair of data points (x_i, y_i) and (x_j, y_j):

$$(A_1)_{ij} = \frac{Y_j(x_j, y_j) - Y_i(x_i, y_i)}{X_j(x_j, A_2) - X_i(x_i, A_2)} \quad (7)$$

Consequently, for given A_1 and A_2 the parameter A_0 is calculated for every point (x_i, y_i) from the equation

$$(A_0)_i = Y_i(x_i, y_i) - A_1X_i(x_i, A_2) \quad (8)$$

Median methods

The general concept of the regression methods considered is to use the median as an estimator of parameters A_0, A_1 and A_2 in the model in Eqn. 3. The median of set of m values, ordered from the lowest to the highest, is defined as the mean of the $m/2$th and $m/2 + 1$th rank if m is even or the value of the $(m + 1)/2$th rank if m is odd.

According to the single median (SM) method, the parameter A_2 is proposed to be estimated as the median of set of values $(A_2)_{ijk}$ calculated according to Eqn. 4 with the use of all possible combinations (without repetitions) of three data points (x_i, y_i), (x_j, y_j), (x_k, y_k) taken from all of n data points:

$$A_2 = \underset{1 \le i < j < k \le n}{\text{med}} (A_2)_{ijk} \quad (9)$$

Then, all combinations of data (x_i, y_i) and (x_j, y_j), in addition to A_2 evaluated above, are used for the calculation of $(A_1)_{ij}$ values according to Eqn. 11 and the median is chosen again as A_1:

$$A_1 = \underset{1 \le i < j \le n}{\text{med}} (A_1)_{ij} \quad (10)$$

Finally, A_0 is estimated as the median of all values $(A_0)_i$ calculated from Eqn. 8 on the basis of the evaluated A_1, A_2 and all single experimental data (x_i, y_i):

$$A_0 = \underset{1 \le i \le n}{\text{med}} (A_0)_i \quad (11)$$

In the repeated median (RM) method, the parameters $(A_1)_{ij}$ and $(A_2)_{ijk}$ are calculated from Eqns. 7 and 4, respectively, according to a procedure different from that for the SM method. In order to estimate A_2, the set of $(A_2)_{ijk}$ values is created for the experimental point i and the pairs of other data j, k (j, $k \neq i$) combined with each other without repetition. This is carried out for all points i ($i = 1, n$). Thus n medians are ob-

TABLE 2

Formulation of the hyperbolic model (c) from Table 1 according to the SM procedure [experimental data: (0.0, 0.0); (1.0, 1.4), (2.0, 3.9), (3.0, 13.0) and (4.0, 11.6)]

A_2			A_1			A_0		
i, j, k	$(A_2)_{ijk}$	Median	i, j	$(A_1)_{ij}$	Median	i	$(A_0)_i$	Median
1, 2, 3	−0.22		1, 2	1.04		1	0.00	
1, 2, 4	−0.25		1, 3	0.95		2	0.16	
1, 2, 5	−0.15		1, 4	0.99		3	0.09	0.16
1, 3, 4	−0.26		1, 5	−0.09		4	0.84	
1, 3, 5	−0.12	−0.26	2, 3	0.90	0.92	5	136.58	
1, 4, 5	−1.02		2, 4	0.98				
2, 3, 4	−0.27		2, 5	−0.07				
2, 3, 5	−0.10		3, 4	1.01				
2, 4, 5	−0.63		3, 5	−0.06				
3, 4, 5	−0.44		4, 5	−0.01				

tained and the median of these medians is the repeated median being an evaluation of A_2:

$$A_2 = \underset{1 \le i \le n}{\text{med}} \; \underset{\substack{1 \le i \le n \\ 1 \le j < k \le n \\ (j,\, k \ne i)}}{\text{med}} \; (A_2)_{ijk} \tag{12}$$

Similarly, the medians are calculated for n sets of $(A_1)_{ij}$ values which are obtained on the basis of every datum i and all other data j $(j \neq i)$. The median of these medians gives an estimation of $(A_1)_{ij}$:

$$A_1 = \underset{1 \le i \le n}{\text{med}} \; \underset{\substack{1 \le i \le n \\ 1 \le j \le n \\ (j \ne i)}}{\text{med}} \; (A_1)_{ij} \tag{13}$$

TABLE 3

Formulation of the hyperbolic model (c) from Table 1 according to the RM procedure [experimental data: (0.0, 0.0); (1.0, 1.4), (2.0, 3.9), (3.0, 13.0) and (4.0, 11.6)]

A_2				A_1				A_0		
i, j, k	$(A_2)_{ijk}$	Median	Median	i, j	$(A_1)_{ij}$	Median	Median	i	$(A_0)_i$	Median
1, 2, 3	−0.22			1, 2	1.06			1	0.00	
1, 2, 4	−0.25			1, 3	1.01					
1, 2, 5	−0.15			1, 4	1.20	1.04				
1, 3, 4	−0.26	−0.24		1, 5	0.10					
1, 3, 5	−0.12									
1, 4, 5	−1.02									
2, 1, 3	−0.22			2, 1	1.06			2	0.05	
2, 1, 4	−0.25			2, 3	0.98					
2, 1, 5	−0.15			2, 4	1.22	1.02				
2, 3, 4	−0.27	−0.24		2, 5	0.09					
2, 3, 5	−0.10									
2, 4, 5	−0.63									
3, 1, 2	−0.22			3, 1	1.01			3	−0.05	0.00
3, 1, 4	−0.26			3, 2	0.98					
3, 1, 5	−0.12			3, 4	1.30	1.00	1.02			
3, 2, 4	−0.27	−0.24	−0.24	3, 5	0.07					
3, 2, 5	−0.10									
3, 4, 5	−0.44									
4, 1, 2	−0.25			4, 1	1.20			4	1.93	
4, 1, 3	−0.26			4, 2	1.22					
4, 1, 5	−1.02			4, 3	1.31	1.21				
4, 2, 3	−0.27	−0.35		4, 5	−0.01					
4, 2, 5	−0.63									
4, 3, 5	−0.44									
5, 1, 2	−0.15			5, 1	0.10			5	−101.46	
5, 1, 3	−0.12			5, 2	0.09					
5, 1, 4	−1.02			5, 3	1.31	0.09				
5, 2, 3	−0.10	−0.29		5, 4	−0.01					
5, 2, 4	−0.63									
5, 3, 4	−0.44									

The parameter A_0 is calculated from Eqn. 11 in the same way as for the SM method.

EXPERIMENTAL

The real calibration graphs for Sr, Mn, Pb, Cd and Ca which are presented in this paper were prepared from Titrisol (Merck) stock solutions in either 1% v/v HNO_3 or 1% v/v HCl. Aluminium at a concentration of 300 μg ml^{-1} was added to the standards of Sr in order to match the standards to the samples. Doubly distilled water was used throughout.

Measurements were carried out on Perkin-Elmer 3100 and AAS-1 (Zeiss, Jena) atomic absorption spectrometers under conditions specific for each element determined. An air–acetylene flame was used in all experiments.

In order to prepare the working solutions according to the calibration methods based on the dilution procedure, a laboratory constructed device [15] was adapted and controlled by a ZX Spectrum (Sinclair) microcomputer.

The program for the non-linear regression methods (LS, SM and RM) was written in QUICK-BASIC for IBM microcomputers.

RESULTS AND DISCUSSION

To make both SM and RM procedures of non-linear regression clearer, the results of calculations of the parameters A_0, A_1 and A_2 in the hyperbolic model (c) in Table 1 are presented in Tables 2 and 3. Figure 1 illustrates the SM and RM calibration graphs and the graph resulting from the approximation by the LS method. It is seen that the median procedures identify the fifth point as an outlier, hence this point is ignored completely, while the other points lie correctly on the SM and RM lines. In contrast all points have been considered by the LS method according to minimizing the sum of the squares of all residuals; as a result the LS line is strongly shifted towards the outlier and fits the other points very badly.

The data in Tables 2 and 3 reveal the efficiency of the median procedures proposed. It can be observed that the values $(A_2)_{ijk}$, $(A_1)_{ij}$ and $(A_0)_i$ calculated on the basis of points 1, 2, 3 and 4 are relatively similar to each other and considerably different from the values corresponding to point 5. Among the values $(A_2)_{ijk}$ and $(A_1)_{ij}$ to which point 5 has contributed, those calculated with point 4 are different from those calculated without this point. Additionally, the value $(A_0)_4$ is clearly greater than $(A_0)_1$, $(A_0)_2$ and $(A_0)_3$. Hence point 5 is revealed definitely as an outlier and point 4 can be suspected to be outlier to a lesser extent. This situation is detected very well when the median is used as an estimator of the parameters A_0, A_1 and A_2: both median methods give rise to rejection of the values $(A_0)_4$ and $(A_0)_5$ and the values $(A_2)_{ijk}$ and $(A_1)_{ij}$ which are disturbed by point 5, and by points 4 and 5 together. As a consequence, the SM and RM calibration graphs fit the first three points excellently, point 4 is a slightly neglected and point 5 is ignored completely.

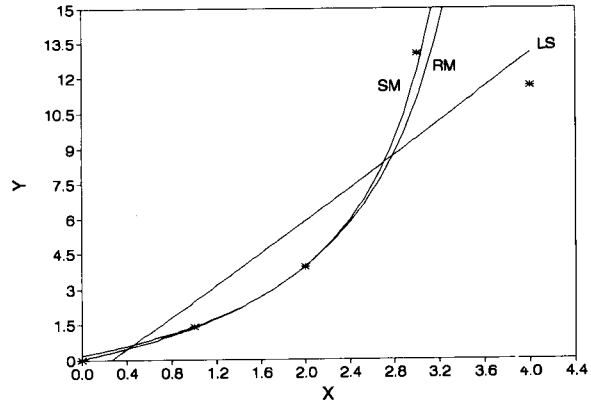

Fig. 1. Examples of calibration lines (hypothetical data given in Tables 2 and 3) obtained by SM, RM and LS methods.

Generally, five points are not always sufficient to reject a single outlier with the aid of the median non-linear procedures proposed. It can be seen from Tables 2 and 3 that the number of values $(A_2)_{ijk}$ calculated with the use of a given point is five from among ten values calculated in the SM method and three from among six values calculated in four (from among five) groups of numbers taken for first evaluation of medians in

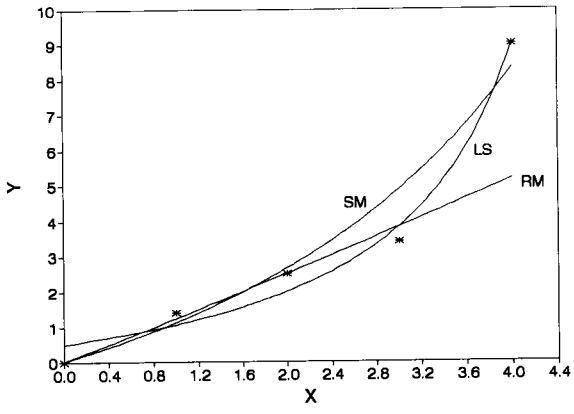

Fig. 2. Examples of calibration lines [hypothetical data: (0.0, 0.0), (1.0, 1.4), (2.0, 2.5), (3.0, 3.4), (4.0, 9.0)] obtained by SM, RM and LS methods.

the RM method. Thus, in a possible situation when all values $(A_2)_{ijk}$ corresponding to an outlier are greater or less than the remaining curvatures, one of them takes part in the calculation of a median and thereby the resulting value A_2 is contaminated by the outlier. This leads to an erroneous estimation of the values A_1 and A_0 giving as a result a calibration line shifted to a greater or lesser extent towards the outlier. Of course, it can be happen that one of the median methods considered will provide a better approximation than the other or each of them will identify the other point as an outlier. The last possibility is shown in Fig. 2, based on the example of some hypothetical data.

The examples presented in Figs. 1 and 2 deal with rather exceptional and extreme situations when five experimental points are taken into consideration (in FAAS more observations are usually made, especially when a non-linear calibration line is expected) and they are distributed in such a manner that the proper detection of an outlier is difficult. However, it is very important from a practical point of view that irrespective of the number and position of outlier(s) recognized by both SM and RM, the graphs, in contrast to LS graphs, fit some of points correctly. This means that even in such difficult cases the median methods are able to give more accurate analytical

TABLE 4

Minimum number of experimental points required by SM and RM linear (L) and non-linear (NL) regression procedures to ignore the outliers

No. of outliers	SM		RM	
	L	NL	L	NL
1	5	7	4	6
2	8	11	6	9
3	11	16	8	12
4	15	21	10	16

results (when using some part of a graphs for calibration) than LS.

The minimum number of experimental points that are needed to be certain that one or more outliers do not contaminate the parameters A_0, A_1 and A_2 in the non-linear model in Eqn. 3 formulated with the use of both median methods are presented in Table 4 (for comparison, the corresponding data dealing with linear regression are also given). It should be stressed that the numbers shown are valid only when all curvatures $(A_2)_{ijk}$ produced by outliers are different from other partial curvatures of the calibration line, i.e., when all experimental points except outliers are distributed in good accordance with the non-linear model assumed. This can be achieved more

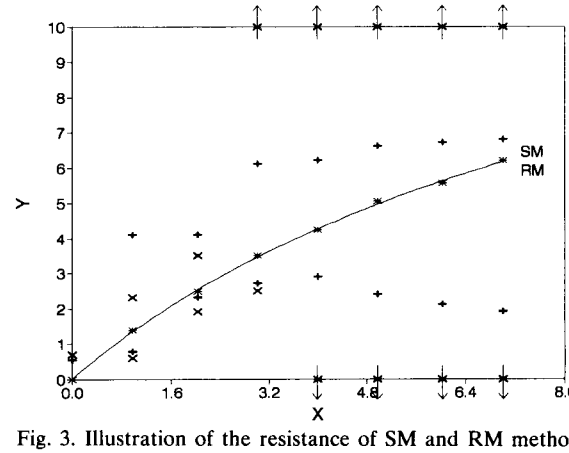

Fig. 3. Illustration of the resistance of SM and RM methods to outliers: plus and cross signs denote the new positions of some hypothetical data (asterisks) changing the QC (Eqn. 14) of SM and RM calibration graphs, respectively, from 1% to 5%.

easily when both the non-linearity of the calibration graph and random fluctuations of the experimental points are less.

The resistance of the non-linear methods proposed to the effect of outliers may be expected to depend on the position of an outlier in relation to the calibration graph. This effect was examined in the model example presented in Fig. 3. It illustrates the SM and RM hyperbolic curves (overlapped with each other) fitting a set of eight points, where the first and last points lie on the lines exactly while the points 2–7 are situated alternately on both sides of the curves with residuals increasing proportionally to the responses Y. The "goodness" of the approximation was estimated with the use of a quality coefficient (QC) [16], defined as

$$QC = \left[\frac{\sum_{i}^{N} \left(\frac{Y_i - \hat{Y}_i}{Y_i} \right)^2}{N - 1} \right]^{1/2} \qquad (14)$$

where Y_i and $\hat{Y}_i$ are the responses measured at each datum and those predicted by model (c) in Table 1, respectively, and N is the number of all data points. In the case presented in Fig. 3, $QC = 1\%$. Now an attempt was made to find the new positions of each individual point (considered at this moment as an outlier) below and above the calibration line giving rise to disturbances of both the SM and RM models to such extent that the QC (calculated without this residual corresponding to the outlier) was increased from 1% to 5%, which is a value still quite acceptable in FAAS.

Considering the results obtained, it is interesting that the outlier's position allowed in relation to the calibration line can be so different. The picture shown depends on such factors such as the degree of curvature of the line and the distribution of the points along this line, so it certainly differs in detail in any particular case considered. However, some rules seem to be valid. First, it is seen again that the resistance of the RM method to outliers is generally greater than that revealed by the SM method. This is evident particularly in the region of high concentrations, where the outlier is rejected by the RM method irrespective of the location related to the calibration line. This is especially important as the probability of finding an outlier among the high analytical signals is greater than that among those signals corresponding to relatively low concentrations of an analyte. The resistance of the SM method to the outlier seems to become larger with increasing concentration, but only when the point rejected is situated below the calibration line, i.e., on the side that corresponds with the direction of curvature of this line. However, one should be very careful of using the SM method when the outlier does appear on the other side of the line among the last experimental points.

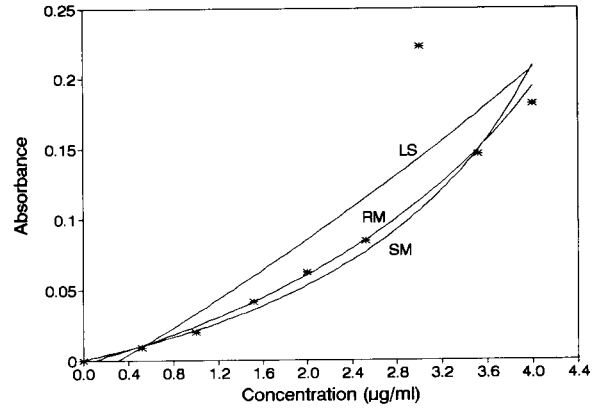

Fig. 4. Calibration lines obtained by SM, RM and LS methods from standards containing Sr in the presence of Al (300 μg ml^{-1}).

In Figs. 4–8 some selected examples of the effective application of both the SM and RM non-linear procedures to the construction of real calibration graphs are presented. In all instances of non-linear approximation the hyperbolic function (c) in Table 1 was used.

Figure 4 is an illustration of the situation where a strongly non-linear configuration of the experimental points is caused by the presence of the interferent added in the same amount to each of standard solutions. The case considered is similar to that shown in Fig. 1 except for a greater number of data, sufficient to identify the outlier beyond any doubt. The point situated very far

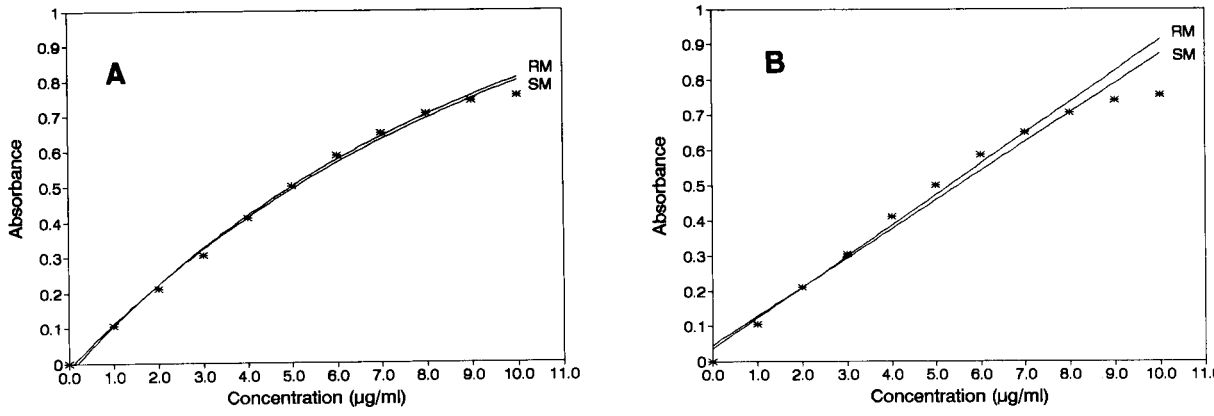

Fig. 5. Calibration lines for Mn obtained by SM and RM methods based on (A) non-linear and (B) linear procedures.

from the remaining ones (presumably because of some error in the preparation of the standard solution) is easily rejected using both of the median methods proposed. In spite of the larger number of data produced (in Fig. 1), the LS curve is still strongly shifted towards the outlier, giving almost a linear approximation of the calibration dependence. As a consequence, the concentrations calculated from this curve must be expected to be much less accurate than those obtained from SM and RM curve.

Figure 5 gives an example where some of data points are outside the linear range of the calibration graph. Both of the non-linear median procedures used (Fig. 5A) do not reflect this complex shape of the curve but they fit almost all points very exactly in fact. Only one point is identified as an outlier in a region which is not practically useful for calibration. For comparison, the straight SM and RM lines based on the same data were also constructed (Fig. 5B); it is seen that they do not detect the partial linearity of the calibration graph and give the wrong approximation over the entire experimental range.

Figure 6 exemplifies another problem that can frequently occur during calibration, namely the experimental points have been produced in the linear range of the calibration dependence but two of these points were measured wrongly. As a result, the distribution of data may seem to be

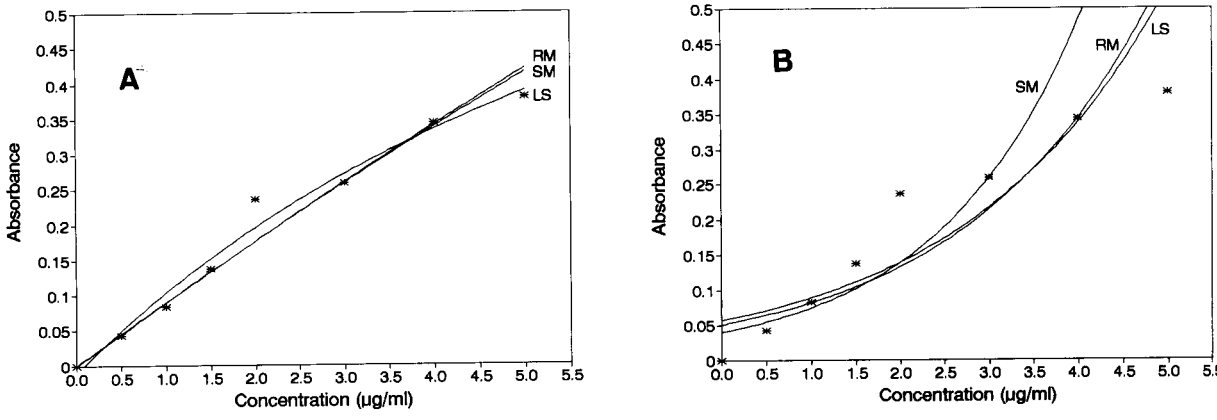

Fig. 6. Calibration lines for Pb obtained by SM, RM and LS methods based on non-linear procedures with (A) hyperbolic [(c) from Table 1] and (B) exponential [$y = a_0 \exp(-a_1 x)$] models.

non-linear, leading to a non-linear approximation. When the LS hyperbolic model is used for this purpose (Fig. 6A) the calibration behaves unsatisfactorily because it is strongly affected by the outliers and becomes too curved. Both the SM and RM hyperbolic models identify the outliers correctly and recognize the linearity of the calibration dependence very well.

As a matter of curiosity, a suggested two-parametric model [8], $y = a_0 \exp(-a_1 x)$, was found to fit the set of points presented in Fig. 6A. After linearization of this model to the form $Y = A_0 + A_1 x$ (where $Y = \ln y$, $A_0 = \ln a_0$ and $A_1 = -a_1$), all three regression methods investigated (LS, SM and RM) were used in their linear mode for estimating the parameters A_0 and A_1. The results of the modelling performed are depicted in Fig. 6B; it is seen that the function considered is evidently too simple to be a useful tool for approximation even when the non-linearity of the calibration graph is very small, as in the example considered.

The question of choice of either a linear or non-linear approximation is also illustrated in Fig. 7. It seems that the data points follow a linear relationship exactly and they do not contain any outlier. In fact, the SM and RM linear models shown in Fig. 7A are found to be acceptable with $QC = 4.6\%$ and 4.8%, respectively. Although some of points are placed beyond the lines they cannot be considered as outliers. What happens when the SM and RM non-linear procedures are then used for the same set of data points can now be observed in Fig. 7B: the hyperbolic models are followed excellently by almost all points except one, which is clearly detected as an outlier. If this point is not taken into account in the QC test, a value of 1.7% is obtained in both instances (SM and RM), but even if the outlier is included values of 5.2% and 4.8%, respectively, are calculated comparable to those corresponding to the linear approximation. Hence it can be concluded that the calibration dependence investigated should be considered rather as non-linear with a single outlier than as linear without outliers.

In Figs. 8 and 9 the relationships between the apparent concentration and the relative dilution are shown which are approximated in calibration methods based on a dilution process, such as the dilution method [1,17] and the addition and successive dilution method [2]. The resulting calibration graphs are usually non-linear because the interference effect is successively eliminated or compensated for during dilution of a sample. They are extrapolated to the concentration axis, allowing an estimate of the concentration of an analyte from the intercept.

The critical feature of the methods considered is the necessity to perform determinations at a sample even more than tenfold diluted, i.e., in the region defined by a relative dilution of less than 0.1 where the analytical signals are usually measured with relatively large fluctuations.

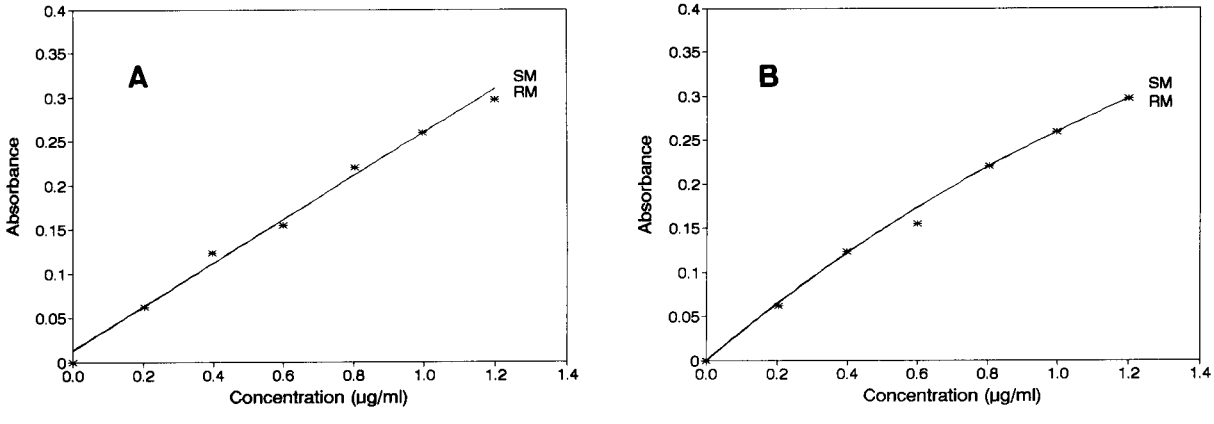

Fig. 7. Calibration lines for Cd obtained by SM and RM methods based on (A) linear and (B) non-linear procedures.

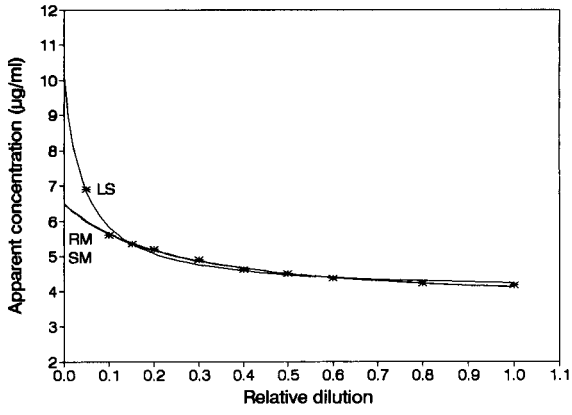

Fig. 8. Calibration lines obtained by SM, RM and LS methods during the determination of Ca (7 μg ml^{-1}) in the presence of Al (80 μg ml^{-1}) in a synthetic sample by the dilution method.

Therefore some of the experimental points obtained in that region can be especially suspected to be outliers. On the other hand, that particular region is also especially important regarding the extrapolation process. The determination error than can then be produced when even a single outlier is not rejected in such an instance can be seen in the example presented in Fig. 8: the LS model leads to the result of 10.1 μg ml^{-1} whereas the SM and RM models give concentrations 6.5 and 6.4 μg ml^{-1}, respectively, which are much closer to the true analyte concentration (7.0 μg ml^{-1}).

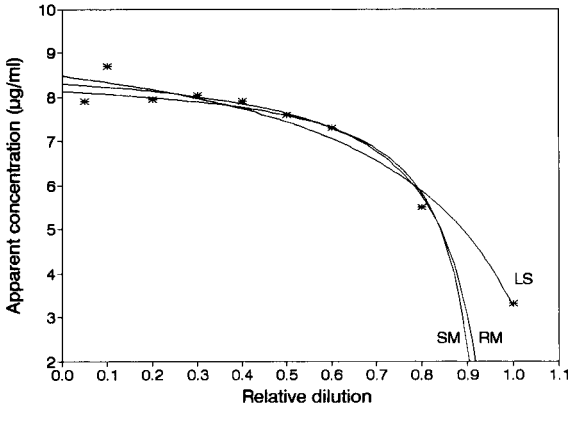

Fig. 9. Calibration lines obtained by SM, RM and LS methods during the determination of Ca (8 μg ml^{-1}) in the presence of Ti (100 μg ml^{-1}) in a synthetic sample by the addition and successive dilution method.

In the addition and successive dilution method (Fig. 9), this critical part of the calibration graph being extrapolated can be expected to be more linear and hence more easily approximated than previously [2]. However, the additional problem may occur when a too concentrated sample is diluted, producing strong non-linearity during the first steps of the dilution process, i.e., in the region of less significance for the calculation of analytical results. As is seen, the use of the SM and RM median non-linear procedures allows one to ignore a point in the region mentioned and to reject a point placed near the concentration axis, giving results (8.1 and 8.3 μg ml^{-1}) that are more accurate than the value (8.5 μg ml^{-1}) obtained with the LS method for a true concentration of the analyte of 8.0 μg ml^{-1}.

Conclusions

Most of the advantages of the robust regression methods based on the median that have been reported previously [8–12] have been confirmed in this work. They are simple and easy mathematical tools providing the possibility of detecting and rejecting outliers. These fundamental features, which are important for calibration purposes, have been preserved in the modified versions of the median methods proposed here. In the present state both the SM and the RM methods can be effectively used in all those instances when the calibration relationships appear to be non-linear irrespective of the reasons for this effect. The algorithm presented can be also easily adapted to some other median approaches, e.g., the method of the least median of squares (LMS) [6,7].

The resistance of non-linear median procedures to the effect of outliers depends on the relationship of the total number of experimental points to the number of outliers suspected. However, it was proved (see Table 4) that the total number of data required to gain a proper non-linear approximation is not much greater than that corresponding to the linear regression and can be accepted in practice even if three outliers are expected to be rejected. Other important factors influencing the efficiency of the proposed methods are a particular position of an outlier in

relation to the calibration line and certainly the curvature of this line and the non-linear function used in modelling. Some of them were investigated here but further research would be needed in order to obtain more valuable information.

The general conclusion seems to be that the RM non-linear method is more robust than SM, i.e., the probability of rejecting outliers from a given set of points is greater when the RM method rather than the SM method is used. Both methods needed sorting procedures, which is relatively time consuming. In spite of the different algorithms the computing time is generally comparable in both instances and it is acceptable even if a relatively large number of data points are produced during calibration (less than 5 s for a calibration graph of ten points on an IBM/AT 16-MHz computer). Taking the above into consideration, the RM method is to be preferred over the SM method.

Some examples have been presented in which the median non-linear procedures were applied to FAAS determinations, giving a better approximation of real calibration relationships than the LS method. However, it seems that the median methods cannot be fully recommended in place of LS in routine analysis. So many possibilities of varied distributions of the experimental points creating a calibration graph can occur that in some situations (especially when only a few points are produced but all with great random fluctuations) it could be very difficult to state if a given point is an outlier and should be rejected or not. Wrong decisions can be followed by more serious consequences than when using an in appropriate regression procedure for linear approximation. Therefore, it is suggested that both RM and LS calibration graphs should always be constructed based on the same set of data. The decision as to which graph should be used for analysis should then be taken on the basis not only of some statistical approach (e.g., calculating the QC values) but also of intuition, which seems still to be an irreplaceable criterion in some of the most difficult cases.

REFERENCES

1 P. Kościelniak, Univ. Iag. Acta Chim., in press.
2 L. Pszonicki and W. Skwara, Talanta, 36 (1989) 1265.
3 M. Sperling, Z. Fang and B. Welz, Anal. Chem., 63 (1991) 151.
4 H. Theil, Ned. Akad. Proc. Ser. A, 53 (1950) 386, 521 and 1397.
5 A.F. Siegel, Biometrica, 69 (1982) 242.
6 A.E. Beaton and J.W. Tukey, Technometrics, 16 (1974) 147.
7 P.J. Rousseuw and A.M. Leroy, Robust Regression and Outlier Detection, Wiley, New York, 1987.
8 G.R. Phillips and E.M. Eyring, Anal. Chem., 55 (1983) 1134.
9 S.C. Rutan and P.W. Carr, Anal. Chim. Acta, 215 (1988) 131.
10 K. Danzer, Fresenius' Z. Anal. Chem., 335 (1989) 869.
11 Y. Hu, J. Smeyers-Verbeke and D.L. Massart, J. Anal. At. Spectrom., 4 (1989) 605.
12 R. Wolters and G. Kateman, J. Chemometr., 3 (1989) 329.
13 P. Kościelniak, Mikrochim. Acta, II (1984) 369.
14 Analytical Methods for Atomic Absorption Spectrometry, Perkin-Elmer, Norwalk, CT, 1982.
15 P. Kościelniak, Chem. Anal. (Warsaw), 34 (1989) 343.
16 J. Knegt and G. Stork, Fresenius' Z. Anal. Chem., 270 (1974) 97.
17 A. Shatkay, Anal. Chem., 40 (1968) 2097.

Analytica Chimica Acta, 278 (1993) 189–196
Elsevier Science Publishers B.V., Amsterdam

Determination of mercury in urine by flow-injection cold vapour atomic absorption spectrometry

Tiezheng Guo and Jörn Baasner

Atomic Absorption Product Department, Bodenseewerk Perkin-Elmer GmbH, Postfach 101164, D(W)-7770 Überlingen (Germany)

(Received 21st October 1992; revised manuscript received 4th January 1993)

Abstract

A simple, rapid and accurate method was developed for the determination of total mercury in urine samples. The method uses on-line addition of $KMnO_4$ after adding a bromate–bromide reagent to the sample to decompose organic mercury compounds to inorganic mercury(II) ions at room temperature, and determines mercury by flow-injection cold vapour atomic absorption spectrometry. The recoveries of five mercury compounds added to urine were studied; with the proposed method the recoveries of all the mercury compounds used were complete. Good agreement with certificate values of urine reference materials was also obtained. The detection limit of the method based on three standard deviations of the blank was 0.1 μg Hg l^{-1} in urine with a 500-μl sample loop, achieving a sample throughput of 100 h^{-1}. The calibration graphs were linear up to 30 μg l^{-1} and with a dynamic range up to 100 μg Hg l^{-1}. At a concentration of 5 μg Hg l^{-1} in urine, the relative standard deviation was about 2%.

Keywords: Atomic absorption spectrometry; Flow injection; Mercury; Urine

The determination of the mercury level in various biological matrices, in particular in blood and urine, is recommended as a means of estimating the degree of mercury contamination at the workplace and in the environment [1]. A knowledge of "normal" mercury levels is of importance in the evaluation of the mercury concentration in body fluids. According to Angerer and Schaller [1], these levels are currently given as less than 5 μg l^{-1} (in both blood and urine). The average mercury levels in the general population are less than 1 μg l^{-1} in blood or urine [1].

For the toxicological evaluation of the mercury levels in the blood and urine of occupationally exposed persons, BAT values (biological tolerance values of working materials) are available. The BAT values for exposure to inorganic mercury compounds or metallic mercury are 50 μg l^{-1} in blood and 200 μg l^{-1} in urine [1].

It is generally agreed that oxidative conversion of all forms of mercury in the sample to Hg(II) is necessary prior to reduction to elemental Hg [2–6]. A wide variety of combinations of strong acids (HCl, H_2SO_4, HNO_3), oxidants (H_2O_2, $KMnO_4$, $K_2Cr_2O_7$, $K_2S_2O_8$), UV irradiation and elevated temperatures have been used and recommended [2–11]. The main concerns are the loss of mercury during elevated temperature digestion procedures, contamination and the problem with using a large amount of any reagent during pretreatment which gives rise to increased blank values and deteriorated detection limits.

In the method described here, organic mercury compounds are decomposed by using a bromate–bromide reagent and $KMnO_4$ together. The samples need only limited manipulation and then the addition of $KMnO_4$ and the measurement of total mercury are completed automatically with a

Correspondence to: T. Guo, Atomic Absorption Product Department, Bodenseewerk Perkin-Elmer GmbH, Postfach 101164, D(W)-7770 Überlingen (Germany).

flow-injection system with cold vapour atomic absorption spectrometric detection. The whole process is carried out at room temperature.

EXPERIMENTAL

Apparatus

A Perkin-Elmer Model 2100 atomic absorption spectrometer in conjunction with a Perkin-Elmer FIAS-200 flow injection instrument and AS-90 autosampler were used in this study. The system was operated through an Epson EL 3s personal computer and the associated software, version 9.0. An LQ-850 + printer was used to print out the results and signal traces.

Figure 1 shows the set-up of the FIAS-200 for the on-line addition of $KMnO_4$. The flow-rates of $NaBH_4$ and $KMnO_4$ were each 6.2 ml min^{-1}; the colour codes of the pump tubes used were red–red. The flow-rates of the carrier solution and the sample solution were each 10 ml min^{-1}; the colour codes of the pump tubes used were blue–yellow. The carrier gas used was argon and the flow-rate was 110 ml min^{-1}. Details of the connecting tubes employed and other information can be found in the recommended conditions in the FIA manual [12] provided by the manufacture. A filter was placed between the gas–liquid separator and the quartz cuvette; it can prevent aerosol droplets from entering the cuvette and improve the measurement precision.

TABLE 1

FIAS-200 programme [a]

Step No.	Time (s)	Pump 1 (rpm)	Pump 2 (rpm)	Valve	Read
1	10	100	120	Fill	
2	20		120	Inject	0

[a] Cell temperature = 200°C; prefill time = 10 s.

The FIAS-200 program used is given in Table 1. The prefill time was 10 s and the sampling time was 10 s, which was performed in step 1. Next the sample was injected into the carrier stream and then mixed with $KMnO_4$ and $NaBH_4$ solutions in sequence in the chemifold, after mixing with the carrier gas the reaction products (mercury vapour, hydrogen, etc.) and the remaining liquid as well as argon entered the gas–liquid separator. The gas phase was swept into an electrically heated quartz cell assembly maintained at 200°C, where the mercury vapour was measured. This process was completed in step 2 within 20 s.

Both a Perkin-Elmer hollow-cathode lamp (operated at 4 mA) and a Perkin-Elmer electrodless discharge lamp (EDL) (system I, operated at 6 W) were used as the primary light sources. For the measurement of detection limits the EDL was used. The measurement was carried out at 253.6 nm with a slit width of 0.7 nm (low). An integration time of 20 s and the peak-height measurement (0.5 peak height) mode were used.

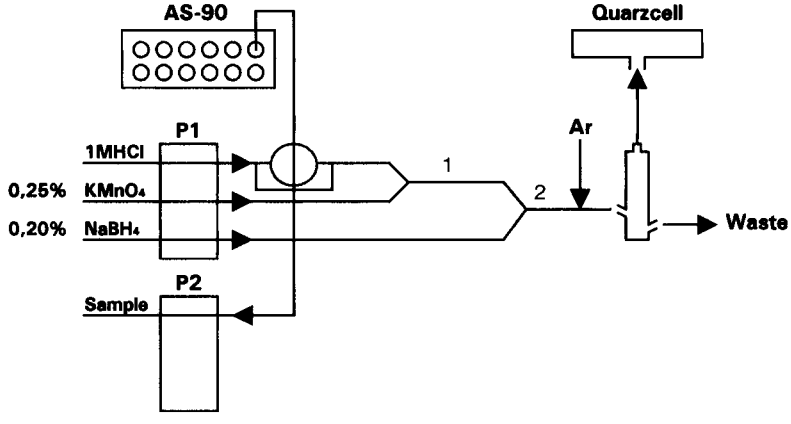

Fig. 1. FIAS-200 set-up for on-line addition of $KMnO_4$.

Reagents and solutions

All chemicals were of analytical reagent grade unless specified otherwise, and deionized water was used throughout.

Dow Corning DB 110A. Silicon antifoaming agent for FIAS/MHS analyses, Batch No. 9203, Part No. B050 7226 (Perkin-Elmer).

$NaBH_4$ solution. A 0.2% (w/v) solution of $NaBH_4$ in 0.05% (w/v) NaOH was prepared. To 1 l of this solution 200 μl of Dow Corning DB 110A were added and shaken well. This solution must be freshly prepared every day.

$KMnO_4$ solution, 0.25% (w/v). This solution is kept in a dark brown bottle to prevent it from decomposing. Experience has shown that it is preferable to prepare this solution daily.

Bromate–bromide reagent. A 2-g amount of KBr and 0.56 g of $KBrO_3$ were dissolved in 25 ml of deionized water. This solution should be prepared freshly every week [4].

Triton X-100 solution A 600-mg amount of Triton X-100 was dissolved in 50 ml of deionized water.

$K_2Cr_2O_7$ stabilizing solution, 0.5% (w/v). A 0.5-g amount of $K_2Cr_2O_7$ was dissolved in 100 ml of dilute (65%, w/v) HNO_3 (1 + 1).

Carrier solution. HCl (1 mol l^{-1}).

Carrier gas. Argon.

Calibration standards. A 1000 ml l^{-1} stock standard solution of mercury was prepared from Merk Titrisol reagent. A 10 mg Hg l^{-1} solution was prepared by taking 1 ml of the stock standard solution and 1 ml of stabilizing solution and diluting the mixture to 100 ml with water. This solution is stable for at least 6 months.

Calibration standards at different mercury levels were prepared from the stock standard solution by further dilution with 1 mol l^{-1} HCl. These working standard solutions should contain 1% (v/v) of the stabilizing solution [0.5% (w/v) $K_2Cr_2O_7$] and are stable for a few days; however, it is recommended that these solutions be prepared freshly every day.

Specimen collection

To prevent any exogenous contamination, all plastic bottles (Greiner Labortechnic) used for specimen collection must be cleaned with 1 mol l^{-1} nitric acid before use and then rinsed three times with ultrapure water and dried at room temperature.

Urine specimens were collected in clean plastic bottles, acidified with acetic acid (1 ml to 100 ml of urine) and then stored at 4°C until required for analysis [1]. In this study, both 24-h urine and spot urine specimens were collected for the test.

Precautions in preparing the flow-injection system

It is important to ensure that when $KMnO_4$ is flowing through the system, $NaBH_4$ is also flowing. This prevents the $KMnO_4$ solution from entering the system alone and forming hydrated manganese(IV) oxide, which remains in the gas–liquid separator and drastically reduces the mercury signal (see the discussion of $KMnO_4$ as an oxidizing agent). If MnO_2 does form in the system, then the system must be cleaned by pumping 5 mol l^{-1} HCl through it (see Determination of mercury in control urine samples). Therefore, it is suggested that before starting measurements $NaBH_4$ and carrier solution should be pumped through the respective channels while pumping water or air through the $KMnO_4$ channel. Pumping of $KMnO_4$ should only be started when the $NaBH_4$ and carrier channels are filled with solutions.

Recovery test

The following mercury compounds were used for the recovery test to check the efficiency of different oxidation reagents and their combinations on the decomposition of mercury compounds: MMC = methyl mercury chloride (CH_3HgCl); MA = mercury(II) acetate [$Hg(CH_3COO)_2$]; MS = mercurescein sodium ($C_{20}H_8Br_2HgNa_2O_6$); PMC = phenylmercury(II) chloride (C_6H_5HgCl); and MN = mercury(II) nitrate [$Hg(NO_3)_2$].

The solutions were prepared as described [6]. For the recovery tests, pooled urine samples from subjects unexposed to mercury were spiked with these mercury compounds at a level of 10 μg l^{-1}.

The recoveries of these tested organic and inorganic mercury compounds were measured using combinations of four $NaBH_4$ concentrations

0.4, 0.2, 0.1 and 0.05% (w/v) in 0.05% (w/v) NaOH, and four $KMnO_4$ concentrations, 0.5, 0.3, 0.1 and 0.05% (w/v).

Measurement

Place 5-ml aliquots of the urine specimens in 10-ml plastic test-tubes (Sarstedt), add 0.5 ml of HCl (32%, w/v), 0.2 ml of bromate–bromide reagent and 25 μl of Triton X-100 solution and mix well. These solutions are ready for analysis. The volume change of the sample due to the addition of the reagents to the samples should be taken into account; under the above-mentioned conditions, the measured value of mercury should be multiplied by a factor of 1.14 to obtain the actual concentration in the original sample.

Normally a 5-ml sample of the urine specimen is analysed to determine the level of mercury (three replicates). If the mercury level is too high (higher than 100 $\mu g\ l^{-1}$), the specimen must be diluted appropriately.

RESULTS AND DISCUSSION

Recovery test

Figure 2 shows the results of the recovery test on mercury compounds under different conditions: without any oxidizing reagent, with $KMnO_4$ or bromate–bromide reagent only and with both of them.

Use of $NaBH_4$ as reductant. Sodium tetrahydroborate(III) ($NaBH_4$) has been shown to be an effective reductant for both inorganic and organic forms of mercury. Some reports claim that $NaBH_4$ in combination with copper will allow the determination of total mercury without prior oxidative treatment [13,14]. Other workers have also shown

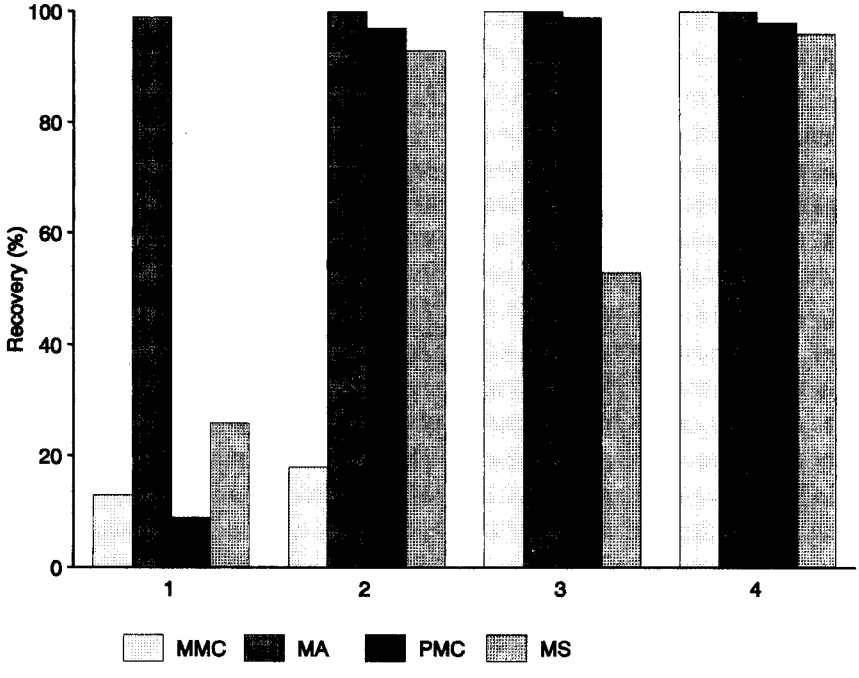

Fig. 2. Results of recovery tests on organic mercurials under various conditions. 1 = Without $KMnO_4$ and bromate–bromide reagent; 2 = bromate–bromide reagent only; 3 = 0.3% $KMnO_4$ only; 4 = with both $KMnO_4$ and Bromate–bromide reagent. All measurements used 0.2 (w/v) $NaBH_4$ as the reductant.

that $NaBH_4$ could more readily attack those organic mercury compounds which are not reduced to the metal by tin(II) chloride [15]. However, in a more recent study [6] it was found that $NaBH_4$ cannot reduce all organomercurials to elemental mercury equally. All the above-mentioned studies were based on the use of a batch system.

In this work the flow-injection (FI) technique was used. First $NaBH_4$ was used alone for the recovery test on organic mercury compounds in urine, and low results were found for MMC, PMC and MS (Fig. 2, signal groups 1). This is in contrast to the results of the work mentioned above [13,14]. The reasons are probably the lower $NaBH_4$ concentration, i.e., 0.2% (w/v) in this work as opposed to 3–5% in the batch system [6,13], and that the reaction time in the FI set-up is very short, of the order of a few tenths of a second, whereas in the batch system it is of the order of a few seconds.

On-line addition of $KMnO_4$. Potassium permanganate can oxidize many organic compounds, but it is also known that a number of organic compounds, e.g., phenylmercury(II) acetate and methylmercury chloride, are only partially oxidized by this reagent.

It was expected that using $KMnO_4$ and $NaBH_4$ together could be effective in decomposing most of the organic mercury compounds in samples such as urine. However, there are problems associated with the use of $KMnO_4$ if it is added to urine samples before the measurements are started. The most serious problem originates from the adsorption of mercury on hydrated manganese(IV) oxide, which forms a film on the surfaces of sample vessels, tubing and other manifold components [4]. In some instances e.g., for the measurement of mercury in water samples, hydroxylamine hydrochloride was used to dissolve the hydrated manganese oxide [5] and to remove excess of $KMnO_4$. However, by using the method of on-line addition of $KMnO_4$, the advantages of $KMnO_4$ as a powerful oxidant can be exploited while the problems mentioned above can be effectively avoided owing to the short residence time of the reaction mixture in the system. Under the conditions used here, the use of hydroxylamine hydrochloride to reduce the excess of MnO_4^-/Mn(IV) is not required, which makes the experimental set-up simpler.

The combinations of 0.1% $NaBH_4$ with 0.5% $KMnO_4$ and 0.05% $NaBH_4$ with 0.5% and 0.3% $KMnO_4$ did not work properly because of the relatively high concentration of $KMnO_4$ compared with $NaBH_4$, and the purple colour of the $KMnO_4$ solution did not totally disappear after mixing with the $NaBH_4$ solution, as in this instance the Hg(II) cannot be reduced to Hg(0). With all the other combinations the measurement proceeded properly.

It was found that the combination of $NaBH_4$ and $KMnO_4$ was very effective for the decomposition of MMC, MA and PMC. Even at a very low concentration of $KMnO_4$, e.g., 0.05%, the recoveries of these three compounds were 100% compared with aqueous standard solutions. However, the recovery of MS was only about 50% under the same conditions (Fig. 2, signal group 3).

It should be stressed that the reaction time between the sample and $KMnO_4$ and the time between the reaction mixture of sample and $KMnO_4$ and $NaBH_4$ depend on the dimensions of the connecting tubes in the system, i.e., tubes 1 and 2 in Fig. 1. In the present set-up both of these tubes have a length of 10 cm and a i.d. of 1 mm, which corresponds to a volume of about 0.08 ml. The residence time (or the reaction time) of the fluids in these tubes can be calculated approximately from the volume of these tubes and the flow-rate of the fluids through them. The calculated residence time of the solution in tube 1 is ca. 300 ms (the fluid flow-rate is ca. 16 ml min^{-1}) and that in tube 2 is ca. 220 ms (fluid flow-rate ca. 22 ml min^{-1}). This means that the decomposition of some organic compounds by $KMnO_4$ and $NaBH_4$ is very rapid. An increase in the length of tube 1, i.e., an increase in the reaction time between sample and $KMnO_4$, can improve the recovery of MS. In this work a 10 m × 0.9 mm i.d. tube was used and with the same fluid flow-rate as with tube 1 the residence time of the solution in this long tube was ca. 30 s. Under such conditions the recovery of MS could reach 100%; however, an increase in the residence time of sample and $KMnO_4$ in the tube will increase the risk of contamination of the

system by decomposition products of $KMnO_4$, i.e., hydrated manganese(IV) oxide. Therefore, the idea of using a long reaction tube to improve the recovery of MS was abandoned, also because it was found that the addition of bromate–bromide reagent was effective for the decomposition of MS (see below).

An interesting and reproducible observation during this work was the enhancement of the Hg(II) signal when $KMnO_4$ was added on-line. This proved to be another advantage of using $KMnO_4$. Despite the dilution of the sample plug in the carrier stream, which was unavoidable during the on-line addition process, the signal (both peak height and peak area) was increased rather than decreased when $KMnO_4$ was added. This effect if illustrated in Fig. 3. The reason for this phenomenon is not clear and further work is required to elucidate the chemistry of this enhancement effect.

Use of bromate–bromide reagent. The use of bromate–bromide reagent was first proposed by Farey and co-workers [10,11] for the determination of organic mercury in natural water in which bromate–bromide reagent in hydrochloric acid was used to generate bromine in the sample. Later it was also used by Welz et al. [4] for the determination of mercury in urine.

In this study it was found that the recovery of MS in urine increased when bromate–bromide reagent was added (Fig. 4). These measurements were carried out shortly after the addition of

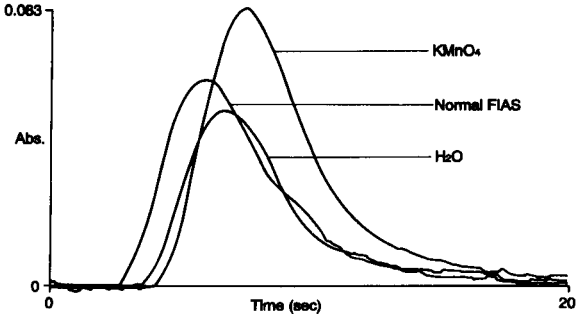

Fig. 3. Enhancement of mercury signal by on-line addition of $KMnO_4$. Normal FIAS = set-up without additional channel for $KMnO_4$; $KMnO_4$ = on-line addition of $KMnO_4$; H_2O = on-line Addition of water instead of $KMnO_4$.

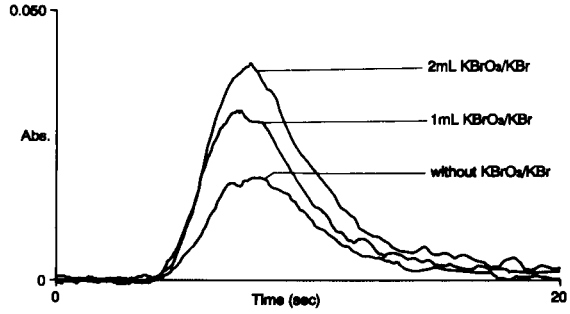

Fig. 4. Mercury signals from mercurescein sodium in urine showing effect of varying the amounts of bromate–bromide reagent.

bromate–bromide reagent to the urine samples. In a urine sample that contained 4% (v/v) bromate–bromide reagent, the recovery of the added MS could reach 93%. It was also found that the bromate–bromide reagent was effective for MA and PMC, but alone it was not effective for MMC (Fig. 2, signal group 2)

Use of $KMnO_4$ and bromate–bromide reagent together. Based on the recovery tests described above, the use of $KMnO_4$ or bromate–bromide reagent alone was effective only for some of the organic mercury compounds tested and their effects on organic mercury compounds are complementary. The natural conclusion was to use both $KMnO_4$ (effective for MMC, MA and PMC) and bromate–bromide reagent (effective for MA, PMC and MS) together in order to obtain the most powerful decomposition effect. In this work, the bromate–bromide reagent was added off-line; the results of using $KMnO_4$ and bromate–bromide reagent together are shown in Fig. 2 (signal group 4). The recoveries of all the organic mercury compounds tested were nearly complete.

It should be mentioned that the organic compounds used in this recovery test cannot represent all of the organic mercurials that may possibly exist in urine; some may not exist in urine and there may be also other organic mercury compounds that are not included in this list. However, these compounds, MA, PMC and MS, were deliberately chosen for the test because it was known that they had very low recoveries even in distilled water and using $NaBH_4$ as the reductant

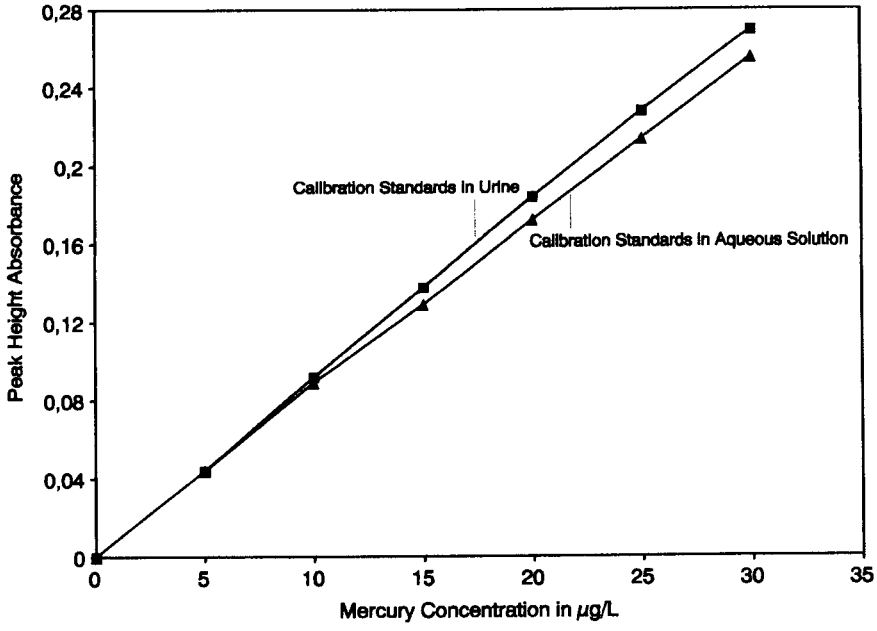

Fig. 5. Calibration C graphs for the determination of mercury in urine (with the cold vapour technique) using atomic absorption spectrometry. ■ = Calibration standards in urine; ▲ = calibration standards in aqueous solution.

[6]. It is reasonable to infer that when the recoveries of these compounds are complete under the selected conditions, then other organic mercury compounds could also be completely measured. In this work, this method was checked by the measurement of urine control samples.

Calibration

The system was calibrated with a series of Hg(II) standards with concentrations up to 30 μg l^{-1}; the standard series were 0.00, 5.00, 15.00, 20.00, 25.00 and 30.00 μg l^{-1} Hg. The calibration graphs obeyed the equation $H = 7.7 \times 10^{-3}\ C + 1.7 \times 10^{-3}$ (correlation coefficient $r = 0.999$), where H is peak-height absorbance and C is the mercury concentration in μg l^{-1}. The between-batch relative standard deviation of the slope was 1.3% and that of the intercept was 34% for three measurements made on three consecutive days.

Under the experimental conditions described above, the measured signal of mercury in urine was about 5% higher than that for the same concentration in aqueous solution (both were blank corrected).

TABLE 2

Results of measurements on control urine samples

Sample	Assigned [a] value (μg l^{-1})	Confidence range [b] (μg l^{-1})	Results by proposed method [c] (μg l^{-1})
Lanonorm Metalle 1	11.8	9.8–13.7	11.4 ± 0.2 (n = 6)
Lanonorm Metalle 2	114	101–128	119 ± 3 (n = 4)
Lyphochek Urine 1	5.2	2.8–7.6	7.8 ± 0.9 (n = 5)
Lyphochek Urine 2	30.5	20.5–40.5	31.3 ± 1.9 (n = 4)
Seronorm Urine No. 115	35		33 ± 0.5 (n = 5)

[a] "Mean" for Lyphochek samples and "preliminary recommended values" for seronorm samples. [b] "Acceptable range" for Lyphochek samples. [c] The ± values indicate the standard deviations for n measurements, each measurement being the mean of three replicates.

Calibration graphs obtained with standards in urine and in aqueous solution are shown in Fig. 5. These results are in good agreement with the observations with the batch system [1]. The reason for the difference in the signals is probably the different physical properties of urine and aqueous solution, e.g., viscosity and surface tension. Adding Triton X-100 solution to urine at a level of 0.4% (v/v) was found to be effective in reducing or even eliminating the sensitivity difference between the two matrices.

Detection limit and precision

The detection limit of the method based on three standard deviations of the blank was 0.1 μg Hg l^{-1} in urine with a 500-μl sample loop.

The relative standard deviation of the signal at a level of 5 μg Hg(II) l^{-1} in urine was 1.7% ($n = 11$) and the between-batch precision was ca. 2%. When the filter-paper was wet then the precision deteriorated; if this occurs the filter-paper should be replaced.

Determination of mercury in control urine samples

This method for the determination of total mercury in urine was tested by measuring the mercury contents in control urine samples. The results are summarized in Table 2 and are in agreement with the known contents.

After a large number of measurements, the reaction coil tube 1 becomes brown, obviously owing to the decomposition products of $KMnO_4$. However, this does not affect the determinations. It is recommended that the system is cleared every day by pumping 1 + 1 HCl through all three channels, i.e., the $KMnO_4$, the $NaBH_4$ and the carrier channels. This procedure removes the brown colour in tube 1.

Sometimes excess $KMnO_4$ or $KMnO_4$ alone may enter the system, which would result in a severe decrease in the sensitivity of the system. Pumping 1 + 1 HCl through the system as described above restores the sensitivity.

Conclusion

A rapid and reliable procedure for the determination of total mercury in urine samples has been described. Because the flow-injection technique was used for on-line addition of $KMnO_4$, the advantages of this powerful oxidizing agent and its enhancement of the mercury signals can be fully exploited, while the disadvantages can be effectively avoided.

The samples need very limited manipulation before measurement, and the reactions take place at room temperature within the FI system, which reduces the risk of analyte loss or contamination. In addition, the method has a low detection limit, wide dynamic range and high throughput.

The authors thank Professor Z.L. Fang and Dr. I. Shuttler for their valuable comments on and discussions of this work. Mr. Stephen Helliwell is thanked for this kind revision of the manuscript.

REFERENCES

1 J. Angerer and K.H. Schaller (Eds.), Deutsche Forschungsgemeinschaft, Analyses of Hazardous Substances in Biological Materials (Methods for Biological Monitoring, Vol. 2), VCH, Weinheim, 1988, pp. 196–211.
2 L. Ping and P.K. Dasgupta, Anal. Chem., 61 (1989) 1230.
3 R. Ahmed; K. May and M. Stoeppler, Fresenius' Z. Anal. Chem., 326 (1987) 510.
4 B. Welz, D.L. Tsalev and M. Sperling, Anal. Chim. Acta, 261 (1992) 91.
5 H.W. Sinemus and H.H. Stabel, in B. Welz (Ed.), in 5. CAS (Colloquium Atomspektrometrische Spurenanalytik), 1989, Bodenseewerk Perkin-Elmer, Überlingen, 1989, p. 711.
6 D.C. Baxter and W. Frech, Anal. Chim. Acta, 236 (1990) 377.
7 H. Brandenberger and H. Bader, At. Absorpt. Newsl., 6 (1967) 101.
8 W.R. Hatch and W.L. Ott, Anal. Chem., 40 (1968) 2085.
9 United States Environmental Protection Agency, Mercury Method 245.1 (Manual Cold Vapor Technique), EPA, Washington, DC, 1974, p. 1.
10 B.J. Farey, L.A. Nelson and M.G. Rolph, Analyst, 103 (1978) 656.
11 B.J. Farey and L.A. Nelson, Anal. Chem., 50 (1978), 2147.
12 FIAS-200 Flow-Injection Analysis System, User Documentation, B019-3807 (B 3502/E), Release A 2.0, Bodenseewerk Perkin-Elmer, Überlingen, 1991.
13 J. Toffaletti and J. Savory, Anal. Chem., 47 (1975) 2091.
14 S. Margel and J. Hirsch, Clin. Chem., 30 (1984) 243.
15 B. Welz and M. Melcher, At. Spectrosc., 5 (1984) 37.

Analytica Chimica Acta, 278 (1993) 197–203
Elsevier Science Publishers B.V., Amsterdam

Tensammetric studies of the separation of surfactants

Part 1. Investigation of sources of error in precipitation of non-ionic surfactants with modified Dragendorff reagent

Bogdan Wyrwas, Andrzej Szymanski and Zenon Lukaszewski

Institute of Chemistry, Technical University of Poznan, 60-965 Poznan (Poland)

(Received 4th November 1992)

Abstract

Precipitation of surfactants with modified Dragendorff reagent, being a part of the bismuth active substance (BiAS) standard procedure, was investigated with the use of adsorptive stripping tensammetry and an indirect tensammetric method. Triton X-100 was used as a representative surfactant. The washing step with glacial acetic acid, part of the investigated procedure, was found to be a serious source of loss of precipitate and therefore the main source of error of determination in the BiAS procedure. The concentration of surfactant in the filtrate and adsorptive losses on the filter were also determined.

Keywords: UV–Visible spectrophotometry; Bismuth active substances; Surfactants; Tensammetry

Precipitation of ethoxylates with modified Dragendorff reagent is part of a standard procedure used for determination of non-ionic surfactants in environmental samples known as the bismuth active substance (BiAS) procedure [1]. It is an indirect method. Bismuth is determined in the precipitate by different methods (potentiometry [1] or UV spectrophotometry [2–4]). Therefore, substances determined with this method are called bismuth active substances (BiAS). The precipitation stage is preceded by sublation of ethoxylates from a water matrix to the ethyl acetate phase.

Dragendorff reagent is an acidic solution of the iodide complex of bismuth(III). In fact, it is one of the numerous Dragendorff reagents used for identification of different organic substances [5]. The iodide complex of bismuth(III) has been used for identification of alkaloids since 1867. This reagent has been modified for precipitation of ethoxylates [6]. Barium(II) cations have been added and acetic acid for acidification instead of the nitric acid which was used in the original procedure. Ethoxylates, in the form of the complex with barium(II) ions, exhibit an ability to be precipitated with the bismuth(III)–iodide complex. The property concerns those ethoxylates having at least 4–5 ethoxylene subunits in the molecule. The orange precipitate obtained is filtered and washed with glacial acetic acid to remove the residue of non-precipitated bismuth(III).

The use of the BiAS procedure starting from the 1970s allowed the assessment of the level of non-ionic surfactants in surface waters, and influents and effluents of sewage treatment plants and biodegradibility tests on the surfactants. The results stimulated changes in the profile of manufacture of non-ionic surfactants with the aim of eliminating these hardly biodegradable compounds and, in consequence, of achieving sub-

Correspondence to: Z. Lukaszewski, Institute of Chemistry, Technical University of Poznan, 60-965 Poznan (Poland)

stantial drop in the level of non-ionic surfactants in surface waters [7]. On the other hand, interlaboratory tests showed large unidentified errors in the determination of non-ionic surfactants in the final effluent of sewage treatment plants using the BiAS procedure [8]. The results obtained differed by almost half an order of magnitude. Because of this error, only amounts of ethoxylates higher than 100 μg in a sample are recommended for determination. This is a serious limitation on the use of the BiAS method for surface water analysis. At the normal levels of concentration of non-ionic surfactants a large volume of surface water (5 l) would be needed in the BiAS procedure to achieve an amount exceeding 100 μg.

The aim of this work was the examination of different stages of precipitation of ethoxylates with modified Dragendorff reagent to find the sources of error. This work is part of a wider attempt to investigate the whole BiAS procedure. Two tensammetric techniques, adsorptive stripping tensammetry (AST) and the indirect tensammetric method (ITM), were used in these investigations. AST uses preconcentration on a hanging mercury drop electrode preceding recording of the tensammetric curve [9,10]. The analytical signal in this technique is specific, to a certain extent. ITM uses the lowering of the tensammetric peak of ethyl acetate (caused by competitive adsorption of surfactant) as an analytical signal [11]. This technique is not specific. Both techniques are sufficiently sensitive to detect signals of surfactant in precipitates and processing solutions and to indicate losses of surfactant on the filter during the analytical procedure. The BiAS procedure was performed in parallel and bismuth(III) was determined using UV spectrophotometry. The absorbance of the bismuth(III)–EDTA complex was measured at 264 nm. Triton X-100 was used as a representative non-ionic surfactant.

EXPERIMENTAL

Apparatus and reagents

A Carl-Zeiss Jena Specord M40 UV–visible spectrophotometer was used. Measurements were performed using a 1-cm cell at 264 nm versus a 0.05 M aqueous solution of ammonium tartrate containing 0.8 mM EDTA.

A Radelkis OH-105 polarograph was used with a voltage scan rate of 400 mV min^{-1}. The applied amplitude of the alternating voltage was 2 mV. Controlled-temperature HMDE equipment (Radiometer), having an additional platinum wire auxiliary electrode, was used. All potentials cited are versus the saturated calomel electrode (SCE). The beaker of the measuring cell was replaced with a quartz beaker. The ceramic frit on the end of the salt bridge was protected by fitting a polyethylene tube. This ceramic frit exhibits a large adsorptive ability [10], and this protection very effectively reduces the adsorptive loss of surfactant. The investigated cell was first carefully cleaned with methanol.

Triton X-100 (Rohm and Haas, supplied by Serva) was used without additional purification. Ethyl acetate (POCh) of gas chromatographic grade was used. Other reagents used were of analytical-reagent grade.

Modified Dragendorff reagent [1] was prepared, consisting of two solutions (A and B) that were mixed before use. Solution A was prepared by dissolving 1.7 g of basic bismuth(III) nitrate and 65 g of potassium iodide in 220 ml of glacial acetic acid and diluting to 1 l with water. Solution B was an aqueous solution containing 290 g of barium chloride dihydrate in 1 l.

The solution for dissolving the precipitate was prepared by mixing 12.4 g of tartaric acid and 18 ml of 25% ammonia solution and diluting to 1 l with water.

Purified sodium sulphate was used for the preparation of the aqueous 0.5 M base electrolyte [10]. All solutions were prepared in water triply distilled from quartz. Only freshly distilled water was used.

In AST measurements preconcentration was done in a stirred solution at the required potential with a new mercury drop [10]. The preconcentration time was measured from the moment of drop formation. The tensammetric curve was recorded in the negative direction after a 30-s quiescent period. ITM measurements were performed without preconcentration. The tensam-

metric curve was recorded 15 s after the formation of a new mercury drop, in the negative direction.

Precipitation of oxyethylates with modified Dragendorff reagent according to the BiAS procedure and their determination by UV spectrophotometry [3,4]

A sample of 100–1000 μg of Triton X-100 was added in the form of a solution to a mixture of 5 ml of methanol and 40 ml of water, then 20 ml of solution A and 10 ml of solution B of the modified Dragendorff reagent were mixed and added to the sample. The reaction mixture was left for 15–60 min. The orange precipitate obtained was filtered through a glass filter (G4) and washed with a limited volume of glacial acetic acid (40 ml is recommended). The precipitate was then dissolved in 60 ml of hot ammonium tartrate solution. After cooling the solution, 4 ml of 0.2 M EDTA solution were added and the volume was made up to 100 ml with water.

The absorbance was measured at 264 nm. The results were evaluated using a calibration graph obtained after the whole cycle, i.e., including precipitation, washing and dissolution of the precipitate, to compensate for losses during procedure.

Determination of Triton X-100 in the filtrate, in the washing agent, on the glass filter and in the precipitate obtained or used during the BiAS procedure

A 10-g amount of sodium chloride was added to the filtrate obtained in the BiAS procedure and the solution was diluted to 100 ml with water. Non-ionic surfactants were extracted with 5 ml of ethyl acetate. A 50-μl volume of the extract was dissolved in the base electrolyte. AST measurements were performed using a 5-min preconcentration at −1.20 V vs. SCE. The results were evaluated using a calibration graph obtained in the presence of 50 μl of ethyl acetate. Excess of complex of bismuth(III) with iodide also passes to the ethyl acetate phase under the applied conditions. A 50-μl amount of extract contains a maximum amount of this complex tolerated in AST measurement of non-ionic surfactant concentrations.

The glacial acetic acid used for washing the precipitate in the BiAS procedure was evaporated and the residue was dissolved in 100 ml of water. Triton X-100 was extracted with 5 ml of ethyl acetate and the further procedure was performed as described above.

The glass filter used for filtration of precipitate in the BiAS procedure was washed with methanol after filtration was completed. The methanol was evaporated, the residue was dissolved in 100 ml of water and the further procedure was performed as described above.

The same solution prepared for the determination of bismuth(III) by the BiAS–UV procedure (see above) was used for the determination of Triton X-100 by the AST and ITM methods. A 100–1000-μl volume of solution prepared for UV spectrophotometric measurement was introduced into the base electrolyte and an AST measurement was performed using a 5-min preconcentration at −1.20 V vs. SCE. A 1–2 ml volume of the same solution was introduced into the base electrolyte for ITM measurement. A 1.5-ml volume of ethyl acetate was added. ITM measurement was performed starting from −1.20 V in the negative direction.

RESULTS AND DISCUSSION

Determination of surfactant not precipitated during the BiAS procedure

The concentration of Triton X-100 was measured in the filtrate after precipitation of the surfactant with modified Dragendorff reagent. Two different times of precipitation were used and different amounts of Triton X-100 were added. Two experiments were added to this series with separation of the filtrate by decantation instead of filtration of the precipitate. AST was employed for the measurement the concentration of Triton X-100 in the filtrate. The results are given in Table 1.

The concentration of Triton X-100 in the filtrate changes irregularly within the range 13–48 μg of sample. This indicates that the conditions

TABLE 1

Amounts of surfactant determined by AST in the filtrate in the BiAS procedure

Added Triton X-100 (μg in the sample)	Time of precipitation (min)	Triton X-100 found in the filtrate (μg)
100	15	44; 48
	60	20; 20; 13
500	15	25
	60	40
1000	15	42
	60	42; 37; 16; 17
		30 [a]
2000		20 [a]

[a] In the decantate.

of precipitation were not completely controlled. Although the loss of Triton X-100 due to incomplete precipitation remains roughly the same, irrespective of the amount of precipitated Triton X-100, the percentage loss is much higher in with small amounts of surfactant to be determined than with large amounts.

Loss of surfactant during washing of the precipitate with glacial acetic acid

Four series of experiments were performed, the first with 100 μg of precipitated Triton X-100 and the other three with 1000 μg of Triton X-100. In two series the recommended amount of washing agent was added and in the other two an exaggerated amount of washing agent was used to enhance and reveal the errors connected with this operation. The content of Triton X-100 in each portion of washing agent was determined by AST. The results are given in Table 2 and examples of the analytical signals in AST obtained after the first two washings are shown in Fig. 1. The amount of Triton X-100 in the precipitate and in the filtrate and the loss of Triton X-100 on the glass filter are also given for a total balance.

A serious loss during washing of the precipitate with glacial acetic acid is obvious from the results. In the last two experiments an exaggerated volume of washing agent was used and the

TABLE 2

Loss of surfactant during washing of the precipitate obtained in the BiAS procedure with glacial acetic acid (as determined by AST)

Triton X-100 processed in the BiAS procedure (μg)	Portion of glacial acetic acid (ml)	Triton X-100 found (μg)
100	20	25
	20	8
	40 [a]	33 [b]
		63 [c]
		13 [d]
		4 [e]
		50 [f]
Total		113
1000	20	22
	20	22
	20	48
	60 [a]	92 [b]
		904 [c]
		37 [d]
		6 [e]
		87 [f]
Total		1039
1000	20	112
	20	53
	20	29
	40	33
	40	29
	40	21
	40	39
	80	26
	300 [a]	342 [b]
		670 [c]
		16 [d]
		8 [e]
		179 [f]
Total		1036
1000	20	93
	20	40
	200	223
	240 [a]	356 [b]
		657 [c]
		17 [d]
		8 [e]
		158 [f]
Total		1038

[a] Total volume. [b] Total loss. [c] Triton X-100 found in the precipitate. [d] Triton X-100 found in the filtrate. [e] Loss of Triton X-100 on the filter. [f] Total loss of two washings, content in the filtrate and adsorptive loss.

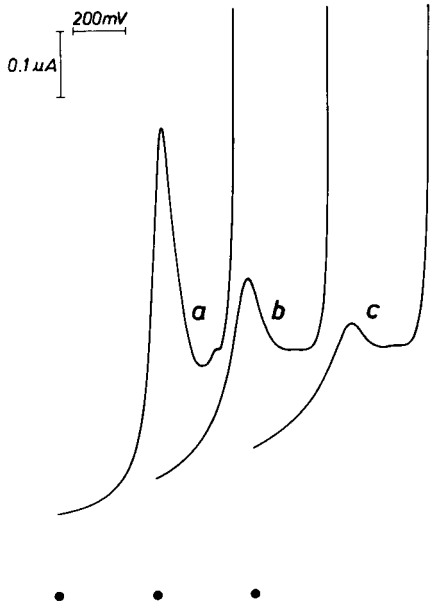

Fig. 1. Examples of tensammetric curves (AST) of Triton X-100 as determined in portions of glacial acetic acid used during washing of the precipitate in the BiAS standard procedure. (a) Standard (200 μg of Triton X-100 in the sample); (b and c) signals for the first and second washing solutions, respectively.

loss is abnormally high. However, these experiments show that each excessive portion of washing agent increases the loss of surfactant. Even if first two portions of washing agent are considered the loss from 1000 μg of precipitated Triton X-100 during washing ranges from 44 to 165 μg. Undoubtedly, the washing with glacial acetic acid is the main source of error during the BiAS procedure. The loss due to non-precipitated surfactant in the filtrate is of the order of 15–45 μg (see Table 1) and the adsorptive loss on the filter is in the range 4–8 μg. On the other hand, if washing is not complete, the results of analysis will be too high. It is necessary to stress the irregularity of the losses during washing. Consecutive portions of washing agent dissolve different amounts of precipitate. One of the factors responsible for this irregularity seems to be the flow-rate of the washing agent. The discussed irregularity makes it difficult to compensate for this loss by carrying out calibration in the full cycle.

The total loss from the 1000 μg of Triton X-100 precipitate for three series of experiments shown in Table 2 (i.e. the loss in the first two 20-ml portions of washing, the loss in the filtrate and the adsorptive loss) is as high as 87–179 μg, i.e., 9–18% of the precipitated amount of surfactant. However, if 100 μg of Triton X-100 are precipitated the total loss is 50 μg, i.e., 50% of the precipitated amount. Therefore, it is obvious why only comparatively large amounts of non-ionic surfactants are recommended for the determination by means of the BiAS procedure (> 100–200 μg). It is also clear why interlaboratory experiments with the BiAS procedure [8] gave satisfactory results for the samples containing a high concentration of surfactants and simultaneously very poor results for samples containing a low concentration of surfactants. The total balance of all kinds of losses and the amount of surfactant in the precipitate is satisfactory.

Comparison of recoveries in the BiAS procedure as determined by UV spectrophotometry and by tensammetric techniques

The recovery of Triton X-100 in the BiAS procedure was investigated by the determination of bismuth(III) in the precipitate using UV spectrophotometry (BiAS–UV) and by the determination of Triton X-100 in the precipitate using AST and ITM. The amount of spiked Triton X-100 was varied within the range 100–1000 μg, i.e., within the range recommended for the BiAS procedure [1–4]. Each determination of Triton X-100 by the BiAS–UV method was accompanied with the AST measurement of the Triton X-100 concentration performed on the same solution.

Numerous measurements were simultaneously made with the BiAS–UV method, AST and ITM. Supplementary single experiments with AST and ITM were also performed. The results for Triton X-100 as determined with both tensammetric techniques concerned the real amount of Triton X-100 in the precipitate, i.e., they should indicate the loss of surfactant during the procedure. In contrast, the results obtained with the BiAS–UV method should have this loss compensated for by the calibration performed in the full cycle, i.e., the given amount of surfactant was processed

according to the full BiAS procedure including precipitation, filtration, washing and dissolution of precipitate. Therefore, the error of loss should be compensated for. The results of recovery experiments are given in Table 3.

The average amount of surfactant determined by BiAS–UV measurements is higher than those for the tensammetric techniques, which supports expectations and again supports the evidence for losses of surfactant during the BiAS procedure. The very poor precision of the results for BiAS–UV measurements if a small amount of surfactant is determined is apparent from the results for 100 μg of Triton X-100. The precision of the tensammetric measurements is roughly twice as good. The precision of measurements becomes better and typical for trace analysis if the determined amount of surfactant increases. Several cases of overestimation are also apparent. Incomplete washing can be the reason for such results. This overestimation is not supported by the tensammetric measurements because only additional bismuth(III) (detected by the BiAS–UV method) appears in the system and not the additional amount of surfactant determined by tensammetric measurements. The two tensammetric techniques gave similar results.

Other sources of error

Adsorptive loss of Triton X-100 on the walls of the vessels and filtration material is shown in Table 3. It is not the main source of error within the range of concentration used but it is not negligible and should be controlled.

Insufficient washing of the precipitate can cause a serious source of errors leading to overestimation. Such an error can be easily made because attempts to minimize the loss by washing. Several such cases appear in the results given in Table 3 and they have already been briefly discussed.

Qualitative evidence was found for several further sources of errors. Dilution of the modified Dragendorff reagent with glacial acetic acid or water causes the formation of precipitates including bismuth(III). Another source of error can be the glass filter used for filtration, which seems to adsorb barium(II) ions. This effect influences the subsequent filtration, resulting in a slower flow-rate, and it changes the loss of precipitate during the washing with glacial acetic acid in this way. To prevent this poorly defined effect the filter was stored in alkaline EDTA solution between

TABLE 3

Comparison of recovery in the BiAS procedure as determined by UV–spectrophotometry (BiAS–UV) and by the tensammetric techniques (AST and ITM)

Triton X-100 added (μg)	Found (μg) [a]		
	BiAS–UV	AST	ITM
0	30	0	0
100	148	76	–
	–	78	–
	34	43	36
	–	–	35
	61	35	38
	48	64	74
	–	–	68
	56	68	64
	102	63	–
Average	75	61	53
S.D.	42	16	53
R.S.D.	56%	26%	34%
200	205	170	–
	–	175	–
Average		172	
300	315	264	–
	–	286	–
Average		275	
400	473	456	–
	–	368	
Average		412	
500	489	540	–
	–	448	–
	436	500	490
	406	460	450
Average	443	487	470
S.D.	42	42	
R.S.D.	9.5%	8.5%	
700	794	750	–
	–	675	–
Average		712	
1000	948	905	–
	–	930	–
	1026	963	920
	1083	976	940
	932	904	–
Average	997	935	930
S.D.	71	33	
R.S.D.	7%	3.5%	

[a] Dashes indicate not measured.

measurements. Filtration required a porous filter of G4 density. The use of a glass filter of lower density causes losses of the precipitate during filtration. Blind tests on glacial acetic acid did not show evidence of a substantial error from this source.

This work was supported by the Technical University of Poznan (grant No. R3KB/500/37/92/BW-31/1).

REFERENCES

1 R. Wickbold, Tenside Deterg., 9 (1972) 173.
2 J. Waters and G.F. Longman, Anal. Chim. Acta, 93 (1977) 341.
3 J. Waters, J.T. Garigan and A.M. Paulson, Water Res., 20 (1986) 247.
4 Polish Standard PN-88-C-04550/11, Determination of non-ionic surfactants in waters by spectrophotometric method using Dragendorff reagent, Polish Committee for Standardization, Measures and Quality Control, 1988.
5 Merck's Reagenzien-Verzeichnis, Merck, Darmstadt, 1939.
6 K. Bürger, Fresenius' Z. Anal. Chem., 196 (1963) 251.
7 H. Hellmann, Tenside Surfact. Deterg., 27 (1990) 318.
8 D. Brown, H. De Henau, J.T. Garigan, P. Gerike, M. Holt, E. Keck, E. Kunkel, E. Matthijs, J. Waters and J. Watkinson, Tenside Deterg., 23 (1986) 190.
9 H. Batycka and Z. Lukaszewski, Anal. Chim. Acta, 162 (1984) 215.
10 A. Szymanski and Z. Lukaszewski, Anal. Chim. Acta, 231 (1990) 77.
11 A. Szymanski and Z. Lukaszewski, Anal. Chim. Acta, 260 (1992) 25.

Analytica Chimica Acta, 278 (1993) 205–206
Elsevier Science Publishers B.V., Amsterdam

Discussion on "On-line determination of bromide ion in spent brine"

Wei Li and Jian Chen

Department of Pharmacy, Xin Jiang Medical College, Wulumuqi 830054 (China)

Deng-kui An

Department of Pharmaceutical Analysis, China Pharmaceutical University, Nanjing 210009 (China)

(Received 20th October 1992)

Abstract

Some errors in the mathematical treatment of a dual-cell system in the paper "On-line determination of bromide ion in spent brine" [Anal. Chim. Acta, 256 (1992) 97] were found and some necessary corrections to the mathematical treatment have been made.

Keywords: UV–Visible spectrophotometry; Bromide; Fibre-optic sensors; Spent brine

The paper "On-line determination of bromide ion in spent brine" [1] reported the on-line determination of bromide in spent brine by combining fibre-optic techniques and continuous-flow sampling. Simultaneously, the dynamic range of an absorption measurement can be extended by using a dual absorption cell system. However, we found some errors in the mathematical treatment of a dual-cell system in the Appendix, and some comments and corrections are presented here.

The cited paper considers two light beams passing through two absorption cells in parallel, the transmitted light being combined and sent to a single detector:

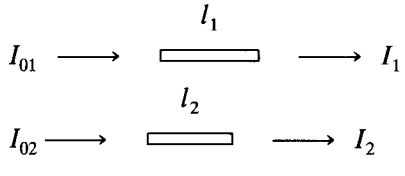

Correspondence to: Deng-kui An, Department of Pharmaceutical Analysis, China Pharmaceutical University, Nanjing 210009 (China).

where I_{01} and I_{02} are incident intensities, I_1 and I_2 the intensities of the transmitted light and l_1 and l_2 the path lengths of the two cells.

Assume that the light incident on both absorption cells has the same intensity, I_0; the total intensity of the transmitted light is then

$$I = I_1 + I_2 = I_0[\exp(-al_1c) + \exp(-al_2c)]$$

$$A = \log(I_0/I)$$

$$= -\log[\exp(-al_1c) + \exp(-al_2c)]$$

When c approaches zero, $\exp[a(l_1 - l_2)c]$ will approach zero:

$$A = al_1c - \log\{1 + \exp[a(l_1 - l_2)c]\} = al_1c$$

When c approaches infinity, then $\exp[-a(l_2 - l_1)c]$ will approach zero:

$$A = al_2c - \log\{1 + \exp[-a(l_2 - l_1)c]\} = al_2c$$

A calibration graph obtained with the dual-cell instrumentation is linear and produces a zero intercept when c approaches zero and is linear but produces a non-zero intercept when c approaches infinity.

There are some errors in the underlined sections. The mathematical treatment of a dual-cell system should be as follows:

$$A = \log[(I_{01} + I_{02})/(I_1 + I_2)] = \log(2I_0/I)$$
$$= -\log[\exp(-al_1c) + \exp(-al_2c)] + \log 2$$

When c approaches zero, $\exp[a(l_1 - l_2)c]$ will approach 1:

$$A = al_1c - \log\{1 + \exp[a(l_1 - l_2)c]\} + \log 2$$
$$= al_1c$$

When c approaches infinity, then $\exp[-a(l_1 - l_2)c]$ will approach zero:

$$A = al_2c - \log\{\exp[-a(l_1 - l_2)c] + 1\} + \log 2$$
$$= al_2c + \log 2$$

Our deductions conform to the calibration graph obtained with a dual absorption cell and the conclusions drawn by the authors: the use of a dual absorption cell will produce a non-linear Beer's law response, but will offer a greatly enhanced dynamic range.

Editor's note. The authors of the original paper agree that the errors detected may be corrected in this way.

REFERENCE

1 C. Zhu and G.M. Hieftje, Anal. Chim. Acta, 256 (1992) 97.

Analytica Chimica Acta, 278 (1993) 207–210
Elsevier Science Publishers B.V., Amsterdam

BOOK REVIEWS

I. Weeks, *Chemiluminescence Immunoassay* (Vol. XXIX of *Wilson and Wilson's Comprehensive Analytical Chemistry*, series Editor: G. Svehla), Elsevier, Amsterdam, 1992 (ISBN 0-444-89035-1). xvi + 293 pp. Price US$151.50/Dfl.295.00.

This is the latest addition to Wilson and Wilson's Comprehensive Analytical Chemistry series (Volume XXIX). It is a timely contribution in view of the dramatic increase in the use of non-isotopic immunoassays in recent years and the expansion of the application base to include non-clinical areas, e.g., environmental monitoring.

The overall presentation is good although the index is brief and the appendix dealing with instrumentation contains a series of uninspiring black and white photographs. The material presented follows a logical progression and the style of writing makes it very easy to read.

The opening chapters deal succinctly with the separate topics of chemiluminescence and immunoassay and are followed by discussion of the immunochemical/photochemical interface, with emphasis on the chemical coupling of the chemiluminescent reactant with the immunoreactant. The historical evolution of chemiluminescent immunoassays, from the initial experiences with luminol through to indirect enzyme-mediated systems, is then overviewed and illustrates some of the pitfalls that can be encountered during method development.

Homogeneous immunoassays with chemiluminescent labels are also discussed with the attraction of eliminating the separation stage balanced against the potential matrix interferences. Successful assays based on this approach, e.g., the determination of cortisol using aminopentylethylisoluminol as the label and the determination of cyclic adenosine monophosphate using aminobutylethylisoluminol as the label, are described in some detail.

The current status of chemiluminescence immunoassays is covered at length and includes indirect systems, phthalhydrazide and acridinium labels and practical aspects. Given the interests of the author it is not surprising that acridinium labels are considered in particular detail.

Finally, future prospects for the technique are outlined, e.g., the use of monoclonal antibodies, recombinant DNA technology and the impact of the technique on veterinary testing and agricultural, food and environmental analysis.

Overall the book is an authoritative and comprehensive account of chemiluminescence immunoassays and is recommended to those with an interest in either of the parent subjects.

Paul J. Worsfold

L.H.J. Lajunen, *Spectrochemical Analysis by Atomic Absorption and Emission*, The Royal Society of Chemistry, Cambridge, 1992 (ISBN 0-85186-873-8). xii + 233 pp. Price £18.50.

The book covers the theory, instrumentation and sample preparation associated with analytical atomic absorption and emission spectroscopy. It therefore seems rather unusual for the book to use a minor technique within emission spectroscopy, i.e., a direct current plasma, for the cover diagram! Detailed chapters within the book cover atomic absorption spectrometry (flame and graphite furnace, background correction, hydride generation/cold vapour, calibration, interferences and flow injection), atomic emission spectrometry (plasma sources, sample introduction, spectrometers and background correction), inductively coupled plasma mass spectrometry (sample introduction and interferences) and atomic fluorescence spectrometry (sources, atomizer and interference effects). A curious two page chapter on flame emission spectrometry appears to be an adjunct to the book. Of particular importance within the book is the coverage of sample preparation methods for liquid and solid samples, an area frequently omitted in texts. Although limited

details of solid sample preparation including ashing, dissolution by acids with and without microwave heating, and fusion methods are provided, their inclusion is noteworthy. Also, methods for the separation and preconcentration of analytes by liquid–liquid extraction, ion exchange, precipitation and evaporation are useful sections of the book if rather limited in detail.

For a publication from The Royal Society of Chemistry it is rather poor that within the further reading chapter the author should get the name of its main journal in this field wrong, i.e., Journal of Analytical Atomic Spectrometry (JAAS) and not that quoted in the book. Also, the Annual Reports on Analytical Atomic Spectroscopy (ARAAS) has not been published since 1986 when it was superseded by Atomic Spectrometry Updates (ASU). In addition, further reading in books should quote the latest edition of a particular book, e.g., Thompson and Walsh's book has been available as a second edition since 1989 while a better introductory text on ICP-MS is "Applications of ICP-MS", A.R. Date and A.L. Gray, Blackie and Son, Glasgow, 1989. Another major omission from the reading list for a book presumably aimed at the undergraduate/postgraduate student market is "An introduction to AAS", L. Ebdon, Heyden and Son, London, 1982. Overall, however, the book does cover some of the recent innovations in analytical atomic spectroscopy and for this reason is probably of use as an undergraduate/postgraduate text.

J.R. Dean

W. Neagle and D.A. Randell (Eds.), *Surface Analysis Techniques and Applications*, The Royal Society of Chemistry, Cambridge, 1990 (ISBN 0-85186-597-6). vi + 173 pp. Price £37.50.

This booklet contains papers presented at an international symposium held at UMIST in 1989. Consequently it is more a conference report with survey character than a real introductory book. It starts with an overview on surface analytical techniques by D.M. Hercules, which is well written and useful, however somewhat short for the size of the topic. Further methodological chapters deal with surface enhanced Raman spectroscopy, ellipsometry and static SIMS. Further chapters are more problem oriented; they cover a wide variety of applications in industry, for corrosion studies, for mechanical studies, for investigation of glasses, metallized surfaces, etc.

The overall impression is that the book might be useful as a conference report. However it is not recommendable as a real book on surface analysis which would be used by a beginner or practitioner. There are other monographs which have to be definitely preferred. Furthermore I think that the price is not justified, neither for the size of the book nor the content.

Manfred Grasserbauer

B. Volesky and J. Votruba, *Modeling and Optimization of Fermentation Processes*, Elsevier, Amsterdam, 1992 (ISBN 0-444-89588-4). ix + 266 pp. Price Dfl.235.00.

This book is apparently the first in a series on process simulation and modeling, but no indication is given about the forthcoming issues in this series. Therefore it is difficult to assess the aim of the publisher in starting this new series, the more so because in another newly started series from the same publisher devoted to process measurement and control the first volume also deals with bioreactors.

The present volume consists of three parts: the first is devoted to mathematical modeling of microbial processes, the second describes the fundamentals of mass balances and the final part gives an extensive treatment of a case study. According to the introduction, this volume is meant for those who are dealing with bioprocess elements in the laboratory or on a large scale, for the engineer as well as for the science student, stressing the interdisciplinarity of the field.

The interesting approach chosen by the authors is that they give many examples throughout the text by defining problems and discussing the solutions. This will certainly help the reader to digest the material in a proper way. However, in

the reviewer's opinion it will be difficult to appreciate the discussions when not being familiar already to some extent with the concepts of process control, process simulation and optimization on the one hand and with the principles of biotechnology on the other. This is one of the weaker points of this book: it is suggested that it is meant for the newcomers in the field whereas it supposes knowledge on the level of more advanced students who are familiar with reaction kinetics and microbiology. This latter category will certainly like the last chapter where the acetone–butanol–ethanol fermentation process is modeled for batch cultures, for continuous-flow cultures, fed-batch cultures and immobilized cells culture systems. The description is comprehensive and gives a very good insight in the way how systematic modeling can be performed.

In one respect there is a big question mark: that is the information concerning computer programs. With one or two exceptions all programs to which reference is made date back to the sixties or seventies. Furthermore extensive use is made of a program published in 1982 by one of the authors of this book. It is hard to believe that in the eighties no further progress has been made in this area. So it is not clear if this book presents the state-of-the-art in 1992.

In summary, this is a book which has some informative parts but which is less suitable as an introduction in the field of modeling of bioprocesses.

W.E. van der Linden

R.C. Ropp, *Luminescence and the Solid State* (*Studies in Inorganic Chemistry*, Vol. 12), Elsevier, Amsterdam, 1991 (ISBN-0-444-88940-X). xv + 453 pp. Price Dfl.325.00/US$185.50.

Solid state luminescence in the UV–visible region, of the type described in this book, finds surprisingly little application in analytical science. It is essentially restricted to cathode-ray and X-ray stimulated luminescence, and the similar emissions stimulated in certain solids by cool flames (candoluminescence) or by electrochemical processes (electroluminescence). And none of these has progressed further than the research stage as regards its analytical use. What have become more analytically valuable have been techniques like room temperature phosphorescence and low temperature luminescence, but these are not covered in the present text.

The book gives an extremely comprehensive account of the solid state, and its luminescent properties. Indeed, the coverage is probably too wide ranging, because it provides background information on many areas, such as a whole chapter on thermal analysis, and discussions of tristimulus colorimetry, nucleation, growth of single crystals, and the separation of lanthanides, the consequences of which are important, but which topics are well covered in other texts. The strength of the book lies in its detailed coverage of the nature of the solid state and of its luminescence, and of the details of the preparation of solid phosphors. For this it is highly recommended.

Finally, the book deserves a more extensive subject index, and, at least in my copy, the typesetting seemed to be a random mixture of near letter quality and normal typescript.

Alan Townshend

A.E. Martell and R.J. Motekaitis, *The Determination and Use of Stability Constants*, 2nd edn., VCH, Weinheim, 1992 (ISBN 1-560-81516-7). vii + 200 pp. and a 5.25″ disc. Price DM82.00.

In this second edition (see *Anal. Chim. Acta*, 231 (1990) 330) for review of the 1st edition) the typography has been improved, the text clarified in response to readers' comments, and the programs on the diskette revised to run faster on a PC with or without a maths coprocessor. If you get into trouble running the programs, technical support is available. Like the first edition, this is a highly recommended book for those concerned with speciation problems or determination of stability constants.

J.R. Chipperfield

T. Hanai (Ed.), *Liquid Chromatography in Biomedical Analysis* (*Journal of Chromatography Library*, Vol. 50), Elsevier, Amsterdam, 1991 (ISBN 0-444-87451-8). xi + 292 pp. Price Dfl.270.00.

The book begins with an account of collection and pretreatment of the various types of sample (blood, urine and faeces), including on-line procedures, followed by a discussion of the optimisation of liquid chromatography (LC) for biologically important compounds. The remaining ten chapters are devoted to detailed discussion of the LC of particular classes of compound (amino acids, bile acids, carbohydrates, catecholamines, fatty acids, nucleotides, porphyrins, prostaglandins, steroid hormones, and catecholamine metabolites and indoleacetic acid). Most of the chapters are written by C.K. Lim, T. Hirai and T. Hanai.

Barry A.J. Fisher, *Techniques of Crime Scene Investigation*, 5th edn., Elsevier, New York, 1992 (ISBN 0-444-01636-8). xxv + 526 pp. Price US$44.50/Dfl.145.00.

This is the 5th edition of a most useful and interesting text. It gives a comprehensive account of modern forensic science in the scene of crime context. It is liberally supplied with case studies, clearly illustrated, with many new photographs. The book is intended "to introduce the reader to the concepts, procedures and technical information concerning crime scene investigations...", where the reader might well be a non-technical person. Thus the depth of treatment is often insufficient for the knowledgeable scientist, but the breadth of coverage will make a tremendous impression. This book is essential reading for anyone with an interest in forensic science.

Jeffrey C. Hoch, Flemming M. Poulsen and Christina Redfield (Eds.), *Computational Aspects of the Study of Biological Macromolecules by Nuclear Magnetic Resonance Spectroscopy*, Plenum Press, New York, 1991 (ISBN 0-306-44114-4). x + 464 pp. Price US$115.00.

These are the *Proceedings of the NATO Advanced Research Workshop* on the above topic held at IC Ciocco, Barga, Italy, June 3–8, 1990. It contains 37 papers, printed in uniform format, which cover the whole range of current NMR techniques and applications to biological macromolecules and provide an impressive account of powerful computers in NMR spectroscopy. The introductory lecture by R.R. Ernst has its thesis that modern NMR would not be possible without such computers; this is admirably borne out by the contents of this volume.

L. Poppe and L. Novak, *Selective Biocatalysis*, VCH, Weinheim, 1992 (ISBN 3-527-28372-2). xii + 319 pp. Price £63.00.

The target audience for this book is synthetic organic chemists, particularly those with an interest in the production of stereoisomers and high purity compounds in general. A brief introduction to biotransformation makes reference to immobilization techniques for enzymes and whole cells but that is the only aspect of the book that is of direct interest to analytical chemists. The remainder of the text is devoted to stereochemical aspects of biocatalysis, with particular reference to hydrolases, oxidoreductases and baker's yeast.

EUROANALYSIS VIII: European Conference on Analytical Chemistry

September 5-11, 1993, Edinburgh, Scotland, UK

EUROANALYSIS VIII, the eighth in a series of Triennial European Conferences on Analytical Chemistry, will be held at the University of Edinburgh from Sunday to Saturday, September 5-11, 1993. The organisation by the Analytical Division of The Royal Society of Chemistry is on behalf of the Working Party on Analytical Chemistry of the Federation of European Chemical Societies (FECS). There is also sponsorship by the International Union of Pure and Applied Chemistry, and the Conference carries the designation of FECS Event No. 188.

The Scientific Programme has 39 oral sessions to follow the Opening Session on Monday morning, September 6. In addition to the hefty Oral Presentation Programme there are Poster Sessions, an Educational Discussion Session, and throughout the week there will be an Exhibition of Books and Journals.

There is a full day-time programme of visits and trips available to Accompanying Persons and Social events are planned to permit Participants to exchange views and to discuss the Scientific part of the Programme as much as to enjoy the surroundings and to renew friendships and to make new ones.

The various Oral Presentation Streams have by now settled down to be devoted to the following:

Monday:	Sensors; Pharmaceutical and Biomedical Analysis; Atmospheric Analysis; Conservation of Arts; Laser-based Techniques.
Tuesday:	Materials and Surface Analysis; Pharmaceutical and Biomedical Analysis (continued); Analysis of Water; Flow Analysis; Biosensors; Education Discussion Session.
Wednesday:	Electroanalytical Approaches; Analysis of Soils and Sediments; Separation Science; Validation of Analytical Measurements (VAM).
Thursday:	Validity of Forensic Analysis; New Methods and Strategies in Environmental Analysis (sponsored by *Analytica Chimica Acta*); Atomic Spectrometry; Separation Science; Bioselective Methods; COBAC.
Friday:	Industrial Analysis; Coupled Techniques; Food and Drink Analysis; Molecular Spectroscopy; Chemometrics and COBAC.

The Poster Sessions will be on Monday, Tuesday and Thursday at times when there will be breaks in the Oral Presentation Programme. Manuscripts of accepted contributed papers will be considered for publication in a special issue of *The Analyst*. Papers may also be offered for publication in the *Journal of Analytical Atomic Spectrometry* and *Analytical Proceedings*. Papers for "New Methods and Strategies in Environmental Analysis" will be published in *Analytica Chimica Acta*. The invited lectures will be published in a volume of the Proceedings of the Conference.

For more information, please contact: Miss P.E. Hutchinson, Secretary, Analytical Division, The Royal Society of Chemistry, Burlington House, Piccadilly, London W1V 0BN, UK; FAX: 071 734 1227.

Announcement from the Publisher

Elsevier Science Publishers encourages submission of articles on floppy disk.

All manuscripts may now be submitted on computer disk, with the eventual aim of reducing production times still further.

The preferred storage medium is a 5¼ or 3½ inch disk in MS-DOS format, although other systems are welcome, e.g. Macintosh.

After **final acceptance**, your disk plus one final, printed and exactly matching version (as a printout) should be submitted together to the editor. **It is important that the file on disk and the printout are identical.** Both will then be forwarded by the editor to Elsevier.

Illustrations should be provided in the usual manner.

Please follow the general instructions on style/arrangement and, in particular, the reference style of this journal as given in 'Instructions to Authors'.

Please label the disk with your name, the software & hardware used and the name of the file to be processed.

Contact the Publisher for further information:

Elsevier Science Publishers
Analytica Chimica Acta
P.O. Box 330
1000 AH Amsterdam, The Netherlands
Phone: (+31-20) 5862 791 Fax: (+31-20) 5862 459

ELSEVIER SCIENCE PUBLISHERS

CHEMOMETRICS AND INTELLIGENT LABORATORY SYSTEMS

An International Journal Sponsored by the Chemometrics Society

With the Chemometric Newsletter, official bulletin of the Chemometrics Society and including "Laboratory Information Management"

AIMS AND SCOPE

This international journal publishes articles about new developments on laboratory techniques in chemistry and related disciplines which are characterized by the application of statistical and computer methods. Special attention is given to emerging new technologies and techniques for the building of intelligent laboratory systems, i.e. artificial intelligence and robotics. The journal aims to be interdisciplinary; more particularly it intends to bridge the gap between chemists and scientists from related fields, statisticians, and designers of laboratory systems. In order to promote understanding between scientists from different fields the journal features a special section containing tutorial articles.

The journal deals with the following topics: Chemometrics; Computerized acquisition, processing and evaluation of data; Robotics; Developments in statistical theory and mathematics with application to chemistry; Intelligent laboratory systems; Application (case studies) of statistical and computational methods; New software; Imaging techniques and graphical software applied in chemistry. The research papers and tutorials are complemented by the Monitor Section which contains news, a calendar of forthcoming meetings, reports on meetings, software reviews, book reviews, news on societies and announcements of courses and meetings.

ABSTRACTED/INDEXED IN: ASCA, Analytical Abstracts, BioSciences Information Service, Cambridge Scientific Abstracts, Chemical Abstracts, Chromatography Abstracts, Current Contents, Current Index to Statistics, Excerpta Medica, INSPEC, SCISEARCH.

1993 SUBSCRIPTION INFORMATION
Volumes 18-21 (in 12 issues)
Dfl. 1444.00 / US $ 825.00 (including postage) ISSN 0169-7439

Audience

Chemists and physical and life scientists as well as statisticians and information specialists working in a variety of fields of chemistry, including analytical chemistry, organic chemistry and synthesis, environmental chemistry, food chemistry, industrial chemistry, pharmaceutical chemistry and pharmacy.

I would like ☐ a free sample copy of Chemometrics and Intelligent Laboratory Systems.

☐ Instructions to Authors.

☐ to enter a subscription for 1993. Please send me a Proforma Invoice.

Name _____

Address _____

_____

_____

Elsevier Science Publishers
Attn. Carla G.C. Stokman
P.O. Box 330, 1000 AH Amsterdam
The Netherlands
Fax: (+31-20) 5862 845
In the USA & Canada
Attn. Judy Weislogel
P.O. Box 945, Madison Square Station
New York, NY 10160-0757, USA
Fax: (212) 633 3880

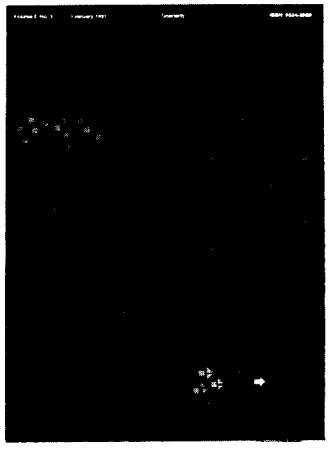

Audience

Scientists and engineers involved in research, plant design, process quality control and environmental monitoring. Chemists, chemical / mechanical / electrical and instrument engineers, computer scientists, quality assurance engineers, instrument manufacturers and consultants.

PROCESS CONTROL AND QUALITY

The science and technology of process quality measurement systems. An international journal

AIMS AND SCOPE

The journal provides a multidisciplinary forum for scientists and engineers involved in research, plant design, processs quality control and environmental monitoring

Topics covered include:

- sampling
- sample handling, instrumentation
- on-line measurement techniques
- automation
- (real-time) expert systems
- control theory
- system validation
- data management and statistical process control.

ABSTRACTED/INDEXED IN: Chemical Abstracts, Chemical Engineering and Biochemical Abstracts (CEBA), Engineering Index, Fluid Abstracts: Process Engineering, Food Science and Technology Abstracts, INSPEC.

SUBSCRIPTION INFORMATION

1993: Volumes 4 – 5 in 8 issues
Dfl. 886.00 / US $ 506.50 (including postage)
ISSN 0924-3089

I would like ☐ a free sample copy of Process Control and Quality.
☐ Instructions to Authors.
☐ to enter a subscription for 1993.
Please send me a Proforma Invoice.

Name _____

Address _____

_____

_____

The Dutch Guilder price (Dfl.) is definitive. US$ prices are for your convenience only and are subject to exchange fluctuations. Customers in the European Community should add the appropriate VAT rate applicable in their country to the price(s).

Elsevier Science Publishers
Attn. Carla G.C. Stokman
P.O. Box 330, 1000 AH Amsterdam
The Netherlands
Fax: (+31-20) 5862 845
In the USA & Canada
Attn. Judy Weislogel
P.O. Box 945, Madison Square Station
New York, NY 10160-0757, USA
Fax: (212) 633 3880

PUBLICATION SCHEDULE FOR 1993

	S'92	O'92	N'92	D'92	J	F	M	A	M	J	J	A
Analytica Chimica Acta	267/1 267/2	268/1 268/2	269/1 269/2	270/1 270/2	271/1 271/2	272/1 272/2 273/1–2	274/1 274/2	275/1–2 276/1 276/2	277/1 277/2	278/1 278/2	279/1 279/2	280/1 280/2
Vibrational Spectroscopy		4/1			4/2		4/3	5/1		5/2		5/3

INFORMATION FOR AUTHORS

Manuscripts. The language of the journal is English. English linguistic improvement is provided as part of the normal editorial processing. Authors should submit three copies of the manuscript in clear double-spaced typing on one side of the paper only. *Vibrational Spectroscopy* also accepts papers in English only.

Abstract. All papers and reviews begin with an Abstract (50–250 words) which should comprise a factual account of the contents of the paper, with emphasis on new information.

Figures. Figures should be prepared in black waterproof drawing ink on drawing or tracing paper of the same size as that on which the manuscript is typed. One original (or sharp glossy print) and two photostat (or other) copies are required. Attention should be given to line thickness, lettering (which should be kept to a minimum) and spacing on axes of graphs, to ensure suitability for reduction in size on printing. Axes of a graph should be clearly labelled, along the axes, outside the graph itself. All figures should be numbered with Arabic numerals, and require descriptive legends which should be typed on a separate sheet of paper. Simple straight-line graphs are not acceptable, because they can readily be described in the text by means of an equation or a sentence. Claims of linearity should be supported by regression data that include slope, intercept, standard deviations of the slope and intercept, standard error and the number of data points; correlation coefficients are optional.

Photographs should be glossy prints and be as rich in contrast as possible; colour photographs cannot be accepted. Line diagrams are generally preferred to photographs of equipment.

Computer outputs for reproduction as figures must be good quality on blank paper, and should preferably be submitted as glossy prints.

Nomenclature, abbreviations and symbols. In general, the recommendations of the International Union of Pure and Applied Chemistry (IUPAC) should be followed, and attention should be given to the recommendations of the Analytical Chemistry Division in the journal *Pure and Applied Chemistry* (see also *IUPAC Compendium of Analytical Nomenclature, Definitive Rules*, 1987).

References. The references should be collected at the end of the paper, numbered in the order of their appearance in the text (*not* alphabetically) and typed on a separate sheet.

Reprints. Fifty reprints will be supplied free of charge. Additional reprints (minimum 100) can be ordered. An order form containing price quotations will be sent to the authors together with the proofs of their article.

Papers dealing with vibrational spectroscopy should be sent to: Dr J.G. Grasselli, 150 Greentree Road, Chagrin Falls, OH 44022, U.S.A. Telefax: (+1-216) 2473360 (Americas, Canada, Australia and New Zealand) or Dr J.H. van der Maas, Department of Analytical Molecule Spectrometry, Faculty of Chemistry, University of Utrecht, P.O. Box 80083, 3508 TB Utrecht, The Netherlands. Telefax: (+31-30) 518219 (all other countries).

0003-2670/93/$06.00

This issue is printed on acid-free paper.

PRINTED IN THE NETHERLANDS

TrAC - Trends in Analytical Chemistry: Reference Edition

Volume 11: 1992

TrAC Compendium Series Volume 11

The Reference Edition of Trends in Analytical Chemistry (TrAC) is a compilation of the archival material reprinted from the regular issues of the journal. TrAC provides a topical digest of current developments and new ideas in the analytical sciences. It does so in the form of broadly-based, easy-to-read scientific reviews, backed up by news and other features of interest to the international analytical chemistry community. For subscribers to the library edition of TrAC, the reference editions form an integral part of the annual subscription, but for others these indispensable sources of information can be purchased individually. They provide informative and stimulating reading for all those who use analytical methods.

This latest volume contains all the archival material published in 1992. It covers a wide range of analytical techniques and applications of interest to academic and research workers in chemistry, biochemistry, clinical chemistry, pharmaceutical chemistry and toxicology.

A selection of the Contents.

Capillary Electrophoresis in Chemical/Pharmaceutical Quality Control *(A. Pluym, W. Van Ael, M. De Smet)*. Image Analysis in Chemistry. I. Properties of Images, Greylevel Operations, the Multivariate Image. II. Multivariate Image Analysis *(P. Geladi et al.)*. Silica Based, Solid Phase Reagents for Derivatizations in Chromatography *(F.-X. Zhou, J.M. Thorne, I.S. Krull)*. Mapping Post-Translational Modifications of Viral Proteins by Mass Spectrometry *(J.J. Gormann)*. Fluorescence Detection in Capillary Electrophoresis *(L.N. Amankwa, M. Albin, W.G. Kuhr)*. Biomolecular Tracing through Accelerator Mass Spectrometry *(J.S. Vogel, K.W. Turteltaub)*. Solid-Phase Reactors in Flow Injection Analysis *(M.D. Luque de Castro)*. Capillary Electrophoresis: A Powerful Tool for Biomedical Analysis and Research? *(D. Perrett, J. Ross)*. Bioanalytical Sample Preparation using Microdialysis and Ultrafiltration Capillaries *(M.C. Linhares, P.T. Kissinger)*. Models of Time-Series Analysis - a Helpful Tool for Evaluation of Noisy Data in Distribution Analysis *(K. Doerffel)*. Bio-Analytical Applications of Fourier Transform Infrared Spectroscopy *(M. Jackson, H.H. Mantsch)*. X-ray Absorption Spectroscopy in Chemistry. I. Extended X-ray Absorption Fine Structure. II. X-ray Absorption near Edge Structure *(P. Behrens)*. Mechanism of the Peroxyoxalate Chemiluminescence Reaction *(P.J.M. Kwakman, G.J. de Jong, U.A.Th. Brinkman)*. Plasma Spectrometric Detection for Supercritical Fluid Chromatography *(J.M. Carey, J.A. Caruso)*. Electrochemistry of Biopolymers *(J.A. Cox, A. Pryzjazny)*. High-Field NMR Spectroscopy as an Analytical Tool for Quantitative Determinations: Pitfalls, Limitations and Possible Solutions *(Cs. Szántay, Jr.)*. Abrasive Stripping Voltammetry - an Electrochemical Solid State Spectroscopy of Wide Applicability *(F. Scholz, B. Lange)*. Polymer Coatings as Stationary Phases in High-Performance Liquid Chromatography *(M. Hanson, K.K. Unger)*. Lasers in Mass Spectrometry *(J. Gorbally)*. Author Index. Subject Index.

1993 viii + 402 pages
Price: US $ 354.25 / Dfl. 620.00
ISBN 0-444-89926-X

ORDER INFORMATION

For USA and Canada
ELSEVIER SCIENCE PUBLISHERS
Judy Weislogel
P.O. Box 945
Madison Square Station,
New York, NY 10160-0757
Tel: (212) 989 5800
Fax: (212) 633 3880

In all other countries
ELSEVIER SCIENCE PUBLISHERS
P.O. Box 211
1000 AE Amsterdam
The Netherlands
Tel: (+31-20) 5803 753
Fax: (+31-20) 5803 705

US$ prices are valid only for the USA & Canada and are subject to exchange rate fluctuations; in all other countries the Dutch guilder price (Dfl.) is definitive. Customers in the European Community should add the appropriate VAT rate applicable in their country to the price(s). Books are sent postfree if prepaid.

ELSEVIER
SCIENCE PUBLISHERS

0003-2670(19930606)278:1;1-A